A study of the interaction of the electromagnetic field with slotted cylindrical structures employing the Method of Regularization

Kaiser Lock

This thesis is presented for the degree of

Doctor of Philosophy

Department of Mathematics

2011

Thesis directed by

Prof. Paul D. Smith

&

Dr. Elena Vinogradova

Abstract

The research program described in this thesis analyzes the interaction of the electromagnetic field with several classes of open cylindrical structures, by using the semi-analytical Method of Regularization (MoR). The dielectric cylinders considered in this thesis are partially shielded by conformal perfectly electric conducting (PEC) strips, where significant coupling and re-radiation of energy are created by the presence of apertures and sharp edges. The problems studied include the scattering problem of a single cylindrical lens reflector (CLR) illuminated by an obliquely incident plane wave, the scattering problem of a finite array of CLR with different characteristics when illuminated by a normal plane wave, the analysis of the scattering from and penetration through a multi-layered CLR and a multi-conductor cylinder, as well as the transmission line problem involving a multi-conductor cable. Each of the problems studied is interesting from both a theoretical point of view and as an idealization of scattering and coupling mechanism in real devices of technological interest.

When the structures are of moderate or large electrical size, standard numerical approaches to solving these mixed boundary valued problems (MBVP) often encounter difficulties of convergence and accuracy of computed solution. Therefore, the MoR — which transforms the ill-posed nature of the standard formulation of the problem to a well-conditioned second kind Fredholm matrix equation — is well-suited for the class of problems considered here. Numerical algorithms based upon the solution of the matrix equation, after truncation to a finite system of N_{tr} equations, converge with guaranteed and predictable accuracy, as $N_{\text{tr}} \to \infty$. Because the computed solutions to these problems are rigorously accurate (in the sense of guaranteed convergence — theoretically and numerically), they provide benchmark solutions to problems of significant complexity against which solutions computed by more general purpose numerical codes (which although of wider applicability have less firm theoretical underpinnings) may be validated.

Statement of Originality

I hereby declare that this submission is my own work and that this thesis contains no material which to a substantial extent has been accepted for the award of any other degree or diploma at any educational institution. To the best of my knowledge and belief, this thesis contains no material previously published or written by another person, except where due reference has been made in the thesis.

Kaiser Lock

Acknowledgements

I would like to sincerely thank Prof. Paul D. Smith and Dr. Elena Vinogradova for their supervision, support and guidance throughout the study program. Their valuable advice for technical issues, and assistance for thesis preparation were much appreciated. I am also greatly indebted to Prof. Sergey Vinogradov for his advice and suggestions regarding many issues relating to the data investigations.

The research reported in this thesis has been financially supported by the Australian Postgraduate Award (APA) and the research training scheme (RTS). I will also like to gratefully acknowledge the Faculty of Science, Macquarie University for the hardware and software support as well as for the financial assistance which makes it possible to attend international conferences and make academic visits during my candidature.

During these years in Australia, the support and friendship of the fellow students have been very helpful through many difficult times. Last but by no means the least, I wish to express my appreciation to my family and Yung for their patience in allowing me to complete this endeavour and to share my problems with them.

Contents

Abbreviations

Acronyms	Description
CLLR	cylindrical Luneburg lens reflector
CLR	cylindrical lens reflector
DSE	dual series equations
FDM	Finite Difference Method
FEM	Finite Element Method
HEM	hybrid electromagnetic mode
HPBW	half power beam width
ISLAE	infinite system of linear algebraic equations
LL	Luneburg lens
MBC	mixed boundary conditions
MBVP	mixed boundary valued problem
MoM	Method of Moments
MoR	Method of Regularization
ODE	ordinary differential equation
PEC	perfectly electric conducting
RCS	radar cross section
SLR	spherical lens reflectors
TE	transverse electric
TEM	transverse electromagnetic mode
TM	transverse magnetic

Chapter 1

Introduction

1.1 Electromagnetic interaction with open cylinders

Structures (in *e.g.*, electrical devices and equipment) with apertures on the surface or that are partially shielded by metals are often termed open structures. The scattering from and penetration through the openings on the surface of these structures are of great interest in engineering applications such as aperture antennas and microstrip transmission lines. In addition, the mass production of telecommunication networks has led to the development of transmitting and receiving structures with metals packed between layers of dielectrics. Dielectric loading has been widely used as a convenient way to modify the scattering behavior of a structure. For example, careful selection of the structure's geometry and physical parameters (such as its dimension, dielectric constants and aperture size) allows one to control and/or reduce the structure's radar cross section (RCS). At the same time, by using flexible dielectric materials, nonplanar transmission lines and reflectors which wrap around a cylinder can be easily constructed.

This thesis focuses on the interaction between electromagnetic fields and infinitely-long, partially-shielded dielectric cylinders, as opposed to the conventional closed cylinders (which are either full dielectric or PEC). In the literature, these open cylinders are also frequently termed slotted cylinders when the angular size of the aperture is less than π. Underground water pipes provide approximate examples of these ideal cylinders, when their lengths are substantially greater than the other dimensions encountered (such as the diameter, screen thickness, and the wavelength of the incident radiation). The presence of sharp edges in these open cylinders requires more careful attention in all solution methods than that of a closed cylinder, due to the mixed

boundary conditions (MBC) that apply.

The problems studied are classified by the scatterers involved, which include a cylindrical lens reflector (CLR), a finite array of CLR with different characteristics, a multi-layered CLR, a multi-conductor cylindrical scatterer and a multi-conductor transmission line. The studies are carried out in the frequency domain and time dependence $e^{j\omega t}$ is assumed. All these problems are solved using the semi-analytical Method of Regularization (MoR) documented in Section 2.2 of [84]. The rigorous solutions computed are not only of direct technological interest, they also provide quantitative predictions for more general and complex structures that are more reliable than those obtained by purely numerical methods.

1.2 A brief survey of solution methods

There are essentially three main groups of computational methods to solve these MBVP where an analytical solution method is intractable. They are the purely-numerical methods, the high frequency methods and the semi-analytical methods.

Purely-numerical methods:

This group consists of the differential equation methods and the integral equation methods. They are usually only feasible at low to intermediate frequencies. Short introduction to and discussions of these methods are given in the following paragraphs. In-depth introduction and review of these purely-numerical methods can be found in classical literature such as [53, 57, 62, 86]. These methods are versatile methods for handling complex scatterer and media but they suffer from some intrinsic weaknesses. Many of them require large computational resources (both time and storage) that may exhaust resources available, especially in the quasi-optical regime ($\lambda \ll R$)[1]. In addition, it is often hard to establish the accuracy of the computed solution based upon these methods.

The Finite Difference Methods (FDM), a popular example of the differential equation methods, was popularized by A. Thom in the 1920s [73]. The method is based upon direct discretization of the differential equations encountered (Maxwell's equations or equivalent) and approximating them by the equivalent finite differences. In another words, it is derived using a truncated Taylor series expansion to approximate the derivatives in the differential equations. The Finite Element Method (FEM)

[1]Here, λ is the wavelength, while R is a typical dimension of the scatterer.

[11, 61] — another example of the differential equation methods — is relatively the simplest method to implement for problems involving complex geometries and inhomogeneity. Its key ideas involve discretizing the solution region into a finite number of elements and deriving the governing equations for a typical element. For the scattering problem in regions of infinite extent (*i.e.*, in the open domain), the Sommerfeld radiation condition is normally approximated by some artificial boundary condition on the exterior of the truncated domain. A survey of various treatments of this artificial boundary condition can be found in [78]. The equations are assembled and solved using methods such as Gaussian elimination, or for large problems where this method is too computationally demanding, iterative methods or band matrix methods can be applied.

For the FDM, truncation error arises because some higher order terms in the Taylor series expansion were neglected in deriving the finite difference schemes. One way to tackle this is by increasing the number of terms in the series expansion of derivatives. However, instability may result if the order of the finite difference is higher than that of the original differential equation. Another way is by reducing the mesh size, which results in an increase in the number of arithmetic operations and thus, an increase in the roundoff error due to the finite storage capacity of the computer. In other words, the accuracy of the FDM is limited [88], as the truncation error is inversely proportional to the roundoff error. A similar limitation exists for the FEM as it requires discretization of the domain. Additionally, any area of highly concentrated energy (such as in the vicinity of edges) needs to be carefully analyzed by using a sufficiently refined mesh.

Integral equation solution methods rely on the integral equation obtained from Maxwell's equations with an appropriately constructed Green's function. An example is the MoM which became widely popular since the work by Harrington [24]. The conventional MoM converts the integral equation encountered — *e.g.*, the electric field integral equation (EFIE) — into an infinite system of linear algebraic equations (ISLAE) by using some properly chosen weighting functions in the process of taking moments, and using basis functions to represent the related surface current. The ISLAE is subsequently truncated (by restriction to a finite basis and weighting set) and solved numerically for the coefficients of the basis functions.

Although the methods avoid discretization of the entire domain by solving only for the fields on the surface of the scatterer, instability may still arise when they rely on numerical solving of a first kind Fredholm equation. We consider the EFIE of a

slotted PEC cylinder as an example: it is a first kind Fredholm equation, of the form

$$\mathcal{A}\mathbf{x} = \mathbf{b}\,, \tag{1.1}$$

where $\mathcal{A}$ is a compact operator on the Hilbert space ℓ_2. It is inherently weakly ill-posed [43]. The solution of this equation, when solved with direct numerical methods, is unreliable [27, 51]. Thus, the computational scheme for the conventional MoM is not stable, especially for the nearly-resonant open cylinders. In addition, due to the capacity limitation of computers, this method is less desirable for electrically large scatterers.

High frequency methods:

The high frequency methods are based on the assumption that the electromagnetic fields act like optical rays. They play an important part in developing solution for problems in the quasi-optical regime (*i.e.*, when the wavelength is much smaller than the dimension of the structures). The Geometrical Optics (GO) and the Physical Optics (PO) are two classical examples from this group.

The classical GO uses the ray concepts to approximate the propagation of electromagnetic fields, ignoring the wave effects. Its correction in [36, 37, 47] describes the fields by the leading term of the Luneburg-Kline asymptotic series expansion. Contrasting to the GO, the PO is a wave optical approach. Under the PO, the scatterer is replaced by a set of equivalent electric and magnetic surface currents on the surface, where the surface currents are often approximated by the GO. Via the radiation integral of the surface currents over the surface, the diffracted fields are subsequently found.

The main weakness of this group is the neglect of the finiteness of wavelength. For the open cylinders considered, this disregard may lead to the case where the fields are trapped inside the structures and hence provide a poor estimate of true solution. The GO method provides an approximation to the dominant part of the diffracted field only along the direction of reflection (if that direction is not near the caustics[2]). In addition, the GO fails near the sharp edges as well as in the shadow region, even with the improvement by including additional terms of the Luneburg-Kline series. On the other hand, although the PO ameliorates the problems encountered by the GO near the caustics, it fails to model the dependence of the diffraction on polarization.

[2]A caustic refers to the cross-sectional area where all the rays pass.

The PO is also inaccurate in bistatic scattering direction away from the direction of reflection, when the GO is used to approximate the surface currents.

Semi-analytical methods:

It is these limitations of the purely-numerical methods and the high frequency methods that motivate the development of the final group of solution methods — the semi-analytical methods. The semi-analytical methods include the Tikhonov regularization and the Method of Regularization (MoR) — which sometimes referred to as the Analytical Regularization Method (ARM) or Method of Analytical Regularization (MAR). Although using different means and steps, the key idea of all these semi-analytical methods lies in converting the ill-posed, first kind equation of the form (1.1) to a well-conditioned, second kind Fredholm equation of the form

$$(\mathcal{I} + \mathcal{H})\,\mathbf{x} = \mathbf{b}\,, \tag{1.2}$$

where $\mathcal{I}$ is the identity operator, and $\mathcal{H}$ is a compact operator in the Hilbert space ℓ_2. The benefit of this second kind system is that it is well-conditioned and has a numerically stable, converging computational scheme simply implemented by truncating the infinite system to a finite one. By increasing the truncation number, any desired accuracy of the computed solution can be reached.

The Tikhonov regularization [74, 75] was proposed to find a stable solution to (1.1), by seeking the solution $\mathbf{x}$ that minimizes

$$||\mathcal{A}\mathbf{x} - \mathbf{b}||^2 + \alpha||\mathcal{B}\mathbf{x}||^2\,, \tag{1.3}$$

where $\alpha > 0$ is called the regularization parameter and $\mathcal{B}$ is some suitably chosen bounded operator (*e.g.*, the identity operator). It is worth noting that the operator $(\mathcal{A}^*\mathcal{A} + \alpha\mathcal{B}^*\mathcal{B})$ is a self-adjoint, bounded and invertible operator[3]. For any $\alpha > 0$, the regularized problem is well-posed. An explicit form of the solution is given by

$$\mathbf{x} = (\mathcal{A}^*\mathcal{A} + \alpha\mathcal{B}^*\mathcal{B})^{-1}\,\mathcal{A}^*\mathbf{b}\,. \tag{1.4}$$

It is clear that the approximated solution depend on the choice of α and $\mathcal{B}$ [74, 75]. In general, α is chosen to be as close to 0 as possible, so that the regularized problem is consistent with the original problem, with a good condition number (that of $\mathcal{A}^*\mathcal{A} + \alpha\mathcal{B}^*\mathcal{B}$). In many cases, $\mathcal{B}$ is chosen as the identity operator and α as 1.

[3]Here, * indicates complex conjugation.

Even though the theoretical scheme of the MoR can be found in many functional analysis textbooks [42], the practical implementation of the scheme is not straightforward. Many different treatments have been developed over the years to regularize a set of ill-conditioned dual series or dual integral equations. The older publications of these treatments include the definition-extension method [90] and the multiplying factor method [55]. One popular example of the MoR is the dual series approach based on the Riemann-Hilbert problem of complex analysis. It was first formally documented by Shestopalov *et al* in [41, 66] and popularized in the western area by Ziolkowski *et al* in [32, 96, 97, 98]. Since then, the method has been extended to the study of various 3D and 2D structures, *e.g.*, in [59]. In [79, 80], Tuchkin proposed a method to transform the singular kernel of the original integral equation (*e.g.*, EFIE) to an infinite set of decoupled integral equations, which are eventually transformed to a second kind system of equations by constructing a pair of two-sided regularizator. The MoR has been successfully applied to solve many mixed boundary value scattering and potential problems, such as those involving punctured/slotted spherical, spheroidal and toroidal shells in [84, 85]. Detailed review and survey of some recent work of the MoR can be found in [56, 59, 84].

These methods are uniformly valid for analysis in a broad frequency band, including not only the Rayleigh regime ($\lambda \gg R$) and the resonance regime ($\lambda \approx R$), but also the quasi-optical regime ($\lambda \ll R$). They offer a way to obtain reliable solutions to the benchmark problems of more complex problems and provide a means to check for the validity of other numerical methods. Apart from the crucial advantages coming from a second kind equation, these semi-analytical methods also have a similar advantage to that of the boundary integral equation method; *i.e.*, they avoid the discretization of an infinite domain by expanding the fields as a series of special analytic solutions of the governing equation and solving these coefficients in a linear system.

1.3 Outline of the thesis

This thesis structurally consists of seven parts and is organized in the following manner:

The introductory Chapter 1 consists of an overall description for the electromagnetic problems under study, a short survey of solution methods for the MBVP encountered, as well as a sketch of the thesis structure.

The aim of Chapter 2 is to allow us to establish the terminology and notations that will be used in this thesis. The mathematical framework of electromagnetism

is introduced, particularly when the structures under consideration are infinitely-long cylinders. The expressions for some of the physical quantities of interest that are subsequently employed in the numerical analysis (*e.g.*, energy distribution, RCS, normalized relative error and surface current densities) are also presented.

In Chapter 3, the MoR approach (documented in Section 2.2 of [84]) to transform a set of ill-posed DSE involving the trigonometric functions to a well-conditioned second kind equation is formulated for the sake of completeness of the thesis. In addition, more thorough justifications of the steps of the regularization process are presented.

We study the diffraction problem of an oblique incident plane wave impinging on a cylindrical lens reflector (CLR) in Chapter 4. As opposed to the 2D normal incident problems, the E- and H-polarizations in this 3D oblique incident problem are mixed and exist simultaneously. The effect of incident angle on the scattering behavior is studied numerically by considering the RCS and energy distribution.

Analysis and comparison of the performance of a CLR versus a cylindrical Luneburg lens reflector (CLLR) is carried out in Chapter 5. The energy distribution of a constant-K lens is studied for proper placement of the reflecting PEC cylindrical strip of the CLR. Here, we use the term constant-K lens to refer to the homogeneous dielectric cylinder with constant K (an alternative symbol for the relative permittivity, ϵ_r). Special attention is paid to the RCS calculations when the incidence angle varies from normal incidence to so-called grazing incidence. Because of similar underlying physical principles, these studies are also useful for the 3D version of the spherical lens reflector.

Chapter 6 focusses on the mutual interaction of the scattering from an array of CLR under normal incidence. Suppose a finite number of parallel CLR of different geometry and physical parameters (*e.g.*, radius, PEC strip size, dielectric constant and center of cylinder) are located in the near region of one another. Due to the close proximity to one another, mutual interaction of these CLR under the a plane wave incidence is significant, which therefore has to be taken into account in the problem formulation. We consider the multi-body scattering problem of this finite array by a TM_z normally incident plane wave.

The oblique plane wave scattering problem of a braided cylindrical shield is considered in Chapter 7. The scatterer under consideration is a dielectric cylinder with multiple conformal PEC strips attached. The PEC strips are placed periodically on the surface of the inner dielectric cylinder and are taken to be the same width.

In Chapter 8, the MBVP associated with a shielded, inhomogeneous transmission line is formulated in terms of a rigorous hybrid electromagnetic mode (HEM) representation. We consider a shielded transmission line consisting of an inner coaxial cylinder with multiple PEC strip lines, the structure of which bears great similarity to that of the scatterer considered in Chapter 6. The resulting DSE are transformed, via the application of the MoR in the spectral domain, to yield a characteristic equation for the dispersion properties of the transmission line. The cutoff frequency of the HEM is computed by finding the zeros of the determinant of the block matrix obtained from the MoR approach.

Lastly, in Chapter 9, the main conclusions and observations are drawn of the work that is reported in this thesis. Related future considerations and development are also summarized here.

Chapter 2

Mathematical formulations

Some basic concepts and equations of electromagnetic theory used are briefly reviewed in this chapter. Whilst the material is purely expository, it allows us to establish terminology and notations that will be subsequently used. The series representations for general field components and classical incident waves are formulated. Definitions and expressions for some of the electrical and numerical quantities of interest are also included.

2.1 Maxwell's equations and the constitutive relations

The behavior of electromagnetic fields is governed by the Maxwell's equations and the medium dependent constitutive relations. The time domain[1] Maxwell's equations in the differential form are

$$\nabla \times \mathtt{E}(\mathbf{r},t) = -\frac{\partial}{\partial t}\mathtt{B}(\mathbf{r},t)\,, \tag{2.1a}$$

$$\nabla \times \mathtt{H}(\mathbf{r},t) = \frac{\partial}{\partial t}\mathtt{D}(\mathbf{r},t) + \mathtt{J}(\mathbf{r},t)\,, \tag{2.1b}$$

$$\nabla \cdot \mathtt{D}(\mathbf{r},t) = \rho(\mathbf{r},t)\,, \tag{2.1c}$$

$$\nabla \cdot \mathtt{B}(\mathbf{r},t) = 0\,, \tag{2.1d}$$

where E and H are the electric and magnetic field intensities (in volt/meter and ampere/meter, respectively), D and B are the electric and magnetic flux densities (in coulomb/meter^2 and weber/meter^2, respectively), J is the electric current density (in ampere/meter^2), ρ is the volume charge density (in coulomb/meter^3), and $(\mathbf{r},t)$ denotes an arbitrary point of position $\mathbf{r}$ and time t.

[1]The teletype fonts are used to represent the time varying (vector) functions.

The fields are assumed to be finite, single-valued as well as continuous with continuous derivatives in both time and space excluding the scattering structure (particularly any edges of the scatterer). It may be noted that (2.1b) and (2.1c) may be combined to give the continuity equation, which connects the current and charge densities,

$$\nabla \cdot \mathtt{J}(\mathbf{r}, t) + \frac{\partial}{\partial t}\rho(\mathbf{r}, t) = 0\,. \tag{2.2}$$

The constitutive relations supplementing the Maxwell's equations describe the macroscopic properties of the medium being considered. They give a relation between the quantities $\{\mathtt{D}, \mathtt{B}, \mathtt{J}\}$ and $\{\mathtt{E}, \mathtt{H}\}$. For a linear, homogeneous and non-dispersive medium,

$$\mathtt{D}(\mathbf{r}, t) = \epsilon\, \mathtt{E}(\mathbf{r}, t)\,, \tag{2.3a}$$

$$\mathtt{B}(\mathbf{r}, t) = \mu\, \mathtt{H}(\mathbf{r}, t)\,, \tag{2.3b}$$

$$\mathtt{J}(\mathbf{r}, t) = \sigma\, \mathtt{E}(\mathbf{r}, t)\,, \tag{2.3c}$$

where the scalars ϵ, μ and σ are the permittivity, permeability and conductivity of the medium (in farad/meter, henrie/meter and mho/meter, respectively).

In the frequency domain, the time variation for all fields can be represented by $e^{j\omega t}$. A time varying function can be reconstructed from its Fourier transform by explicitly evaluating the integral (2.4a), which acts as the inverse Fourier transformation[2].

$$\mathtt{F}\,(\mathbf{r}, t) = \frac{1}{2\pi}\int_{-\infty}^{\infty} \mathbf{F}\,(\mathbf{r}, \omega)\, e^{j\omega t} \mathrm{d}\omega\,, \tag{2.4a}$$

where ω is the sinusoidal frequency. The unknown $\mathbf{F}$ is the Fourier transform of $\mathtt{F}$ in the frequency domain. It is defined by the direct transformation

$$\mathbf{F}\,(\mathbf{r}, \omega) = \int_{-\infty}^{\infty} \mathtt{F}\,(\mathbf{r}, t)\, e^{-j\omega t} \mathrm{d}t\,. \tag{2.4b}$$

All the electromagnetic fields having sinusoidal time variation can be related to their corresponding time-varying fields by

$$\mathtt{F}\,(\mathbf{r}, t) = \mathrm{Re}\left[\mathbf{F}\,(\mathbf{r}, \omega)\, e^{j\omega t}\right].$$

The time dependence $e^{j\omega t}$ common to all the time-harmonic field is omitted throughout this thesis. It is worth noting that as any transient electromagnetic field is

[2]The conventional bold fonts in mathematical mode are used to represent the (vector) functions in the frequency domain.

bounded in value, the Fourier transformation exists for all $\omega \in \mathbb{C}$, provided that $\mathrm{Im}(\omega) < 0$ [52]. The Fourier transform at real values of ω are obtained by letting $\mathrm{Im}(\omega) \to 0$.

The Maxwell's equations in frequency domain read

$$\nabla \times \mathbf{E}(\mathbf{r}, \omega) = -j\omega\mu\mathbf{H}(\mathbf{r}, \omega)\,, \tag{2.5a}$$

$$\nabla \times \mathbf{H}(\mathbf{r}, \omega) = j\omega\epsilon\mathbf{E}(\mathbf{r}, \omega) + \mathbf{J}(\mathbf{r}, \omega)\,, \tag{2.5b}$$

$$\nabla \cdot \mathbf{D}(\mathbf{r}, \omega) = \hat{\rho}(\mathbf{r}, \omega)\,, \tag{2.5c}$$

$$\nabla \cdot \mathbf{B}(\mathbf{r}, \omega) = 0\,, \tag{2.5d}$$

where $\hat{\rho}(\mathbf{r}, \omega)$ denotes the transform of the transient volume charge density $\rho(\mathbf{r}, t)$ in the frequency domain.

2.2 Conditions for existence and uniqueness of solution

Maxwell's equations, which completely specify the electromagnetic fields over time in a continuous medium, are common to every electromagnetic problem. To ensure that the solution exists and is unique, a complete description of an electromagnetic problem should also include information about the domain. These conditions include the boundary conditions specified along the geometrical configuration of the problem, the Sommerfeld radiation condition in the case when the medium extends to infinity, and the Meixner finite energy condition in the case of scatterers with edges. A proof of solution uniqueness upon the enforcement of these boundary conditions is given in Chapter 9 of [33].

2.2.1 Boundary conditions

Consider a closed smooth surface Ω separating two different homogeneous media with parameters $(\epsilon_1, \mu_1, \sigma_1)$ and $(\epsilon_2, \mu_2, \sigma_2)$. The fields in regions 1 and 2 are denoted by $(\mathbf{E}_1, \mathbf{H}_1)$ and $(\mathbf{E}_2, \mathbf{H}_2)$, respectively. The boundary conditions at Ω can be derived from the integral form of Maxwell's equations as

$$\mathbf{n} \times (\mathbf{E}_2 - \mathbf{E}_1) = 0\,, \tag{2.6a}$$

$$\mathbf{n} \times (\mathbf{H}_2 - \mathbf{H}_1) = -\mathbf{J}_S\,, \tag{2.6b}$$

$$\mathbf{n} \cdot (\epsilon_2\mathbf{E}_2 - \epsilon_1\mathbf{E}_1) = -\rho_S\,, \tag{2.6c}$$

$$\mathbf{n} \cdot (\mu_2\mathbf{H}_2 - \mu_1\mathbf{H}_1) = 0\,, \tag{2.6d}$$

where $\mathbf{n}$ is a (unit) normal vector pointing from medium 2 into medium 1, $\mathbf{J}_S$ is the electric surface current density on the boundary and ρ_S is the electric surface charge density on the boundary.

(2.6a) and (2.6d) state that the tangential components of electric field and the normal components of magnetic flux density are continuous at all points, including points on Ω for which the physical quantities (ϵ, μ) may change discontinuously. At the interface Ω, (2.6b) states that the discontinuity of the tangential components of magnetic field equals the surface current density; while (2.6c) states that the normal components of magnetic flux density exhibit a jump discontinuity of size ρ_S.

These four boundary conditions are not independent when solving for an electromagnetic problem. By enforcing that the fields satisfy the Maxwell's equations as well as the first two boundary conditions (2.6a) and (2.6b), it is automatically ensured that the normal components of the corresponding flux densities satisfy the remaining pair (2.6c) and (2.6d). Therefore, only (2.6a) and (2.6b) are needed [6].

When there is no current nor charge on the surface Ω (*i.e.*, $\mathbf{J}_S$ and ρ_S are absent), the tangential components of the magnetic fields are continuous across Ω; *i.e.*, (2.6b) becomes

$$\mathbf{n} \times \mathbf{H}_1 = \mathbf{n} \times \mathbf{H}_2 \,. \tag{2.7}$$

In most cases, transmission lines and scatterers are made from highly conducting materials such as brass or copper and it is valid to assume that the conductors are perfect (ideal with infinite conductivity). If the surface Ω enclosing the interior region 2 is a perfect electric conductor, the electric and magnetic fields vanish in the impenetrable region 2, *i.e.*, $\mathbf{E}_2 = 0 = \mathbf{H}_2$. The boundary conditions (2.6a) and (2.6b) simplify to

$$\mathbf{n} \times \mathbf{E}_1 = 0 \,, \tag{2.8a}$$

$$\mathbf{n} \times \mathbf{H}_1 = \mathbf{J}_S \,. \tag{2.8b}$$

If there is an aperture in the perfectly electric conducting (PEC) surface Ω, mixed boundary conditions (MBC) are required. We denote the aperture surface as Ω_0, and the remaining PEC portion as Ω_1, where $\Omega = \Omega_0 \cup \Omega_1$, as depicted in Figure 2.1. Besides the continuity conditions given by (2.6a) which applies over the total surface Ω, the MBC on Ω are

$$\mathbf{n} \times \mathbf{E}_2 = \begin{cases} \mathbf{n} \times \mathbf{E}_1 & , \text{on } \Omega_0 \\ 0 & , \text{on } \Omega_1 \end{cases} \tag{2.9a}$$

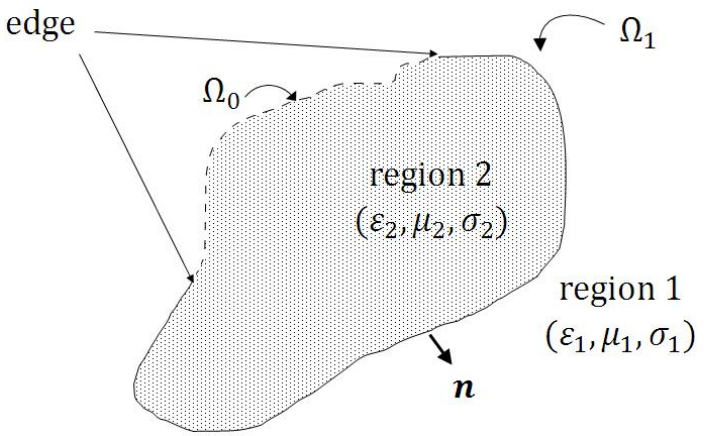

Figure 2.1: Contour Ω comprising discontinuities and sharp edges.

$$\mathbf{n} \times \mathbf{H}_2 = \begin{cases} \mathbf{n} \times \mathbf{H}_1 & , \text{ on } \Omega_0 \\ -\mathbf{J}_S & , \text{ on } \Omega_1 \end{cases} \tag{2.9b}$$

As $\mathbf{J}_S$ is due to the induced field that is yet to be determined, the second half of (2.9b) defined over Ω_1 is redundant.

2.2.2 Radiation condition

Due to the superposition principle, the electric and magnetic fields can be separated with respect to their origin. Consider a general scattering problem involving a source located somewhere in space, and illuminating a particular structure. In the absence of the structure, this source produces the primary fields, the incident fields ($\mathbf{E}^{\text{inc}}$ and $\mathbf{H}^{\text{inc}}$). The secondary fields induced in the presence of the structure are the referred to as the transmitted fields ($\mathbf{E}^{\text{tr}}$ and $\mathbf{H}^{\text{tr}}$) when inside the structure, and as the scattered fields ($\mathbf{E}^{\text{sc}}$ and $\mathbf{H}^{\text{sc}}$) when outside the structure. The total fields ($\mathbf{E}^{\text{tot}}$ and $\mathbf{H}^{\text{tot}}$) in the exterior of the structure is the sum of the incident and scattered fields.

When the outer boundary of the domain recedes to infinity, physics demands that the scattered field acts as an outgoing wave, and vanishes at infinity if the electromagnetic contrast of the structure with respect to the background remains of finite support. These can be summarized by the Sommerfeld radiation condition. For the cylindrical structures considered in this thesis, the Sommerfeld radiation condition is expressed in the polar coordinates (ρ, ϕ, z), where the z-axis is taken to be the cylinder axis. Assuming that the structures are immersed in free space with wave number k_0, and located within a finite distance from the origin, the z-components of

the scattered fields are required to satisfy

$$|\sqrt{\rho}U| < K\,, \tag{2.10a}$$

$$\lim_{\rho\to\infty} \sqrt{\rho}\left(\frac{\partial}{\partial\rho}U + jk_0U\right) = 0\,. \tag{2.10b}$$

In the above equations, U may denote either E_z^{sc} or H_z^{sc}[3], while ρ is the radial distance from the origin, and K is some constant. This is equivalent to enforcing a boundary condition at infinity so that the only incoming waves come from the incident field.

2.2.3 Finite energy condition

For a closed scatterer, the implementation of the boundary conditions and the Sommerfeld radiation condition is adequate to ensure a unique solution to the scattering problem. However, when the structure considered has singular points (*e.g.*, a slotted PEC cylinder), the solutions are not always unique. In particular, it is found that some of the field components become infinite. To guarantee the existence of a unique solution, the order of singularity allowed is such that the energy stored in the vicinity of the diffracting edge is finite. The Meixner finite energy condition [49, 50], which states that the total electromagnetic energy contained in any finite volume V is bounded, can be expressed mathematically as

$$\frac{1}{2}\iiint_V \left\{\epsilon\,|\mathbf{E}|^2 + \mu\,|\mathbf{H}|^2\right\} \mathrm{d}V < \infty\,. \tag{2.11}$$

This condition provides the correct choice of the solution class for the field and its expansion coefficients, when the field is expanded in cylindrical harmonics. It ensures that the field in the volume V containing the edges displays a weaker singularity than that of the real source.

2.3 Wave equations for configurations uniform in z-direction

The cylindrical structures considered in this thesis are uniform in the z-direction. By taking this geometrical property into consideration, the analysis can be made much simpler by expressing all fields in terms of their longitudinal and transverse components. This is done by first separating the longitudinal and transverse components

[3]In this thesis, the scalar functions are represented by the conventional slanted font in mathematical mode.

with respect to the z-axis as follows

$$\mathbf{E}(\mathbf{r}) = \mathbf{E}_t(\mathbf{r}) + \mathbf{i}_z E_z(\mathbf{r}) \,, \tag{2.12}$$

$$\mathbf{H}(\mathbf{r}) = \mathbf{H}_t(\mathbf{r}) + \mathbf{i}_z H_z(\mathbf{r}) \,, \tag{2.13}$$

$$\nabla = \nabla_t + \mathbf{i}_z \frac{\partial}{\partial z} \,, \tag{2.14}$$

where $\mathbf{i}_z$ is the unit vector in the z-direction, the subscript t indicates the component transverse to the z-direction, the subscript z indicates the z-component, and ∇_t is the transverse gradient operator.

Substitution of above expressions into (2.5a) leads to

$$\left(\nabla_t + \mathbf{i}_z \frac{\partial}{\partial z}\right) \times (\mathbf{E}_t + \mathbf{i}_z E_z) = -j\omega\mu \left(\mathbf{H}_t + \mathbf{i}_z H_z\right) \,. \tag{2.15}$$

By using the identities $\nabla_t \cdot \mathbf{i}_z = 0$, $\mathbf{i}_z \cdot \mathbf{E}_t = \mathbf{i}_z \cdot \mathbf{H}_t = 0$ and (A.1), the operation "$\mathbf{i}_z \cdot$" on (2.15) gives an expression for the longitudinal part of the magnetic field in (2.16). On the other hand, by using (A.2), the transverse part is obtained in (2.17), by using the operation "$\mathbf{i}_z \times \mathbf{i}_z \times$" on (2.15).

$$-j\omega\mu H_z = \mathbf{i}_z \cdot (\nabla_t \times \mathbf{E}_t) \,, \tag{2.16}$$

$$-j\omega\mu \mathbf{H}_t = \nabla_t \times (\mathbf{i}_z \, E_z) + \mathbf{i}_z \times \left(\frac{\partial}{\partial z} \mathbf{E}_t\right) \,. \tag{2.17}$$

Using the same arguments, the longitudinal and transverse parts of the electric fields can be obtained from (2.5b) as

$$j\omega\epsilon E_z = \mathbf{i}_z \cdot (\nabla_t \times \mathbf{H}_t) \,, \tag{2.18}$$

$$j\omega\epsilon \mathbf{E}_t = \nabla_t \times (\mathbf{i}_z \, H_z) + \mathbf{i}_z \times \left(\frac{\partial}{\partial z} \mathbf{H}_t\right) \,. \tag{2.19}$$

Therefore, the following two expressions of $\mathbf{E}_t$ and $\mathbf{H}_t$ in terms of E_z and H_z are derived from (2.16)–(2.19),

$$\left(\frac{\partial^2}{\partial z^2} + k^2\right) \mathbf{E}_t = j\omega\mu \left(\mathbf{i}_z \times \nabla_t H_z\right) + \frac{\partial}{\partial z} \nabla_t E_z \,, \tag{2.20a}$$

$$\left(\frac{\partial^2}{\partial z^2} + k^2\right) \mathbf{H}_t = -j\omega\epsilon \left(\mathbf{i}_z \times \nabla_t E_z\right) + \frac{\partial}{\partial z} \nabla_t H_z \,, \tag{2.20b}$$

where $k = \omega\sqrt{\epsilon\mu} = 2\pi/\lambda$ (in radian/meter) is the wavenumber of the electromagnetic field in the medium, with λ (in meter) being the wavelength of the field. This points out that all components of electromagnetic fields can be readily calculated once the

values of the scalar functions E_z and H_z are known. The following section concentrates on deriving the scalar wave equations for E_z and H_z.

In regions where μ is independent of x and y, the operation "$\nabla_t \times$" on (2.17), with the aid of (A.4), gives

$$-j\omega\mu\left(\nabla_t \times \mathbf{H}_t\right) = -\nabla_t^2\left(\mathbf{i}_z\, E_z\right) + \mathbf{i}_z \frac{\partial}{\partial z}\left(\nabla_t \cdot \mathbf{E}_t\right) . \tag{2.21}$$

In regions where μ is independent of x and y, taking the transverse divergence of (2.19), and making use of (A.3) gives

$$j\omega\epsilon\left(\nabla_t \cdot \mathbf{E}_t\right) = -\frac{\partial}{\partial z}\left[\mathbf{i}_z \cdot \left(\nabla_t \times \mathbf{H}_t\right)\right] , \tag{2.22}$$

which when combined with (2.18) becomes

$$\nabla_t \cdot \mathbf{E}_t = -\frac{\partial}{\partial z} E_z \, . \tag{2.23}$$

We obtain the scalar wave equation for E_z by substitution of (2.23) and (2.18) into (2.21):

$$\left(\nabla_t^2 + \frac{\partial^2}{\partial z^2} + k^2\right) E_z = 0 \, . \tag{2.24a}$$

With similar arguments and steps on (2.16), (2.17) and (2.19), the scalar wave equation can be obtained for H_z as

$$\left(\nabla_t^2 + \frac{\partial^2}{\partial z^2} + k^2\right) H_z = 0 \, . \tag{2.24b}$$

2.4 General field expressions for circular cylinder

In this section, the method of separation of variables is employed to find a series representation of the solution to the scalar wave equations given in (2.24). When the structure involved is closed, an exact solution (Mie series) can be derived for the problem, by exploiting the orthogonality of the kernel functions [9]. However, separation of variables method has strict restrictions on the boundary conditions defining the problem, making it not applicable to an open problem (which has MBC). Nevertheless, it is this approach that MoR depends on in formulating the set of DSE.

With U denoting either of E_z and H_z, the scalar wave equations in (2.24) in polar cylindrical coordinates (ρ, ϕ, z) read

$$\left[\frac{1}{\rho}\frac{\partial}{\partial \rho}\left(\rho \frac{\partial}{\partial \rho}\right) + \frac{1}{\rho^2}\frac{\partial^2}{\partial \phi^2} + \frac{\partial^2}{\partial z^2} + k^2\right] U(\rho, \phi, z) = 0 \, . \tag{2.25}$$

The solutions of the form $U(\rho, \phi, z) = P(\rho)Q(\phi)Z(z)$ are sought, using separation of variables method. By substitution of this separable solution into (2.25), the Helmholtz equation decouples into the following ordinary differential equations (ODE)

$$\frac{\mathrm{d}^2 Z}{\mathrm{d}z^2} + k_z^2 Z = 0\,, \tag{2.26}$$

$$\frac{\mathrm{d}^2 Q}{\mathrm{d}\phi^2} + n^2 Q = 0\,, \tag{2.27}$$

$$\frac{\rho}{P}\frac{\mathrm{d}}{\mathrm{d}\rho}\left(\rho\frac{\mathrm{d}P}{\mathrm{d}\rho}\right) - n^2 + \left(k^2 - k_z^2\right)\rho^2 = 0\,, \tag{2.28}$$

where k_z and n are separation constants. It is worth noting that k_z is termed the propagation constant in the z-direction (or the longitudinal wavenumber).

The ODE for variable z is harmonic, and its commonly-used solutions are $e^{jk_z z}$, $e^{-jk_z z}$, $\sin(k_z z)$ and $\cos(k_z z)$. With respect to the time dependence $e^{j\omega t}$, both $\sin(k_z z)$ and $\cos(k_z z)$ represent standing waves. When k_z is real-valued, $e^{jk_z z}$ and $e^{-jk_z z}$ represent waves traveling in the negative- and positive-z direction, respectively. When k_z is purely-imaginary, $e^{\pm jk_z z}$ represents evanescent waves, as $z \to \pm\infty$. For complex valued k_z, $e^{jk_z z}$ and $e^{-jk_z z}$ represent attenuated-traveling waves. To simplify the notation, we assume that the source is located such that the waves are traveling only in the negative-z direction, thus involving only $e^{jk_z z}$.

The ODE for variable ϕ is also harmonic. In addition, ϕ is an angle coordinate, and only solutions in the full azimuthal domain $-\pi \leq \phi \leq \pi$ are considered. As the electromagnetic fields are single-valued, the requirement of $Q(-\pi) = Q(\pi)$ leads to n taking on integer values only.

For propagating waves $k^2 \neq k_z^2$, k_ρ is introduced to denote $k_\rho^2 = k^2 - k_z^2$. It is worth noting that k_ρ is the propagation constant in the ρ-direction (or termed the transverse wavenumber). The ODE for variable ρ is essentially Bessel's equation of order n and argument $k_\rho\rho$

$$(k_\rho\rho)^2\frac{\mathrm{d}^2 P}{\mathrm{d}(k_\rho\rho)^2} + (k_\rho\rho)\frac{\mathrm{d}P}{\mathrm{d}(k_\rho\rho)} + \left[(k_\rho\rho)^2 - n^2\right]P = 0\,. \tag{2.29}$$

Any two of the Bessel function $J_n(k_\rho\rho)$, Neumann function $Y_n(k_\rho\rho)$, the Hankel functions of the first and second kind $H_n^{(1)}(k_\rho\rho)$, $H_n^{(2)}(k_\rho\rho)$ form a pair of linearly-independent solutions to the equation. The characteristics of these functions are documented in the Appendix B.2.1. From the definitions given in (B.10)–(B.13), only $J_n(k_\rho\rho)$ is bounded as $\rho \to 0$. Due to the boundedness of electromagnetic fields, the radial function $P(\rho)$ can contain only $J_n(k_\rho\rho)$, when the origin is included in the domain. On the other hand, from the asymptotic behaviors of the functions when

$\rho \to \infty$ given in (B.18)–(B.21), $H_n^{(2)}(k_\rho \rho)$ is the only function that represents outgoing and vanishing waves, for the choice of time variation $e^{j\omega t}$. In compliance with the Sommerfeld radiation condition (2.10), $P(\rho)$ contains only $H_n^{(2)}(k_\rho \rho)$, if the domain considered is unbounded.

As a result of the choice of solutions to each of the ODE, an elementary wave function traveling in the negative z-direction, and satisfying (2.25) is

$$U_{k_z,n,k_\rho} = e^{jk_z z} \left\{ \begin{array}{c} J_n(k_\rho \rho) \\ H_n^{(2)}(k_\rho \rho) \end{array} \right\} e^{jn\phi}, \text{ for the } \left\{ \begin{array}{c} \text{“interior”} \\ \text{“exterior”} \end{array} \right\} \text{problem} \tag{2.30}$$

for some fixed values of k_z and n. Due to the superposition principle, the summation of all the elementary wave functions gives a general solution to (2.25). Thus, the z-component of a electric or magnetic field has the following expansion:

$$U(\rho, \phi, z) = e^{jk_z z} \sum_{n=-\infty}^{\infty} \left[a_n H_n^{(2)}(k_\rho \rho) + b_n J_n(k_\rho \rho) \right] e^{jn\phi}, \tag{2.31}$$

where $\{a_n\}_{n=-\infty}^{\infty}$ and $\{b_n\}_{n=-\infty}^{\infty}$ are unknown coefficients to be determined from boundary conditions, with $\{a_n\}_{n=-\infty}^{\infty} \equiv 0$ for domains including the origin, and $\{b_n\}_{n=-\infty}^{\infty} \equiv 0$ for unbounded domains.

For the special case when $k^2 = k_z^2$, the Helmholtz equation (2.25) becomes the Laplace equation encountered in the transverse electromagnetic mode (TEM) in transmission line problem. The corresponding radial solutions for (2.28) are ρ^n and ρ^{-n}, for positive integer n. For $n = 0$, the radial solutions are simply 1 and $\ln \rho$. Therefore, a general solution to (2.25), when $k^2 = k_z^2$, has the expression

$$u(\rho, \phi, k_z) = e^{jk_z z} \left\{ a_0 \ln(\rho) + b_0 + \sum_{n=1}^{\infty} \left[a_n \rho^{-n} + b_n \rho^n \right] \cos n\phi \right\}. \tag{2.32}$$

Similarly, as electromagnetic fields are finite, and satisfy the Sommerfeld radiation condition, a_0 and $\{a_n\}_{n=1}^{\infty}$ and a_0 vanish for domains including the origin, while $b_0, \{b_n\}_{n=1}^{\infty} \equiv 0$ for unbounded domains.

The expressions for all other field components can be obtained from (2.20a) and (2.20b) upon setting $\frac{\partial}{\partial z} \equiv jk_z$ as

$$\left\{ \begin{array}{c} E_\rho \\ H_\rho \end{array} \right\} = \frac{j\omega}{k_\rho^2 \rho} \frac{\partial}{\partial \phi} \left\{ \begin{array}{c} -\mu H_z \\ \epsilon E_z \end{array} \right\} + \frac{jk_z}{k_\rho^2} \frac{\partial}{\partial \rho} \left\{ \begin{array}{c} E_z \\ H_z \end{array} \right\}, \tag{2.33a}$$

$$\left\{ \begin{array}{c} E_\phi \\ H_\phi \end{array} \right\} = -\frac{j\omega}{k_\rho^2} \frac{\partial}{\partial \rho} \left\{ \begin{array}{c} -\mu H_z \\ \epsilon E_z \end{array} \right\} + \frac{jk_z}{k_\rho^2 \rho} \frac{\partial}{\partial \phi} \left\{ \begin{array}{c} E_z \\ H_z \end{array} \right\}. \tag{2.33b}$$

2.5 Plane wave

A plane wave consists of the electric and magnetic fields of uniform phase over a set of infinite parallel planes (called the equiphase surfaces) that are perpendicular to the direction of propagation. For a uniform plane wave, the fields are of constant amplitude over the equiphase surfaces. The electric and magnetic fields of a plane wave are orthogonal to each other. For a linearly-polarized plane wave, the fields always point to the same direction in space. The source of a plane wave is considered to be at infinity to produce such planar equiphase surfaces. Plane waves are the type of electromagnetic waves that predominate at each fixed observation point in the far zone of an antenna.

Suppose a uniform plane wave propagates in the direction of a unit vector $\mathbf{w}$, in the free space with intrinsic impedance $\eta_0 = \sqrt{\mu_0/\epsilon_0} \approx 120\pi$ (ohm), and wavenumber $k_0 = \omega\sqrt{\epsilon_0\mu_0} = 2\pi/\lambda$. Here, $\epsilon_0 \approx \pi/36 \times 10^{-9}$ (farad/meter), and $\mu_0 = 4\pi \times 10^{-7}$ (henry/meter) are the permittivity and permeability of vacuum, respectively; whereas ω and λ are the frequency and wavelength of the radiation, respectively. It can be expressed mathematically as

$$\mathbf{E}^{\text{pw}} = A_0 e^{-jk_0\mathbf{w}\cdot\mathbf{r}}\,\mathbf{v}\,, \tag{2.34a}$$

$$\mathbf{H}^{\text{pw}} = \frac{A_0}{\eta_0} e^{-jk_0\mathbf{w}\cdot\mathbf{r}}\,(\mathbf{w}\times\mathbf{v})\,, \tag{2.34b}$$

where the constant A_0 is the amplitude of the uniform plane wave, $\mathbf{v}$ is a unit vector on the equiphase surfaces indicating the direction the electric field points to, and $\mathbf{r} = (x, y, z)$ is the arbitrary position vector. As the equiphase surfaces are perpendicular to the direction of propagation, $\mathbf{v}\cdot\mathbf{w} = 0$.

Consider a uniform plane wave which direction of propagation $\mathbf{w}$ is completely defined by the polar angle θ_z^{pw} and the azimuthal angle θ_x^{pw}, as shown in Figure 2.2. That is, $\mathbf{w} = (-\cos\theta_x^{\text{pw}}\sin\theta_z^{\text{pw}}, -\sin\theta_x^{\text{pw}}\sin\theta_z^{\text{pw}}, -\cos\theta_z^{\text{pw}})$ in Cartesian coordinates. Here, the polar angle θ_z^{pw} is the angle the propagation direction $\mathbf{w}$ makes with the $z-$axis, while the azimuthal angle θ_x^{pw} is the angle between incidence of the plane wave in the xy-plane and the positive x-axis. The electric field of the plane wave may be either parallel (TM_z) or orthogonal (TE_z) to the plane of incidence[4].

TM_z case (i.e., $H_z^{\text{pw}} = 0$) :

From the definition of magnetic field given in (2.34b), and the condition $\mathbf{v}\cdot\mathbf{w} = 0$, we have $\mathbf{v}_{\text{TM}} = (-\cos\theta_x^{\text{pw}}\cos\theta_z^{\text{pw}}, -\sin\theta_x^{\text{pw}}\cos\theta_z^{\text{pw}}, \sin\theta_z^{\text{pw}})$. Due to the geometry

[4]The plane containing the direction of propagation $\mathbf{w}$ and the cylinder axis, the z-axis.

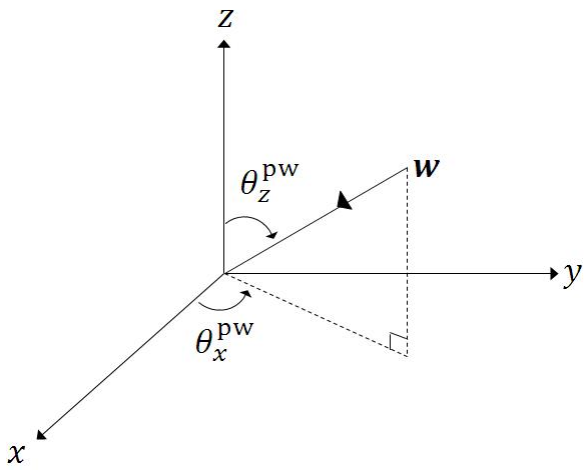

Figure 2.2: Direction of propagation of a plane wave.

of the structure, it is desirable to express the plane wave in the polar cylindrical coordinates, where $x = \rho\cos\phi$ and $y = \rho\sin\phi$. From (2.34a), we get

$$E_z^{\mathrm{pw}}(\rho,\phi,z) = A_0 \sin\theta_z^{\mathrm{pw}} e^{jk_0 z\cos\theta_z^{\mathrm{pw}}} e^{jk_0\rho\sin\theta_z^{\mathrm{pw}}\cos(\phi-\theta_x^{\mathrm{pw}})}\,, \tag{2.35a}$$

$$= A_0 \sin\theta_z^{\mathrm{pw}} e^{jk_0 z\cos\theta_z^{\mathrm{pw}}} \sum_{n=-\infty}^{\infty} j^n J_n(k_0\rho\sin\theta_z^{\mathrm{pw}}) e^{jn(\phi-\theta_x^{\mathrm{pw}})}\,, \tag{2.35b}$$

where the series expansions is obtained using (B.27).

The series expansion for other components of the TM_z plane wave can be derived from (2.34a) and (2.34b), with the help of (A.5), (B.16) and (B.15). Alternatively and more straightforwardly, they can also be obtained using (2.33) with $k_z = k_0\cos\theta_z^{\mathrm{pw}}$ (and thus, $k_\rho = k_0\sin\theta_z^{\mathrm{pw}}$).

When the special case of normal incidence (*i.e.*, $\theta_z^{\mathrm{pw}} = \frac{\pi}{2}$) is considered, the problem reduces to 2D as $k_z = 0$. Only the components E_z^{pw}, H_ρ^{pw} and H_ϕ^{pw} are non-zero for this special case.

TE_z case (i.e., $E_z^{\mathrm{pw}} = 0$):

In this case, we have $\mathbf{v}_{\mathrm{TE}} = (\sin\theta_x^{\mathrm{pw}}, -\cos\theta_x^{\mathrm{pw}}, 0)$. Clearly, $\mathbf{w}\times\mathbf{v}_{\mathrm{TE}} = \mathbf{v}_{\mathrm{TM}}$ and $\mathbf{w}\times\mathbf{v}_{\mathrm{TM}} = -\mathbf{v}_{\mathrm{TE}}$. Consequently, $\mathbf{E}^{\mathrm{TE}} = -\eta_0\mathbf{H}^{\mathrm{TM}}$ and $\mathbf{H}^{\mathrm{TE}} = \frac{1}{\eta_0}\mathbf{E}^{\mathrm{TM}}$. Thus,

$$H_z^{\mathrm{pw}}(\rho,\phi,z) = \frac{A_0}{\eta_0}\sin\theta_z^{\mathrm{pw}} e^{jk_0 z\cos\theta_z^{\mathrm{pw}}} \sum_{n=-\infty}^{\infty} j^n J_n(k_0\rho\sin\theta_z^{\mathrm{pw}}) e^{jn(\phi-\theta_x^{\mathrm{pw}})}\,. \tag{2.36a}$$

Similarly, for normal incidence problem, only H_z^{pw}, E_ρ^{pw} and E_ϕ^{pw} are non-zero.

2.6 Quantities of interest

2.6.1 Energy density

The energy density w (Joule/meter^3) of an electromagnetic field is simply the sum of the electric and magnetic energy densities

$$w := \frac{1}{2}\left(\epsilon\left|\mathbf{E}\right|^2 + \mu\left|\mathbf{H}\right|^2\right) . \tag{2.37}$$

The integral expression in (2.11) gives the total electromagnetic energy contained in any finite volume V.

2.6.2 Radiation pattern and radar cross section

The radiation pattern $\mathbf{R}(\phi)$ is an alternative representation for the scattered field, valid for observation point in the far zone where $\rho \to \infty$. The large argument approximation for the Hankel function is given in (B.21) while the approximation for its derivative can be deduced to be

$$H_n^{\prime(2)}(\kappa\rho) \approx -\, j\sqrt{\frac{2}{\pi\kappa\rho}}e^{-j\left(\kappa\rho - \frac{2n+1}{4}\pi\right)} , \qquad \text{as } \rho \gg R. \tag{2.38}$$

From these approximations, magnitudes of the scattered fields in free space are approximately

$$\mathbf{U}^{\text{sc}} \approx \mathbf{R}(\phi)\frac{e^{-jk_0\rho}}{\sqrt{\rho}} , \tag{2.39}$$

where $\mathbf{U}$ is either $\mathbf{E}$ or $\mathbf{H}$.

Another important parameter in radar communication study is the radar cross section (RCS) of a scattering structure, $\sigma(\phi)$. It is defined as the area intercepting the amount of power that, when scattered isotropically, produces at the receiver a density that is equal to the density scattered by the actual target [5]. For the cylindrical structures considered, the mathematical expression for RCS is

$$\sigma = \lim_{\rho\to\infty} 2\pi\rho\frac{\left|\mathbf{U}^{\text{sc}}\right|^2}{\left|\mathbf{U}^{\text{inc}}\right|^2} . \tag{2.40}$$

The same value of RCS can be calculated for a scattering problem by using either choice of $\mathbf{E}$ or $\mathbf{H}$ because of (2.33).

Without loss of generality, the incident field is assumed to have amplitude A_0 of one throughout this thesis. The normalized RCS (against the dimension of the scatterer πR), $\hat{\sigma}(\phi)$, can be written in terms of the radiation pattern $\mathbf{R}(\phi)$ as

$$\hat{\sigma}(\phi) = \frac{2}{R}\left|\mathbf{R}(\phi)\right|^2 . \tag{2.41}$$

In particular, the backscattering RCS ($\hat{\sigma}_{\rm b}$) (when $\phi = \theta_x^{\rm pw} + \pi$) indicates the efficiency of the structure in scattering the incident plane wave back to its source. The RCS is depicted in decibel scale in most of the numerical investigations carried out; *i.e.*, $\hat{\sigma}(\text{dB}) = 10 \log_{10} \hat{\sigma}$.

2.6.3 Surface current densities

The surface current density measures the jump in the magnetic field across the contour of the PEC strip. In general, the surface current density flows both parallel and transverse to the cylinder axis on the strip, it can be written as

$$\mathbf{J} = \mathbf{n} \times (\mathbf{H}_1 - \mathbf{H}_2) \ , \tag{2.42}$$

where $\mathbf{n}$ is a unit normal vector pointing from medium 2 into medium 1. For the special case of normal incidence, the surface current density has only the z-component and depends only on the angular variable ϕ.

2.6.4 Relative error

For a numerical solution to be reliable and useful, it is important that the approximated solution derived is indeed close to the exact solution (if exists), as well as being stable. Suppose when the infinite system (derived upon the application of the MoR) is truncated to $N_{\rm tr}$ equations. We denote the computed solution as $\left\{x_n^{N_{\rm tr}}\right\}_{n=1}^{N_{\rm tr}}$. The normalized relative error of the computed coefficients in maximum norm sense, $e_{\max}(N_{\rm tr})$, can be defined mathematically as

$$e_{\max}(N_{\rm tr}) = \frac{\max_{n \le N_{\rm tr}} \left| x_n^{N_{\rm tr}+1} - x_n^{N_{\rm tr}} \right|}{\max_{n \le N_{\rm tr}} |x_n^{N_{\rm tr}}|} \, . \tag{2.43}$$

The relative error of the RCS in ℓ_2-norm sense, $e_{\hat{\sigma}}(N_{\rm tr})$, provides another useful measure of the value of $N_{\rm tr}$ required for a desired accuracy of the physical quantities computed. We denote the normalized RCS value computed based on the coefficients $\left\{x_n^{N_{\rm tr}}\right\}_{n=1}^{N_{\rm tr}}$ as $\hat{\sigma}^{N_{\rm tr}}$. The relative error of the RCS in ℓ_2-norm sense, $e_{\hat{\sigma}}(N_{\rm tr})$, is defined as

$$e_{\hat{\sigma}}(N_{\rm tr}) = \frac{\left| \hat{\sigma}^{N_{\rm tr}+1} - \hat{\sigma}^{N_{\rm tr}} \right|}{|\hat{\sigma}^{N_{\rm tr}}|} \, . \tag{2.44}$$

2.6.5 Condition number

Another useful numerical quantity is the condition number, $\chi(\mathcal{A})$, associating with the matrix operator $\mathcal{A}$. In ℓ_2-norm, $\chi(\mathcal{A})$ is defined as the ratio of the maximal to the minimal singular values of $\mathcal{A}$. It gives an indication of the accuracy of the results from matrix inversion and the linear equation solution. For our purpose, the condition numbers for each considered problem are computed using the built-in MATLAB function, `cond`, directly.

Suppose we have $\chi(\mathcal{A}) = 10^{\alpha}$ for our final system of equations. As a general rule of thumb, $\log_{10}[\chi(\mathcal{A})]$ indicates the number of decimal places lost by computer due to roundoff errors arising from the matrix inversion of $\mathcal{A}$. In other words, with the 16 decimal digits of computer precision, the results computed will be accurate to at most $(16 - \alpha)$ decimal places of accuracy.

Chapter 3

Method of Regularization

3.1 Introduction

Although there is a variety of regularization techniques for electromagnetic problems, this thesis deals exclusively with the Abel integral transformation method. In particular, for the cylindrical problems considered, this thesis deals with the regularization of the DSE involving trigonometric functions documented in Section 2.2 of the monograph [84]. This type of DSE has also been previously reported in [69, 76, 77]. For the sake of completeness of this thesis, the regularization process involved is presented in this chapter. The final solutions are the same as those documented in [84], though different notations are employed. In addition, more thorough justifications of the steps are formulated, and a more compressed process is presented here. This method has been applied to the study of the scattering problem of a slotted cylinder illuminated by a normal incident plane wave in [85]. It is the aim of this thesis to extend the application of this method to consider some of the more generalized problems in subsequent chapters.

The first step of the regularization involves rewriting the DSE (derived from the MBC) in terms of Jacobi polynomials. By rescaling and levelling the convergence rate of them, the DSE are then transformed into a set of Abel integral equations. An ISLAE is subsequently obtained by employing the corresponding inversion formulas. Upon converting the original DSE into a Fredholm matrix equation of the second kind (with the relevant matrix operator being a compact perturbation of the identity operator), the equation is then solved by the truncation method and numerical matrix inversion. The accuracy of the solution computed can be controlled by altering the truncation number N_{tr} of the ISLAE. The most notable feature of this approach is that the solution computed converges not only theoretically, but also numerically to the exact solution of the ISLAE, as $N_{\text{tr}} \to \infty$.

3.2 Dual series equations with kernels $\cos n\phi$

We consider the following DSE involving the cosine functions

$$ax_0 + c + \sum_{n=1}^{\infty} [x_n (1 - s_n) + e_n] \cos n\phi = 0 \qquad (A)\,, \quad \phi \in (0, \phi_0), \tag{3.1a}$$

$$bx_0 + d + \sum_{n=1}^{\infty} n\,[x_n (1 - t_n) + f_n] \cos n\phi = 0 \qquad (A)\,, \quad \phi \in (\phi_0, \pi), \tag{3.1b}$$

where a, b, c and d and $\{e_n, f_n, s_n, t_n\}_{n=1}^{\infty}$ are assumed to be known, while $\{x_n\}_{n=0}^{\infty}$ is the unknown sequence to be determined. Here, ϕ_0 is some fixed value in $(0, \pi)$. The notation (A) implies that each member of the DSE above is to be read as being Abel-summable (see Appendix D.1.2) to the right hand value on its corresponding interval; *i.e.*,

$$ax_0 + c + \lim_{|r|\to 1^-} \left\{ \sum_{n=1}^{\infty} [x_n (1 - s_n) + e_n]\, r^n \cos n\phi \right\} = 0\,, \qquad \phi \in (0, \phi_0), \tag{3.2a}$$

$$bx_0 + d + \lim_{|r|\to 1^-} \left\{ \sum_{n=1}^{\infty} n\,[x_n (1 - t_n) + f_n]\, r^n \cos n\phi \right\} = 0\,, \qquad \phi \in (\phi_0, \pi). \tag{3.2b}$$

For the regularization process, it is assumed that $\{\sqrt{n}x_n\}_{n=0}^{\infty}$ belongs to the set of square-summable Fourier coefficients ℓ_2; *i.e.*,

$$\sum_{n=1}^{\infty} n|x_n|^2 < \infty\,. \tag{3.3}$$

The known sequences $\{\sqrt{n}e_n, \sqrt{n}f_n\}_{n=1}^{\infty}$ are also assumed to belong to the same class, ℓ_2. In other words, $\{x_n, e_n, f_n\}_{n=1}^{\infty}$ are assumed to satisfy the Fejér's Tauberian condition (D.4). Additionally, it is assumed that

$$\lim_{n\to\infty} s_n = \lim_{n\to\infty} t_n = 0\,, \tag{3.4}$$

which is why they are often termed the asymptotically small parameters. In the electromagnetic problems considered, these assumptions arise naturally from the Meixner condition required for a structure with apertures, as well as the general properties of fields in space excluding the scatterer.

From these assumptions, we can see that the general terms of series in (3.1a) and (3.1b) decay at rates $O\left(n^{-3/2}\right)$ and $O\left(n^{-1/2}\right)$, respectively, as $n \to \infty$. In the key step of the regularization process, the slower converging series equation (3.1b) is subjected to an integration operation to equilibrate the rates of convergence of the DSE. These assumptions provide sufficient conditions for the justification for the termwise integration operations, as shown in the next subsection.

3.2.1 Justification of term-by-term integration

Although its convergence is not assumed, this series in (3.1a) is convergent as its terms satisfy (D.4). In fact, the series can be shown by the Weierstrass M Test to be absolutely (and hence, uniformly) convergent for all real-valued ϕ. Therefore, (3.1a) can be integrated termwise over any interval $(0, \phi')$, for some $\phi' \in (0, \pi)$. In addition, the notation (A) is omitted for (3.1a) from here onwards.

However, the slower converging series in (3.1b) are not uniformly convergent for the interval (ϕ_0, π), if convergent at all. While uniformity of convergence is a sufficient condition for term-by-term integrability, it is not a necessary condition.

For brevity, we denote the Abel mean of the series in (3.1b) as

$$\lambda(\phi, r) := \sum_{n=1}^{\infty} n \left[x_n (1 - t_n) + f_n\right] r^n \cos n\phi \,. \tag{3.5}$$

Clearly, $\lambda(\phi, r)$ is absolutely convergent as long as $|r| < 1$, for all $\phi \in (0, \pi)$. Therefore, for $|r| < 1$, $\lambda(\phi, r)$ is integrable term-by-term over the interval (ϕ', π), for some $\phi' \in (\phi_0, \pi)$, to give

$$\int_{\phi'}^{\pi} \lambda(\phi, r) \mathrm{d}\phi = -\sum_{n=1}^{\infty} \left[x_n (1 - t_n) + f_n\right] r^n \sin n\phi' \,. \tag{3.6}$$

We introduce the following sequence from $\lambda(\phi, r)$:

$$\lambda_k(\phi) := \lambda\left(\phi, 1 - \tfrac{1}{k}\right) = \sum_{n=1}^{\infty} n \left[x_n (1 - t_n) + f_n\right] \left(1 - \tfrac{1}{k}\right)^n \cos n\phi \,, \tag{3.7}$$

for $k = 1, 2, \ldots$ From (3.2b), we know

$$\lim_{|r| \to 1^-} \lambda(\phi, r) = -(bx_0 + d) \,, \quad \text{for } \phi \in (\phi_0, \pi). \tag{3.8}$$

Hence, from the definition of $\{\lambda_k\}_{k=1}^{\infty}$ give in (3.7),

$$\lim_{k \to \infty} \lambda_k(\phi) = -(bx_0 + d) \,, \quad \text{for } \phi \in (\phi_0, \pi). \tag{3.9}$$

In addition, as $\lambda(\phi, r)$ is piecewise continuous for $|r| < 1$, each $\lambda_k(\phi)$ for $k = 1, 2, \ldots$ is integrable over the interval (ϕ', π), for some $\phi' \in (\phi_0, \pi)$. Moreover, $|\lambda_k(\phi)| \leq C$, for all $k = 1, 2, \ldots$, on (ϕ', π) for some $\phi' \in (\phi_0, \pi)$, where C is some positive constant. Accordingly,

$$\lim_{k \to \infty} \int_{\phi'}^{\pi} \lambda_k(\phi) \, \mathrm{d}\phi = \int_{\phi'}^{\pi} \lim_{k \to \infty} \lambda_k(\phi) \, \mathrm{d}\phi = \int_{\phi'}^{\pi} -(bx_0 + d) \, \mathrm{d}\phi \,, \tag{3.10}$$

by Arzelà's Dominated Convergence Theorem, and the term-by-term integration of (3.1b) is justified.

3.2.2 Levelling of the rates of convergence

To ensure both members of the DSE will involve the same kernel after the transformation, the DSE in (3.1) are first rewritten in terms of the Jacobi polynomials using (B.35b),

$$ax_0 + c + \sum_{n=1}^{\infty} \left[x_n \left(1 - s_n\right) + e_n\right] \frac{\sqrt{\pi} n!}{\Gamma\left(n + \frac{1}{2}\right)} P_n^{\left(-\frac{1}{2}, -\frac{1}{2}\right)}(\psi) = 0\,, \qquad \psi \in (\psi_0, 1), \tag{3.11a}$$

$$bx_0 + d + \sum_{n=1}^{\infty} n \left[x_n \left(1 - t_n\right) + f_n\right] \frac{\sqrt{\pi} n!}{\Gamma\left(n + \frac{1}{2}\right)} P_n^{\left(-\frac{1}{2}, -\frac{1}{2}\right)}(\psi) = 0\ (A), \quad \psi \in (-1, \psi_0), \tag{3.11b}$$

by means of new variables $\psi := \cos\phi$ and $\psi_0 := \cos\phi_0$.

An additional step of transforming the parameter values α and β in $P_n^{(\alpha,\beta)}(\psi)$ occurring in (3.11) is required before the equilibration of the convergence rates of the DSE. This is to ensure the condition $\alpha, \beta > -1$ is satisfied after the equilibration. It is accomplished by multiplying (3.11a) and (3.11b) by $(1-\psi)^{-1/2}(1+\psi)^{-1/2}$, then integrating over $(\psi, 1)$ and $(-1, \psi)$, respectively. The term-by-term integration has been justified in the previous subsection, as the DSE in (3.11) in terms of $P_n^{\left(-\frac{1}{2}, -\frac{1}{2}\right)}(\psi)$ are essentially those in (3.1) with kernels $\cos n\phi$. We obtain the following from the integration with the aid of (B.37) with $\alpha = \beta = -1/2$:

$$\begin{aligned}
&(ax_0 + c)\left(\tfrac{\pi}{2} - \sin^{-1}\psi\right) + \frac{\sqrt{\pi}}{2}(1-\psi)^{\frac{1}{2}}(1+\psi)^{\frac{1}{2}} \\
&\quad \times \sum_{n=1}^{\infty} \left[x_n \left(1 - s_n\right) + e_n\right] \frac{(n-1)!}{\Gamma\left(n + \frac{1}{2}\right)} P_{n-1}^{\left(\frac{1}{2}, \frac{1}{2}\right)}(\psi) = 0\,, \qquad \psi \in (\psi_0, 1), \qquad (3.12a) \\
&(bx_0 + d)\left(\tfrac{\pi}{2} + \sin^{-1}\psi\right) - \frac{\sqrt{\pi}}{2}(1-\psi)^{\frac{1}{2}}(1+\psi)^{\frac{1}{2}} \\
&\quad \times \sum_{n=1}^{\infty} \left[x_n \left(1 - t_n\right) + f_n\right] \frac{n!}{\Gamma\left(n + \frac{1}{2}\right)} P_{n-1}^{\left(\frac{1}{2}, \frac{1}{2}\right)}(\psi) = 0\,, \qquad \psi \in (-1, \psi_0). \qquad (3.12b)
\end{aligned}$$

The convergence rates of the series terms in (3.12a) and (3.12b) are $O\left(n^{-5/2}\right)$ and $O\left(n^{-3/2}\right)$, respectively, as $P_n^{(\alpha,\beta)} = O\left(n^{-1/2}\right)$ as given in (B.34). Both series are now uniformly convergent in their corresponding intervals. In order to level the convergence rates, the slower converging (3.12b) is integrated over $(-1, \psi)$ for $\psi \in (-1, \psi_0)$, with weight function $(1+\psi)^{-1/2}$. With the aid of integration by parts and

(B.36b) with $\eta = 0$, the integration gives

$$\begin{aligned}
&(bx_0 + d)\left[4\sqrt{1+\psi} - 2\sqrt{1-\psi}\left(\tfrac{\pi}{2} + \sin^{-1}\psi\right)\right] \\
&\quad - \frac{\sqrt{\pi}}{2}(1+\psi)^{\frac{3}{2}}\sum_{n=1}^{\infty}\left[x_n\left(1-t_n\right) + f_n\right]\frac{n!}{\Gamma\left(n+\frac{3}{2}\right)}P_{n-1}^{\left(-\frac{1}{2},\frac{3}{2}\right)}(\psi) = 0\,,
\end{aligned} \tag{3.13}$$

for all $\psi \in (-1, \psi_0)$. Both series in (3.12a) and (3.13) now have the same convergence rate $O\left(n^{-5/2}\right)$, but different kernels.

3.2.3 Abel integral transformation

The next step involved in the regularization process is reformulating (3.12a) and (3.13) as Abel integral equations. For (3.13), this is done by using (B.36b) when $\eta = 1/2$. We obtain

$$\int_{-1}^{\psi}\frac{S(t)}{\sqrt{\psi - t}}\mathrm{d}t = 4\left(bx_0 + d\right)\left[2\sqrt{1+\psi} - \sqrt{1-\psi}\left(\tfrac{\pi}{2} + \sin^{-1}\psi\right)\right]\,, \tag{3.14}$$

for all $\psi \in (-1, \psi_0)$, where $S(t)$ is defined as

$$S(t) := (1+t)\sum_{n=1}^{\infty}\left[x_n\left(1-t_n\right) + f_n\right]P_{n-1}^{(0,1)}(t)\,. \tag{3.15}$$

The interchange of the order of summation and integration is justified because of the weighted mean square convergence of the series in (3.13). The equation (3.14) is of the form of (C.1). Using the inversion formula (C.7), it can be derived that, for all $t \in (-1, \psi_0)$

$$S(t) = \frac{4}{\pi}\left(bx_0 + d\right)\frac{\mathrm{d}}{\mathrm{d}t}\int_{-1}^{t}\frac{2\sqrt{1+\psi} - \sqrt{1-\psi}\left(\frac{\pi}{2} + \sin^{-1}\psi\right)}{\sqrt{t-\psi}}\mathrm{d}\psi\,, \tag{3.16a}$$

$$= \frac{4}{\pi}\left(bx_0 + d\right)\frac{\mathrm{d}}{\mathrm{d}t}\int_{-1}^{t}\sqrt{\frac{t-\psi}{1-\psi}}\left(\tfrac{\pi}{2} + \sin^{-1}\psi\right)\mathrm{d}\psi\,, \tag{3.16b}$$

$$= \frac{2}{\pi}\left(bx_0 + d\right)\int_{-1}^{t}\frac{\frac{\pi}{2} + \sin^{-1}\psi}{\sqrt{t-\psi}\sqrt{1-\psi}}\mathrm{d}\psi\,, \tag{3.16c}$$

$$= -2\left(bx_0 + d\right)\ln\left(\frac{1-t}{2}\right)\,. \tag{3.16d}$$

It is noted that integration by parts was used to evaluate the integral in (3.16a). Since the integrand in the right hand side of (3.16b) is continuous everywhere in $(-1, t]$ as $t < 1$, the integral can be evaluated making use of the fundamental theorem of

integral calculus and chain rule. The resulting integral in (3.16c) is solved by change of variable ($\psi = -\cos\theta, t = -\cos\beta$) and the Dirichlet-Mehler formula [21, 69]

$$\int_0^{\beta} \frac{\theta \sin\frac{\theta}{2}}{\sqrt{\cos\theta - \cos\beta}} \mathrm{d}\theta = -\sqrt{2}\pi \ln\left(\cos\frac{\beta}{2}\right) . \tag{3.17}$$

Similarly, (3.12a) defined over $(\psi_0, 1)$ can be transformed using (B.36a) when $\eta = 1/2$ to

$$\int_{\psi}^{1} \frac{T(t)}{\sqrt{t-\psi}} \mathrm{d}t = -2\left(ax_0 + c\right) \frac{\frac{\pi}{2} - \sin^{-1}\psi}{\sqrt{1+\psi}} , \tag{3.18}$$

for all $\psi \in (\psi_0, 1)$, where $T(t)$ is defined as:

$$T(t) := \sum_{n=1}^{\infty} \left[x_n\left(1 - s_n\right) + e_n\right] P_{n-1}^{(0,1)}(t) . \tag{3.19}$$

Repeating parallel operations used in the derivation of (3.16d) with the aid of (C.8) and (3.17), we obtain a series equation of $\{x_n\}_{n=0}^{\infty}$ in terms of the same kernels, $P_{n-1}^{(0,1)}(t)$, as that in (3.16d):

$$T(t) = -2\left(ax_0 + c\right)\left(1 + t\right)^{-1} , \qquad t \in (\psi_0, 1). \tag{3.20}$$

We convert the kernels to the normalized form, $\hat{P}_{n-1}^{(0,1)}(t)$, defined in (B.31), and introduce following normalized coefficients for brevity:

$$\left\{\hat{x}_n, \hat{e}_n, \hat{f}_n\right\} := \sqrt{n}\left\{x_n, e_n, f_n\right\} , \tag{3.21}$$

for $n = 1, 2, \ldots$ It is worth noting that these new coefficients lie in ℓ_2. Combining (3.16d) and (3.20), we obtain a series equation defined over the entire interval:

$$\begin{aligned} &-\frac{1+\psi}{\sqrt{2}} \sum_{n=1}^{\infty} \hat{x}_n \frac{\hat{P}_{n-1}^{(0,1)}(\psi)}{n} \\ &= \begin{cases} \left(ax_0 + c\right) - \dfrac{1+\psi}{\sqrt{2}} \displaystyle\sum_{n=1}^{\infty} \left(\hat{x}_n s_n - \hat{e}_n\right) \frac{\hat{P}_{n-1}^{(0,1)}(\psi)}{n} , & \psi \in (\psi_0, 1), \\ \left(bx_0 + d\right) \ln\left(\dfrac{1-\psi}{2}\right) - \dfrac{1+\psi}{\sqrt{2}} \displaystyle\sum_{n=1}^{\infty} \left(\hat{x}_n t_n - \hat{f}_n\right) \frac{\hat{P}_{n-1}^{(0,1)}(\psi)}{n} , & \psi \in (-1, \psi_0). \end{cases} \end{aligned} \tag{3.22}$$

3.2.4 Conversion to an ISLAE

The last step of regularization process involves converting (3.22) into an ISLAE, which can be solved numerically by truncation method and matrix inversion. This process

is achieved by exploiting the orthonormality and completeness of $\left\{\hat{P}_n^{(0,1)}(\psi)\right\}_{n=1}^{\infty}$ on $(-1,1)$ as given in (B.32). The following integrals which occur in the conversion are evaluated using integration by parts, (B.38) and (B.39),

$$\int_{\psi_0}^{1} \hat{P}_{m-1}^{(0,1)}(t)\,\mathrm{d}t = (1-\psi_0)\frac{\hat{P}_{m-1}^{(1,0)}(\psi_0)}{m}\,, \tag{3.23}$$

$$\begin{aligned}\int_{-1}^{\psi_0} \ln\left(\frac{1-t}{2}\right)\hat{P}_{m-1}^{(0,1)}(t)\,\mathrm{d}t = &-(1-\psi_0)\ln\left(\frac{1-\psi_0}{2}\right)\frac{\hat{P}_{m-1}^{(1,0)}(\psi_0)}{m}\\ &-(1+\psi_0)\frac{\hat{P}_{m-1}^{(0,1)}(\psi_0)}{m^2}\,.\end{aligned} \tag{3.24}$$

It is worth noting that every series in (3.22) is Fourier-Jacobi and uniformly convergent. By exploiting the completeness and orthonormality of the kernels, the infinite system below is obtained from (3.22), for $m = 1, 2, \ldots$

$$\begin{aligned}&\hat{x}_m\,(1-t_m)\\ &= \sqrt{2}\,(bx_0+d)\left[(1-\psi_0)\ln\left(\frac{1-\psi_0}{2}\right)\hat{P}_{m-1}^{(1,0)}(\psi_0) + (1+\psi_0)\,\frac{\hat{P}_{m-1}^{(0,1)}(\psi_0)}{m}\right]\\ &\quad - \sqrt{2}\,(ax_0+c)\left[(1-\psi_0)\,\hat{P}_{m-1}^{(1,0)}(\psi_0)\right] - \hat{f}_m\\ &\quad + \sum_{n=1}^{\infty}\left[\hat{x}_n\,(s_n-t_n) + \hat{f}_n - \hat{e}_n\right]\frac{m}{n}\hat{Q}_{m-1,n-1}^{(0,1)}(\psi_0)\,.\end{aligned} \tag{3.25}$$

The function $\hat{Q}_{nm}^{(0,1)}(\psi_0)$ (see Appendix B.4.2) denotes the incomplete scalar product of the normalized Jacobi polynomials encountered; *i.e.*,

$$\hat{Q}_{nm}^{(0,1)}(\psi_0) := \int_{\psi_0}^{1}(1+t)\hat{P}_n^{(0,1)}(t)\,\hat{P}_m^{(0,1)}(t)\,\mathrm{d}t\,. \tag{3.26}$$

The solution of $\{\hat{x}_n\}_{n=1}^{\infty}$ is square summable, regardless of the value of the unknown x_0. However, x_0 must be chosen to ensure that it also lies in ℓ_2. Since the series on the left side of (3.22) is uniformly convergent (as $\{\hat{x}_n\}_{n=1}^{\infty} \in \ell_2$), the right side must be continuous everywhere on $(-1,1)$, including at the point $\psi = \psi_0$. It is worth noting that both sub-functions on the right side of (3.22) are continuous on their corresponding intervals $(\psi_0, 1)$ and $(-1, \psi_0)$, due to the assumptions made on $\{e_n, f_n, s_n, t_n, x_n\}_{n=1}^{\infty}$. For the continuity at $\psi = \psi_0$, the sub-functions on the right side of (3.22) are equated to give an equation for x_0

$$\begin{aligned}x_0 =&\frac{c - d\ln\left(\frac{1-\psi_0}{2}\right)}{b\ln\left(\frac{1-\psi_0}{2}\right) - a}\\ &+ \frac{1+\psi_0}{\sqrt{2}\left[b\ln\left(\frac{1-\psi_0}{2}\right) - a\right]}\sum_{n=1}^{\infty}\left[\hat{x}_n\,(t_n-s_n) + \hat{e}_n - \hat{f}_n\right]\frac{\hat{P}_{n-1}^{(0,1)}(\psi_0)}{n}\,,\end{aligned} \tag{3.27}$$

provided $\left[b\ln\left(\frac{1-\psi_0}{2}\right)-a\right]\neq 0$. Subsequently, the value of x_0 can be calculated once the values of $\{\hat{x}_n\}_{n=1}^{\infty}$ are known. Therefore, by substitution of (3.27) into (3.25), and by exploiting (B.47a) when $\alpha=1$ and $\beta=0$, an ISLAE involving only $\{x_n\}_{n=1}^{\infty}$ is obtained

$$\begin{aligned}
&\hat{x}_m\,(1-t_m)+\sum_{n=1}^{\infty}\hat{x}_n\,(t_n-s_n)\,\hat{R}_{m-1,n-1}(\psi_0)\\
&=\sqrt{2}(1+\psi_0)\frac{bc-ad}{b\ln\left(\frac{1-\psi_0}{2}\right)-a}\frac{\hat{P}_{m-1}^{(0,1)}(\psi_0)}{m}\\
&\quad-\hat{f}_m+\sum_{n=1}^{\infty}\left[\hat{f}_n-\hat{e}_n\right]\hat{R}_{m-1,n-1}(\psi_0),
\end{aligned}\tag{3.28}$$

for $m=1,2,3,\ldots$, where the following notation is used for brevity

$$\hat{R}_{m-1,n-1}(\psi_0):=\hat{Q}_{m-1,n-1}^{(1,0)}(\psi_0)-\frac{b(1+\psi_0)^2}{b\ln\left(\frac{1-\psi_0}{2}\right)-a}\frac{\hat{P}_{m-1}^{(0,1)}(\psi_0)}{m}\frac{\hat{P}_{n-1}^{(0,1)}(\psi_0)}{n}\,.\tag{3.29}$$

When $\left[b\ln\left(\frac{1-\psi_0}{2}\right)-a\right]=0$, the continuity at $t=\psi_0$ gives rise to an additional series equation involving only $\{\hat{x}_n\}_{n=1}^{\infty}$,

$$c-d\ln\left(\frac{1-\psi_0}{2}\right)+\frac{1+\psi_0}{\sqrt{2}}\sum_{n=1}^{\infty}\left[\hat{x}_n\,(t_n-s_n)+\hat{e}_n-\hat{f}_n\right]\frac{\hat{P}_{n-1}^{(0,1)}(\psi_0)}{n}=0\,.\tag{3.30}$$

The original ISLAE in (3.25) can be reduced to the following by using (3.30), and (B.47a) when $\alpha=1$ and $\beta=0$,

$$\begin{aligned}
&-\sqrt{2}b(1+\psi_0)\frac{\hat{P}_{m-1}^{(0,1)}(\psi_0)}{m}x_0+\hat{x}_m\,(1-t_m)+\sum_{n=1}^{\infty}\hat{x}_n\,(t_n-s_n)\,\hat{Q}_{m-1,n-1}^{(1,0)}(\psi_0)\\
&=\sqrt{2}d(1+\psi_0)\frac{\hat{P}_{m-1}^{(0,1)}(\psi_0)}{m}-\hat{f}_m+\sum_{n=1}^{\infty}\left[\hat{f}_n-\hat{e}_n\right]\hat{Q}_{m-1,n-1}^{(1,0)}(\psi_0)\,,
\end{aligned}\tag{3.31}$$

for $m=1,2,\ldots$ The additional series equation (3.30) and the above ISLAE are to be solved simultaneously for the values of x_0 and $\{\hat{x}_n\}_{n=1}^{\infty}$.

3.2.5 ISLAE in matrix operator form

The ISLAE in (3.28) can be written in matrix operator form as[1]

$$(\mathcal{I}+\mathcal{H})\,\mathbf{x}=\mathbf{b}\,,\tag{3.32}$$

[1]The Calligraphic fonts are used to represent the matrix operators.

where $\mathcal{I}$ denotes the identity operator on the Hilbert space ℓ_2, the column vector $\mathbf{b}$ represents the right side of (3.28), $\mathbf{x}$ is the column vector containing the solution $\{\hat{x}_n\}_{n=1}^{\infty}$, and $\mathcal{H}$ is defined as

$$\mathcal{H} := \mathcal{R}\,(\mathcal{T} - \mathcal{S}) - \mathcal{T}\,. \tag{3.33}$$

Here, $\mathcal{R} := \left\{\hat{R}_{n-1,m-1}(\psi_0)\right\}_{n,m=1}^{\infty}$ denotes the matrix operator of function defined in (3.29), whereas $\mathcal{S} := \text{diag}\,(\{s_n\}_{n=1}^{\infty})$ and $\mathcal{T} := \text{diag}\,(\{t_n\}_{n=1}^{\infty})$. It is worth noting that the column vectors $\mathbf{x}$ and $\mathbf{b}$ are square-summable.

As s_n, $t_n \to 0$ when $n \to \infty$, the diagonal matrix operators $\mathcal{S}$ and $\mathcal{T}$ are compact in ℓ_2. The linear matrix operator $\mathcal{R}$ is bounded as it is a superposition of two linear bounded operators. In fact, because of the property of $\hat{Q}^{(1,0)}_{m-1,n-1}(\psi_0)$ given in (B.46), the first part of $\mathcal{R}$ in (3.29) is idempotent and hence, a projection operator having norm at most 1. The second part of $\mathcal{R}$ in (3.29) can be shown to be Hilbert-Schmidt and bounded, by using (B.34). As a product of a bounded operator and compact operator is compact, $\mathcal{R}\,(\mathcal{T} - \mathcal{S})$ is compact. Consequently, the matrix operator $\mathcal{H}$ is compact because the sum of compact operators is also compact. As $\mathcal{I}$ in the infinite-dimensional ℓ_2 is a Fredholm operator with index zero and $\mathcal{H}$ is compact, the matrix operator $(\mathcal{I} + \mathcal{H})$ is Fredholm with index zero[2].

As a result, $(\mathcal{I} + \mathcal{H})$ satisfies the Fredholm alternative theorem. If the solution is unique, the Fredholm alternative theorem implies the solution existence and stability. For the electromagnetic MBVP considered, one can prove the uniqueness of solution by using the standard technique in [12]. The infinite system in (3.28) is truncated to a finite system of N_{tr} equations and solved numerically. The computed solution of this finite system ($\mathbf{x}^{N_{\text{tr}}}$) converges to the true solution of the infinite system ($\mathbf{x}^{\infty}$), as $N_{\text{tr}} \to \infty$. The condition number of the truncated system is uniformly bounded (*i.e.*, $\chi^{N_{\text{tr}}} \leq C$, for some positive constant C) and converges to that of the infinite system (*i.e.*, $\chi^{N_{\text{tr}}} \to \chi^{\infty}$). Therefore, the numerical process of solving these truncated system is stable for arbitrarily large N_{tr}. The solution of the MBVP can be computed numerically with any predetermined accuracy, limited only by the computer's digital precision [2, 4, 34].

[2]The background definitions and theorems from functional analysis are omitted. We refer to [2, 15, 30, 34].

3.2.6 Companion pair of DSE

Consider a companion pair to the DSE given in (3.1), where the subintervals on which (3.1a) and (3.1b) are defined are interchanged:

$$ax_0 + c + \sum_{n=1}^{\infty} \left[x_n \left(1 - s_n\right) + e_n\right] \cos n\phi = 0 \qquad (A)\,, \quad \phi \in (\phi_0, \pi), \tag{3.34a}$$

$$bx_0 + d + \sum_{n=1}^{\infty} n \left[x_n \left(1 - t_n\right) + f_n\right] \cos n\phi = 0 \qquad (A)\,, \quad \phi \in (0, \phi_0). \tag{3.34b}$$

Same assumptions as those for the previous pair of DSE are made on the coefficients x_0 and $\{x_n, e_n, f_n, s_n, t_n\}_{n=1}^{\infty}$.

This pair of DSE can be regularized and transformed to a second kind ISLAE, by following the same process used for the pair in (3.1). Alternatively, the final form of system can be obtained from (3.28) by means of new variables $\phi' := \pi - \phi$ and $\phi_0' := \pi - \phi_0$. The DSE in (3.35) can be rewritten as

$$ax_0 + c + \sum_{n=1}^{\infty} (-1)^n \left[x_n \left(1 - s_n\right) + e_n\right] \cos n\phi' = 0 \quad (A)\,, \quad \phi' \in (0, \phi_0'), \tag{3.35a}$$

$$bx_0 + d + \sum_{n=1}^{\infty} (-1)^n n \left[x_n \left(1 - t_n\right) + f_n\right] \cos n\phi' = 0 \quad (A)\,, \quad \phi' \in (\phi_0', \pi). \tag{3.35b}$$

By putting $x_n \mapsto (-1)^n x_n$, $e_n \mapsto (-1)^n e_n$, $f_n \mapsto (-1)^n f_n$, $\psi_0 \mapsto \cos\phi_0' = -\cos\phi_0 = \psi_0$ in (3.28) with the rest remaining unchanged, we obtain

$$\begin{aligned}
&(-1)^m \hat{x}_m \left(1 - t_m\right) + \sum_{n=1}^{\infty} (-1)^n \hat{x}_n \left(t_n - s_n\right) \hat{R}_{m-1,n-1}(-\psi_0) \\
&= \sqrt{2}(1 + \psi_0) \frac{bc - ad}{b \ln\left(\frac{1-\psi_0}{2}\right) - a} \frac{\hat{P}_{m-1}^{(0,1)}(-\psi_0)}{m} \\
&\quad - (-1)^m \hat{f}_m + \sum_{n=1}^{\infty} (-1)^n \left[\hat{f}_n - \hat{e}_n\right] \hat{R}_{m-1,n-1}(-\psi_0)\,,
\end{aligned} \tag{3.36}$$

provided $\left[b \ln\left(\frac{1-\psi_0}{2}\right) - a\right] \neq 0$. An alternative form of the above can be obtained by making use of the identities (B.33) and (B.45),

$$\begin{aligned}
&\hat{x}_m \left(1 - s_m\right) - \sum_{n=1}^{\infty} \hat{x}_n \left(t_n - s_n\right) \hat{S}_{m-1,n-1}(\psi_0) \\
&= -\sqrt{2}(1 - \psi_0) \frac{bc - ad}{b \ln\left(\frac{1+\psi_0}{2}\right) - a} \frac{\hat{P}_{m-1}^{(1,0)}(\psi_0)}{m} \\
&\quad - \hat{e}_m - \sum_{n=1}^{\infty} \left[\hat{f}_n - \hat{e}_n\right] \hat{S}_{m-1,n-1}(\psi_0),
\end{aligned} \tag{3.37}$$

for $m = 1, 2, 3, \ldots$, where we define:

$$\hat{S}_{m-1,n-1}(\psi_0) := \hat{Q}^{(0,1)}_{m-1,n-1}(\psi_0) + \frac{b(1-\psi_0)^2}{b\ln\left(\frac{1+\psi_0}{2}\right) - a} \frac{\hat{P}^{(1,0)}_{m-1}(\psi_0)}{m} \frac{\hat{P}^{(1,0)}_{n-1}(\psi_0)}{n}\,. \tag{3.38}$$

Similarly, the expression for x_0 can be obtained from (3.27) and (B.33) as

$$\begin{aligned} x_0 =& \frac{c - d\ln\left(\frac{1+\psi_0}{2}\right)}{b\ln\left(\frac{1+\psi_0}{2}\right) - a} \\ & - \frac{1-\psi_0}{\sqrt{2}\left[b\ln\left(\frac{1+\psi_0}{2}\right) - a\right]} \sum_{n=1}^{\infty} \left[\hat{x}_n\left(t_n - s_n\right) + \hat{e}_n - \hat{f}_n\right] \frac{\hat{P}^{(1,0)}_{n-1}(\psi_0)}{n}\,. \end{aligned} \tag{3.39}$$

The infinite system when $\left[b\ln\left(\frac{1-\psi_0}{2}\right) - a\right] = 0$, can be obtained directly from (3.30) and (3.31), by substitution of ϕ' and ϕ'_0.

3.3 Dual series equations with kernels $\sin n\phi$

We consider the following DSE involving the sine functions

$$\sum_{n=1}^{\infty} \left[y_n\left(1 - s_n\right) + g_n\right] \sin n\phi = 0 \quad (A)\,, \qquad \phi \in (0, \phi_0), \tag{3.40a}$$

$$\sum_{n=1}^{\infty} n\left[y_n\left(1 - t_n\right) + h_n\right] \sin n\phi = 0 \quad (A)\,, \qquad \phi \in (\phi_0, \pi), \tag{3.40b}$$

where the coefficients $\{g_n, h_n, s_n, t_n\}_{n=1}^{\infty}$ are assumed to be known, and $\{y_n\}_{n=1}^{\infty}$ is the unknown sequence to be determined. As with the case where the DSE involving $\cos n\phi$, $\{y_n, g_n, h_n\}_{n=1}^{\infty}$ are assumed to satisfy the Fejér's Tauberian condition (D.4); whereas $\{s_n, t_n\}_{n=1}^{\infty}$ tend to zero, when $n \to \infty$. Term-by-term integration of (3.40a) and (3.40b) can be justified following the same arguments given in the previous section for the DSE involving $\cos n\phi$.

3.3.1 Leveling of the rates of convergences

The conversion of the weakly ill-posed DSE in (3.40) follows parallel operations as those in previous section, except that the transformation of the values of α and β of $P_n^{(\alpha,\beta)}(\psi)$ is not required. The justification of each of the mathematical operations is similar to those given in previous section, and hence omitted.

By using (B.35a), we rewrite the DSE in (3.40) as

$$\sum_{n=1}^{\infty}\left[y_n\left(1-s_n\right)+g_n\right]\frac{n!}{\Gamma\left(n+\frac{1}{2}\right)}P_{n-1}^{\left(\frac{1}{2},\frac{1}{2}\right)}(\psi)=0\,,\qquad\qquad \psi\in(\psi_0,1),\tag{3.41a}$$

$$\sum_{n=1}^{\infty}n\left[y_n\left(1-t_n\right)+h_n\right]\frac{n!}{\Gamma\left(n+\frac{1}{2}\right)}P_{n-1}^{\left(\frac{1}{2},\frac{1}{2}\right)}(\psi)=0\quad(A)\,,\qquad \psi\in(-1,\psi_0).\tag{3.41b}$$

To equilibrate the convergence rates, we integrate (3.41b) over $(-1,\psi)$ with weight function $(1+\psi)^{1/2}$, for some $\psi\in(-1,\psi_0)$. By using (B.36a) when $\eta=0$, we get:

$$(1+\psi)^{\frac{3}{2}}\sum_{n=1}^{\infty}n\left[y_n\left(1-t_n\right)+h_n\right]\frac{n!}{\Gamma\left(n+\frac{3}{2}\right)}P_{n-1}^{\left(-\frac{1}{2},\frac{3}{2}\right)}(\psi)=0\,,\psi\in(-1,\psi_0).\tag{3.42}$$

3.3.2 Abel integral transformation

Abel integral transformation is carried out on (3.42), by using (B.36a) when $\eta=1/2$, and the homogeneous form of (C.1). We obtain

$$\sum_{n=1}^{\infty}n\left[y_n\left(1-t_n\right)+h_n\right]P_{n-1}^{(0,1)}(t)=0\,,\qquad\qquad t\in(-1,\psi_0).\tag{3.43}$$

Using (B.36a) when $\eta=1/2$, and the homogeneous form of (C.8), Abel transformation of (3.41a) gives

$$\sum_{n=1}^{\infty}n\left[y_n\left(1-s_n\right)+g_n\right]P_{n-1}^{(0,1)}(t)=0\,,\qquad\qquad t\in(\psi_0,1).\tag{3.44}$$

Combining (3.43) and (3.44), we get a series equation defined over $(-1,1)$:

$$\sum_{n=1}^{\infty}\hat{y}_n\hat{P}_{n-1}^{(0,1)}(\psi)=\qquad\begin{cases}\displaystyle\sum_{n=1}^{\infty}\left(\hat{y}_n s_n-\hat{g}_n\right)\hat{P}_{n-1}^{(0,1)}(\psi)\,, & \psi\in(\psi_0,1),\\[2ex] \displaystyle\sum_{n=1}^{\infty}\left(\hat{y}_n t_n-\hat{h}_n\right)\hat{P}_{n-1}^{(0,1)}(\psi)\,, & \psi\in(-1,\psi_0),\end{cases}\tag{3.45}$$

where the following normalized coefficients have been introduced for $n=1,2,3,\ldots$

$$\left\{\hat{y}_n,\hat{g}_n,\hat{h}_n\right\}:=\sqrt{n}\left\{y_n,g_n,h_n\right\}.\tag{3.46}$$

3.3.3 Conversion to an ISLAE

By making use of the properties of orthonormality and completeness of the set $\left\{\hat{P}_n^{(0,1)}(\psi)\right\}_{n=1}^{\infty}$ on $(-1,1)$, (3.45) is converted to the following ISLAE where $m=$

$1, 2, 3, \ldots$

$$\hat{y}_m\,(1-t_m) + \sum_{n=1}^{\infty} \hat{y}_n\,(t_n - s_n)\,\hat{Q}^{(0,1)}_{m-1,n-1}(\psi_0)$$
$$= -\hat{h}_m + \sum_{n=1}^{\infty} \left(\hat{h}_n - \hat{g}_n\right) \hat{Q}^{(0,1)}_{m-1,n-1}(\psi_0)\,. \tag{3.47}$$

3.3.4 ISLAE in matrix operator form

It is evident that (3.47) is a Fredholm equation of the second-kind, and can be written in the following matrix operator form

$$(\mathcal{I} + \mathcal{H}')\,\mathbf{y} = \mathbf{b}'\,, \tag{3.48}$$

where the column vector $\mathbf{b}'$ represents the right side of (3.47), $\mathbf{y}$ is the column vector containing the solution $\{\hat{y}\}_{n=1}^{\infty}$, and $\mathcal{H}'$ is defined as

$$\mathcal{H}' := \mathcal{Q}\,(\mathcal{T} - \mathcal{S}) - \mathcal{T}\,. \tag{3.49}$$

The operators $\mathcal{I}$, $\mathcal{S}$ and $\mathcal{T}$ are as defined in the previous section for the DSE involving $\cos n\phi$. The matrix operator $\mathcal{Q} := \left\{\hat{Q}^{(0,1)}_{m-1,n-1}(\psi_0)\right\}_{n,m=1}^{\infty}$ is idempotent because of (B.46). Hence, $\mathcal{Q}$ is linear bounded operator having norm atmost 1, and $\mathcal{H}'$ is a compact operator. Therefore, $(\mathcal{I} + \mathcal{H}')$ is a Fredholm operator with index zero, and (3.47) offers a stable computation scheme to solve the originally ill-posed DSE in (3.40).

3.3.5 Companion pair of DSE

The companion pair to the DSE given in (3.40) is

$$\sum_{n=1}^{\infty} \left[y_n\,(1-s_n) + g_n\right] \sin n\phi = 0 \quad (A)\,, \qquad \phi \in (\phi_0, \pi), \tag{3.50a}$$

$$\sum_{n=1}^{\infty} n\left[y_n\,(1-t_n) + h_n\right] \sin n\phi = 0 \quad (A)\,, \qquad \phi \in (0, \phi_0). \tag{3.50b}$$

This pair of DSE can be regularized and transformed to the following second kind ISLAE, where $m = 1, 2, 3, \ldots$

$$\hat{y}_m\,(1-s_m) - \sum_{n=1}^{\infty} \hat{y}_n\,(t_n - s_n)\,\hat{Q}^{(1,0)}_{m-1,n-1}(\psi_0)$$
$$= -\hat{g}_m - \sum_{n=1}^{\infty} \left(\hat{h}_n - \hat{g}_n\right) \hat{Q}^{(1,0)}_{m-1,n-1}(\psi_0)\,. \tag{3.51}$$

Chapter 4

Scattering from a CLR under oblique incidence

4.1 Introduction

In this chapter, the scattering of an oblique incident plane wave on a dielectric cylinder with a conformal PEC strip[1] (as depicted in Figure 4.1) is considered. Assuming that it is aligned parallel to the z-axis, the structure has constant cross-section with respect to z. The terminology cylindrical lens reflector (CLR) is used to refer to this partially-shielded dielectric cylinder.

The scattering problem of an axially-slotted PEC cylinder is one of the simplest and most investigated geometries in the area of scattering and radiation. A very large number of papers have been written on the determination of the near-field quantities due to normal plane wave incidence. For example, Senior [65] and Beren [7] used the integral equation approach to determine the field around an axially slotted cylinder, the rigorous regularization method was used to solved the same problem first by Shestopalov *et al* in [41], then by Ziolkowski *et al* in [32, 97], Harrington treated the field penetration inside a conducting circular cylinder through a narrow slot in using method of moments [17], *etc.*

Most of these studies are for incidence at normal incidence with respect to the cylinder axis (*i.e.*, the z-axis). In this special case, the vector boundary value problem can be studied in terms of two separate scalar boundary value problems. They are the E-polarization (the TM_z case) and the H-polarization (the TE_z case). For normal incidence case, the E- and H-polarized waves are separate, and are solved

[1] Alternatively, when the strip subtends an angle greater than π (*i.e.*, the slit is small), the structure is often referred to as a slotted cylinder with dielectric loading.

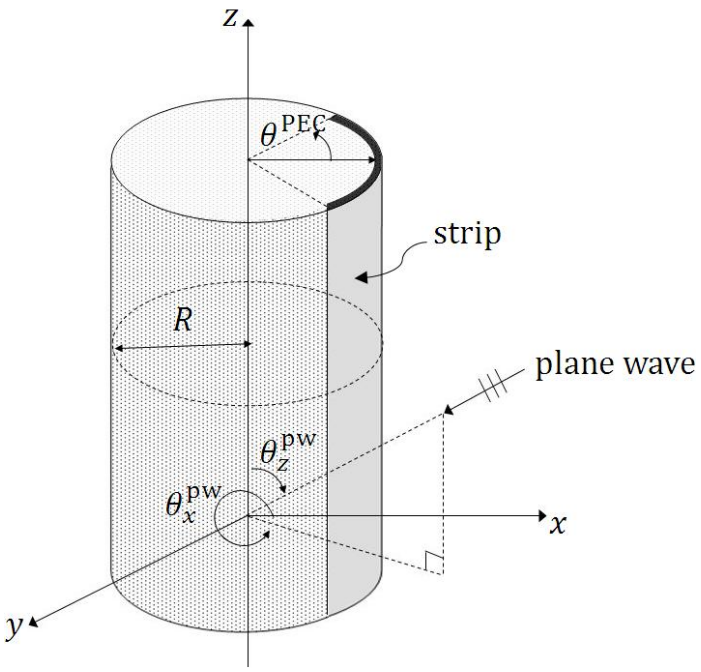

Figure 4.1: The infinitely-long CLR and the oblique incident plane wave.

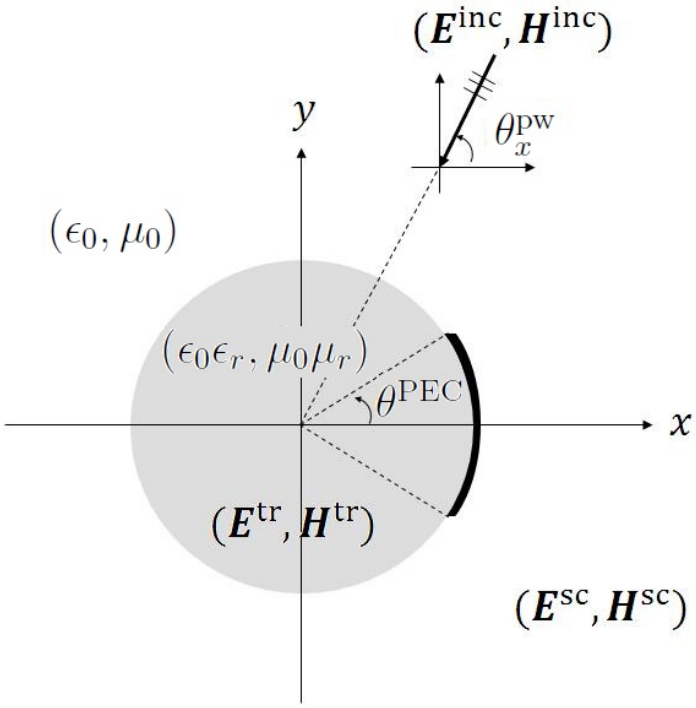

Figure 4.2: Cross-sectional view of the CLR.

independently. The secondary (reflected or transmitted) fields for a general incident wave polarization are simply a vector sum from each one of these two polarizations.

However, when the incident wave is at an oblique angle (angle other than perpendicular) to the z-axis, the two polarizations are mixed and exist simultaneously. The oblique scattering problem has important practical applications in various areas such as diffraction grating analysis. The problem also forms a fundamental building block in the analysis of the fields induced by a finite source, which may be decomposed into a spectrum of oblique incident plane waves. In spite of the fact that for many real-world applications the excitation is not normal to the cylinder, results for this general case of oblique incidence are rather sparse. Surprisingly, despite the simplicity of the scatterer considered, the oblique scattering problem of a slotted cylinder has only been considered in [94], to the best of our knowledge. However, [94] neglected the crossed polarization in its conformal mapping formulation.

In order to provide an accurate and constructive assessment, as well as understanding of the scattering properties of the CLR, the 3D oblique incident problem is considered in this chapter. The detailed derivation for the pure TM_z excitation is first formulated, and the extension to the pure TE_z case is outlined. The formalism can be readily adapted to the problem with incident wave coming from an infinitely thin straight wire of infinite length running parallel to the z-axis and carrying a current $I_0 e^{-jk_z z}$, which represents a wave with axial wavenumber k_z propagating in the positive z-direction. A single-layered dielectric substrate is assumed in the problem formulation for simplicity, although the approach is applicable to the problem involving a multi-layered and/or overlaid structure.

Section 4.2 is devoted to give a full description of the problem, and to establish the notations used. In Section 4.3–4.4, the MBVP is transformed into two independent 2-by-2 block matrix equations of the second kind by using the MoR approach. The result is extended to the case involving a pure TE_z incident plane wave in Section 4.5. Series representations of the energy distribution, RCS and surface current are derived in Section 4.6.3, where an approach to improve the convergence rate of the series terms is also proposed in Section 4.7.

The numerical investigation for this chapter is documented in Section 4.8. It first deals with the numerical verification of the problem formulation and numerical algorithm through internal as well as external tests. Internal tests based on the calculations of the near fields to verify the MBC on the contour (to within the roundoff errors) are applied. In addition, comparisons with the results from the literature (for the normal incident problem) have been carried out as an external test. The

agreement in all cases is excellent. The second part of the numerical investigation focuses on the stability and convergence of the algorithm. Specific information about the dependence of the truncation number $N_{\rm tr}$ (for a chosen degree of accuracy) on the radius of the CLR and the dielectric loading is obtained through convergence checks of the unknown coefficients and the RCS. Numerical results also show that the condition numbers of the matrices are bounded, as $N_{\rm tr}$ increases. In the final part of the numerical investigation, the effects of the oblique incident angle on the RCS and internal energy are plotted.

4.2 Geometrical description of the problem

Consider an infinitely long CLR of radius R, with cylindrical lens made of dielectric material of relative permittivity and permeability (ϵ_r, μ_r)[2]. The conformal PEC strip on the surface of the CLR is assumed to be infinitely thin, and has an angular width of $2\theta^{\rm PEC}$. Without loss of generality, we suppose that the CLR is embedded in free space, and is aligned parallel to the z-axis, and the PEC strip is located at $\Omega_{\rm PEC} = \big\{(\rho,\phi) : \rho = R \text{ and } |\phi| < \theta^{\rm PEC}\big\}$. We use the term "aperture" to refer to the interface on the cylindrical lens that is not shielded by the PEC strip; *i.e.*, $\Omega_{\rm aper} = \big\{(\rho,\phi) : \rho = R \text{ and } |\phi| > \theta^{\rm PEC}\big\}$.

Suppose the CLR is illuminated by a purely TM_z oblique incident plane wave (*i.e.*, $H_z^{\rm inc} \equiv 0$), with vacuum wavenumber $k_0 = \omega\sqrt{\epsilon_0\mu_0}$. The plane wave propagates in the direction which makes a polar angle $\theta_z^{\rm pw}$ with the z-axis, and an azimuthal angle $\theta_x^{\rm pw}$ in the xy-plane with the positive x-axis. The geometrical description of the CLR, and the propagation direction of the oblique incident plane wave is given in Figure 4.1. The time dependence $e^{j\omega t}$ is assumed and suppressed.

4.3 Derivation of the four sets of DSE

The series expansions for the field components have been derived in Section 2.4, by replacing k_z with $k_0 \cos\theta_z^{\rm pw}$. Due to phase matching, all of the primary and secondary fields exhibit the same phase dependence on z through the factor $e^{jk_0 z\cos\theta_z^{\rm pw}}$ (which is suppressed throughout this chapter). For oblique incidence (when $k_z \neq 0$), even a pure TM_z or TE_z plane wave will give rise to a mixed-polarized field, due to the dependence of E_ϕ and H_ϕ on both E_z and H_z as seen in (2.33). As a result, four sets

[2]Under the assumption that the permittivity is independent of frequency, for any material, $\epsilon_r \geq 1$; whereas μ_r is essentially 1 for most materials, except for nonlinear ferromagnetic material.

of connected DSE are derived from the MBC, instead of two independent sets of DSE for the normal incidence problem.

4.3.1 Series representations for the field components

The complete scattering domain is divided into two regions by the contour of the CLR; *i.e.*, region 0 which denotes the exterior with $\rho > R$ (free space), and region 1 which denotes the interior with $\rho < R$ (the dielectric lens).

In region 0, the transverse wavenumber $k_\rho = \sqrt{k_0^2 - k_z^2} = k_0 \sin\theta_z^{\text{pw}}$. It is denoted as κ_0 to avoid confusion with the vacuum wavenumber k_0. From Section 2.5, the field components of the TM_z incident plane wave have the following series representations:

$$E_z^{\text{inc}} = \sum_{n=-\infty}^{\infty} c_n(\kappa_0\rho)e^{jn\phi}\,, \tag{4.1a}$$

$$H_z^{\text{inc}} = 0\,, \tag{4.1b}$$

$$E_\phi^{\text{inc}} = -\frac{k_0\cos\theta_z^{\text{pw}}}{\kappa_0^2\rho}\sum_{n=-\infty}^{\infty} nc_n(\kappa_0\rho)e^{jn\phi}\,, \tag{4.1c}$$

$$H_\phi^{\text{inc}} = -\frac{jk_0}{\eta_0\kappa_0}\sum_{n=-\infty}^{\infty} c_n'(\kappa_0\rho)e^{jn\phi}\,, \tag{4.1d}$$

$$E_\rho^{\text{inc}} = \frac{jk_0\cos\theta_z^{\text{pw}}}{\kappa_0}\sum_{n=-\infty}^{\infty} c_n'(\kappa_0\rho)e^{jn\phi}\,, \tag{4.1e}$$

$$H_\rho^{\text{inc}} = -\frac{k_0}{\eta_0\kappa_0^2\rho}\sum_{n=-\infty}^{\infty} nc_n(\kappa_0\rho)e^{jn\phi}\,, \tag{4.1f}$$

where the following parameters have been introduced for brevity,

$$c_n(\kappa_0\rho) := A_0\sin\theta_z^{\text{pw}} j^n J_n(\kappa_0\rho)e^{-jn\theta_x^{\text{pw}}}\,, \tag{4.2a}$$

$$c_n'(\kappa_0\rho) := A_0\sin\theta_z^{\text{pw}} j^n J_n'(\kappa_0\rho)e^{-jn\theta_x^{\text{pw}}}\,. \tag{4.2b}$$

The presence of the CLR causes a scattered field in the region 0. We represent the z-components of the fields by:

$$\begin{Bmatrix} E_z^{\text{sc}} \\ H_z^{\text{sc}} \end{Bmatrix} := \sum_{n=-\infty}^{\infty} \begin{Bmatrix} a_n^{(0)} \\ b_n^{(0)} \end{Bmatrix} \frac{H_n^{(2)}(\kappa_0\rho)}{H_n^{(2)}(\kappa_0 R)} e^{jn\phi}\,, \tag{4.3}$$

where $\left\{a_n^{(0)}, b_n^{(0)}\right\}_{n\in\mathbb{Z}}$ are unknowns to be determined. By normalizing the coefficients in (4.3) with respect $H_n^{(2)}(\kappa_0 R)$, the overflow problems encountered when computing large order Hankel function are improved [14]. In fact, after the normalization, it

follows from the Meixner condition that $\left\{a_n^{(0)}, b_n^{(0)}\right\}_{n\in\mathbb{Z}}$ satisfy the Fejér's Tauberian condition (D.4) (shown in next subsection). It is worth noting that, the scattered field components represented by (4.3) automatically satisfy the Sommerfeld radiation condition.

In region 1, we denote the transverse wavenumber as $\kappa_1 = \sqrt{k_1^2 - k_0^2 \cos^2\theta_z^{\mathrm{pw}}}$. Here, $k_1 = k_0\sqrt{\epsilon_r\mu_r}$ is the wavenumber in the dielectric lens. In terms of the unknowns $\left\{a_n^{(1)}, b_n^{(1)}\right\}_{n\in\mathbb{Z}}$, we write the z-components of the transmitted fields as

$$\begin{Bmatrix} E_z^{\mathrm{tr}} \\ H_z^{\mathrm{tr}} \end{Bmatrix} := \sum_{n=-\infty}^{\infty} \begin{Bmatrix} a_n^{(1)} \\ b_n^{(1)} \end{Bmatrix} J_n(\kappa_1\rho) H_n^{\prime(2)}(\kappa_1 R) e^{jn\phi}\,. \tag{4.4}$$

We have chosen this normalization instead of one in the same form as (4.3) to avoid the division by $J_n(\kappa_1 R)$, which could vanish for a finite number of ω, when the argument $\kappa_1 R$ coincides with one of the zeros for $J_n(x)$. This normalization also ensures that $\left\{a_n^{(1)}, b_n^{(1)}\right\}_{n\in\mathbb{Z}}$ satisfy the Fejér's Tauberian condition, for the Meixner condition to be satisfied. It is worth noting that these series representations satisfy the boundedness of fields at the origin.

Due to (2.33), the transverse components can be expressed in terms of the transverse derivatives of E_z and H_z. Therefore, all the transverse components can be expressed in terms of $\left\{a_n^{(i)}, b_n^{(i)}\right\}_{n\in\mathbb{Z}}$ $(i = 0, 1)$ as:

$$\begin{cases}
E_\phi^{\mathrm{sc}} = -\dfrac{k_0}{\kappa_0}\displaystyle\sum_{n=-\infty}^{\infty}\left\{\frac{\cos\theta_z^{\mathrm{pw}}}{\kappa_0\rho} n a_n^{(0)} \frac{H_n^{(2)}(\kappa_0\rho)}{H_n^{(2)}(\kappa_0 R)} + \frac{\eta_0}{j} b_n^{(0)} \frac{H_n^{\prime(2)}(\kappa_0\rho)}{H_n^{(2)}(\kappa_0 R)}\right\} e^{jn\phi}\,, & \text{(4.5a)}\\
H_\phi^{\mathrm{sc}} = -\dfrac{k_0}{\kappa_0}\displaystyle\sum_{n=-\infty}^{\infty}\left\{\frac{j}{\eta_0} a_n^{(0)} \frac{H_n^{\prime(2)}(\kappa_0\rho)}{H_n^{(2)}(\kappa_0 R)} + \frac{\cos\theta_z^{\mathrm{pw}}}{\kappa_0\rho} n b_n^{(0)} \frac{H_n^{(2)}(\kappa_0\rho)}{H_n^{(2)}(\kappa_0 R)}\right\} e^{jn\phi}\,, & \text{(4.5b)}\\
E_\phi^{\mathrm{tr}} = -\dfrac{k_0}{\kappa_1}\displaystyle\sum_{n=-\infty}^{\infty}\left\{\frac{\cos\theta_z^{\mathrm{pw}}}{\kappa_1\rho} n a_n^{(1)} J_n(\kappa_1\rho) H_n^{\prime(2)}(\kappa_1 R)\right. & \\
\qquad\left. + \dfrac{\eta_0\mu_r}{j} b_n^{(1)} J_n'(\kappa_1\rho) H_n^{\prime(2)}(\kappa_1 R)\right\} e^{jn\phi}\,, & \text{(4.5c)}\\
H_\phi^{\mathrm{tr}} = -\dfrac{k_0}{\kappa_1}\displaystyle\sum_{n=-\infty}^{\infty}\left\{\frac{j\epsilon_r}{\eta_0} a_n^{(1)} J_n'(\kappa_1\rho) H_n^{\prime(2)}(\kappa_1 R)\right. & \\
\qquad\left. + \dfrac{\cos\theta_z^{\mathrm{pw}}}{\kappa_1\rho} n b_n^{(1)} J_n(\kappa_1\rho) H_n^{\prime(2)}(\kappa_1 R)\right\} e^{jn\phi}\,, & \text{(4.5d)}
\end{cases}$$

$$
\begin{cases}
E_\rho^{\mathrm{sc}} = \dfrac{k_0}{\kappa_0}\displaystyle\sum_{n=-\infty}^{\infty}\left\{ j\cos\theta_z^{\mathrm{pw}} a_n^{(0)} \dfrac{H_n^{'(2)}(\kappa_0\rho)}{H_n^{(2)}(\kappa_0 R)} + \dfrac{\eta_0}{\kappa_0\rho} n b_n^{(0)} \dfrac{H_n^{(2)}(\kappa_0\rho)}{H_n^{(2)}(\kappa_0 R)} \right\} e^{jn\phi}\,, & \text{(4.6a)} \\
H_\rho^{\mathrm{sc}} = -\dfrac{k_0}{\kappa_0}\displaystyle\sum_{n=-\infty}^{\infty}\left\{ \dfrac{1}{\eta_0\kappa_0\rho} n a_n^{(0)} \dfrac{H_n^{(2)}(\kappa_0\rho)}{H_n^{(2)}(\kappa_0 R)} - j\cos\theta_z^{\mathrm{pw}} b_n^{(0)} \dfrac{H_n^{'(2)}(\kappa_0\rho)}{H_n^{(2)}(\kappa_0 R)} \right\} e^{jn\phi}\,, & \text{(4.6b)} \\
E_\rho^{\mathrm{tr}} = \dfrac{k_0}{\kappa_1}\displaystyle\sum_{n=-\infty}^{\infty}\Big\{ j\cos\theta_z^{\mathrm{pw}} a_n^{(1)} J_n'(\kappa_1\rho) H_n^{'(2)}(\kappa_1 R) \\
\qquad\qquad + \dfrac{\eta_0\mu_r}{\kappa_1\rho} n b_n^{(1)} J_n(\kappa_1\rho) H_n^{'(2)}(\kappa_1 R) \Big\} e^{jn\phi}\,, & \text{(4.6c)} \\
H_\rho^{\mathrm{tr}} = -\dfrac{k_0}{\kappa_1}\displaystyle\sum_{n=-\infty}^{\infty}\Big\{ \dfrac{\epsilon_r}{\eta_0\kappa_1\rho} n a_n^{(1)} J_n(\kappa_1\rho) H_n^{'(2)}(\kappa_1 R) \\
\qquad\qquad - j\cos\theta_z^{\mathrm{pw}} b_n^{(1)} J_n'(\kappa_1\rho) H_n^{'(2)}(\kappa_1 R) \Big\} e^{jn\phi}\,, & \text{(4.6d)}
\end{cases}
$$

where the prime on the Bessel and Hankel functions denotes differentiation with respect to the argument $\kappa_i\rho$ $(i = 0, 1)$.

As all electromagnetic fields are finite, single-valued as well as continuous with continuous derivatives everywhere in space, excluding the contour of the scatterer, the representations given in (4.3)–(4.6) need to be bounded, convergent and continuous, as long as $\rho > R$ (for the scattered field) or $\rho < R$ (for the transmitted field). These series can be shown to satisfy these properties by using the ratio test, and considering the solution class established in next subsection for the coefficients $\left\{a_n^{(i)}, b_n^{(i)}\right\}_{n\in\mathbb{Z}}$ $(i = 0, 1)$.

4.3.2 Solution class of the unknown coefficients

The electromagnetic energy contained per unit length of the CLR is

$$
\begin{aligned}
\mathrm{W} = & \frac{1}{2}\int_0^1 \left| e^{jk_0 z\cos\theta_z^{\mathrm{pw}}} \right|^2 \mathrm{d}z \times \int_0^R \int_{-\pi}^{\pi} \Big\{ \epsilon_0\epsilon_r \left(\left|E_\rho^{\mathrm{tr}}\right|^2 + \left|E_\phi^{\mathrm{tr}}\right|^2 + \left|E_z^{\mathrm{tr}}\right|^2 \right) \\
& + \mu_0\mu_r \left(\left|H_\rho^{\mathrm{tr}}\right|^2 + \left|H_\phi^{\mathrm{tr}}\right|^2 + \left|H_z^{\mathrm{tr}}\right|^2 \right) \Big\} \mathrm{d}\phi\, \rho\, \mathrm{d}\rho\,. \qquad \text{(4.7)}
\end{aligned}
$$

The original triple integral in (2.11) can be evaluated as this iterated integral according to Tonelli's theorem, as the integrands are all nonnegative. It is worth noting that not all integrands are bounded in the region of integration; *e.g.*, $H_\phi\left(R, \pm\theta^{\mathrm{PEC}}\right)$. A series expression for W can be obtained by substitution of the representations given

in (4.3)–(4.6) into (4.7). The double summations encountered can be reduced by making use of the orthogonality of the exponential function:

$$\int_{-\pi}^{\pi} e^{j(n-m)\phi}\mathrm{d}\phi = \begin{cases} 0, & \text{if } n \neq m, \\ 2\pi, & \text{if } n = m. \end{cases} \tag{4.8}$$

The series expression for W can be simplified to

$$W = \pi \sum_{n=-\infty}^{\infty} \left\{ \left(\epsilon_0 \epsilon_r \left| a_n^{(1)} \right|^2 + \mu_0 \mu_r \left| b_n^{(1)} \right|^2 \right) \Phi_n + \left(\overline{b}_n^{(1)} a_n^{(1)} - b_n^{(1)} \overline{a}_n^{(1)} \right) \Gamma_n \right\}, \tag{4.9}$$

where the following quantities are introduced for a neater expression,

$$\begin{aligned} \Phi_n :=& \int_0^R \left\{ J_n^2(\kappa_1\rho) + \frac{k_0^2 \cos^2\theta_z^{\mathrm{pw}} + k_1^2}{\kappa_1^2} \left[J_n'^{\,2}(\kappa_1\rho) + \frac{n^2}{\kappa_1^2\rho^2} J_n^2(\kappa_1\rho) \right] \right\} \rho \,\mathrm{d}\rho \\ & \times \left| H_n'^{(2)}(\kappa_1 R) \right|^2, \end{aligned} \tag{4.10a}$$

$$\Gamma_n := \frac{4jk_1^2 \cos\theta_z^{\mathrm{pw}}}{\kappa_1^3} \sqrt{\epsilon_0\mu_0} \int_0^R n J_n(\kappa_1\rho) J_n'(\kappa_1\rho)\,\mathrm{d}\rho \times \left| H_n'^{(2)}(\kappa_1 R) \right|^2. \tag{4.10b}$$

The integrals in (4.10a)–(4.10b) are evaluated by a change of variable, $z = \kappa_1\rho$. By using integration by parts and the Bessel equation (B.7), we derive

$$\int z J_n^2(z)\mathrm{d}z = \tfrac{1}{2} \left\{ z^2 J_n'^{\,2}(z) + \left(z^2 - n^2 \right) J_n^2(z) \right\}, \tag{4.11}$$

$$\int z J_n'^{\,2}(z)\mathrm{d}z = z J_n(z) J_n'(z) + \int z J_n^2(z)\mathrm{d}z - \int \frac{n^2}{z} J_n^2(z)\mathrm{d}z\,, \tag{4.12}$$

$$\int J_n(z) J_n'(z)\,\mathrm{d}z = \tfrac{1}{2} J_n^2(z)\,. \tag{4.13}$$

Substitution of these into (4.10a)–(4.10b) leads to

$$\begin{aligned} \Phi_n =& \left| H_n'^{(2)}(\kappa_1 R) \right|^2 \times \left\{ \frac{k_1^2 R^2}{\kappa_1^2} \left[J_n'^{\,2}(\kappa_1 R) + \left(1 - \frac{n^2}{\kappa_1^2 R^2} \right) J_n^2(\kappa_1 R) \right] \right. \\ & \left. + \frac{(k_z^2 + k_1^2)\, R}{\kappa_1^3} J_n'(\kappa_1 R) J_n(\kappa_1 R) \right\}, \end{aligned} \tag{4.14a}$$

$$\Gamma_n = \frac{2jk_1^2 \cos\theta_z^{\mathrm{pw}}}{\kappa_1^4} \sqrt{\epsilon_0\mu_0}\, n J_n^2(\kappa_1 R) \left| H_n'^{(2)}(\kappa_1 R) \right|^2. \tag{4.14b}$$

For the series in (4.9) to be bounded, as required by the Meixner finite energy condition stated in (2.11), the behaviors of Φ_n and Γ_n when $n \to \infty$ need to be

inspected. According to the characteristics of the Bessel and Hankel functions given in (B.22)–(B.25), we have for large order n:

$$J_n(z)H_n^{'(2)}(z) = -\frac{j}{\pi z}\left\{1 + O\left(\frac{z}{n}\right)^2\right\}, \tag{4.15a}$$

$$J_n'(z)H_n^{'(2)}(z) = -\frac{j|n|}{\pi z^2}\left\{1 + O\left(\frac{z}{n}\right)^2\right\}. \tag{4.15b}$$

Therefore, for large order n, the magnitudes of Φ_n and Γ_n are approximately $C|n|$ $\times \left\{1 + O\left(\kappa_1 R/n\right)^2\right\}$, for some constant C. As a result, the unknowns coefficients $\left\{a_n^{(1)}, b_n^{(1)}\right\}_{n\in\mathbb{Z}}$ are required to satisfy the following conditions

$$\sum_{n=-\infty}^{\infty} |n| \left|a_n^{(1)}\right|^2 < \infty \text{ and } \sum_{n=-\infty}^{\infty} |n| \left|b_n^{(1)}\right|^2 < \infty\,. \tag{4.16}$$

Due to the continuity condition, it is clear that the remaining pair of unknowns $\left\{a_n^{(0)}, b_n^{(0)}\right\}_{n\in\mathbb{Z}}$ (which are the coefficients for the scattered field in region 0) belong to the same solution class, as follows from (4.19) and (4.20).

4.3.3 Enforcing the MBC

The solution of the unknowns $\left\{a_n^{(i)}, b_n^{(i)}\right\}_{n\in\mathbb{Z}}$ $(i = 0, 1)$ can be obtained by applying the continuity condition and MBC on the contour of the CLR. The tangential components of the total electric field are continuous across the contour of the CLR as according to (2.6a). Thus,

$$\lim_{\rho\to R^+}\left(E_z^{\text{sc}} + E_z^{\text{inc}}\right) = \lim_{\rho\to R^-} E_z^{\text{tr}}\,, \tag{4.17}$$

$$\lim_{\rho\to R^+}\left(E_\phi^{\text{sc}} + E_\phi^{\text{inc}}\right) = \lim_{\rho\to R^-} E_\phi^{\text{tr}}\,. \tag{4.18}$$

for all $\phi \in (-\pi, \pi)$. As these components are matched over the entire contour of the CLR, the coefficients may be equated termwise,

$$a_n^{(0)} = a_n^{(1)} J_n(\kappa_1 R) H_n^{'(2)}(\kappa_1 R) - c_n(\kappa_0 R)\,, \tag{4.19}$$

$$\begin{aligned} b_n^{(0)} =& \frac{j\cos\theta_z^{\text{pw}}}{\eta_0\kappa_0 R}\left(\frac{\kappa_0^2}{\kappa_1^2} - 1\right) n a_n^{(1)} J_n(\kappa_1 R) H_n^{'(2)}(\kappa_1 R) \frac{H_n^{(2)}(\kappa_0 R)}{H_n^{'(2)}(\kappa_0 R)} \\ &+ \mu_r \frac{\kappa_0}{\kappa_1} b_n^{(1)} J_n'(\kappa_1 R) H_n^{'(2)}(\kappa_1 R) \frac{H_n^{(2)}(\kappa_0 R)}{H_n^{'(2)}(\kappa_0 R)}\,. \end{aligned} \tag{4.20}$$

Therefore, only $\left\{a_n^{(1)}, b_n^{(1)}\right\}_{n\in\mathbb{Z}}$ are left to be determined from the MBC.

According to (2.9a), the tangential components of the total electric field vanish on the PEC strip, $\Omega_{\rm PEC}$; *i.e.*,

$$\lim_{\rho\to R^+}\left(E_z^{\rm sc}+E_z^{\rm inc}\right)=0=\lim_{\rho\to R^-}E_z^{\rm tr}\,, \tag{4.21}$$

$$\lim_{\rho\to R^+}\left(E_\phi^{\rm sc}+E_\phi^{\rm inc}\right)=0=\lim_{\rho\to R^-}E_\phi^{\rm tr}\,. \tag{4.22}$$

Imposing these two conditions leads to the following series equations

$$\sum_{n=-\infty}^{\infty}a_n^{(1)}o_n e^{jn\phi}=0\quad(A)\,, \tag{4.23}$$

$$\sum_{n=-\infty}^{\infty}\left\{a_n^{(1)}p_n+b_n^{(1)}q_n\right\}e^{jn\phi}=0\quad(A)\,, \tag{4.24}$$

for $\phi\in(-\theta^{\rm PEC},\theta^{\rm PEC})$, where we introduce

$$o_n:=J_n(\kappa_1R)H_n^{'(2)}(\kappa_1R)\,, \tag{4.25}$$

$$p_n:=\frac{j\cos\theta_z^{\rm pw}}{\eta_0\mu_r\kappa_1R}\,n\,J_n(\kappa_1R)H_n^{'(2)}(\kappa_1R)\,, \tag{4.26}$$

$$q_n:=J_n'(\kappa_1R)H_n^{'(2)}(\kappa_1R)\,. \tag{4.27}$$

On the other hand, according to (2.9b), the tangential components of the total magnetic field are continuous across the aperture (where the PEC strip is absent), $\Omega_{\rm aper}$. Therefore, we have

$$\lim_{\rho\to R^+}\left(H_z^{\rm sc}+H_z^{\rm inc}\right)=\lim_{\rho\to R^-}H_z^{\rm tr}\,, \tag{4.28}$$

$$\lim_{\rho\to R^+}\left(H_\phi^{\rm sc}+H_\phi^{\rm inc}\right)=\lim_{\rho\to R^-}H_\phi^{\rm tr}\,, \tag{4.29}$$

for $\phi\in(\theta^{\rm PEC},\pi)\cup[-\pi,-\theta^{\rm PEC})$, which result in:

$$\sum_{n=-\infty}^{\infty}\left\{a_n^{(1)}r_n+b_n^{(1)}s_n\right\}e^{jn\phi}=0\quad(A)\,, \tag{4.30}$$

$$\sum_{n=-\infty}^{\infty}\left\{a_n^{(1)}t_n+b_n^{(1)}u_n+z_n\right\}e^{jn\phi}=0\quad(A)\,. \tag{4.31}$$

In the above series equations, the following coefficients have been introduced:

$$r_n:=\frac{j\cos\theta_z^{\rm pw}}{\eta_0\kappa_0R}\left(1-\frac{\kappa_0^2}{\kappa_1^2}\right)n\,J_n(\kappa_1R)H_n^{'(2)}(\kappa_1R)\frac{H_n^{(2)}(\kappa_0R)}{H_n^{'(2)}(\kappa_0R)}\,, \tag{4.32}$$

$$s_n:=J_n(\kappa_1R)H_n^{'(2)}(\kappa_1R)-\mu_r\frac{\kappa_0}{\kappa_1}J_n'(\kappa_1R)H_n^{'(2)}(\kappa_1R)\frac{H_n^{(2)}(\kappa_0R)}{H_n^{'(2)}(\kappa_0R)}\,, \tag{4.33}$$

$$t_n :=\epsilon_r\kappa_0 J_n'(\kappa_1 R)H_n^{'(2)}(\kappa_1 R) - \kappa_1 J_n(\kappa_1 R)H_n^{'(2)}(\kappa_1 R)\frac{H_n^{'(2)}(\kappa_0 R)}{H_n^{(2)}(\kappa_0 R)}$$
$$+ n^2\frac{\cos^2\theta_z^{\mathrm{pw}}\kappa_1}{\kappa_0^2 R^2}\left(1-\frac{\kappa_0^2}{\kappa_1^2}\right)J_n(\kappa_1 R)H_n^{'(2)}(\kappa_1 R)\frac{H_n^{(2)}(\kappa_0 R)}{H_n^{'(2)}(\kappa_0 R)}\,, \tag{4.34}$$

$$u_n :=n\frac{\eta_0\kappa_0\cos\theta_z^{\mathrm{pw}}}{j\kappa_1 R}\left[J_n(\kappa_1 R)H_n^{'(2)}(\kappa_1 R)\right.$$
$$\left.-\mu_r\frac{\kappa_1}{\kappa_0}J_n'(\kappa_1 R)H_n^{'(2)}(\kappa_1 R)\frac{H_n^{(2)}(\kappa_0 R)}{H_n^{'(2)}(\kappa_0 R)}\right]\,, \tag{4.35}$$

$$z_n :=\kappa_1\left[c_n(\kappa_0 R)\frac{H_n^{'(2)}(\kappa_0 R)}{H_n^{(2)}(\kappa_0 R)} - c_n'(\kappa_0 R)\right]\,. \tag{4.36}$$

From (B.14) and (B.16), we can see that for $n = 1, 2, \ldots$, if we have $h_n \equiv \{o_n, q_n, s_n, t_n\}$, then $h_n = h_{-n}$; whereas when $h_n \equiv \{p_n, r_n, u_n\}$, we have $h_n = -h_{-n}$. In addition, by using the Wronskian identity given in (B.17), $\{z_n\}_{n\in\mathbb{Z}}$ (which collects all the information about the incident field) can be simplified to

$$z_n = -\frac{2A_0\kappa_1\sin\theta_z^{\mathrm{pw}}j^{n+1}e^{-jn\theta_x^{\mathrm{pw}}}}{\pi\kappa_0 R\,H_n^{(2)}(\kappa_0 R)}\,. \tag{4.37}$$

Due to the symmetry of the intervals $(-\theta^{\mathrm{PEC}}, \theta^{\mathrm{PEC}})$ and $(-\pi, -\theta^{\mathrm{PEC}}) \cup (\theta^{\mathrm{PEC}}, \pi)$, the four series equations (4.23), (4.24), (4.30) and (4.31) remain valid when ϕ is replaced by $-\phi$. These equations defined over $(-\pi, \pi)$ are thus equivalent to the following four sets of DSE defined over $(0, \pi)$ in terms of the trigonometric functions,

$$\begin{cases} a_0^{(1)}o_0 + \displaystyle\sum_{n=1}^{\infty} x_n^{(1)}o_n\cos n\phi = 0\ (A),\ \phi\in(0,\theta^{\mathrm{PEC}}), & \text{(4.38a)}\\ a_0^{(1)}t_0 + z_0 + \displaystyle\sum_{n=1}^{\infty}\left[x_n^{(1)}t_n + y_n^{(2)}u_n + nz_n^{(1)}\right]\cos n\phi = 0\ (A),\ \phi\in(\theta^{\mathrm{PEC}},\pi), & \text{(4.38b)}\end{cases}$$

$$\begin{cases} \displaystyle\sum_{n=1}^{\infty}\left[x_n^{(1)}p_n + y_n^{(2)}q_n\right]\sin n\phi = 0\ (A), & \phi\in(0,\theta^{\mathrm{PEC}}), & \text{(4.39a)}\\ \displaystyle\sum_{n=1}^{\infty}\left[x_n^{(1)}r_n + y_n^{(2)}s_n\right]\sin n\phi = 0\ (A), & \phi\in(\theta^{\mathrm{PEC}},\pi), & \text{(4.39b)}\end{cases}$$

$$\begin{cases} b_0^{(1)}q_0 + \displaystyle\sum_{n=1}^{\infty}\left[y_n^{(1)}p_n + x_n^{(2)}q_n\right]\cos n\phi = 0\ (A), & \phi\in(0,\theta^{\mathrm{PEC}}), & \text{(4.40a)}\\ b_0^{(1)}s_0 + \displaystyle\sum_{n=1}^{\infty}\left[y_n^{(1)}r_n + x_n^{(2)}s_n\right]\cos n\phi = 0\ (A), & \phi\in(\theta^{\mathrm{PEC}},\pi), & \text{(4.40b)}\end{cases}$$

$$\begin{cases} \displaystyle\sum_{n=1}^{\infty} y_n^{(1)} o_n \sin n\phi = 0 \ (A), & \phi \in (0, \theta^{\mathrm{PEC}}), \qquad (4.41a) \\ \displaystyle\sum_{n=1}^{\infty} \left[y_n^{(1)} t_n + x_n^{(2)} u_n + n z_n^{(2)} \right] \sin n\phi = 0 \ (A), & \phi \in (\theta^{\mathrm{PEC}}, \pi), \qquad (4.41b) \end{cases}$$

where the following notations are used:

$$x_n^{(1)} := a_n^{(1)} + a_{-n}^{(1)}, \qquad x_n^{(2)} := b_n^{(1)} + b_{-n}^{(1)}, \qquad (4.42a)$$

$$y_n^{(1)} := a_n^{(1)} - a_{-n}^{(1)}, \qquad y_n^{(2)} := b_n^{(1)} - b_{-n}^{(1)}, \qquad (4.42b)$$

$$z_n^{(1)} := \frac{z_n + z_{-n}}{n}, \qquad z_n^{(2)} := \frac{z_n - z_{-n}}{n}, \qquad (4.42c)$$

for $n = 1, 2, 3, \ldots$ It can be easily seen that the new coefficients $\left\{ x_n^{(i)}, y_n^{(i)} \right\}_{n=1}^{\infty}$ $(i = 0, 1)$ belong to the same solution class as $\left\{ a_n^{(1)}, b_n^{(1)} \right\}_{n \in \mathbb{Z}}$ and thus, also satisfy the Fejér's Tauberian condition (D.4).

For the normal incidence problem, $\{p_n, r_n, u_n\}_{n=1}^{\infty} \equiv 0$, and the four sets of DSE decouple. The formulation above reduces to the E-polarization formulation (or the H-polarization formulation if the TE_z incidence is considered) by merely enforcing $H_z \equiv 0$ (or $E_z \equiv 0$). In other words, the second and third sets (4.39) and (4.40) are redundant for the TM_z normal incidence problem, as solving these homogeneous DSE leads to the trivial solutions; *i.e.*, $\left\{ x_n^{(2)}, y_n^{(2)} \right\}_{n=1}^{\infty} \equiv 0$.

For the oblique incident problem, both sets of the DSE (4.38) and (4.39) involve $\left\{ x_n^{(1)}, y_n^{(2)} \right\}_{n=-\infty}^{\infty}$. As a result, these two sets of DSE are coupled, and need to be solved simultaneously. Similarly, the remaining two sets of DSE (4.40) and (4.41) are coupled, as they both involve $\left\{ x_n^{(2)}, y_n^{(1)} \right\}_{n=-\infty}^{\infty}$.

4.4 Regularization process

Each of the four sets of DSE derived in Subsection 4.3.3 is regularized to an ISLAE using MoR, by first introducing the asymptotically small parameters to extract the singular parts of the series equations. As two pairs of coupled DSE — the first pair: (4.38), (4.39) and the second pair: (4.40), (4.41) — are involved, each pair of the coupled ISLAE can be written in the form of a 2-by-2 block matrix equation. Each of the block matrix operators encountered will be shown to be a compact perturbation of the identity operator in ℓ_2.

4.4.1 Introducing the asymptotically small parameters

The first step of the regularization process lies in the identification of suitable asymptotically small parameters, so that the singular part of each of the series equations can be extracted. By using the asymptotic formulas given in Appendix B.2.1, we deduce that, when $n \to +\infty$,

$$o_n = -\frac{j}{\pi\kappa_1 R}\left\{1 + O\left(\frac{\kappa_1^2 R^2}{n^2}\right)\right\}, \tag{4.43a}$$

$$p_n = \frac{n\cos\theta_z^{\mathrm{pw}}}{\pi\kappa_1^2 R^2 \mu_r \eta_0}\left\{1 + O\left(\frac{\kappa_1^2 R^2}{n^2}\right)\right\}, \tag{4.43b}$$

$$q_n = -\frac{jn}{\pi\kappa_1^2 R^2}\left\{1 + O\left(\frac{\kappa_1^2 R^2}{n^2}\right)\right\}, \tag{4.43c}$$

$$r_n = -\frac{\cos\theta_z^{\mathrm{pw}}}{\pi\kappa_1 R\eta_0}\left(1 - \frac{\kappa_0^2}{\kappa_1^2}\right)\left\{1 + O\left(\frac{\kappa_1^2 R^2}{n^2}\right)\right\}, \tag{4.43d}$$

$$s_n = -\frac{j}{\pi\kappa_1 R}\left(1 + \mu_r\frac{\kappa_0^2}{\kappa_1^2}\right)\left\{1 + O\left(\frac{\kappa_1^2 R^2}{n^2}\right)\right\}, \tag{4.43e}$$

$$t_n = -\frac{jn\zeta}{\pi\kappa_0 R^2}\left\{1 + O\left(\frac{\kappa_1^2 R^2}{n^2}\right)\right\}. \tag{4.43f}$$

$$u_n = -\frac{n\cos\theta_z^{\mathrm{pw}}\eta_0\kappa_0(1+\mu_r)}{\pi\kappa_1^2 R^2}\left\{1 + O\left(\frac{\kappa_1^2 R^2}{n^2}\right)\right\}. \tag{4.43g}$$

In (4.43f), we have introduced the constant ζ for brevity:

$$\zeta = 1 + \epsilon_r\frac{\kappa_0^2}{\kappa_1^2} - \cos^2\theta_z^{\mathrm{pw}}\left(1 - \frac{\kappa_0^2}{\kappa_1^2}\right). \tag{4.44}$$

It is worth noting that, $\zeta \neq 0$, and $\zeta \geq (1+\epsilon_r)\,(\kappa_0^2/\kappa_1^2)$, for all values of θ_z^{pw}.

Considering above observation, asymptotically small parameters of magnitude $O\left(n^{-2}\right)$ when $n \to +\infty$ can be introduced. These parameters are denoted with a tilde above their corresponding counterparts. For $n = 1, 2, 3, \ldots$, we define

$$\tilde{o}_n := 1 - (j\pi\kappa_1 R)\, o_n, \tag{4.45a}$$

$$\tilde{p}_n := 1 - \left(\frac{\mu_r\eta_0\pi\kappa_1^2 R^2}{\cos\theta_z^{\mathrm{pw}} n}\right) p_n = 1 - (j\pi\kappa_1 R)\, o_n = \tilde{o}_n, \tag{4.45b}$$

$$\tilde{q}_n := 1 - \left(\frac{j\pi\kappa_1^2 R^2}{n}\right) q_n, \tag{4.45c}$$

$$\tilde{r}_n := 1 + \left(\frac{\eta_0\pi\kappa_1^3 R}{\cos\theta_z^{\mathrm{pw}}(\kappa_1^2 - \kappa_0^2)}\right) r_n = 1 + \left(\frac{j\pi\kappa_1 n}{\kappa_0}\right)\frac{H_n^{(2)}(\kappa_0 R)}{H_n^{\prime(2)}(\kappa_0 R)}\, o_n, \tag{4.45d}$$

$$\tilde{s}_n := 1 - \left(\frac{j\pi\kappa_1^3 R}{\kappa_1^2 + \mu_r\kappa_0^2}\right) s_n, \tag{4.45e}$$

$$\tilde{t}_n := 1 - \left(\frac{j\pi\kappa_0 R^2}{\zeta n}\right) t_n \,, \tag{4.45f}$$

$$\begin{aligned}\tilde{u}_n &:= 1 + \frac{\pi\kappa_1^2 R^2}{(1+\mu_r)\cos\theta_z^{\mathrm{pw}}\eta_0\kappa_0 n}\, u_n \,, \\ &= 1 + \frac{\pi\kappa_1 R}{j(1+\mu_r)}\left[o_n - \mu_r \frac{\kappa_1}{\kappa_0}\frac{H_n^{(2)}(\kappa_0 R)}{H_n^{\prime(2)}(\kappa_0 R)}\, q_n\right].\end{aligned} \tag{4.45g}$$

The behaviors of these parameters for three different values of wavenumber ($k_0 =$ 20, 50 and 100) are shown in Figure 4.1, where $R = 1$, $(\epsilon_r, \mu_r) = (2.1, 1)$ (PTFE), and $\theta_z^{\mathrm{pw}} = \frac{\pi}{3}$. The plots for the parameter $\{\tilde{o}_n\}_{n=1}^{\infty}$ are omitted, as $\tilde{o}_n = \tilde{p}_n$, for all n. The top sub-figures for each parameter are plotted on logarithmic scale for both axes. By comparison with the function $f(n) = n^{-2}$ (or $f(n) = n^{-3}$ for $\{\tilde{p}_n\}_{n=1}^{\infty}$) displayed as the green dot-dashed line, it is clear that all of the parameters are of order at least $O\left(n^{-2}\right)$ for large n. For a closer examination of the decay rates of these parameters, the bottom sub-figures are plotted on logarithmic scale for the vertical axis only. Evidently, all the parameters decay rapidly once $n > \kappa_1 R$. Therefore, it is only sensible to chose a truncation number N_{tr} that is somewhat greater than $\kappa_1 R$ in the final step of matrix truncation.

By substitution of these asymptotically small parameters into (4.38)–(4.41), the four pairs of DSE can be rewritten with the singular parts isolated as:

$$\begin{cases} a_0^{(1)}\tilde{o}_0 + \displaystyle\sum_{n=1}^{\infty} x_n^{(1)}\left(1-\tilde{o}_n\right)\cos n\phi = 0 \ (A), & \phi \in (0, \theta^{\mathrm{PEC}}), \quad (4.46a) \\ a_0^{(1)}\tilde{t}_0 + \tilde{z}_0 + \displaystyle\sum_{n=1}^{\infty} n\left[x_n^{(1)}\left(1-\tilde{t}_n\right)\right. & \\ \left. \quad + y_n^{(2)}\left(1-\tilde{u}_n\right)\varsigma + \tilde{z}_n^{(1)}\right]\cos n\phi = 0 \ (A), & \phi \in (\theta^{\mathrm{PEC}}, \pi), \quad (4.46b) \end{cases}$$

$$\begin{cases} \displaystyle\sum_{n=1}^{\infty} n\left[x_n^{(1)}\left(1-\tilde{p}_n\right)\tau + y_n^{(2)}\left(1-\tilde{q}_n\right)\right]\sin n\phi = 0 \ (A), & \phi \in (0, \theta^{\mathrm{PEC}}), \quad (4.47a) \\ \displaystyle\sum_{n=1}^{\infty} \left[x_n^{(1)}\left(1-\tilde{r}_n\right)\upsilon + y_n^{(2)}\left(1-\tilde{s}_n\right)\right]\sin n\phi = 0 \ (A), & \phi \in (\theta^{\mathrm{PEC}}, \pi), \quad (4.47b) \end{cases}$$

$$\begin{cases} b_0^{(1)}\tilde{q}_0 + \displaystyle\sum_{n=1}^{\infty} n\left[y_n^{(1)}\left(1-\tilde{p}_n\right)\tau + x_n^{(2)}\left(1-\tilde{q}_n\right)\right]\cos n\phi = 0\,(A), & \phi \in (0, \theta^{\mathrm{PEC}}), \quad (4.48a) \\ b_0^{(1)}\tilde{s}_0 + \displaystyle\sum_{n=1}^{\infty} \left[y_n^{(1)}\left(1-\tilde{r}_n\right)\upsilon + x_n^{(2)}\left(1-\tilde{s}_n\right)\right]\cos n\phi = 0\,(A), & \phi \in (\theta^{\mathrm{PEC}}, \pi), \quad (4.48b) \end{cases}$$

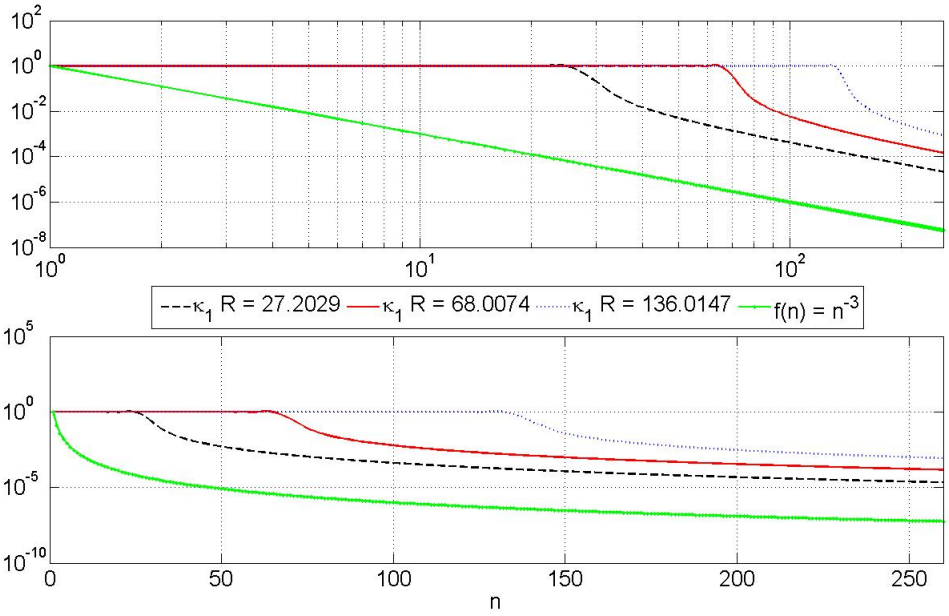
10^{2}
10^{0}
10^{-2}
10^{-4}
10^{-6}
10^{-8}
10^{0}
10^{1}
10^{2}
---κ_1 R = 27.2029 —κ_1 R = 68.0074 ·····κ_1 R = 136.0147 —f(n) = n^{-3}
10^{5}
10^{0}
10^{-5}
10^{-10}
0
50
100
150
200
250
n

(a) p_n

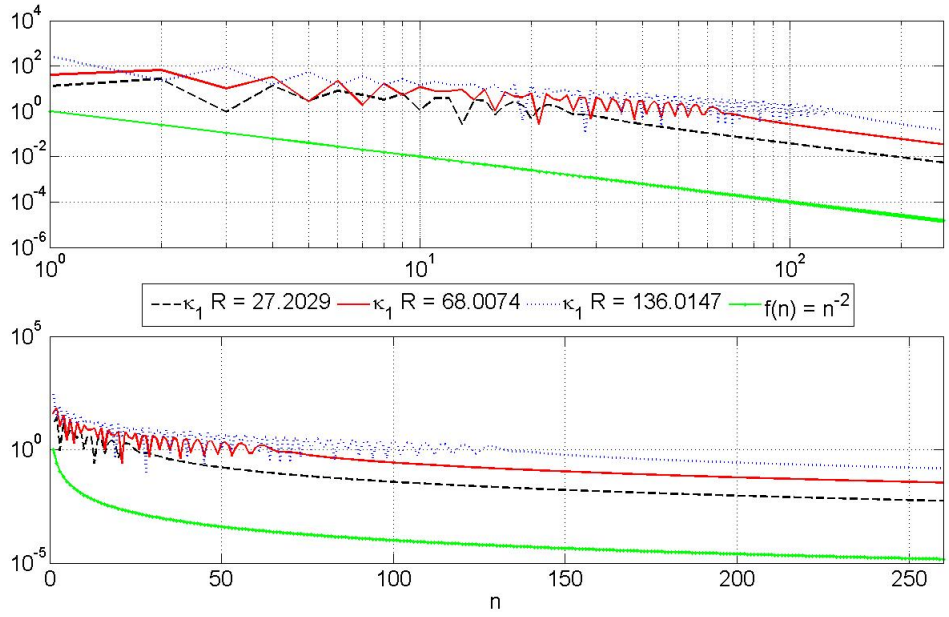
10^{4}
10^{2}
10^{0}
10^{-2}
10^{-4}
10^{-6}
10^{0}
10^{1}
10^{2}
---κ_1 R = 27.2029 —κ_1 R = 68.0074 ·····κ_1 R = 136.0147 —f(n) = n^{-2}
10^{5}
10^{0}
10^{-5}
0
50
100
150
200
250
n

(b) q_n

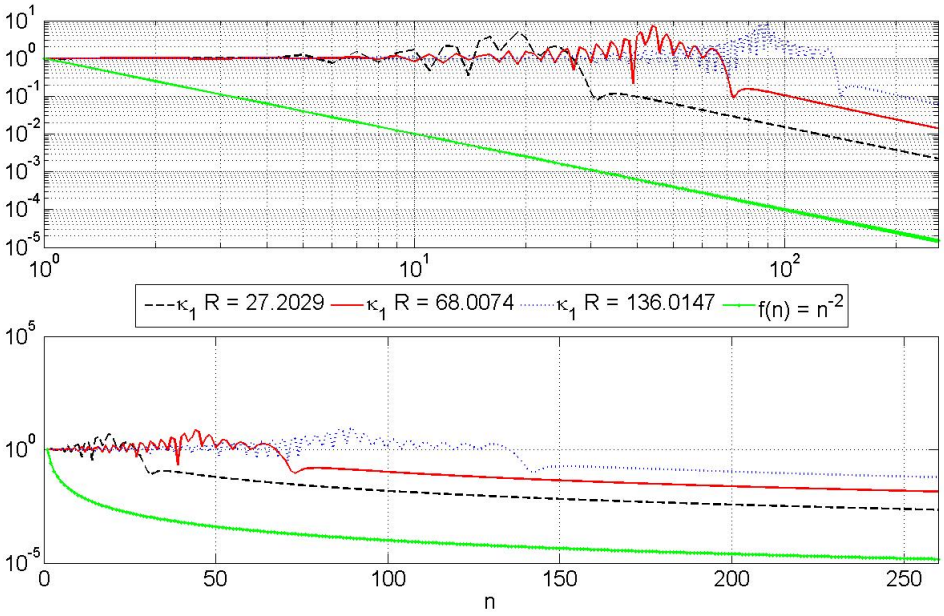
10^{1}
10^{0}
10^{-1}
10^{-2}
10^{-3}
10^{-4}
10^{-5}
10^{0}
10^{1}
10^{2}
---κ_1 R = 27.2029
κ_1 R = 68.0074
κ_1 R = 136.0147
f(n) = n^{-2}
10^{5}
10^{0}
10^{-5}
0
50
100
150
200
250
n

(c) r_n

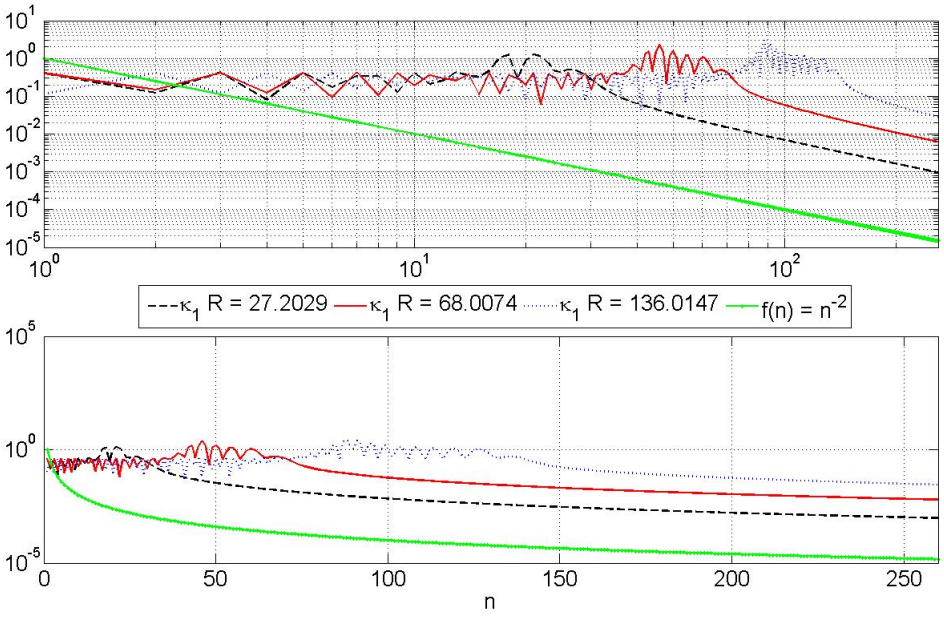
10^{1}
10^{0}
10^{-1}
10^{-2}
10^{-3}
10^{-4}
10^{-5}
10^{0}
10^{1}
10^{2}
---κ_1 R = 27.2029
κ_1 R = 68.0074
κ_1 R = 136.0147
f(n) = n^{-2}
10^{5}
10^{0}
10^{-5}
0
50
100
150
200
250
n

(d) s_n

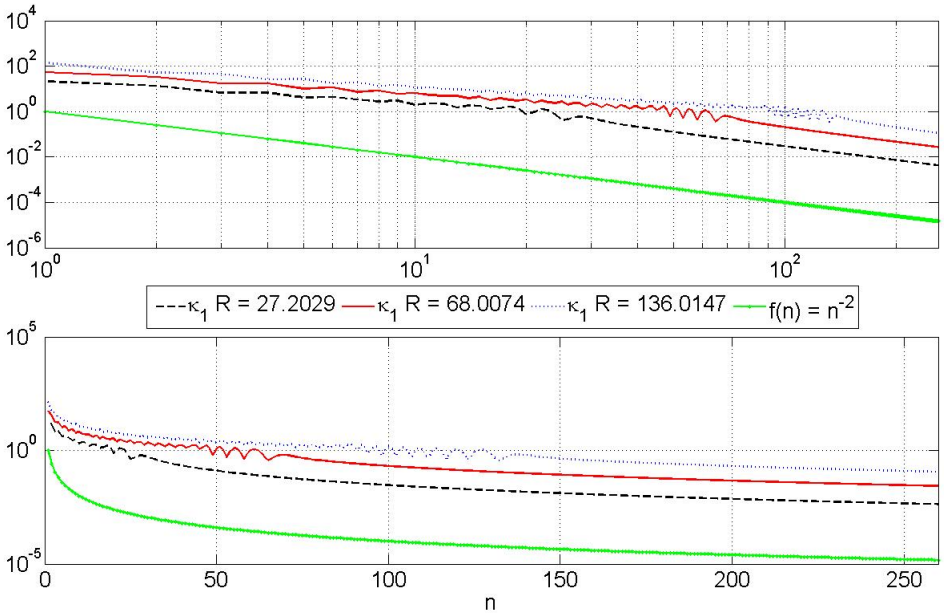

(e) t_n

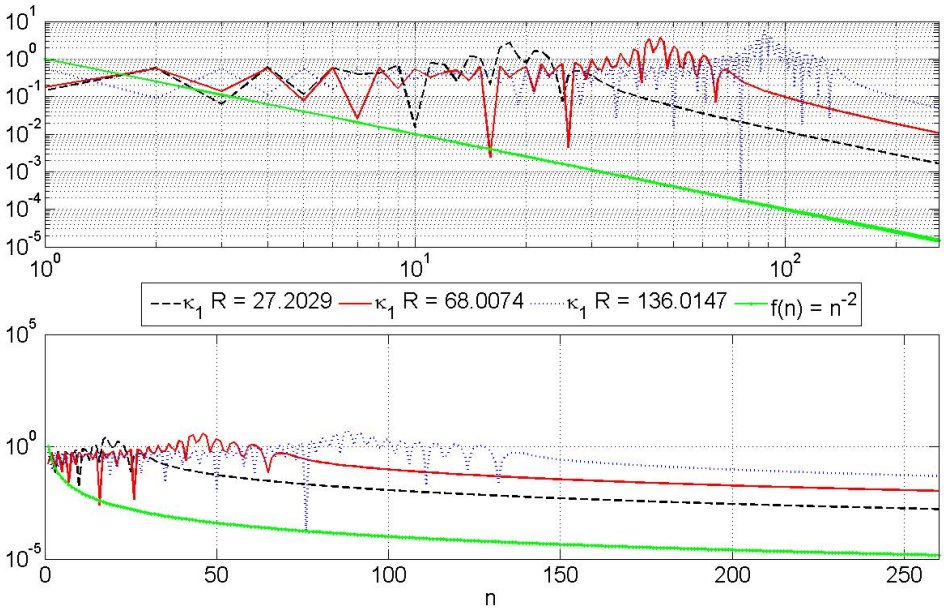

(f) u_n

Figure 4.1: The magnitude of the asymptotically small parameters as n increases, at different values of k_0: $k_0 = 20$ (black dashed), $k_0 = 50$ (red solid), $k_0 = 100$ (blue dotted), $f(n) = n^{-2}$ or $f(n) = n^{-3}$ (green dot-dashed). $[\epsilon_r = 2.1, \mu_r = 1, R = 1, \theta_z^{\text{pw}} = \frac{\pi}{3}]$

$$\begin{cases} \displaystyle\sum_{n=1}^{\infty} y_n^{(1)}\,(1-\tilde{o}_n)\sin n\phi = 0\ (A),\ \phi\in(0,\theta^{\mathrm{PEC}}), & \text{(4.49a)} \\ \displaystyle\sum_{n=1}^{\infty} n\left[y_n^{(1)}\left(1-\tilde{t}_n\right)+x_n^{(2)}\,(1-\tilde{u}_n)\,\varsigma+\tilde{z}_n^{(2)}\right]\sin n\phi = 0\ (A),\ \phi\in(\theta^{\mathrm{PEC}},\pi), & \text{(4.49b)} \end{cases}$$

where the following parameters have been introduced:

$$\varsigma := \frac{\eta_0\cos\theta_z^{\mathrm{pw}}(1+\mu_r)\kappa_0^2}{j\zeta\kappa_1^2}\,, \qquad \tau := \frac{j\cos\theta_z^{\mathrm{pw}}}{\eta_0\mu_r}\,, \qquad \upsilon := \frac{(\kappa_1^2-\kappa_0^2)\cos\theta_z^{\mathrm{pw}}}{j\eta_0\left(\kappa_1^2+\mu_r\kappa_0^2\right)}\,, \tag{4.50a}$$

$$\tilde{o}_0 := j\pi\kappa_1 R\,o_0\,, \qquad \tilde{q}_0 := j\pi\kappa_1^2R^2\,q_0\,, \qquad \tilde{s}_0 := \frac{j\pi\kappa_1^3R}{\kappa_1^2+\mu_r\kappa_0^2}\,s_0\,, \tag{4.50b}$$

$$\tilde{t}_0 := \frac{j\pi\kappa_0R^2}{\zeta}\,t_0\,, \qquad \tilde{z}_0 := \frac{j\pi\kappa_0R^2}{\zeta}\,z_0\,, \qquad \tilde{z}_n^{(1,2)} := \frac{j\pi\kappa_0R^2}{\zeta}\,z_n^{(1,2)}\,. \tag{4.50c}$$

4.4.2 Conversion to ISLAE

Each of the four sets of DSE given in (4.46)–(4.49) can be regularized to a second kind ISLAE following the steps described in Chapter 3. The four sets form two independent pairs of interconnected DSE; *i.e.*, the first pair: (4.46), (4.47) and the second pair: (4.48), (4.49). In the following, each of these two pairs are reformulated as a 2-by-2 block matrix equation, which is subsequently shown to be a second kind Fredholm equation.

The first pair of coupled DSE (4.46) **and** (4.47) We start by considering the first pair, (4.46) and (4.47), from which the unknowns $a_0^{(1)}$ and $\left\{x_n^{(1)},y_n^{(2)}\right\}_{n=1}^{\infty}$ are to be determined. For the DSE given in (4.46), we make the following replacement in (3.27): $a\mapsto\tilde{o}_0$, $b\mapsto\tilde{t}_0$, $c\mapsto 0$, $d\mapsto\tilde{z}_0$, $x_0\mapsto x_0^{(1)}$, $x_n\mapsto x_n^{(1)}$, $s_n\mapsto\tilde{o}_n$, $t_n\mapsto\tilde{t}_n$, $e_n\mapsto 0$, $f_n\mapsto y_n^{(2)}\,(1-\tilde{u}_n)\,\varsigma+\tilde{z}_n^{(1)}$, $x_0\mapsto a_0^{(1)}$, $x_n\mapsto x_n^{(1)}$, and $\psi_0\mapsto\cos\theta^{\mathrm{PEC}}=\psi_{\mathrm{PEC}}$. The notation $\psi_{\mathrm{PEC}}=\cos\theta^{\mathrm{PEC}}$ has been introduced for brevity. An equation for $a_0^{(1)}$ in terms of $\left\{x_n^{(1)},y_n^{(2)}\right\}_{n=1}^{\infty}$ is obtained from (3.27) as

$$\begin{aligned} a_0^{(1)} =& \frac{-\tilde{z}_0\ln\left(\frac{1-\psi_{\mathrm{PEC}}}{2}\right)}{\tilde{t}_0\ln\left(\frac{1-\psi_{\mathrm{PEC}}}{2}\right)-\tilde{o}_0}+\frac{1+\psi_{\mathrm{PEC}}}{\sqrt{2}\left[\tilde{t}_0\ln\left(\frac{1-\psi_{\mathrm{PEC}}}{2}\right)-\tilde{o}_0\right]} \\ & \times\sum_{n=1}^{\infty}\sqrt{n}\left[x_n^{(1)}\left(\tilde{t}_n-\tilde{o}_n\right)-y_n^{(2)}\,(1-\tilde{u}_n)\,\varsigma-\tilde{z}_n^{(1)}\right]\frac{\hat{P}_{n-1}^{(0,1)}(\psi_{\mathrm{PEC}})}{n}\,. \end{aligned} \tag{4.51}$$

An ISLAE in terms of $\left\{x_n^{(1)}, y_n^{(2)}\right\}_{n=1}^{\infty}$ can be derived from (3.28) as

$$\begin{aligned}
&\sqrt{m}\left[x_m^{(1)}\left(1-\tilde{t}_m\right)+y_m^{(2)}\left(1-\tilde{u}_m\right)\varsigma\right] \\
&+\sum_{n=1}^{\infty}\sqrt{n}\left[x_n^{(1)}\left(\tilde{t}_n-\tilde{o}_n\right)-y_n^{(2)}\left(1-\tilde{u}_n\right)\varsigma\right]\hat{R}_{m-1,n-1}(\psi_{\mathrm{PEC}}) \\
&=-\frac{\sqrt{2}(1+\psi_{\mathrm{PEC}})\,\tilde{o}_0\,\tilde{z}_0}{\tilde{t}_0\ln\left(\frac{1-\psi_{\mathrm{PEC}}}{2}\right)-\tilde{o}_0}\frac{\hat{P}_{m-1}^{(0,1)}(\psi_{\mathrm{PEC}})}{m}-\sqrt{m}\tilde{z}_m^{(1)}+\sum_{n=1}^{\infty}\sqrt{n}\tilde{z}_n^{(1)}\hat{R}_{m-1,n-1}(\psi_{\mathrm{PEC}})\,,
\end{aligned} \tag{4.52}$$

for $m=1,2,3,\ldots$, where

$$\hat{R}_{m-1,n-1}(\psi_{\mathrm{PEC}}):=\hat{Q}_{m-1,n-1}^{(1,0)}(\psi_{\mathrm{PEC}})-\frac{\tilde{t}_0(1+\psi_{\mathrm{PEC}})^2}{\tilde{t}_0\ln\left(\frac{1-\psi_{\mathrm{PEC}}}{2}\right)-\tilde{o}_0}\frac{\hat{P}_{m-1}^{(0,1)}(\psi_{\mathrm{PEC}})}{m}\frac{\hat{P}_{n-1}^{(0,1)}(\psi_{\mathrm{PEC}})}{n}\,. \tag{4.53}$$

For the second set of DSE, (4.47a) defined over $(0,\theta^{\mathrm{PEC}})$ is slower converging than (4.47b) defined over $(\theta^{\mathrm{PEC}},\pi)$. Thus, the DSE (4.47) has the same form as that of the companion set given in (3.50). By making the following replacements in (3.51): $s_n\mapsto\tilde{s}_n$, $t_n\mapsto\tilde{q}_n$, $g_n\mapsto x_n^{(1)}\left(1-\tilde{r}_n\right)\upsilon$, $h_n\mapsto x_n^{(1)}\left(1-\tilde{p}_n\right)\tau$, $y_n\mapsto y_n^{(2)}$, and $\psi_0\mapsto\psi_{\mathrm{PEC}}$, we get another ISLAE involving $\left\{x_n^{(1)}, y_n^{(2)}\right\}_{n=1}^{\infty}$:

$$\begin{aligned}
&\sqrt{m}\left[x_m^{(1)}\left(1-\tilde{r}_m\right)\upsilon+y_m^{(2)}\left(1-\tilde{s}_m\right)\right] \\
&+\sum_{n=1}^{\infty}\sqrt{n}\left\{x_n^{(1)}\left[\left(1-\tilde{p}_n\right)\tau-\left(1-\tilde{r}_n\right)\upsilon\right]+y_n^{(2)}\left(\tilde{s}_n-\tilde{q}_n\right)\right\}\hat{Q}_{m-1,n-1}^{(1,0)}(\psi_{\mathrm{PEC}})=0\,,
\end{aligned} \tag{4.54}$$

for $m=1,2,3,\ldots$

Writing (4.52) and (4.54) in matrix operator form gives

$$\left[\mathcal{F}_1-\mathcal{C}_1\right]\left(\begin{array}{c}\mathbf{x}_1\\ \hdashline \mathbf{y}_2\end{array}\right)=\left(\begin{array}{c}\mathbf{z}_1\\ \hdashline 0\end{array}\right), \tag{4.55}$$

where the block matrix operators below have been introduced to facilitate following discussion about the advantages of this final form of system:

$$\mathcal{F}_1:=\left(\begin{array}{c:c}\mathcal{I}&0\\ \hdashline 0&\mathcal{I}\end{array}\right)+\left(\begin{array}{c:c}0&\varsigma\left(\mathcal{I}-\mathcal{H}_1\right)\\ \hdashline \upsilon\left(\mathcal{I}-\mathcal{H}_1\right)+\tau\mathcal{H}_1&0\end{array}\right), \tag{4.56}$$

$$\mathcal{C}_1:=\left(\begin{array}{c:c}\mathcal{T}-\left(\mathcal{H}_1-\mathcal{H}_2\right)\left(\mathcal{T}-\mathcal{O}\right)&\varsigma\left(\mathcal{I}-\mathcal{H}_1+\mathcal{H}_2\right)\mathcal{U}-\varsigma\mathcal{H}_2\\ \hdashline \upsilon\left(\mathcal{I}-\mathcal{H}_1\right)\mathcal{R}+\tau\mathcal{H}_1\mathcal{P}&\left(\mathcal{I}-\mathcal{H}_1\right)\mathcal{S}+\mathcal{H}_1\mathcal{Q}\end{array}\right). \tag{4.57}$$

Here, $\mathcal{I}$ denotes the identity operator, $\mathcal{O}$, $\mathcal{P}$, $\mathcal{Q}$, $\mathcal{R}$, $\mathcal{S}$, $\mathcal{T}$ and $\mathcal{U}$ denotes the diagonal operators formed from $\left\{\tilde{o}_n,\tilde{p}_n,\tilde{q}_n,\tilde{r}_n,\tilde{s}_n,\tilde{t}_n,\tilde{u}_n\right\}_{n=1}^{\infty}$. In addition, the following

operators are introduced for brevity,

$$[\mathcal{H}_1]_{n,m} := \hat{Q}^{(1,0)}_{m-1,n-1}(\psi_{\rm PEC})\,, \tag{4.58}$$

$$[\mathcal{H}_2]_{n,m} := \frac{\tilde{t}_0(1+\psi_{\rm PEC})^2}{\tilde{t}_0 \ln\left(\frac{1-\psi_{\rm PEC}}{2}\right) - \tilde{o}_0} \frac{\hat{P}^{(0,1)}_{m-1}(\psi_{\rm PEC})}{m} \frac{\hat{P}^{(0,1)}_{n-1}(\psi_{\rm PEC})}{n}\,, \tag{4.59}$$

for $n, m = 1, 2, \ldots$ The column vectors $\mathbf{x}_1$ and $\mathbf{y}_2$ denote the scaled unknowns $\left\{\sqrt{n}x_n^{(1)}, \sqrt{n}y_n^{(2)}\right\}_{n=1}^{\infty}$, respectively, while the right hand vector $\mathbf{z}_1$ denote the infinite sequence on the right side of (4.52)

$$\begin{aligned}[\mathbf{z}_1]_n := & -\frac{\sqrt{2}(1+\psi_{\rm PEC})\,\tilde{o}_0\,\tilde{z}_0}{\tilde{t}_0 \ln\left(\frac{1-\psi_{\rm PEC}}{2}\right) - \tilde{o}_0} \frac{\hat{P}^{(0,1)}_{m-1}(\psi_{\rm PEC})}{m} \\ & - \sqrt{m}\tilde{z}^{(1)}_m + \sum_{n=1}^{\infty} \sqrt{n}\tilde{z}^{(1)}_n \hat{R}_{m-1,n-1}(\psi_{\rm PEC})\,. \end{aligned} \tag{4.60}$$

Recalling the observations made in Subsection 3.2.5, all the diagonal matrices formed from the asymptotically small parameters (*i.e.*, $\mathcal{O}$, $\mathcal{P}$, $\mathcal{Q}$, $\mathcal{R}$, $\mathcal{S}$, $\mathcal{T}$ and $\mathcal{U}$) are compact in the Hilbert space, ℓ_2. At the same time, from its definition in (4.59), $\mathcal{H}_2$ is clearly symmetric, and satisfies the following because of (B.34):

$$\sum_n \sum_m \left|[\mathcal{H}_2]_{n,m}\right|^2 < \infty\,. \tag{4.61}$$

Hence, $\mathcal{H}_2$ is also a compact operator. On the other hand, the matrix operator $\mathcal{H}_1$, with entries in terms of the incomplete scalar product $\hat{Q}^{(1,0)}_{m,n}(\psi_{\rm PEC})$, is a projection operator having norm at most 1. It is symmetric, bounded, idempotent, and dependent only on $\theta^{\rm PEC}$.

From these properties of the sub-matrices, it can be readily deduced that the block matrix operator $\mathcal{C}_1$ is a compact operator. Although $\mathcal{F}_1$ takes more complicated form that those encountered in Chapter 3, and cannot be readily deduced as a Fredholm operator, (4.55) can be shown to be similar to those matrix operator equations discussed in Chapter 3 as follows.

From the idempotent properties of $\mathcal{H}_1$; *i.e.*, $\mathcal{H}_1(\mathcal{I}-\mathcal{H}_1) = (\mathcal{I}-\mathcal{H}_1)\mathcal{H}_1 = 0$, and $\mathcal{H}_1^2 = \mathcal{H}_1$, the following bounded matrix operator can be easily checked to be the inverse operator of $\mathcal{F}_1$:

$$\mathcal{F}_1^{-1} = \left(\begin{array}{c:c} \xi\mathcal{I} + (1-\xi)\,\mathcal{H}_1 & \varsigma\xi\,(\mathcal{H}_1 - \mathcal{I}) \\ \hdashline \upsilon\xi\,(\mathcal{H}_1 - \mathcal{I}) - \tau\mathcal{H}_1 & \xi\mathcal{I} + (1-\xi)\,\mathcal{H}_1 \end{array}\right)\,, \tag{4.62}$$

where the notation $\xi = (1-\varsigma\upsilon)^{-1}$ is introduced. It can be readily checked that $\xi \geq 1$ for $\epsilon_r, \mu_r \geq 1$, and it is independent of ω. Left multiplication of $\mathcal{F}_1^{-1}$ on both sides of (4.55) leads to

$$\left[\mathcal{I} - \mathcal{F}_1^{-1}\mathcal{C}_1\right] \begin{pmatrix} \mathbf{x}_1 \\ \cdots \\ \mathbf{y}_2 \end{pmatrix} = \mathcal{F}_1^{-1} \begin{pmatrix} \mathbf{z}_1 \\ \cdots \\ 0 \end{pmatrix}, \tag{4.63}$$

which enjoys the same advantages as those discussed in Chapter 3, because $\mathcal{F}_1^{-1}\mathcal{C}_1$ is a compact operator and (4.63) is second kind Fredholm. Suppose truncation number $N_{\rm tr}$ is used to truncate each of the infinite systems (4.52) and (4.54). The $2N_{\rm tr}$-by-$2N_{\rm tr}$ block matrix $(\mathcal{F}_1 - \mathcal{C}_1)$ is solved numerically by MATLAB; *i.e.*, by a standard process of Gaussian elimination for the results obtained in the thesis. As $(\mathcal{F}_1 - \mathcal{C}_1)$ is a complex perturbation of the identity, and there are no modes for the range of axial wavenumbers under consideration, iterative methods also provide an attractive alternative to solving this linear system. By increasing $N_{\rm tr}$, the solutions $\left\{x_n^{(1)}, y_n^{(2)}\right\}_{n=1}^{N_{\rm tr}}$ computed with the truncated systems converge to the exact solution.

The second pair of coupled SE (4.48) **and** (4.49) Similarly, we now convert the second pair, (4.49)–(4.48), to two coupled infinite systems. To regularize (4.48), we make the following replacements to (3.39) and (3.37): $a \mapsto \tilde{s}_0$, $b \mapsto \tilde{q}_0$, $c \mapsto 0$, $d \mapsto 0$, $s_n \mapsto \tilde{s}_n$, $t_n \mapsto \tilde{q}_n$, $e_n \mapsto y_n^{(1)}\,(1-\tilde{r}_n)\,\upsilon$, $f_n \mapsto y_n^{(1)}\,(1-\tilde{p}_n)\,\tau$, $x_0 \mapsto b_0^{(1)}$, $x_n \mapsto x_n^{(2)}$, and $\psi_0 \mapsto \psi_{\rm PEC}$. We get

$$\begin{aligned} b_0^{(1)} = &- \frac{1-\psi_{\rm PEC}}{\sqrt{2}\left[\tilde{q}_0 \ln\left(\frac{1+\psi_{\rm PEC}}{2}\right) - \tilde{s}_0\right]} \\ &\times \sum_{n=1}^{\infty} \sqrt{n}\left\{x_n^{(2)}\left(\tilde{q}_n - \tilde{s}_n\right) + y_n^{(1)}\left[(1-\tilde{r}_n)\,\upsilon - (1-\tilde{p}_n)\,\tau\right]\right\} \frac{\hat{P}_{n-1}^{(1,0)}(\psi_{\rm PEC})}{n}, \end{aligned} \tag{4.64}$$

and the first ISLAE involving the unknowns $\left\{x_n^{(2)}, y_n^{(1)}\right\}_{n=1}^{\infty}$

$$\begin{aligned} &\sqrt{m}\left[x_m^{(2)}\,(1-\tilde{s}_m) + y_m^{(1)}\,(1-\tilde{r}_m)\,\upsilon\right] \\ &+ \sum_{n=1}^{\infty} \sqrt{n}\left\{x_n^{(2)}\left(\tilde{s}_n - \tilde{q}_n\right) + y_n^{(1)}\left[(1-\tilde{p}_n)\,\tau - (1-\tilde{r}_n)\,\upsilon\right]\right\} \hat{S}_{m-1,n-1}(\psi_{\rm PEC}) = 0, \end{aligned} \tag{4.65}$$

for $m = 1, 2, 3, \ldots$, where

$$\hat{S}_{m-1,n-1}(\psi_{\rm PEC}) := \hat{Q}_{m-1,n-1}^{(0,1)}(\psi_{\rm PEC}) + \frac{\tilde{q}_0\,(1-\psi_{\rm PEC})^2}{\tilde{q}_0 \ln\left(\frac{1+\psi_{\rm PEC}}{2}\right) - \tilde{s}_0} \frac{\hat{P}_{m-1}^{(1,0)}(\psi_{\rm PEC})}{m} \frac{\hat{P}_{n-1}^{(1,0)}(\psi_{\rm PEC})}{n}. \tag{4.66}$$

The second set of DSE (4.49) has the same form as that in (3.40). By making these replacements in (3.47): $s_n \mapsto \tilde{o}_n$, $t_n \mapsto \tilde{t}_n$, $g_n \mapsto 0$, $h_n \mapsto x_n^{(2)}\left(1-\tilde{u}_n\right)\varsigma + \tilde{z}_n^{(2)}$, $y_n \mapsto y_n^{(1)}$, and $\psi_0 \mapsto \psi_{\mathrm{PEC}}$, we get another ISLAE involving $\left\{x_n^{(2)}, y_n^{(1)}\right\}_{n=1}^{\infty}$:

$$\begin{aligned}
&\sqrt{m}\left[y_m^{(1)}\left(1-\tilde{t}_m\right) + x_m^{(2)}\left(1-\tilde{u}_m\right)\varsigma\right] \\
&+\sum_{n=1}^{\infty}\sqrt{n}\left\{y_n^{(1)}\left(\tilde{t}_n-\tilde{o}_n\right) - x_n^{(2)}\left(1-\tilde{u}_n\right)\varsigma\right\}\hat{Q}_{m-1,n-1}^{(0,1)}(\psi_{\mathrm{PEC}}) \qquad (4.67)\\
&= -\sqrt{m}\tilde{z}_m^{(2)} + \sum_{n=1}^{\infty}\sqrt{n}\tilde{z}_n^{(2)}\hat{Q}_{m-1,n-1}^{(0,1)}(\psi_{\mathrm{PEC}})\,.
\end{aligned}$$

for $m = 1, 2, \ldots$

In similar manner, we combine the two coupled ISLAE in (4.65), (4.67), and write them in the following matrix operator form,

$$\left[\mathcal{F}_2 - \mathcal{C}_2\right]\begin{pmatrix}\mathbf{x}_2\\ \mathbf{y}_1\end{pmatrix} = \begin{pmatrix}0\\ \mathbf{z}_2\end{pmatrix}, \qquad (4.68)$$

where the block matrix operators are defined

$$\mathcal{F}_2 := \begin{pmatrix}\mathcal{I} & 0\\ 0 & \mathcal{I}\end{pmatrix} + \begin{pmatrix}0 & \upsilon\left(\mathcal{I}-\mathcal{H}_3\right)+\tau\mathcal{H}_3\\ \varsigma\left(\mathcal{I}-\mathcal{H}_3\right) & 0\end{pmatrix}, \qquad (4.69)$$

$$\mathcal{C}_2 := \begin{pmatrix}\mathcal{S} & \upsilon\mathcal{R}+\left(\upsilon-\tau\right)\mathcal{H}_4\\ +\left(\mathcal{H}_3+\mathcal{H}_4\right)\left(\mathcal{Q}-\mathcal{S}\right) & +\left(\mathcal{H}_3+\mathcal{H}_4\right)\left(\tau\mathcal{P}-\upsilon\mathcal{R}\right)\\ \varsigma\left(\mathcal{I}-\mathcal{H}_3\right)\mathcal{U} & \left(\mathcal{I}-\mathcal{H}_3\right)\mathcal{T}\end{pmatrix}. \qquad (4.70)$$

The following sub matrices are introduced

$$\left[\mathcal{H}_3\right]_{n,m} := \hat{Q}_{m-1,n-1}^{(0,1)}(\psi_{\mathrm{PEC}})\,, \qquad (4.71)$$

$$\left[\mathcal{H}_4\right]_{n,m} := \frac{\tilde{q}_0\left(1-\psi_{\mathrm{PEC}}\right)^2}{\tilde{q}_0\ln\left(\frac{1+\psi_{\mathrm{PEC}}}{2}\right)-\tilde{s}_0}\frac{\hat{P}_{m-1}^{(1,0)}(\psi_{\mathrm{PEC}})}{m}\frac{\hat{P}_{n-1}^{(1,0)}(\psi_{\mathrm{PEC}})}{n}\,, \qquad (4.72)$$

for $n, m = 1, 2, \ldots$ The vectors $\mathbf{x}_2$ and $\mathbf{y}_1$ denotes $\left\{\sqrt{n}x_n^{(2)}, \sqrt{n}y_n^{(1)}\right\}_{n=1}^{\infty}$, respectively, and $\mathbf{z}_2$ denotes the right side of (4.67):

$$\left[\mathbf{z}_2\right]_n := -\sqrt{m}\tilde{z}_m^{(2)} + \sum_{n=1}^{\infty}\sqrt{n}\tilde{z}_n^{(2)}\hat{Q}_{m-1,n-1}^{(0,1)}(\psi_{\mathrm{PEC}})\,. \qquad (4.73)$$

Following the same arguments for the previous pair, it can be shown that (4.68) is a Fredholm equation of the second kind, where the inverse operator of $\mathcal{F}_2$ has been found to take the form

$$\mathcal{F}_2^{-1} = \begin{pmatrix}\xi\mathcal{I}+\left(1-\xi\right)\mathcal{H}_3 & \upsilon\xi\left(\mathcal{H}_3-\mathcal{I}\right)-\tau\mathcal{H}_3\\ \varsigma\xi\left(\mathcal{H}_3-\mathcal{I}\right) & \xi\mathcal{I}+\left(1-\xi\right)\mathcal{H}_3\end{pmatrix}. \qquad (4.74)$$

As with the ISLAE given in (4.63), this infinite system is solved numerically using MATLAB, by a standard process of Gaussian elimination. The solutions $\left\{x_n^{(2)}, y_n^{(1)}\right\}_{n=1}^{N_{\text{tr}}}$ computed with the truncated systems converge to the exact solution, for increasing N_{tr}.

4.5 Extension to the TE$_z$ incident plane wave problem

In this section, the same CLR is considered, with the only distinction being the oblique incident plane wave is TE$_z$. Adapting the same series representations for the secondary fields, the formulation and regularization process in solving for the TE$_z$ incident problem are of great similarity as those for the TM$_z$ incident problem. As a result, the detailed working for the problem is omitted here, with only the main differences outlined. In the following, unless otherwise stated, the parameters are as defined for the TM$_z$ case.

From Section 2.5, the field components for the TE$_z$ plane wave can be represented as the following series

$$E_z^{\text{inc}} = 0\,, \tag{4.75a}$$

$$H_z^{\text{inc}} = \frac{1}{\eta_0}\sum_{n=-\infty}^{\infty} c_n(\kappa_0\rho)e^{jn\phi}\,, \tag{4.75b}$$

$$E_\phi^{\text{inc}} = \frac{jk_0}{\kappa_0}\sum_{n=-\infty}^{\infty} c_n'(\kappa_0\rho)e^{jn\phi}\,, \tag{4.75c}$$

$$H_\phi^{\text{inc}} = -\frac{k_0\cos\theta_z^{\text{pw}}}{\eta_0\kappa_0^2\rho}\sum_{n=-\infty}^{\infty} nc_n(\kappa_0\rho)e^{jn\phi}\,, \tag{4.75d}$$

$$E_\rho^{\text{inc}} = \frac{k_0}{\kappa_0^2\rho}\sum_{n=-\infty}^{\infty} nc_n(\kappa_0\rho)e^{jn\phi}\,, \tag{4.75e}$$

$$H_\rho^{\text{inc}} = \frac{jk_0\cos\theta_z^{\text{pw}}}{\eta_0\kappa_0}\sum_{n=-\infty}^{\infty} c_n'(\kappa_0\rho)e^{jn\phi}\,. \tag{4.75f}$$

Upon the enforcement of the continuity condition on the transverse-components

of the total electric field on the entire contour of the CLR, it can be shown that

$$a_n^{(0)} = a_n^{(1)} J_n(\kappa_1 R) H_n^{'(2)}(\kappa_1 R)\,, \tag{4.76}$$

$$\begin{aligned} b_n^{(0)} =& \frac{j\cos\theta_z^{\mathrm{pw}}}{\eta_0\kappa_0 R}\left(\frac{\kappa_0^2}{\kappa_1^2}-1\right) n a_n^{(1)} J_n(\kappa_1 R) H_n^{'(2)}(\kappa_1 R) \frac{H_n^{(2)}(\kappa_0 R)}{H_n^{'(2)}(\kappa_0 R)} \\ &+ \mu_r \frac{\kappa_0}{\kappa_1} b_n^{(1)} J_n'(\kappa_1 R) H_n^{'(2)}(\kappa_1 R) \frac{H_n^{(2)}(\kappa_0 R)}{H_n^{'(2)}(\kappa_0 R)} - \frac{1}{\eta_0} c_n' \frac{H_n^{(2)}(\kappa_0 R)}{H_n^{'(2)}(\kappa_0 R)}\,, \end{aligned} \tag{4.77}$$

for all $n \in \mathbb{Z}$. The MBC on the contour of the CLR give

$$\sum_{n=-\infty}^{\infty} a_n^{(1)} o_n e^{jn\phi} = 0 \quad (A)\,, \qquad \text{on } \Omega_{\mathrm{PEC}}, \tag{4.78}$$

$$\sum_{n=-\infty}^{\infty} \left\{ a_n^{(1)} p_n + b_n^{(1)} q_n \right\} e^{jn\phi} = 0 \quad (A)\,, \qquad \text{on } \Omega_{\mathrm{PEC}}, \tag{4.79}$$

$$\sum_{n=-\infty}^{\infty} \left\{ a_n^{(1)} r_n + b_n^{(1)} s_n + v_n \right\} e^{jn\phi} = 0 \quad (A)\,, \qquad \text{on } \Omega_{\mathrm{aper}}, \tag{4.80}$$

$$\sum_{n=-\infty}^{\infty} \left\{ a_n^{(1)} t_n + b_n^{(1)} u_n + w_n \right\} e^{jn\phi} = 0 \quad (A)\,, \qquad \text{on } \Omega_{\mathrm{aper}}. \tag{4.81}$$

The two new parameters introduced in the above series equations are defined as:

$$v_n := \frac{1}{\eta_0}\left[c_n'(\kappa_0 R) \frac{H_n^{(2)}(\kappa_0 R)}{H_n^{'(2)}(\kappa_0 R)} - c_n(\kappa_0 R) \right], \tag{4.82}$$

$$w_n := \frac{n\kappa_1 \cos\theta_z^{\mathrm{pw}}}{j\kappa_0 R}\left[c_n'(\kappa_0 R) \frac{H_n^{(2)}(\kappa_0 R)}{H_n^{'(2)}(\kappa_0 R)} - c_n(\kappa_0 R) \right] = \frac{\eta_0\kappa_1 \cos\theta_z^{\mathrm{pw}}}{j\kappa_0 R}\, n v_n\,. \tag{4.83}$$

The series equations above are regularized following the same arguments and steps as those in the TM_z problem. As the same structure is considered, the matrix operators in the final form of infinite systems obtained for the TE_z problem are exactly the same as those for the TM_z problem. The difference lies in the right hand vectors, which collect all the contribution from the incident wave. In matrix operator form, the first and second infinite systems can be written as

$$[\mathcal{F}_1 - \mathcal{C}_1] \begin{pmatrix} \mathbf{x}_1 \\ \cdots \\ \mathbf{y}_2 \end{pmatrix} = \begin{pmatrix} \mathbf{z}_1 \\ \cdots \\ \mathbf{z}_2 \end{pmatrix}, \tag{4.84}$$

$$[\mathcal{F}_2 - \mathcal{C}_2] \begin{pmatrix} \mathbf{x}_2 \\ \cdots \\ \mathbf{y}_1 \end{pmatrix} = \begin{pmatrix} \mathbf{z}_3 \\ \cdots \\ \mathbf{z}_4 \end{pmatrix}, \tag{4.85}$$

where the right hand vectors are composed of

$$[\mathbf{z}_1]_n := -\sqrt{m}\tilde{w}_m^{(+)} + \sum_{n=1}^{\infty}\sqrt{n}\tilde{w}_n^{(+)}\hat{R}_{m-1,n-1}(\psi_{\mathrm{PEC}})\,, \tag{4.86a}$$

$$[\mathbf{z}_2]_n := -\sqrt{m}\tilde{v}_m^{(-)} + \sum_{n=1}^{\infty}\sqrt{n}\tilde{v}_n^{(-)}\hat{Q}^{(1,0)}_{m-1,n-1}(\psi_{\mathrm{PEC}})\,, \tag{4.86b}$$

$$\begin{aligned}[\mathbf{z}_3]_n := &-\frac{\sqrt{2}(1-\psi_{\mathrm{PEC}})\,\tilde{q}_0\,\tilde{v}_0}{\tilde{q}_0\ln\left(\frac{1+\psi_{\mathrm{PEC}}}{2}\right)-\tilde{s}_0}\frac{\hat{P}^{(1,0)}_{m-1}(\psi_{\mathrm{PEC}})}{m}\\ &-\sqrt{m}\tilde{v}_m^{(+)} + \sum_{n=1}^{\infty}\sqrt{n}\tilde{v}_n^{(+)}\hat{S}_{m-1,n-1}(\psi_{\mathrm{PEC}})\,,\end{aligned} \tag{4.86c}$$

$$[\mathbf{z}_4]_n := -\sqrt{m}\tilde{w}_m^{(-)} + \sum_{n=1}^{\infty}\sqrt{n}\tilde{w}_n^{(-)}\hat{Q}^{(0,1)}_{m-1,n-1}(\psi_{\mathrm{PEC}})\,, \tag{4.86d}$$

for $n = 1, 2, \ldots$ A few new notations have been adopted in the expressions above:

$$\left\{\tilde{v}_0, \tilde{v}_n^{(+)}, \tilde{v}_n^{(-)}\right\} := \frac{j\pi\kappa_1^3 R}{\kappa_1^2+\mu_r\kappa_0^2}\left\{v_0, (v_n+v_{-n}), (v_n-v_{-n})\right\}\,, \tag{4.87}$$

$$\left\{\tilde{w}_n^{(+)}, \tilde{w}_n^{(-)}\right\} := \frac{j\pi\kappa_0 R^2}{\zeta}\left\{\frac{w_n+w_{-n}}{n}, \frac{w_n-w_{-n}}{n}\right\}\,, \tag{4.88}$$

where $n = 1, 2, \ldots$ The rest of the parameters are as defined previously for the TM_z incidence problem. The two series expressions similar to (4.51) and (4.90) for unknowns $x_0^{(1)}$ and $x_0^{(2)}$ are also obtained:

$$\begin{aligned}a_0^{(1)} =&\frac{1+\psi_{\mathrm{PEC}}}{\sqrt{2}\left[\tilde{t}_0\ln\left(\frac{1-\psi_{\mathrm{PEC}}}{2}\right)-\tilde{o}_0\right]}\\ &\times\sum_{n=1}^{\infty}\sqrt{n}\left[x_n^{(1)}\left(\tilde{t}_n-\tilde{o}_n\right)-y_n^{(2)}\left(1-\tilde{u}_n\right)\varsigma-\tilde{w}_n^{(+)}\right]\frac{\hat{P}^{(0,1)}_{n-1}(\psi_{\mathrm{PEC}})}{n}\,,\end{aligned} \tag{4.89}$$

$$\begin{aligned}b_0^{(1)} =&\frac{\tilde{v}_0}{\tilde{q}_0\ln\left(\frac{1+\psi_{\mathrm{PEC}}}{2}\right)-\tilde{s}_0}-\frac{1-\psi_{\mathrm{PEC}}}{\sqrt{2}\left[\tilde{q}_0\ln\left(\frac{1+\psi_{\mathrm{PEC}}}{2}\right)-\tilde{s}_0\right]}\\ &\times\sum_{n=1}^{\infty}\sqrt{n}\left\{x_n^{(2)}\left(\tilde{q}_n-\tilde{s}_n\right)+y_n^{(1)}\left[\left(1-\tilde{r}_n\right)\upsilon-\left(1-\tilde{p}_n\right)\tau\right]+\tilde{v}_n^{(+)}\right\}\frac{\hat{P}^{(1,0)}_{n-1}(\psi_{\mathrm{PEC}})}{n}\,.\end{aligned} \tag{4.90}$$

4.6 Series representations of physical quantities

4.6.1 Energy

The series representation for the energy accumulated inside a unit length CLR (W) has been derived in Subsection 4.3.2. In order to represent W in terms of $a_0^{(1)}$, $b_0^{(1)}$,

and $\left\{x_n^{(i)}, y_n^{(i)}\right\}_{n=1}^{\infty}$ $(i=1,2)$, we substitute (4.42a)–(4.42b) into (4.9). As $\Phi_{-n}=\Phi_n$, and $\Gamma_{-n}=-\Gamma_n$ for $n=1,2,\ldots$, (4.9) can be simplified to

$$W=\pi\left(\epsilon_0\epsilon_r\left|a_0^{(1)}\right|^2+\mu_0\mu_r\left|b_0^{(1)}\right|^2\right)\Phi_0+\frac{\pi}{2}\sum_{n=1}^{\infty}\gamma_n\,, \tag{4.91}$$

where $\{\Phi_n,\Gamma_n\}_{n=0}^{\infty}$ are as defined in (4.14), and we introduce

$$\begin{aligned}\gamma_n:=&\Phi_n\left[\epsilon_0\epsilon_r\left(\left|x_n^{(1)}\right|^2+\left|y_n^{(1)}\right|^2\right)+\mu_0\mu_r\left(\left|x_n^{(2)}\right|^2+\left|y_n^{(2)}\right|^2\right)\right]\\&+2j\Gamma_n\,\mathrm{Im}\left(\overline{x_n^{(2)}}y_n^{(1)}+x_n^{(1)}\overline{y_n^{(2)}}\right)\,.\end{aligned} \tag{4.92}$$

4.6.2 Radiation pattern and RCS

Expressions for the components of the radiation pattern, $\mathbf{R}(\phi)$, can be obtained by substitution of the large argument approximations for $H_n^{(2)}(x)$ and $H_n^{'(2)}(x)$ into the series representations for E_z^{sc}, E_ϕ^{sc} and E_ρ^{sc}. Expressing the components in terms of $a_0^{(1)}$, $b_0^{(1)}$, and $\left\{x_n^{(i)}, y_n^{(i)}\right\}_{n=1}^{\infty}$ $(i=1,2)$, we get

$$\{R_z,R_\phi,R_\rho\}=\sqrt{\frac{2}{\pi\kappa_0}}e^{j\frac{\pi}{4}}\left\{S_1(\phi),\frac{\eta_0}{\sin\theta_z^{\mathrm{pw}}}S_2(\phi),\cot\theta_z^{\mathrm{pw}}S_1(\phi)\right\}\,, \tag{4.93}$$

where S_1 and S_2 are used to denote the following series for brevity

$$\begin{aligned}S_1(\phi):=&\frac{a_0^{(1)}o_0-c_0}{H_0^{(2)}(\kappa_0R)}\\&+\sum_{n=1}^{\infty}\frac{e^{jn\frac{\pi}{2}}}{H_n^{(2)}(\kappa_0R)}\left[\left(x_n^{(1)}o_n-c_n^{(1)}\right)\cos n\phi+\left(y_n^{(1)}o_n-c_n^{(2)}\right)j\sin n\phi\right]\,,\end{aligned} \tag{4.94a}$$

$$\begin{aligned}S_2(\phi):=&\frac{\mu_r\frac{\kappa_0}{\kappa_1}b_0^{(1)}q_0}{H_0^{'(2)}(\kappa_0R)}+\sum_{n=1}^{\infty}\frac{e^{jn\frac{\pi}{2}}}{H_n^{'(2)}(\kappa_0R)}\\&\times\left\{\left[\frac{j\cos\theta_z^{\mathrm{pw}}}{\eta_0\kappa_0R}\left(\frac{\kappa_0^2}{\kappa_1^2}-1\right)n\,o_ny_n^{(1)}+\mu_r\frac{\kappa_0}{\kappa_1}q_nx_n^{(2)}\right]\cos n\phi\right.\\&\left.+\left[\frac{j\cos\theta_z^{\mathrm{pw}}}{\eta_0\kappa_0R}\left(\frac{\kappa_0^2}{\kappa_1^2}-1\right)n\,o_nx_n^{(1)}+\mu_r\frac{\kappa_0}{\kappa_1}q_ny_n^{(2)}\right]j\sin n\phi\right\}\,.\end{aligned} \tag{4.94b}$$

The parameters $\{c_n,o_n,q_n\}_{n=1}^{\infty}$ are as defined in (4.2a), (4.25) and (4.27), while $\left\{c_n^{(1,2)}\right\}_{n=0}^{\infty}$ are introduced to denote $c_n^{(1,2)}:=c_n\pm c_{-n}$, for $n=1,2,\ldots$

Without loss of generality, we take the amplitude of the incident plane wave A_0 to be 1, and the normalized RCS $\hat{\sigma}(\phi)$ can be expressed as

$$\hat{\sigma}(\phi)=\frac{2}{R}\left|\mathbf{R}(\phi)\right|^2=\frac{4\csc^2\theta_z^{\mathrm{pw}}}{\pi\kappa_0R}\left\{\left(1+\cos^2\theta_z^{\mathrm{pw}}\right)\left|S_1(\phi)\right|^2+\eta_0^2\left|S_2(\phi)\right|^2\right\}\,. \tag{4.95}$$

4.6.3 Surface current density

Due to the oblique incidence, both of the ϕ- and z-components of the surface current density, $\mathbf{J}$, are present on the surface of the PEC strip. From its definition (2.42), $\mathbf{J}$ per unit length along the z-axis depends only on the angular variable ϕ, and can be expressed mathematically as

$$J_\phi(\phi) = -H_z^{\text{tr}}(R,\phi) + \left[H_z^{\text{sc}}(R,\phi) + H_z^{\text{inc}}(R,\phi)\right] , \tag{4.96a}$$

$$J_z(\phi) = H_\phi^{\text{tr}}(R,\phi) - \left[H_\phi^{\text{sc}}(R,\phi) + H_\phi^{\text{inc}}(R,\phi)\right] . \tag{4.96b}$$

From the series representations given in Subsection 4.3.1, J_z and J_ϕ for the TM_z incidence problem can be expressed in terms of $\left\{x_n^{(i)}, y_n^{(i)}\right\}_{n=1}^{\infty}$ $(i = 1, 2)$ as:

$$J_\phi = -s_0 b_0^{(1)} - \sum_{n=1}^{\infty} \left\{ \left[r_n y_n^{(1)} + s_n x_n^{(2)}\right] \cos n\phi + j \left[r_n x_n^{(1)} + s_n y_n^{(2)}\right] \sin n\phi \right\} , \tag{4.97a}$$

$$\begin{aligned} J_z = &- \frac{jk_0}{\eta_0 \kappa_0 \kappa_1} \Bigg\{ a_0^{(1)} t_0 + z_0 + \sum_{n=1}^{\infty} \left[x_n^{(1)} t_n + y_n^{(2)} u_n + n z_n^{(1)}\right] \cos n\phi \\ &+ j \sum_{n=1}^{\infty} \left[x_n^{(2)} u_n + y_n^{(1)} t_n + n z_n^{(2)}\right] \sin n\phi \Bigg\} . \end{aligned} \tag{4.97b}$$

The parameters $\left\{r_n, s_n, t_n, u_n, z_n^{(1,2)}\right\}_{n=1}^{\infty}$ are as defined in (4.32)–(4.36) and (4.42c).

Writing J_ϕ and J_z in terms of the asymptotically small parameters defined in (4.45d)–(4.45g), we have:

$$\begin{aligned} J_\phi = &- \frac{\kappa_1^2 + \mu_r \kappa_0^2}{j\pi \kappa_1^3 R} \Bigg\{ \tilde{s}_0 b_0^{(1)} - \sum_{n=1}^{\infty} \left[y_n^{(1)} \left(1 - \tilde{r}_n\right) \upsilon + x_n^{(2)} \left(1 - \tilde{s}_n\right)\right] \cos n\phi \\ &- j \sum_{n=1}^{\infty} \left[x_n^{(1)} \left(1 - \tilde{r}_n\right) \upsilon + y_n^{(2)} \left(1 - \tilde{s}_n\right)\right] \sin n\phi \Bigg\} , \end{aligned} \tag{4.98a}$$

$$\begin{aligned} J_z = &- \frac{\zeta k_0}{\pi \eta_0 \kappa_0^2 \kappa_1 R^2} \Bigg\{ a_0^{(1)} \tilde{t}_0 + \tilde{z}_0 + \sum_{n=1}^{\infty} n \left[x_n^{(1)} \left(1 - \tilde{t}_n\right) + y_n^{(2)} \left(1 - \tilde{u}_n\right) \varsigma + \tilde{z}_n^{(1)}\right] \cos n\phi \\ &+ j \sum_{n=1}^{\infty} n \left[x_n^{(2)} \left(1 - \tilde{u}_n\right) \varsigma + y_n^{(1)} \left(1 - \tilde{t}_n\right) + \tilde{z}_n^{(2)}\right] \sin n\phi \Bigg\} , \end{aligned} \tag{4.98b}$$

where the remaining scaled parameters are as defined in (4.50a)–(4.50c).

4.7 Improving the rate of convergence

From the series representations given in (4.98a) and (4.98b), we can see that the general series terms for J_z decreases at order $O\left(n^{-1/2}\right)$, while that for J_ϕ decreases

at order $O\left(n^{-3/2}\right)$, as $n \to \infty$. In other words, correspondingly accurate calculation of J_z will require a larger $N_{\rm tr}$ than that for J_ϕ.

To accelerate the decay rate of the terms in the two series in the slower converging (4.98b), we make use of the block matrix equations given in (4.55) and (4.68). Left multiplying (4.55) with the bounded inverse $\mathcal{F}_1^{-1}$ defined in (4.62), followed by rearrangement of the equation, we get

$$\begin{pmatrix} \mathbf{x}_1 \\ \cdots \\ \mathbf{y}_2 \end{pmatrix} = \mathcal{F}_1^{-1}\mathcal{C}_1 \begin{pmatrix} \mathbf{x}_1 \\ \cdots \\ \mathbf{y}_2 \end{pmatrix} + \mathcal{F}_1^{-1} \begin{pmatrix} \mathbf{z}_1 \\ \cdots \\ 0 \end{pmatrix} . \tag{4.99}$$

Similar operations on (4.68), by using $\mathcal{F}_2^{-1}$ defined in (4.74), lead us to

$$\begin{pmatrix} \mathbf{x}_2 \\ \cdots \\ \mathbf{y}_1 \end{pmatrix} = \mathcal{F}_2^{-1}\mathcal{C}_2 \begin{pmatrix} \mathbf{x}_2 \\ \cdots \\ \mathbf{y}_1 \end{pmatrix} + \mathcal{F}_2^{-1} \begin{pmatrix} 0 \\ \cdots \\ \mathbf{z}_2 \end{pmatrix} . \tag{4.100}$$

Recalling the definitions of $\mathcal{C}_i$ and $\mathbf{z}_i$ $(i = 1, 2)$ given in (4.57), (4.60), (4.70), and (4.73), we can rewrite (4.99) and (4.100) in the following forms:

$$\begin{aligned}
\mathbf{x}_1 =& \left\{ \begin{array}{l} \xi\mathcal{T} + (1-\xi)\mathcal{R} + \mathcal{H}_1\left[\mathcal{O} - \xi\mathcal{T} - (1-\xi)\mathcal{R}\right] \\ \quad + \left[\xi\mathcal{I} + (1-\xi)\mathcal{H}_1\right]\mathcal{H}_2\left(\mathcal{T} - \mathcal{O}\right) \end{array} \right\} \mathbf{x}_1 \\
& + \left\{\xi\varsigma\left(\mathcal{I} - \mathcal{H}_1\right)\left(\mathcal{U} - \mathcal{S}\right) - \varsigma\left[\xi\mathcal{I} + (1-\xi)\mathcal{H}_1\right]\mathcal{H}_2\left(\mathcal{I} - \mathcal{U}\right)\right\}\mathbf{y}_2 \\
& + \left\{\xi\mathcal{I} + (1-\xi)\mathcal{H}_1\right\}\mathbf{z}_1 , \qquad (4.101a) \\
\mathbf{y}_2 =& \left\{ \begin{array}{l} \xi\upsilon\left(\mathcal{R} - \mathcal{T}\right) + \mathcal{H}_1\left[\tau\left(\mathcal{P} - \mathcal{O}\right) - \xi\upsilon\left(\mathcal{R} - \mathcal{T}\right)\right] \\ \quad + \left[\left(\xi\upsilon - \tau\right)\mathcal{H}_1 - \xi\upsilon\mathcal{I}\right]\mathcal{H}_2\left(\mathcal{T} - \mathcal{O}\right) \end{array} \right\} \mathbf{x}_1 \\
& + \left\{ \begin{array}{l} \xi\mathcal{S} + (1-\xi)\mathcal{U} + \mathcal{H}_1\left[\mathcal{Q} - \xi\mathcal{S} - (1-\xi)\mathcal{U}\right] \\ \quad + \left[(1 - \xi + \tau\varsigma)\mathcal{H}_1 - (1-\xi)\mathcal{I}\right]\mathcal{H}_2\left(\mathcal{I} - \mathcal{U}\right) \end{array} \right\} \mathbf{y}_2 \\
& + \left\{\left(\xi\upsilon - \tau\right)\mathcal{H}_1 - \xi\upsilon\mathcal{I}\right\}\mathbf{z}_1 , \qquad (4.101b) \\
\mathbf{x}_2 =& \left\{ \begin{array}{l} \xi\mathcal{S} + (1-\xi)\mathcal{U} + \mathcal{H}_3\left[\mathcal{Q} - \xi\mathcal{S} - (1-\xi)\mathcal{U}\right] \\ \quad + \left[\xi\mathcal{I} + (1-\xi)\mathcal{H}_3\right]\mathcal{H}_4\left(\mathcal{Q} - \mathcal{S}\right) \end{array} \right\} \mathbf{x}_2 \\
& + \left\{ \begin{array}{l} \xi\upsilon\left(\mathcal{R} - \mathcal{T}\right) + \mathcal{H}_3\left[\tau\mathcal{P} - \xi\upsilon\left(\mathcal{R} - \mathcal{T}\right)\right] \\ \quad + \left[\xi\mathcal{I} + (1-\xi)\mathcal{H}_3\right]\mathcal{H}_4\left[\upsilon\left(\mathcal{I} - \mathcal{R}\right) - \tau\left(\mathcal{I} - \mathcal{P}\right)\right] \end{array} \right\} \mathbf{y}_1 \\
& + \left\{\left(\xi\upsilon - \tau\right)\mathcal{H}_3 - \xi\upsilon\mathcal{I}\right\}\mathbf{z}_2 , \qquad (4.101c) \\
\mathbf{y}_1 =& \xi\varsigma\left\{\left(\mathcal{U} - \mathcal{S}\right) - \mathcal{H}_3\left(\mathcal{U} - \mathcal{S}\right) - \left(\mathcal{I} - \mathcal{H}_3\right)\mathcal{H}_4\left(\mathcal{Q} - \mathcal{S}\right)\right\}\mathbf{x}_2 \\
& + \left\{ \begin{array}{l} \xi\mathcal{T} + (1-\xi)\mathcal{R} - \mathcal{H}_3\left[\xi\mathcal{T} + (1-\xi)\mathcal{R}\right] \\ \quad + \left(\mathcal{I} - \mathcal{H}_3\right)\mathcal{H}_4\left[(1-\xi)\left(\mathcal{I} - \mathcal{R}\right) + \xi\varsigma\tau\left(\mathcal{I} - \mathcal{P}\right)\right] \end{array} \right\} \mathbf{y}_1 \\
& + \left\{\xi\mathcal{I} + (1-\xi)\mathcal{H}_3\right\}\mathbf{z}_2 , \qquad (4.101d)
\end{aligned}$$

or equivalently in series forms:

$$\sqrt{m}x_m^{(1)} = \sqrt{m}\left\{x_m^{(1)}\left[\xi\tilde{t}_m + (1-\xi)\tilde{r}_m\right] + \xi\varsigma y_m^{(2)}\left(\tilde{u}_m - \tilde{s}_m\right) - \xi\tilde{z}_m^{(1)}\right\} + \hat{e}_m$$

$$+\sum_{n=1}^{\infty}\sqrt{n}\left\{\left[\begin{array}{l}\left(\tilde{o}_n-\xi\tilde{t}_n-(1-\xi)\tilde{r}_n\right)x_n^{(1)}\\+\xi\varsigma\left(\tilde{s}_n-\tilde{u}_n\right)y_n^{(2)}+\xi\tilde{z}_n^{(1)}\end{array}\right]\hat{Q}_{m-1,n-1}^{(1,0)}(\psi_{\mathrm{PEC}})\right.$$
$$\left.+\left[\left(\tilde{t}_n-\tilde{o}_n\right)x_n^{(1)}-\varsigma\left(1-\tilde{u}_n\right)y_n^{(2)}-\tilde{z}_n^{(1)}\right]\hat{T}_{m-1,n-1}\right\},\tag{4.102a}$$

$$\begin{aligned}\sqrt{m}y_m^{(2)}=&\sqrt{m}\left\{\xi\upsilon x_m^{(1)}\left(\tilde{r}_m-\tilde{t}_m\right)+y_m^{(2)}\left[\xi\tilde{s}_m+(1-\xi)\tilde{u}_m\right]+\xi\upsilon\tilde{z}_m^{(1)}\right\}+\hat{f}_m\\&+\sum_{n=1}^{\infty}\sqrt{n}\left\{\left[\begin{array}{l}\left(\tau\left(\tilde{p}_n-\tilde{o}_n\right)-\xi\upsilon\left(\tilde{r}_n-\tilde{t}_n\right)\right)x_n^{(1)}\\+\left(\tilde{q}_n-\xi\tilde{s}_n-(1-\xi)\tilde{u}_n\right)y_n^{(2)}-\xi\upsilon\tilde{z}_n^{(1)}\end{array}\right]\hat{Q}_{m-1,n-1}^{(1,0)}(\psi_{\mathrm{PEC}})\right.\\&\left.+\left[\left(\tilde{t}_n-\tilde{o}_n\right)x_n^{(1)}-\varsigma\left(1-\tilde{u}_n\right)y_n^{(2)}-\tilde{z}_n^{(1)}\right]\hat{U}_{m-1,n-1}\right\},\end{aligned}\tag{4.102b}$$

$$\begin{aligned}\sqrt{m}x_m^{(2)}=&\sqrt{m}\left\{x_m^{(2)}\left[\xi\tilde{s}_m+(1-\xi)\tilde{u}_m\right]+\xi\upsilon y_m^{(1)}\left(\tilde{r}_m-\tilde{t}_m\right)+\xi\upsilon\tilde{z}_m^{(2)}\right\}\\&+\sum_{n=1}^{\infty}\sqrt{n}\left\{\left[\begin{array}{l}\left(\tilde{q}_n-\xi\tilde{s}_n-(1-\xi)\tilde{u}_n\right)x_n^{(2)}\\+\left(\tau\tilde{p}_n-\xi\upsilon(\tilde{r}_n-\tilde{t}_n)\right)y_n^{(1)}-\xi\upsilon\tilde{z}_n^{(2)}\end{array}\right]\hat{Q}_{m-1,n-1}^{(0,1)}(\psi_{\mathrm{PEC}})\right.\\&\left.+\left[\begin{array}{l}\left(\tilde{q}_n-\tilde{s}_n\right)x_n^{(2)}\\+\left(\upsilon(1-\tilde{r}_n)-\tau(1-\tilde{p}_n)\right)y_n^{(1)}\end{array}\right]\hat{V}_{m-1,n-1}\right\},\end{aligned}\tag{4.102c}$$

$$\begin{aligned}\sqrt{m}y_m^{(1)}=&\sqrt{m}\left\{\xi\varsigma x_m^{(2)}\left(\tilde{u}_m-\tilde{s}_m\right)+y_m^{(1)}\left[\xi\tilde{t}_m+(1-\xi)\tilde{r}_m\right])-\xi\tilde{z}_m^{(2)}\right\}\\&+\sum_{n=1}^{\infty}\sqrt{n}\left\{\left[\begin{array}{l}\xi\varsigma\left(\tilde{s}_n-\tilde{u}_n\right)x_n^{(2)}\\-\left(\xi\tilde{t}_n+(1-\xi)\tilde{r}_n\right)y_n^{(1)}+\xi\tilde{z}_n^{(2)}\end{array}\right]\hat{Q}_{m-1,n-1}^{(0,1)}(\psi_{\mathrm{PEC}})\right.\\&\left.+\left[\begin{array}{l}-\xi\varsigma\left(\tilde{q}_n-\tilde{s}_n\right)x_n^{(2)}\\+\left((1-\xi)(1-\tilde{r}_n)+\xi\varsigma\tau(1-\tilde{p}_n)\right)y_n^{(1)}\end{array}\right]\hat{W}_{m-1,n-1}\right\}.\end{aligned}\tag{4.102d}$$

We have introduced the following notations to simplify the above series equations:

$$\begin{aligned}\hat{e}_m:=&-\frac{\sqrt{2}(1+\psi_{\mathrm{PEC}})\tilde{o}_0\tilde{z}_0}{\tilde{t}_0\ln\left(\frac{1-\psi_{\mathrm{PEC}}}{2}\right)-\tilde{o}_0}\times\left\{\xi\frac{\hat{P}_{m-1}^{(0,1)}(\psi_{\mathrm{PEC}})}{m}\right.\\&\left.+(1-\xi)\left[\sum_{k=1}^{\infty}\hat{Q}_{m-1,k-1}^{(1,0)}(\psi_{\mathrm{PEC}})\frac{\hat{P}_{k-1}^{(0,1)}(\psi_{\mathrm{PEC}})}{k}\right]\right\},\end{aligned}\tag{4.103}$$

$$\begin{aligned}\hat{f}_m:=&-\frac{\sqrt{2}(1+\psi_{\mathrm{PEC}})\tilde{o}_0\tilde{z}_0}{\tilde{t}_0\ln\left(\frac{1-\psi_{\mathrm{PEC}}}{2}\right)-\tilde{o}_0}\times\left\{-\xi\upsilon\frac{\hat{P}_{m-1}^{(0,1)}(\psi_{\mathrm{PEC}})}{m}\right.\\&\left.+(\xi\upsilon-\tau)\left[\sum_{k=1}^{\infty}\hat{Q}_{m-1,k-1}^{(1,0)}(\psi_{\mathrm{PEC}})\frac{\hat{P}_{k-1}^{(0,1)}(\psi_{\mathrm{PEC}})}{k}\right]\right\},\end{aligned}\tag{4.104}$$

$$\begin{aligned}\hat{T}_{m-1,n-1}:=&\frac{\tilde{t}_0(1+\psi_{\mathrm{PEC}})^2}{\tilde{t}_0\ln\left(\frac{1-\psi_{\mathrm{PEC}}}{2}\right)-\tilde{o}_0}\frac{\hat{P}_{n-1}^{(0,1)}(\psi_{\mathrm{PEC}})}{n}\times\left\{\xi\frac{\hat{P}_{m-1}^{(0,1)}(\psi_{\mathrm{PEC}})}{m}\right.\\&\left.+(1-\xi)\left[\sum_{k=1}^{\infty}\hat{Q}_{m-1,k-1}^{(1,0)}(\psi_{\mathrm{PEC}})\frac{\hat{P}_{k-1}^{(0,1)}(\psi_{\mathrm{PEC}})}{k}\right]\right\},\end{aligned}\tag{4.105}$$

$$\hat{U}_{m-1,n-1} := \frac{\tilde{t}_0(1+\psi_{\mathrm{PEC}})^2}{\tilde{t}_0 \ln\left(\frac{1-\psi_{\mathrm{PEC}}}{2}\right) - \tilde{o}_0} \frac{\hat{P}_{n-1}^{(0,1)}(\psi_{\mathrm{PEC}})}{n} \times \left\{ -\xi\upsilon \frac{\hat{P}_{m-1}^{(0,1)}(\psi_{\mathrm{PEC}})}{m} + (\xi\upsilon - \tau) \left[\sum_{k=1}^{\infty} \hat{Q}_{m-1,k-1}^{(1,0)}(\psi_{\mathrm{PEC}}) \frac{\hat{P}_{k-1}^{(0,1)}(\psi_{\mathrm{PEC}})}{k} \right] \right\}, \tag{4.106}$$

$$\hat{V}_{m-1,n-1} := \frac{\tilde{q}_0(1-\psi_{\mathrm{PEC}})^2}{\tilde{q}_0 \ln\left(\frac{1+\psi_{\mathrm{PEC}}}{2}\right) - \tilde{s}_0} \frac{\hat{P}_{n-1}^{(1,0)}(\psi_{\mathrm{PEC}})}{n} \times \left\{ \xi \frac{\hat{P}_{m-1}^{(1,0)}(\psi_{\mathrm{PEC}})}{m} + (1-\xi) \left[\sum_{k=1}^{\infty} \hat{Q}_{m-1,k-1}^{(0,1)}(\psi_{\mathrm{PEC}}) \frac{\hat{P}_{k-1}^{(1,0)}(\psi_{\mathrm{PEC}})}{k} \right] \right\}, \tag{4.107}$$

$$\hat{W}_{m-1,n-1} := \frac{\tilde{q}_0(1-\psi_{\mathrm{PEC}})^2}{\tilde{q}_0 \ln\left(\frac{1+\psi_{\mathrm{PEC}}}{2}\right) - \tilde{s}_0} \frac{\hat{P}_{n-1}^{(1,0)}(\psi_{\mathrm{PEC}})}{n} \times \left\{ \frac{\hat{P}_{m-1}^{(1,0)}(\psi_{\mathrm{PEC}})}{m} - \left[\sum_{k=1}^{\infty} \hat{Q}_{m-1,k-1}^{(0,1)}(\psi_{\mathrm{PEC}}) \frac{\hat{P}_{k-1}^{(1,0)}(\psi_{\mathrm{PEC}})}{k} \right] \right\}, \tag{4.108}$$

By substitution of the equations in (4.102) into the series expression for J_z given in (4.98b), we obtain a modified series expression for J_z, for which the general series terms are of order $\left(n^{-3/2}\right)$, as $n \to +\infty$. The modified series expression has the following form:

$$J_z = -\frac{\zeta k_0}{\pi \eta_0 \kappa_0^2 \kappa_1 R^2} \times \left(a_0^{(1)} \tilde{t}_0 + \tilde{z}_0 + \sum_{m=1}^{\infty} \left[\begin{array}{l} \left\{ x_m^{(1)} \left[(1-\tau\varsigma)\,\tilde{o}_m + \tau\varsigma\tilde{p}_m - \tilde{t}_m \right] + \varsigma y_m^{(2)} \left(\tilde{q}_m - \tilde{u}_m \right) + \tilde{z}_m^{(1)} \right\} \hat{A}_m \\ + \left\{ x_m^{(1)} \left(\tilde{t}_m - \tilde{o}_m \right) - \varsigma y_m^{(2)} \left(1 - \tilde{u}_m \right) - \tilde{z}_m^{(1)} \right\} \hat{B}_m \\ + \left\{ \varsigma x_m^{(2)} \left(\tilde{q}_m - \tilde{u}_m \right) + y_m^{(1)} \left(\tau\varsigma\tilde{p}_m - \tilde{t}_m \right) + \tilde{z}_m^{(2)} \right\} \hat{C}_m \\ + \varsigma \left\{ x_m^{(2)} \left(\tilde{q}_m - \tilde{s}_m \right) + y_m^{(1)} \left[\upsilon \left(1 - \tilde{r}_m \right) - \tau \left(1 - \tilde{p}_m \right) \right] \right\} \hat{D}_m \\ + \hat{E}_m \end{array} \right] \right), \tag{4.109}$$

where the following notations are introduced for brevity:

$$\hat{A}_m := \sqrt{m} \sum_{n=1}^{\infty} \sqrt{n} \cos n\phi \, \hat{Q}^{(1,0)}_{n-1,m-1} \left(\psi_{\mathrm{PEC}}\right) , \tag{4.110}$$

$$\begin{aligned} \hat{B}_m := & \frac{\tilde{t}_0 \left(1+\psi_{\mathrm{PEC}}\right)^2}{\tilde{t}_0 \ln\left(\frac{1-\psi_{\mathrm{PEC}}}{2}\right) - \tilde{o}_0} \frac{\hat{P}^{(0,1)}_{m-1} \left(\psi_{\mathrm{PEC}}\right)}{\sqrt{m}} \\ & \times \sum_{n=1}^{\infty} \sqrt{n} \cos n\phi \left[\frac{\hat{P}^{(0,1)}_{n-1} \left(\psi_{\mathrm{PEC}}\right)}{n} - \tau\varsigma \sum_{l=1}^{\infty} \hat{Q}^{(1,0)}_{n-1,l-1} \left(\psi_{\mathrm{PEC}}\right) \frac{\hat{P}^{(0,1)}_{l-1} \left(\psi_{\mathrm{PEC}}\right)}{l} \right] , \end{aligned} \tag{4.111}$$

$$\hat{C}_m := j\sqrt{m} \sum_{n=1}^{\infty} \sqrt{n} \sin n\phi \, \hat{Q}^{(0,1)}_{n-1,m-1} \left(\psi_{\mathrm{PEC}}\right) , \tag{4.112}$$

$$\begin{aligned} \hat{D}_m := & j \frac{\tilde{q}_0 \left(1-\psi_{\mathrm{PEC}}\right)^2}{\tilde{q}_0 \ln\left(\frac{1+\psi_{\mathrm{PEC}}}{2}\right) - \tilde{s}_0} \frac{\hat{P}^{(1,0)}_{m-1} \left(\psi_{\mathrm{PEC}}\right)}{\sqrt{m}} \\ & \times \sum_{n=1}^{\infty} \sqrt{n} \sin n\phi \sum_{l=1}^{\infty} \hat{Q}^{(0,1)}_{n-1,l-1} \left(\psi_{\mathrm{PEC}}\right) \frac{\hat{P}^{(1,0)}_{l-1} \left(\psi_{\mathrm{PEC}}\right)}{l} , \end{aligned} \tag{4.113}$$

$$\hat{E}_m := - \frac{\sqrt{2} \left(1+\psi_{\mathrm{PEC}}\right) \tilde{o}_0 \tilde{z}_0}{\tilde{t}_0 \ln\left(\frac{1-\psi_{\mathrm{PEC}}}{2}\right) - \tilde{o}_0} \left[\frac{\hat{P}^{(0,1)}_{n-1} \left(\psi_{\mathrm{PEC}}\right)}{n} - \tau\varsigma \sum_{l=1}^{\infty} \hat{Q}^{(1,0)}_{n-1,l-1} \left(\psi_{\mathrm{PEC}}\right) \frac{\hat{P}^{(0,1)}_{l-1} \left(\psi_{\mathrm{PEC}}\right)}{l} \right] . \tag{4.114}$$

The above transformation can also be applied to W and J_ϕ by substitution of (4.102) into (4.91) and (4.98a), respectively. Doing so, we can improve the convergence rate of the series terms from $O\left(n^{-3/2}\right)$ to $O\left(n^{-5/2}\right)$ for J_ϕ, and from $O\left(n^{-2}\right)$ to $O\left(n^{-3}\right)$ for W.

4.8 Numerical investigations

In this section, the solutions for the unknowns $\left\{x_n^{(i)}, y_n^{(i)}\right\}_{n=1}^{\infty}$ $(i = 0, 1)$ are computed by two separate numerical matrix inversions of (4.55) and (4.68) for the TM_z incidence case. The values of the physical quantities (*e.g.*, RCS and surface current density) can be computed once the values of these unknowns coefficients are found.

The goal of the first part of this section is to numerically validate the formulation in previous sections, and also the numerical codes developed. Internal as well as external tests have been carried out as follows:

1. the MBC on the contour of the CLR are verified, by substitution of the computed $\left\{x_n^{(i)}, y_n^{(i)}\right\}_{n=1}^{\infty}$ $(i = 0, 1)$ back into the series representations of the field components,

2. the numerical results for near and far-field patterns are compared with available results from the literature.

The second part investigates the rates of convergence of the solution computed by looking at the relative error, as N_{tr} increases. It is shown that for $N_{\text{tr}} > \kappa_1 R$, the relative error decreases steadily as N_{tr} goes up. The condition numbers for the matrices are also computed, and are shown to be bounded.

Finally, some numerical results of the effect of different polar incident angle (θ_z^{pw}) on the RCS and internal stored energy are reported.

4.8.1 Numerical validation

Internal tests:

The computed coefficients are substituted back into (4.3)–(4.6). The values of the tangential components of the fields on the contour are calculated to verify the MBC (2.9a) and (2.9b) numerically. In both Figure 4.2 and Figure 4.3, the characteristics of the CLR were set to take values $R = 1$, $\epsilon_r = 2.1$, $\mu = 1$, and $\theta^{\text{PEC}} = \frac{\pi}{3}$. The incident TM_z plane wave was taken to have $k_0 = 20$, $\theta_z^{\text{pw}} = \frac{\pi}{4}$, and $\theta_x^{\text{pw}} = \frac{\pi}{5}$.

The magnitudes of E_z^{tr} and E_ϕ^{tr} on the contour are displayed in Figure 4.2. Evidently, both E_z^{tr} and E_ϕ^{tr} vanish on the PEC strip, Ω_{PEC}. In fact, although not displayed in the figures, the tangential components of the sum of the incident and scattered electric field, $\left(E_z^{\text{inc}} + E_z^{\text{sc}}\right)$ and $\left(E_\phi^{\text{inc}} + E_\phi^{\text{sc}}\right)$, when plotted for the same problem characteristic, produces exactly the same figures as in Figure 4.2. These observations confirm with both (2.6a) and (2.9a). The oscillations observed near the sharp edges (when $\phi = \pm\theta^{\text{PEC}}$) in both sub-figures are examples of the Gibbs phenomenon. We can see that the phenomenon is more profound in the bottom sub-figure $\left(E_\phi^{\text{tr}}\right)$ than that in the upper sub-figure (E_z^{tr}). This is because the general series terms for E_ϕ^{tr} given in (4.5c) converges at a slower rate $O\left(n^{-1/2}\right)$, when compared with the rate of $O\left(n^{-3/2}\right)$ for E_z^{tr} as given in (4.4). The convergence rate of E_ϕ^{tr} can be improved, by following the same approach proposed in Subsection 4.6.3.

In Figure 4.3, the absolute values of the differences between the exterior and interior tangential components of total magnetic fields along the contour of the CLR are displayed. It is clear from the sub-figures that both H_z and H_ϕ are continuous across the aperture, Ω_{aper}. We observe similar Gibbs phenomenon in both sub-figures. It is worth noting that the magnitudes of the differences over Ω_{PEC} are the ϕ- and

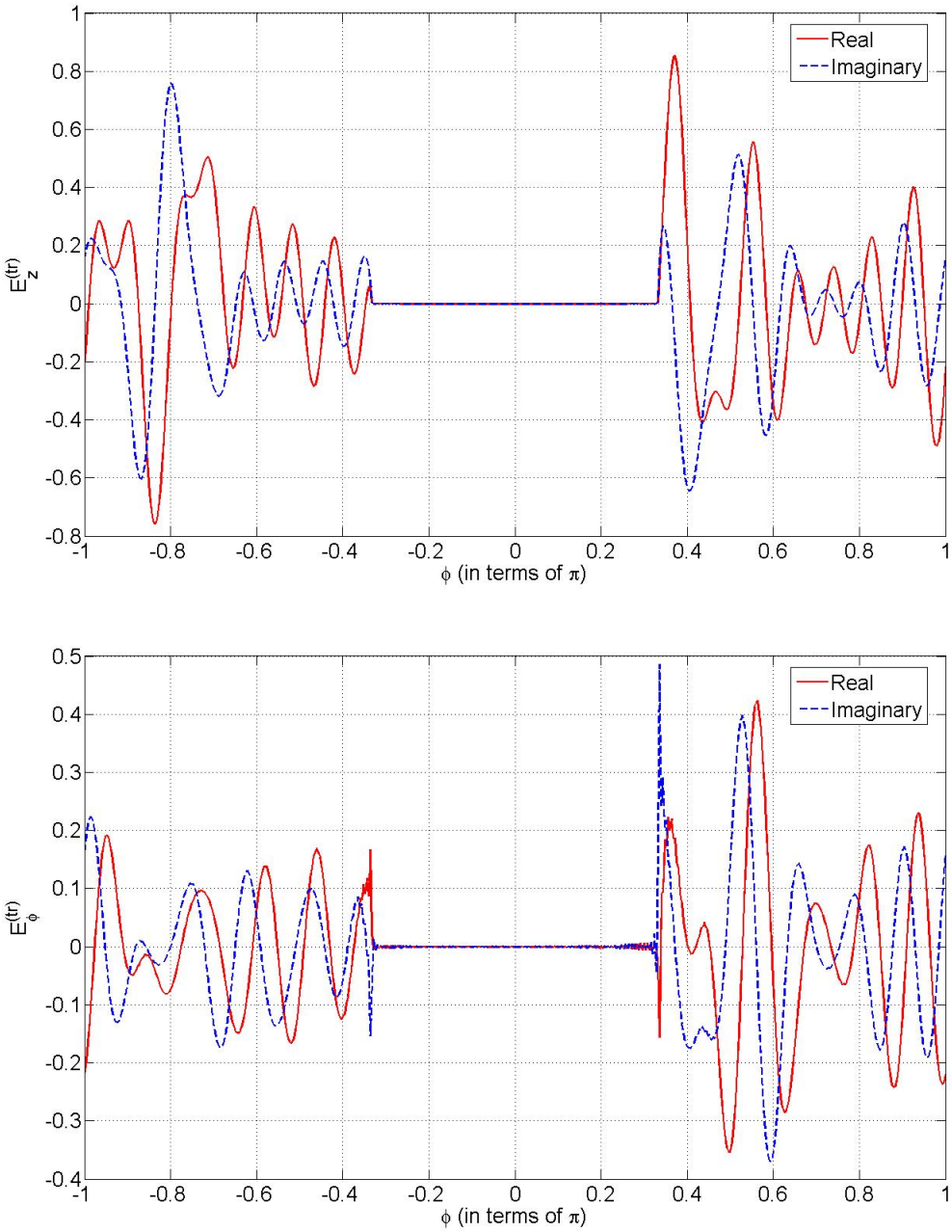

Figure 4.2: Numeric verification of (2.9a); *i.e.*, E_z^{tr} (top) and E_ϕ^{tr} (bottom) vanishes on Ω_{PEC}. [$R = 1$, $\epsilon_r = 2.1$, $\mu_r = 1$, $\theta^{\text{PEC}} = \frac{\pi}{3}$, $k_0 = 20$, $\theta_z^{\text{pw}} = \frac{\pi}{4}$, and $\theta_x^{\text{pw}} = \frac{\pi}{5}$.]

z-components of the induced surface current (in the top and bottom figures, respectively) on the PEC strip.

External tests:

Besides the excellent agreements of the numerical results for the internal tests conducted, the numerical algorithm is also employed to compute for the induced surface current and RCS for the normal incidence case $\left(\theta_z^{\text{pw}} = \frac{\pi}{2}\right)$, in order to compare results externally. Unfortunately, external verification of the algorithm for the oblique incidence case is not available, due to the lack of published results for the problem. To the best of our knowledge, [94] is the only published literature dealing with the oblique scattering problem of a slotted cylinder, using mode matching technique. However, we also notice that the problem formulation in [94] has ignored the presence of mixed polarizations, and neglected the non-vanishing axial-components of the secondary (scattered or transmitted) magnetic field.

In Figure 4.4, the real and imaginary parts, as well as the magnitude of J_z are computed for an empty slit CLR ($\epsilon_r = \mu_r = 1$) of radius $R = 1.0\lambda$, when illuminated by a normally incident TM_z plane wave. The incident wave is characterized by $\theta_z^{\text{pw}} = \frac{\pi}{2}$, and $\theta_x^{\text{pw}} = \pi$. The series representation of J_z in terms of $\left\{x_n^{(i)}, y_n^{(i)}\right\}_{n=1}^{\infty}$ $(i = 0, 1)$, has been obtained in (4.98b). In Figure 4.4, the real (solid red line) and imaginary (dashed black line) parts of J_z are plotted against the angular variable ϕ in the left sub-figure. In the right sub-figure, the absolute value of J_z is depicted. These sub-figures are compared directly to the corresponding results given in Figure 2 (a) from [97]. The curves match with those in Figure 2 (a) from [97]. Although the numerical results are not included here, we have also checked that J_ϕ, as given in (4.98a), vanishes under normal incidence. It is worth noting that Gibbs phenomenon is rather pronounced in these plots, due to the slow convergence rate of the sum resulting from the expansion coefficients of $O\left(n^{-1/2}\right)$. As mentioned previously, these observed Gibbs phenomenon can be suppressed by using the modified series expression for J_z given in (4.109), instead of the originally-derived expression given in (4.97b). In the modified series expression (4.109), the general series term has a magnitude of order $O\left(n^{-3/2}\right)$. Alternative approaches to suppress the Gibbs phenomenon include Fejér's method of summing Cesàro sums, ϵ-algorithm extrapolation method, and the explicit extraction of the square root singularities at the two edges of the strip at $\phi = \pm\theta^{\text{PEC}}$.

Figure 4.5 provides another check of the algorithm under the special case – normal incidence. The backscattering RCS produced by an empty CLR upon a normal

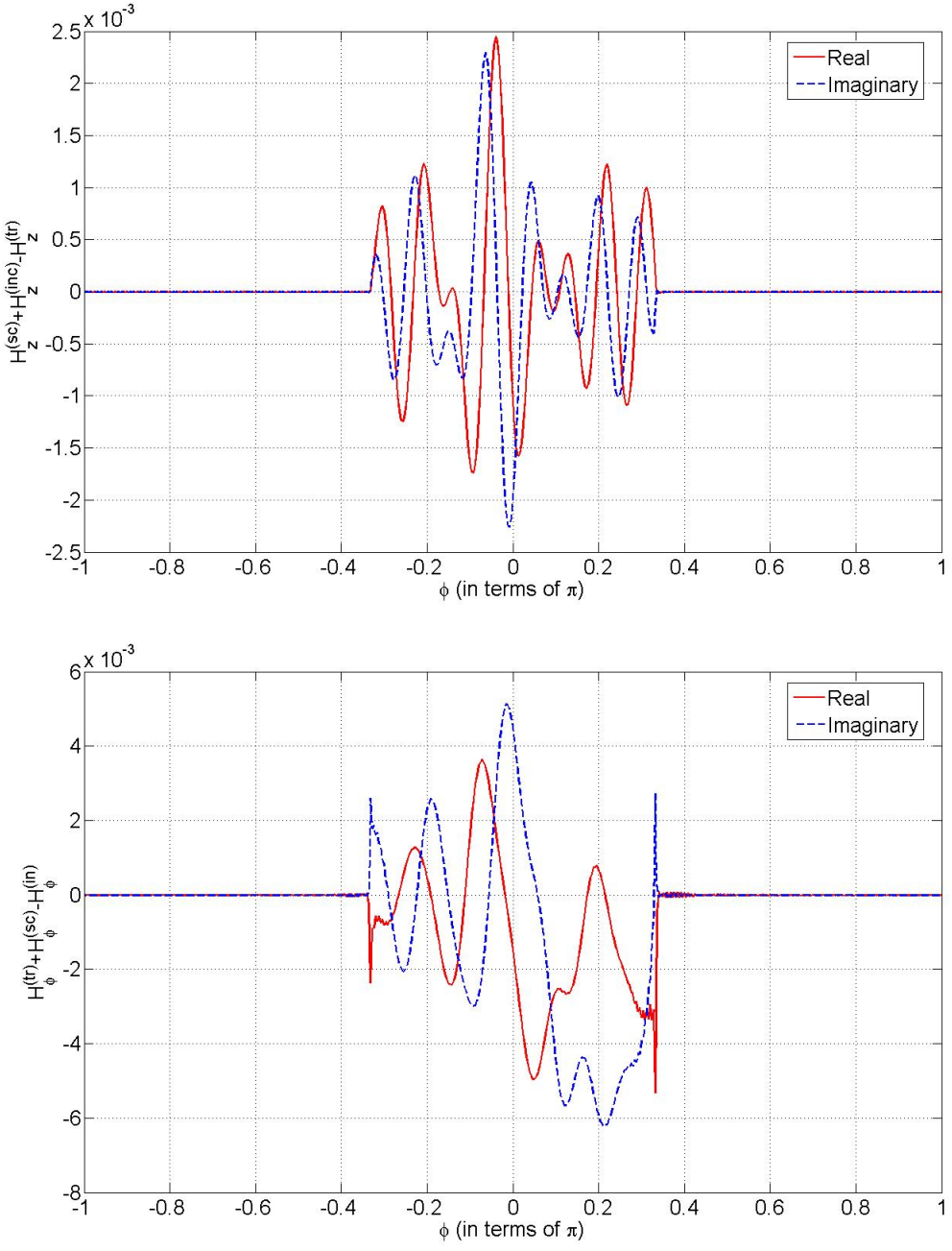

Figure 4.3: Numeric verification of (2.9b); *i.e.*, H_z (top) and H_ϕ (bottom) varies continuously across Ω_{aper}. [$R = 1$, $\epsilon_r = 2.1$, $\mu_r = 1$, $\theta^{\text{PEC}} = \frac{\pi}{3}$, $k_0 = 20$, $\theta_z^{\text{pw}} = \frac{\pi}{4}$, and $\theta_x^{\text{pw}} = \frac{\pi}{5}$.]

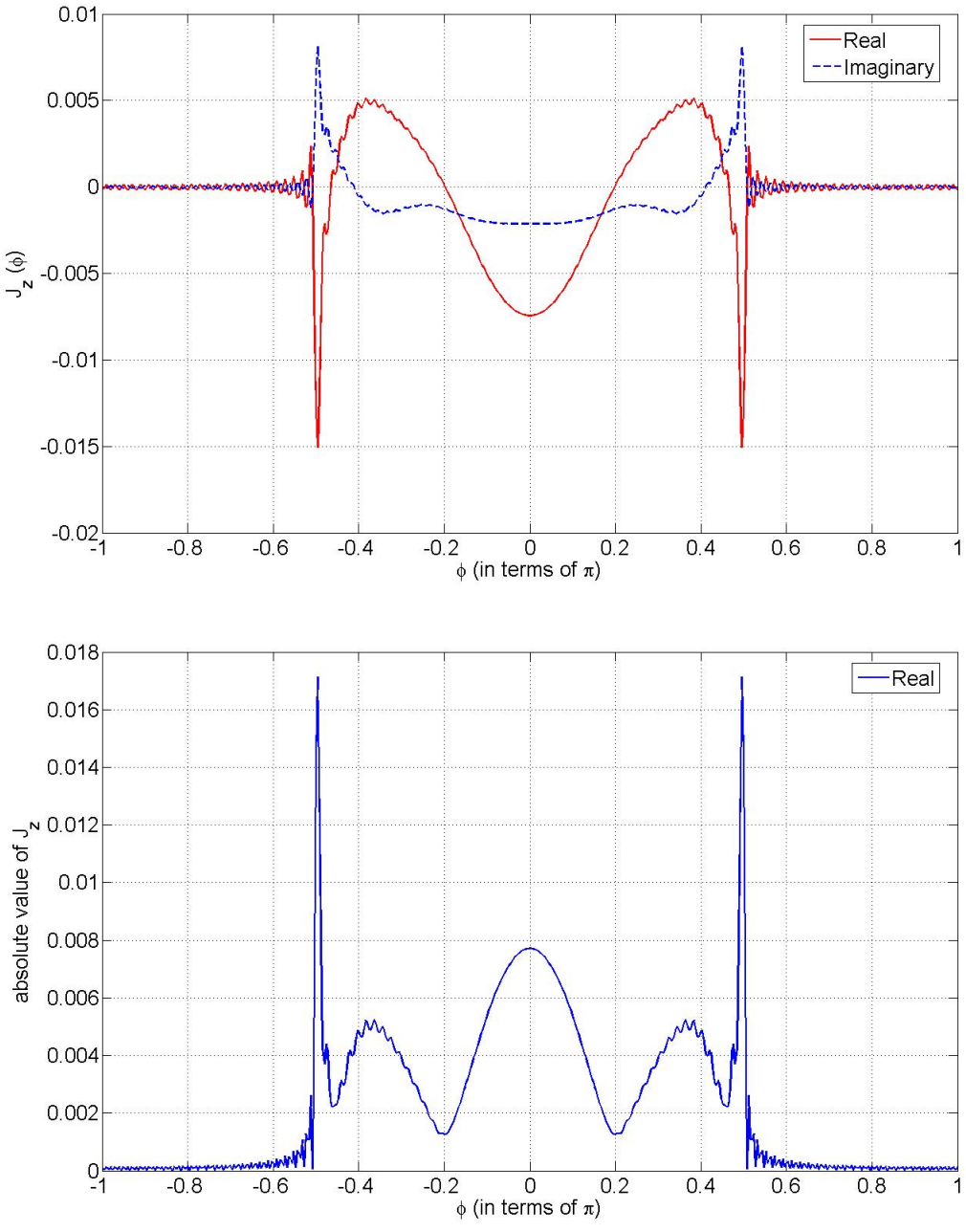

Figure 4.4: Real and imaginary parts (top), as well as magnitude (bottom) of J_z induced when a normal incident plane wave excites an empty CLR (with $\theta^{\text{PEC}} = \frac{\pi}{2}$) at angle $\theta_x^{\text{pw}} = \pi$. [$R = 1.0\lambda$, $\epsilon_r = \mu_r = 1$, $\theta^{\text{PEC}} = \frac{\pi}{2}$, $\theta_z^{\text{pw}} = \frac{\pi}{2}$, and $\theta_x^{\text{pw}} = \pi$.]

incident plane wave excitation is displayed in Figure 4.5. The series representation of the normalized RCS in terms of $\left\{x_n^{(i)}, y_n^{(i)}\right\}_{n=1}^{\infty}$ $(i = 1, 2)$ has been obtained in (4.95). Here, the following values were taken in the computation, $\epsilon_r = 1$, $\mu_r = 1$, $R = 1$, $\theta^{\mathrm{PEC}} = \frac{5}{6}\pi$, $\theta_z^{\mathrm{pw}} = \frac{\pi}{2}$ and $\theta_x^{\mathrm{pw}} = \pi$. The figure is compared directly with the result published on pg.419 in [85], and the curves are indistinguishable from each other.

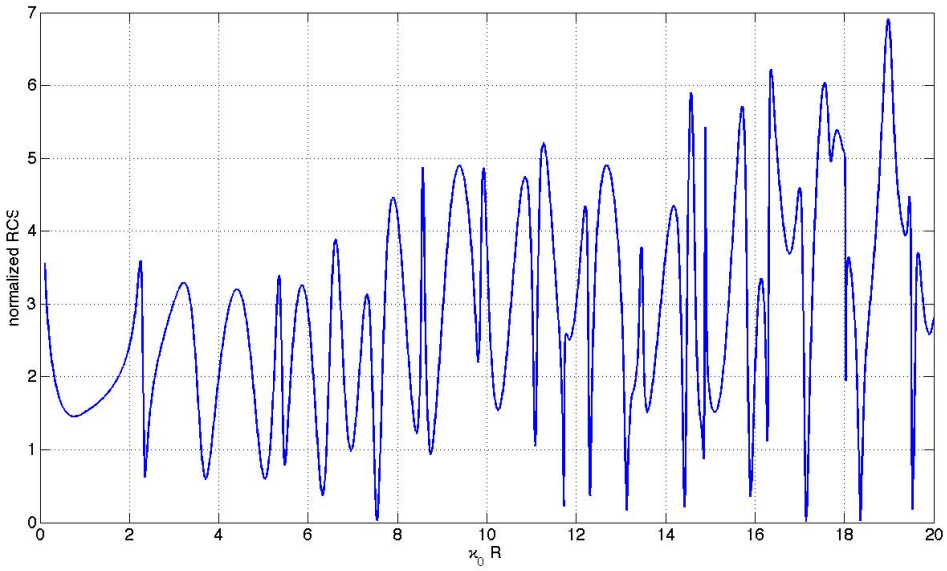

Figure 4.5: RCS induced when a normal incident plane wave excites an empty CLR. [$\epsilon_r = 1$, $\mu_r = 1$, $R = 1$, $\theta^{\mathrm{PEC}} = \frac{5}{6}\pi$, $\theta_z^{\mathrm{pw}} = \frac{\pi}{2}$ and $\theta_x^{\mathrm{pw}} = \pi$.]

4.8.2 Stability and convergence of the algorithm

Rate of convergence of solutions:

As both of the matrix equations are the second kind Fredholm equation, the solutions computed from the truncated systems converge to the exact solutions as $N_{\mathrm{tr}} \to +\infty$. To investigate the accuracy of the computed solutions, the normalized relative error $e(N_{\mathrm{tr}})$ defined in (2.43) is studied. In Figure 4.6–4.8, $e(N_{\mathrm{tr}})$ for each unknown coefficients $\left\{x_n^{(1)}\right\}_{n=1}^{\infty}$ (dotted black), $\left\{y_n^{(1)}\right\}_{n=1}^{\infty}$ (solid green), $\left\{x_n^{(2)}\right\}_{n=1}^{\infty}$ (dashed red), $\left\{y_n^{(2)}\right\}_{n=1}^{\infty}$ (dash-dotted blue) are plotted as functions of the truncation number N_{tr}. The figures are plotted on a logarithmic scale for the vertical axis. For all three of these figures, the characteristics of the CLR were set to take values $R = 1$, $\epsilon_r = 2.1$, $\mu = 1$, and $\theta^{\mathrm{PEC}} = \frac{\pi}{3}$. The incident TM_z plane wave takes fixed values

$\theta_z^{\text{pw}} = \frac{\pi}{4}$, and $\theta_x^{\text{pw}} = \frac{\pi}{5}$. Three different values of k_0 (20, 100 and 200) are considered in Figure 4.6–4.8.

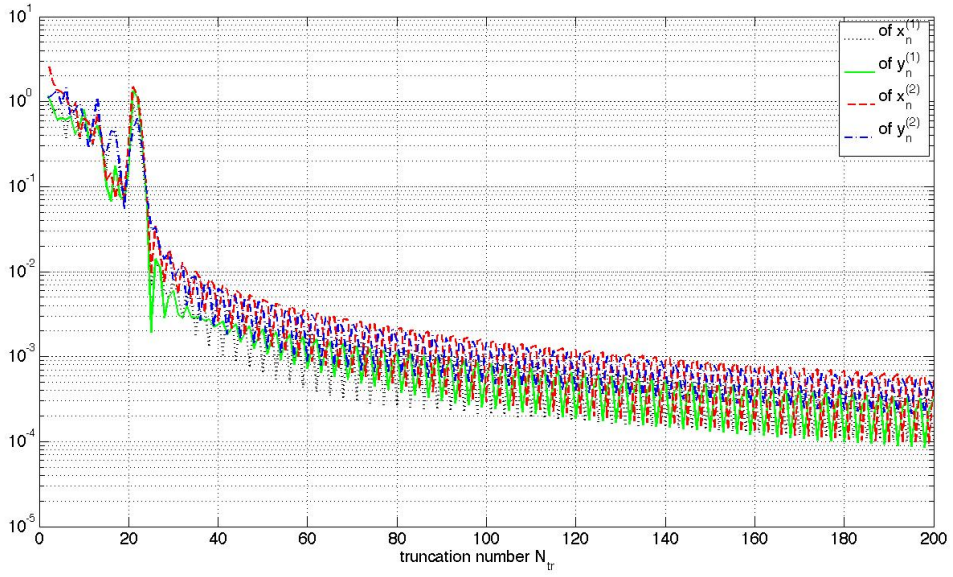

Figure 4.6: The normalized relative error of each unknown coefficients when $k_0 = 20$. [$R = 1$, $\epsilon_r = 2.1$, $\mu_r = 1$, $\theta^{\text{PEC}} = \frac{\pi}{3}$, $\theta_z^{\text{pw}} = \frac{\pi}{4}$ and $\theta_x^{\text{pw}} = \frac{\pi}{5}$]

From Figure 4.6–4.8, we can see that the normalized relative error $e(N_{\text{tr}})$ for each of the computed unknown coefficients is clearly steadily decreasing once the chosen N_{tr} exceeds the parameter $\kappa_1 R$, which has value around 25 (126 or 253) when k_0 is 20 (100 or 200). This is greatly due to the fact that the magnitudes of the asymptotically small parameters diminish at the order $O\left(\left[\frac{\kappa_1 R}{n}\right]^2\right)$. As a result, we can see that N_{tr} required for an aforesaid accuracy increases with the incident wavenumber k_0, by comparing the three plots.

Stability of the systems:

As the computation process of the unknown coefficients involves numerical inversion of the matrices $(\mathcal{F}_1 - \mathcal{C}_1)$ and $(\mathcal{F}_2 - \mathcal{C}_2)$, another useful quantity to investigate is the condition number of each of these two matrices. The scattering problem considered in these figures has the same parameter values as those in Figure 4.6–4.7; that is, $R = 1$, $\epsilon_r = 2.1$, $\mu = 1$, $\theta^{\text{PEC}} = \frac{\pi}{3}$, $\theta_z^{\text{pw}} = \frac{\pi}{4}$ and $\theta_x^{\text{pw}} = \frac{\pi}{5}$. The reason why the solutions can be obtained in any predetermined accuracy can be explained by the plots of the condition numbers against N_{tr} given in Figure 4.9–4.11, for $k_0 = 20$, 50 and 100.

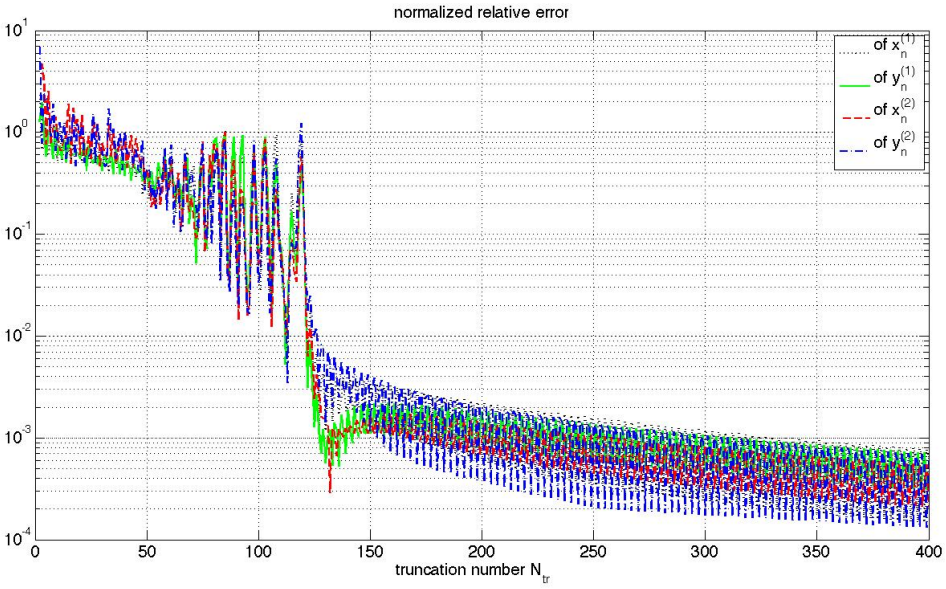

Figure 4.7: The normalized relative error of each unknown coefficients when $k_0 = 100$. $[R = 1,\ \epsilon_r = 2.1,\ \mu_r = 1,\ \theta^{\mathrm{PEC}} = \frac{\pi}{3},\ \theta_z^{\mathrm{pw}} = \frac{\pi}{4}$ and $\theta_x^{\mathrm{pw}} = \frac{\pi}{5}]$

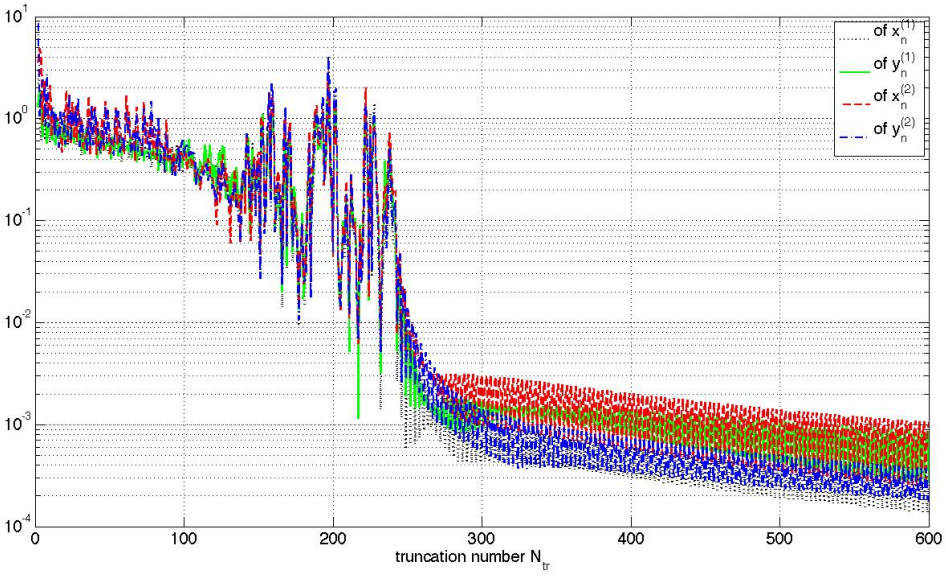

Figure 4.8: The normalized relative error of each unknown coefficients when $k_0 = 200$. $[[R = 1,\ \epsilon_r = 2.1,\ \mu_r = 1,\ \theta^{\mathrm{PEC}} = \frac{\pi}{3},\ \theta_z^{\mathrm{pw}} = \frac{\pi}{4}$ and $\theta_x^{\mathrm{pw}} = \frac{\pi}{5}]$

We can see that the condition numbers — solid blue for $(\mathcal{F}_1 - \mathcal{C}_1)$, and dashed red for $(\mathcal{F}_2 - \mathcal{C}_2)$ — tends to a constant value while the dimension of the systems, N_{tr}, increases and exceeds the value of $\kappa_1 R$. In other words, they are uniformly bounded, as N_{tr} increases. These corresponding condition numbers to the matrix operators of the problem tends to a constant value. That is just the reason why the solution can be obtained in any predetermined accuracy. For condition number of magnitude 10^6 to 10^7, as shown in Figure 4.6–4.7, we can see that about 7 decimal places are lost by computer due to roundoff errors. An accuracy of 9 decimal places can still be achieved with an average computer and 16 decimal places precision. This level of accuracy is more than adequate for most numerical investigations in the field.

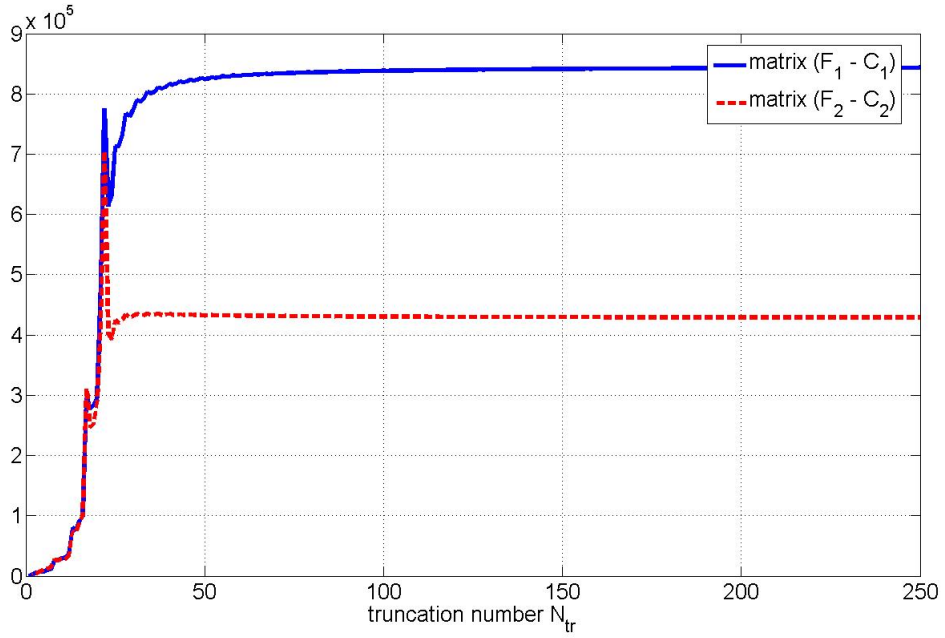

Figure 4.9: The condition numbers of the matrices $(\mathcal{F}_1 - \mathcal{C}_1)$ and $(\mathcal{F}_2 - \mathcal{C}_2)$ when $k_0 = 20$. $[R = 1,\ \epsilon_r = 2.1,\ \mu_r = 1,\ \theta^{\text{PEC}} = \frac{\pi}{3},\ \theta_z^{\text{pw}} = \frac{\pi}{4}$ and $\theta_x^{\text{pw}} = \frac{\pi}{5}]$

Besides the uniformly bounded condition number for the matrices, another interesting feature of the systems is that the condition numbers peak when a resonance frequency is approached. To demonstrate this, the backscattering RCS is plotted against $k_0 R$ in Figure 4.12, in order to locate the resonance frequency. The normalized magnitude of the backscattering RCS in decibels (dB) is depicted; *i.e.*,

$$\hat{\sigma}_{\text{b}}(\text{dB}) = 10 \log_{10} \left(\frac{\sigma_{\text{b}}}{\pi R} \right). \tag{4.115}$$

The two data cursors outlined peak and trough frequencies where $k_0 R = 9.019$ and 9.816, respectively. A closer examination of the rate of convergence and condition

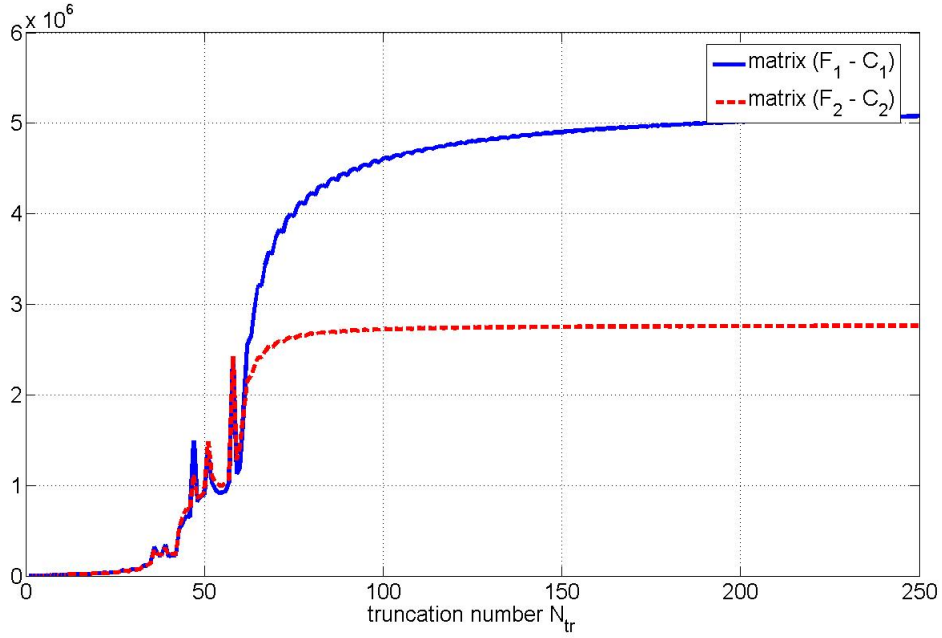

Figure 4.10: The condition numbers of the matrices $(\mathcal{F}_1 - \mathcal{C}_1)$ and $(\mathcal{F}_2 - \mathcal{C}_2)$ when $k_0 = 50$. $[R = 1,\ \epsilon_r = 2.1,\ \mu_r = 1,\ \theta^{\text{PEC}} = \frac{\pi}{3},\ \theta_z^{\text{pw}} = \frac{\pi}{4}$ and $\theta_x^{\text{pw}} = \frac{\pi}{5}]$

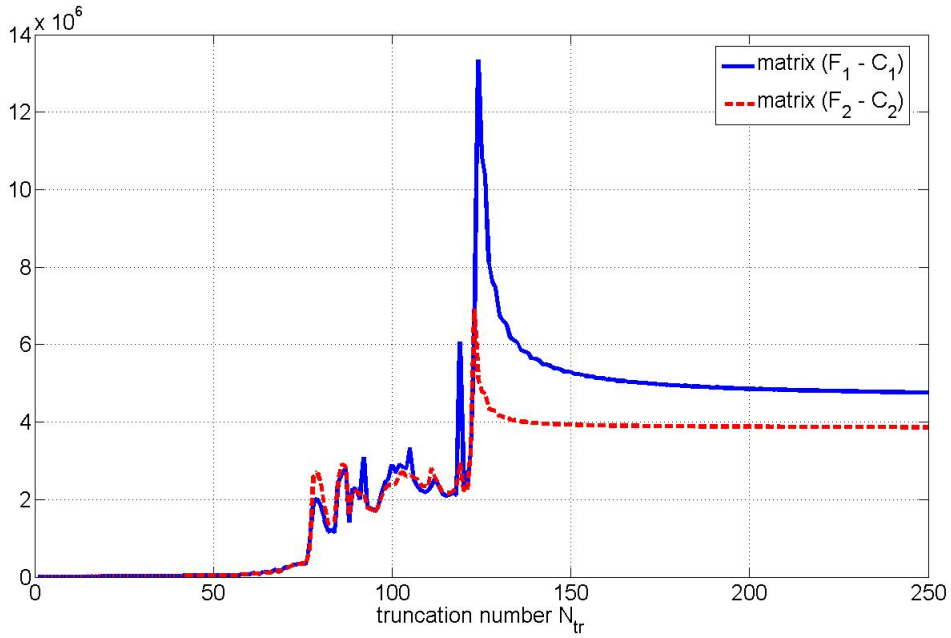

Figure 4.11: The condition numbers of the matrices $(\mathcal{F}_1 - \mathcal{C}_1)$ and $(\mathcal{F}_2 - \mathcal{C}_2)$ when $k_0 = 100$. $[R = 1,\ \epsilon_r = 2.1,\ \mu_r = 1,\ \theta^{\text{PEC}} = \frac{\pi}{3},\ \theta_z^{\text{pw}} = \frac{\pi}{4}$ and $\theta_x^{\text{pw}} = \frac{\pi}{5}]$

number of the problem at these two frequencies is carried out in Figure 4.13 and Figure 4.14. The plots of the condition numbers (the bottom figures) reveals that the matrices have larger condition numbers (about 15 times larger) at the resonance frequency $k_0R = 9.019$ than those at the higher frequency $k_0R = 9.816$. However, the plots of the normalized relative error (the top figures) suggest that 3-digit accuracy may be achieved if $N_{\text{tr}} \approx 100$ for both of the frequencies.

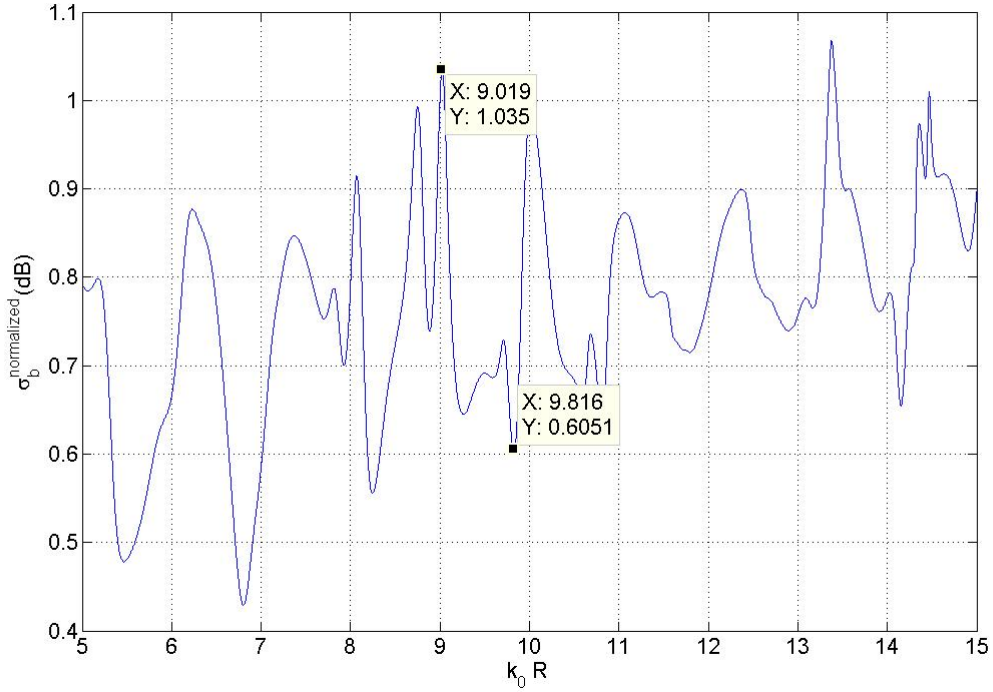

Figure 4.12: The normalized backscattering RCS for $5 \leq k_0R \leq 15$. [$R = 1$, $\epsilon_r = 2$, $\mu_r = 1$, $\theta^{\text{PEC}} = \frac{\pi}{3}$, $\theta_z^{\text{pw}} = \frac{\pi}{4}$ and $\theta_x^{\text{pw}} = \frac{\pi}{5}$]

4.8.3 Effect of the polar incident angle on the scattering behaviors

The frequency dependent, dB-scaled energy stored inside the CLR, W, is plotted in the following figures, for a CLR with characteristics $\theta^{\text{PEC}} = \frac{5}{6}\pi$, $\epsilon_r = 2.1$, $\mu_r = 1$, and $R = 1$. The CLR is excited by a TM_z plane wave at $\theta_x^{\text{pw}} = \pi$, and varying values of θ_z^{pw}. To investigate the effect of polar incident angle θ_z^{pw} has on the scattering behaviors of the CLR, the value of θ_z^{pw} is taken to be $\frac{\pi}{2}$ (dashed red), $\frac{\pi}{3}$ (dotted black), or $\frac{\pi}{6}$ (dot-dashed blue) in Figure 4.15. The effect of the oblique incident angle θ_z^{pw} on RCS (dB) of the same CLR is investigated. The comparison is depicted in Figure 4.16.

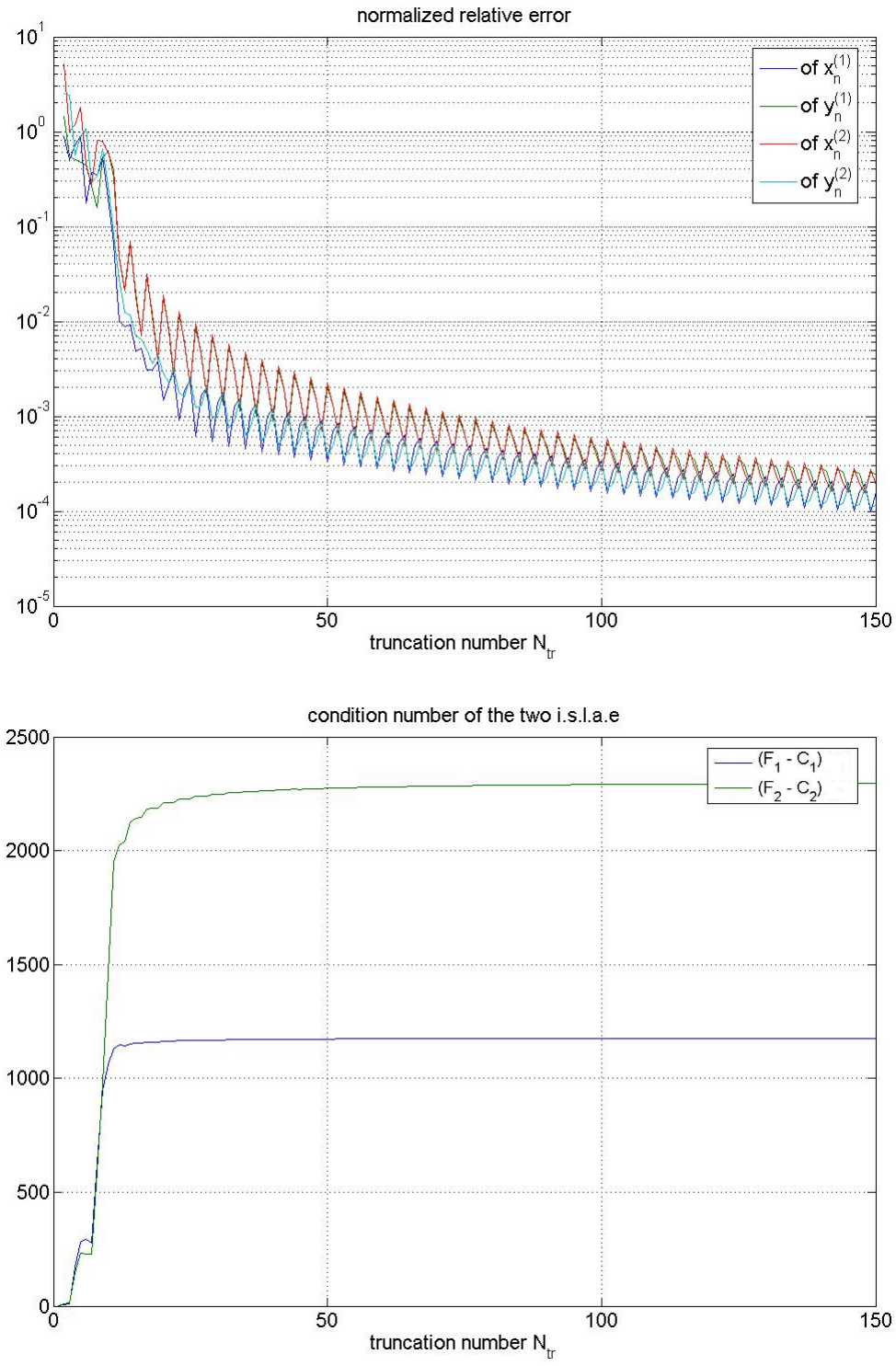

Figure 4.13: The normalized relative error and condition numbers of $(\mathcal{F}_1 - \mathcal{C}_1)$ and $(\mathcal{F}_2 - \mathcal{C}_2)$ at the resonance frequency $k_0 R = 9.019$. [$R = 1$, $\epsilon_r = 2$, $\mu_r = 1$, $\theta^{\mathrm{PEC}} = \frac{\pi}{3}$, $\theta_z^{\mathrm{pw}} = \frac{\pi}{4}$ and $\theta_x^{\mathrm{pw}} = \frac{\pi}{5}$]

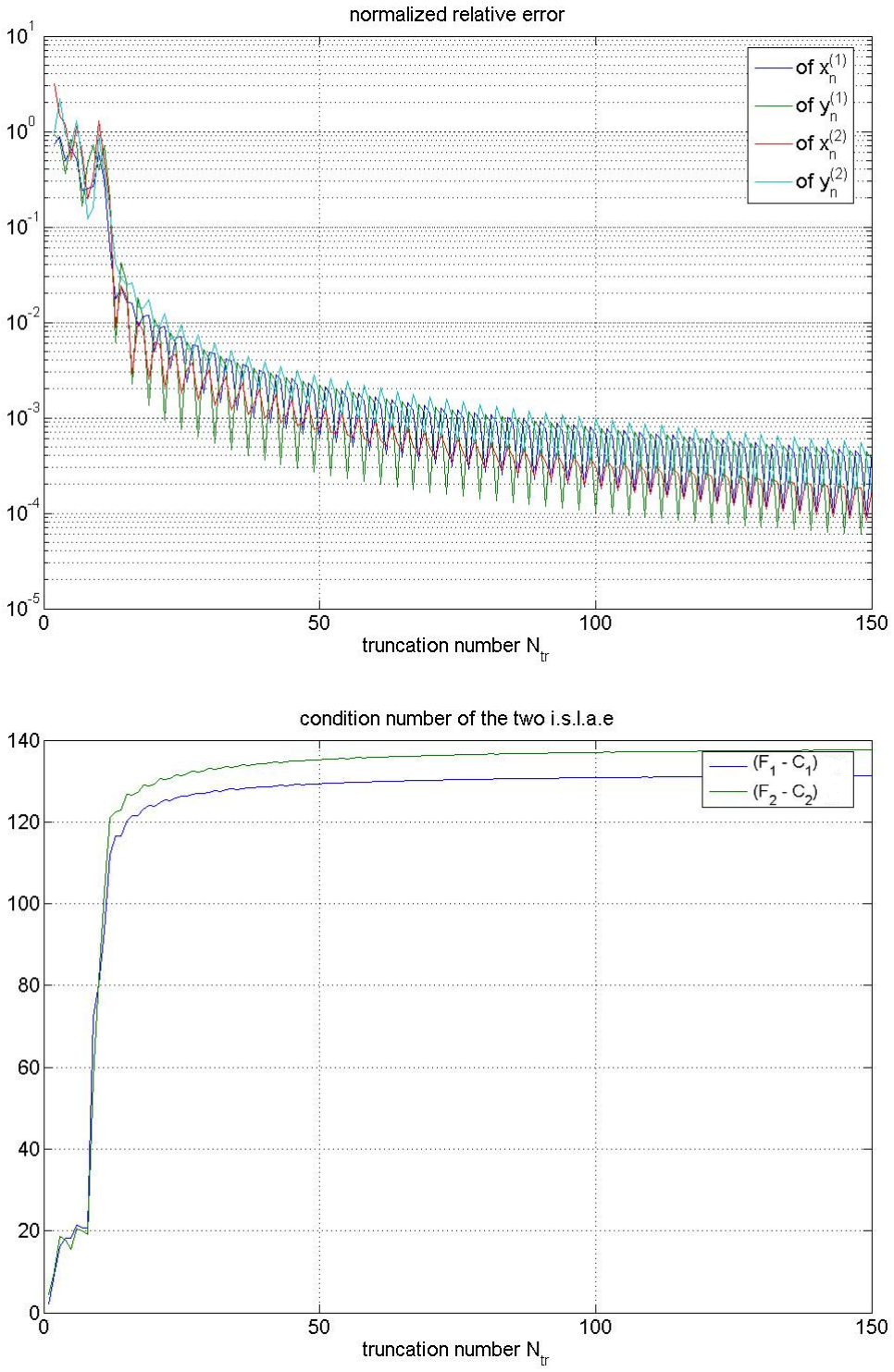

Figure 4.14: The relative error and condition number of $(\mathcal{F}_1 - \mathcal{C}_1)$ and $(\mathcal{F}_2 - \mathcal{C}_2)$ at frequency $k_0 R = 9.816$. $[R = 1,\ \epsilon_r = 2,\ \mu_r = 1,\ \theta^{\mathrm{PEC}} = \frac{\pi}{3},\ \theta_z^{\mathrm{pw}} = \frac{\pi}{4}$ and $\theta_x^{\mathrm{pw}} = \frac{\pi}{5}]$

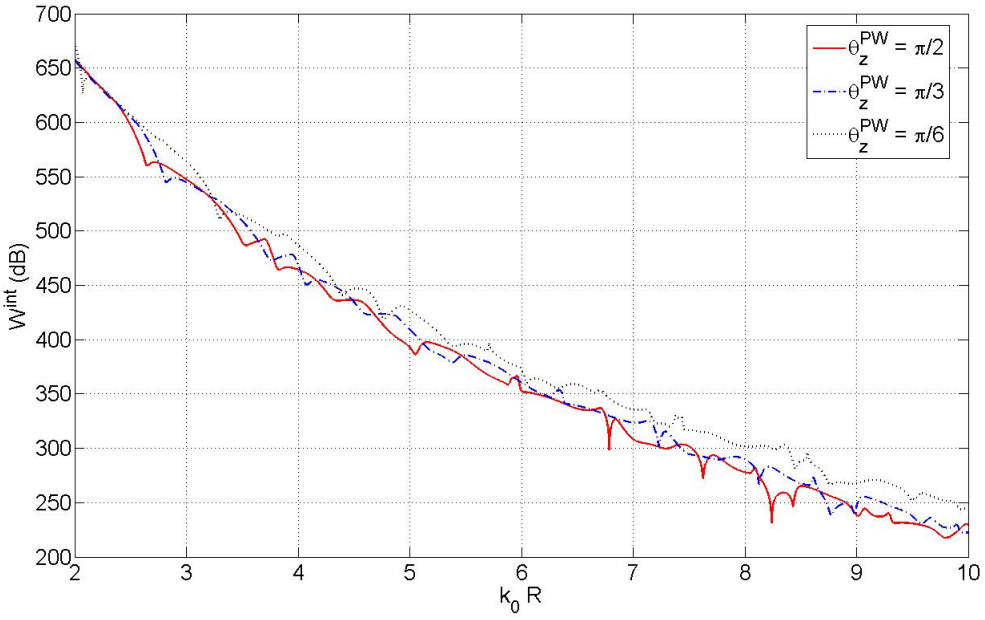

Figure 4.15: Energy stored inside the CLR when excited by a TM_z plane wave at different polar angle; *i.e.*, $\theta_z^{\mathrm{pw}} = \frac{\pi}{2}$ (dashed red), $\frac{\pi}{3}$ (dotted black), or $\frac{\pi}{6}$ (dot-dashed blue). [$R = 1$, $\theta^{\mathrm{PEC}} = \frac{5}{6}\pi$, $\epsilon_r = 2.1$, $\mu_r = 1$, and $\theta_x^{\mathrm{pw}} = \pi$]

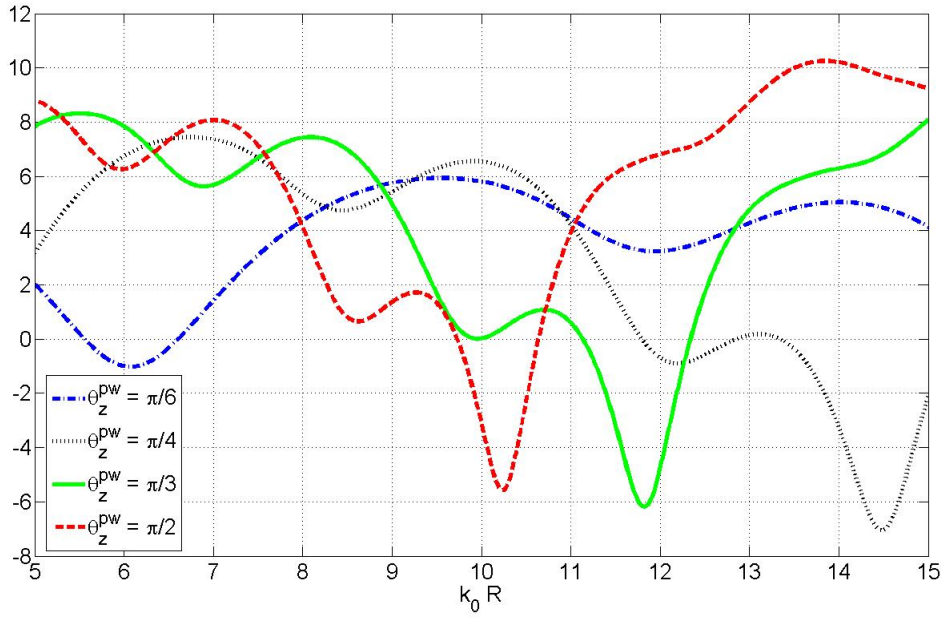

Figure 4.16: Backscattered RCS induced when the CLR is excited by a TM_z plane wave at different polar angle; *i.e.*, $\theta_z^{\mathrm{pw}} = \frac{\pi}{2}$ (dashed red), $\frac{\pi}{3}$ (solid green), $\frac{\pi}{4}$ (dotted black), or $\frac{\pi}{6}$ (dot-dashed blue). [$R = 1$, $\theta^{\mathrm{PEC}} = \frac{\pi}{2}$, $\epsilon_r = 2.1$, $\mu_r = 1$, and $\theta_x^{\mathrm{pw}} = \pi$]

From both Figure 4.15 and Figure 4.16, we can see that as the polar angle θ_z^{pw} moves away from the $\frac{\pi}{2}$ (being perpendicular to the cylinder axis), the resonance frequencies are shifted to the right. It is as though a smaller CLR is excited when θ_z^{pw} decreases. From Figure 4.15, we see that the energy stored in the interior of CLR slightly increases, as θ_z^{pw} decreases. Part of the incident plane wave propagates down the z-axis, and remains in the interior of the CLR, when the incident wavelength exceeds the cut-off for the CLR. In this case, the CLR acts like a waveguide[3]. On the other hand, in addition to the stretching out of the RCS pattern as θ_z^{pw} decreases, we also notice that the magnitude of the peaks and troughs are dampen in Figure 4.16. This is because the obliquely-incident plane wave does not penetrate as deeply into the interior of the CLR as the case for a normal incident plane wave. The smaller θ_z^{pw} is, the more energy is lost to the surrounding due to refraction and transmission, instead of being diffracted back in the direction of the incoming source.

4.9 Comments and conclusion

In this chapter, the MoR is extended to study the scattering characteristics of CLR under an oblique plane wave excitation. This is the first rigorous treatment of this subject necessitating a substantive and extended application of analytical regularization approaches that have previously appeared in the literature. For oblique incidence of either TM_z or TE_z plane wave, the z-components of the electric and magnetic fields are coupled together, and have to be treated simultaneously. Two pairs of coupled ISLAE are obtained for the unknown coefficients. Each pair of them can be formulated as a 2-by-2 block matrix equation of the second kind Fredholm, and solved efficiently, reliably by numerical matrix inversion.

As an internal check of the algorithm, the MBC is validated by substitution of the computed coefficients back into the series representations of fields. To validate the algorithm externally, the surface current density and RCS are computed. The computed results are in good agreement with those which appear in previous studies [97] and [85].

The computed solution is also tested for warranty of stability and convergence by studying the normalized relative error $e(N_{\text{tr}})$ for different values of k_0. We can see that, by choosing $N_{\text{tr}} \approx [\kappa_1 R + 100]$, a 3 decimal places accuracy can be guaranteed

[3]The propagating modes of a closed waveguide have been widely documented in the literature. For the range of dimensions we consider here, several propagating modes are supported by a closed waveguide of these dimensions. Comparing the open CLR problem to this standard closed waveguide, we deduced that guided modes are supported for the dimension considered in the figures.

for the computation of RCS. Series expressions of the internal stored energy, RCS and surface current density are obtained in terms of the coefficients $\left\{x_n^{(i)}, y_n^{(i)}\right\}_{n=1}^{\infty}$ $(i = 0, 1)$. An approach to improve the convergence rate of the series are also proposed. We see that, by using the reformulated series representation for J_z, a smaller valued N_{tr} is required for a predetermined accuracy.

The effect of the oblique incident angle on the scattering behaviors of the CLR are investigated, by studying the energy distribution and RCS. As the oblique incident angle, where $\theta_z^{\text{pw}} \in \left(0, \frac{\pi}{2}\right)$, decreases in value, more energy is stored in the interior of the CLR (as the wave propagates down the cylinder) and less is diffracted back. In addition, the surface current possess both the z- and ϕ- components, for an oblique incident problem. As θ_z^{pw} moves away from $\frac{\pi}{2}$, the value of J_z decreases, while that of J_ϕ increases. Some parametric optimizations maybe introduced to achieve well-suppressed side lobes and powerful backscattering (see next chapter).

Chapter 5

RCS studies of dielectric cylindrical lens reflectors

5.1 Introduction

Lens Reflectors have been used in microwave communications for many years. Most investigations are concerned with the Spherical Lens Reflectors (SLR) [29, 31, 63, 70, 71, 83] in the form of a stepped-index Luneburg Lens (LL) with attached PEC spherical cap. The stepped-index LL has been intensively used as a focusing device. As an approximation to the ideal LL with continuously varying dielectric constant, the stepped-index version reveals the same performance as expected of the ideal LL at a frequency range limited by some "cut-off" frequency strictly depending on the number of concentric layers. It simply means that when using the stepped-index LL, the widening of the frequency range for desired performance is only possible with an increased number of layers. Such an approach is not efficient as manufacturing LL with a larger number of layers is highly costly.

For this reason, some recent investigations, for example [83], have studied a homogeneous dielectric sphere as an alternative choice to the LL. Possessing a less pronounced focusing at any selected frequency, this simple spherical lens is advantageous when it is used as a wide-band frequency lens. It was shown in [83] that, in some cases the RCS spectral characteristics of the reflector attached to a homogeneous sphere are superior to those of based on the LL.

The objective of this chapter is two-fold. First, similar to [83], we study the competitiveness of the reflector based on a constant-K lens (homogeneous dielectric cylinder) with that based on a cylindrical LL. Secondly, we study the properties of the backscattering when the incidence angle varies from that value corresponding to

normal incidence to that describing the grazing incidence. This part of the investigation is of strong interest for 3D lens reflectors, because the dependence of RCS versus incidence angle has not been studied in full, perhaps because the relevance of such results for 3D SLR is of qualitative character. From a general physical approach, it is clear that focusing provided by 2D dielectric lenses is much weaker than that realized by 3D lenses. When implementing the ray-tracing techniques, a 2D lens produces focusing in the plane, whereas a 3D lens produces volumetric focusing. In other words, in the second case the more rays collected at the focus represents a higher intensity of electromagnetic energy density.

To some extent, the study in this chapter may be regarded as "2D version" of [83], with only one but essential addition, which concerns the RCS studies with varying incidence angle. The chapter is organized as follows. In Section 5.2, we describe, in brief, the problem geometry. In Section 5.3, the solution to the scattering problem employing the MoR is obtained. It analytically transforms the singular series equations of the first kind to an ISLAE of the second kind. In Section 5.4, we apply the well-known solution for plane wave scattering by a homogeneous dielectric cylinder to study the focusing effect at different values of permittivity ϵ_r and electrical size $\frac{D}{\lambda}$ $\left(= \frac{k_0 R}{\pi}\right)$. Here, $D = 2R$ is the diameter of the cylindrical lens of radius R, while λ and $k_0 = \frac{2\pi}{\lambda}$ are, respectively, the wavelength and wavenumber in a free space. The study concentrates on the exact calculation of the focal spot location, which is to be further used for proper placement of the reflecting PEC cylindrical strip. This provides the optimal illumination by the focused electromagnetic flux, which leads to the strong backscattering that makes the CLR a powerful reflector. Section 5.5 is related to the comparison of effectiveness of the lenses based on the constant-K lens or LL. The spectral dependence of the RCS versus electric size of structure is studied in a wide frequency range extending up to the quasi-optical region ($\frac{D}{\lambda} \approx 200$). In Section 5.6, we examine the behavior of the RCS depending on the incident angle of the incoming plane wave. In the conclusion, we summarize the basic results and discuss further work.

5.2 Geometrical description of the problem

A multi-layered version of the homogeneous CLR studied in Chapter 4 is considered in the formulation here. Figure 5.1 gives a description of the geometry of a general infinitely-long, L-layered dielectric cylinder with a PEC strip conformally placed on its surface. All the cylinders are assumed to be parallel to the z-direction. The

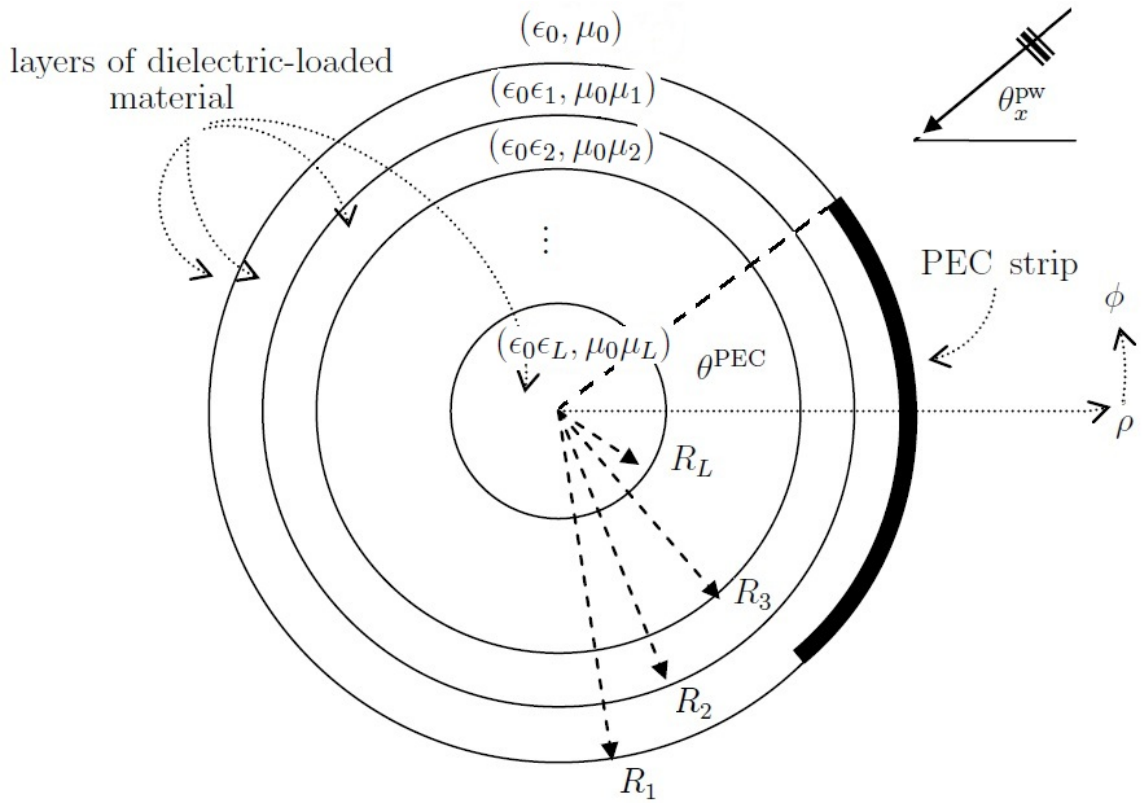

Figure 5.1: A cross-sectional view of a generic multi-layered dielectric-loaded cylinder with attached conformal PEC strip.

whole medium is divided by the L interfaces of the multi-layered cylinder (*i.e.*, when $\rho = R_1, R_2, \ldots, R_L$) into $(L+1)$ regions. The numbering system used here is such that region 0 denotes the scattering region external to the cylinder; while region L denotes the innermost dielectric loaded layer. The outermost region 0 is taken to be the free space with constitutive parameters (ϵ_0, μ_0). Each of the dielectric regions is characterized by its relative permittivity and permeability (ϵ_i, μ_i), $i = 1, 2, \ldots, L$. The PEC strip, assumed to be infinitely thin, is attached to the multi-layered cylinder at $\rho = R_1$. We adopt the same notations as in Chapter 4 for the angles; *i.e.*, θ^{PEC} denotes the half-angular width subtended by the strip at the center, while θ_x^{pw} is the incident angle the normal incident TM_z plane wave makes with respect to the x-axis at the center.

The LL is a dielectric lens with its permittivity varying with the radius of the cylindrical lens. Its relative permittivity is given by the well-known formula

$$\epsilon(\rho) = 2 - \left(\frac{\rho}{R_1}\right)^2, \text{ for } 0 \leq \rho \leq R_1, \tag{5.1}$$

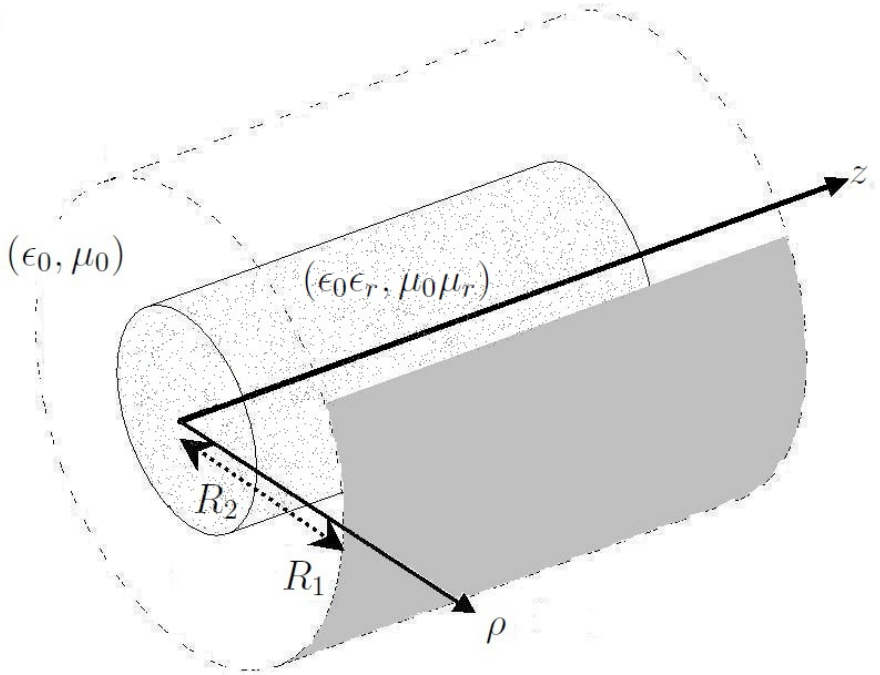

Figure 5.2: Geometry of a infinitely long CLR with a carefully located conformal PEC strip to achieve maximum backscattering.

where R_1 is the radius of the LL. A PEC strip is conformally attached to the surface of the LL. In this construction, the CLLR focuses the incident plane wave to a point at its surface, where the reflecting PEC strip is located. The focusing waves are reflected backward in the opposite direction to the incident plane wave. From the manufacturing point of view, the CLLR is approximated by a stepped-index dielectric-loaded lens. This approximation to the ideal CLLR is a special case of the multi-layered cylinder described in Figure 5.1.

In addition, with appropriate choice of parameters, this multi-layered cylinder can be considered as CLR or Cylindrical Luneburg lens reflector (CLLR). The CLR is a "two-layered" model of this general model, with region 0 and region 1 sharing the same physical quantities; (*i.e.*, they are both the free space), while region 2 represents the homogeneous dielectric lens. We use $(\epsilon_0\epsilon_r, \mu_0\mu_r)$ to denote the physical quantities of this dielectric lens, and R to denote its radius. The PEC strip, which serves as a reflector, is placed at $\rho = R_1$. The location of the reflecting surface (*i.e.*, the PEC strip) is carefully selected to lie close to the spot where incoming plane wave is focused. This is done by studying the energy distribution of the constant-K cylindrical lens after the impingement of the incident plane wave. In other words, we have a concentric layer of air surrounding the core dielectric cylinder, as shown in Figure 5.2.

5.3 Problem formulation

As a normal incident TM_z plane wave is considered (*i.e.*, $\theta_z^{\mathrm{pw}} = \frac{\pi}{2}$ and $k_z = 0$), only E_z, H_ϕ and H_ρ are non-vanishing in this problem. We adopt the following series representation for the secondary E_z in each region i:

$$E_z^{(i)} = \sum_{n=-\infty}^{\infty} \left[a_n^{(i)} \frac{H_n^{(2)}(k_i\rho)}{H_n^{(2)}(k_i R_{i+1})} + b_n^{(i)} J_n(k_i\rho) H_n^{\prime(2)}(k_i R_i) \right] e^{jn\phi}\,, \tag{5.2}$$

where $i = 0, 1, \ldots, L$. In order for the scattered field in the unbounded region 0 to satisfy the Sommerfeld radiation condition, we have $\left\{ b_n^{(0)} \right\}_{n\in\mathbb{Z}} \equiv 0$. On the other hand, for the boundedness of the transmitted field in the innermost region L, we set $\left\{ a_n^{(L)} \right\}_{n\in\mathbb{Z}} \equiv 0$. The series representations for $H_\phi^{(i)}$ and $H_\rho^{(i)}$ in region i can be obtained from (2.33) to be:

$$H_\phi^{(i)} = \frac{1}{j\eta_i} \sum_{n=-\infty}^{\infty} \left[a_n^{(i)} \frac{H_n^{\prime(2)}(k_i\rho)}{H_n^{(2)}(k_i R_{i+1})} + b_n^{(i)} J_n'(k_i\rho) H_n^{\prime(2)}(k_i R_i) \right] e^{jn\phi}\,, \tag{5.3}$$

$$H_\rho^{(i)} = -\frac{1}{\eta_i k_i \rho} \sum_{n=-\infty}^{\infty} n \left[a_n^{(i)} \frac{H_n^{(2)}(k_i\rho)}{H_n^{(2)}(k_i R_{i+1})} + b_n^{(i)} J_n(k_i\rho) H_n^{\prime(2)}(k_i R_i) \right] e^{jn\phi}\,, \tag{5.4}$$

where $\eta_i = \sqrt{\frac{\mu_0\mu_i}{\epsilon_0\epsilon_i}}$ is the characteristic impedance of region i ($i = 0, 1, \ldots, L$).

As stated in (2.6a) and (2.7), the tangential total electric and magnetic fields are continuous across the dielectric interface. That is, for all $\phi \in (-\pi, \pi)$:

$$E_z^{(i-1)}(\phi, R_i) = E_z^{(i)}(\phi, R_i)\,, \qquad \text{for } i = 1, 2, \ldots, L; \tag{5.5}$$

$$H_\phi^{(i-1)}(\phi, R_i) = H_\phi^{(i)}(\phi, R_i)\,, \qquad \text{for } i = 2, 3, \ldots, L. \tag{5.6}$$

Imposing these continuity conditions allows us to write all the unknown coefficients $\left\{ a_n^{(i)}, b_n^{(i)} \right\}_{n\in\mathbb{Z}}$ for $i = 0, 1, \ldots, (L-1)$ in terms of the unknown $\left\{ b_n^{(L)} \right\}_{n\in\mathbb{Z}}$.

Application of the continuity of E_z on each of R_i (for $i = 1, 2, \ldots, L$) allows us to write every one of $\left\{ a_n^{(i)} \right\}_{n\in\mathbb{Z}}$ in terms of the unknowns $\left\{ b_n^{(i)} \right\}_{n\in\mathbb{Z}}$.

$$\begin{aligned} a_n^{(i)} =& b_n^{(L)} J_n(k_L R_L) H_n^{\prime(2)}(k_L R_L) \prod_{j=i+1}^{L-1} \frac{H_n^{(2)}(k_j R_j)}{H_n^{(2)}(k_j R_{j+1})} - b_n^{(i)} J_n(k_i R_{i+1}) H_n^{\prime(2)}(k_i R_i) \\ &+ \sum_{j=i+1}^{L-1} b_n^{(j)} \varsigma_n^{(j)} \frac{H_n^{\prime(2)}(k_j R_j)}{H_n^{(2)}(k_j R_{j+1})} \prod_{k=i+1}^{j-1} \frac{H_n^{(2)}(k_k R_k)}{H_n^{(2)}(k_k R_{k+1})}\,, \end{aligned} \tag{5.7}$$

for $i = 1, 2, \ldots, L-1$; while for $i = 0$, we have:

$$a_n^{(0)} = -c_n + b_n^{(L)} J_n(k_L R_L) H_n^{\prime(2)}(k_L R_L) \prod_{j=1}^{L-1} \frac{H_n^{(2)}(k_j R_j)}{H_n^{(2)}(k_j R_{j+1})}$$

$$+\sum_{j=1}^{L-1} b_n^{(j)} \varsigma_n^{(j)} \frac{H_n^{'(2)}(k_j R_j)}{H_n^{(2)}(k_j R_{j+1})} \prod_{k=1}^{j-1} \frac{H_n^{(2)}(k_k R_k)}{H_n^{(2)}(k_k R_{k+1})} \,. \tag{5.8}$$

In the above, we have introduced $\left\{\varsigma_n^{(i)}\right\}_{n\in\mathbb{Z}}$ to simplify the expressions. For $i = 1, 2, \ldots, (L-1)$,

$$\varsigma_n^{(i)} := J_n(k_i R_i) H_n^{(2)}(k_i R_{i+1}) - J_n(k_i R_{i+1}) H_n^{(2)}(k_i R_i) \,. \tag{5.9}$$

In addition, the application of the continuity of H_ϕ across each of R_i for $i = 2, 3, \ldots, L$ (that is, the interface of the inner dielectric layers), allows us write $\left\{b_n^{(i)}\right\}_{n\in\mathbb{Z}}$ (for $i = 1, 2, \ldots, L-1$) in terms of one single unknown sequence $\left\{b_n^{(L)}\right\}_{n\in\mathbb{Z}}$. For $i = 1, 2, \ldots, (L-1)$, we have

$$b_n^{(i)} = b_n^{(L)} \zeta_i \alpha_n^{(i)} \beta_n^{(i)} \,, \tag{5.10}$$

where the following notations are introduced for $i = 1, 2, \ldots, (L-1)$:

$$\zeta_i := \frac{\pi k_i R_{i+1}}{2j} \,, \tag{5.11a}$$

$$\alpha_n^{(i)} := \frac{H_n^{'(2)}(k_L R_L)}{H_n^{'(2)}(k_i R_i)} \frac{H_n^{(2)}(k_i R_{i+1})}{H_n^{(2)}(k_{L-1} R_L)} \,, \tag{5.11b}$$

$$\beta_n^{(i)} := \begin{cases} \varrho_n^{(L-1)} \,, & \text{for } i = L-1, \\ \gamma_n^{(i)} \upsilon_n^{(i)} + \zeta_{i+1} \left(\varrho_n^{(i)} - \psi_n^{(i)} \varsigma_n^{(i+1)}\right) \beta_n^{(i+1)} \,, & \text{otherwise,} \end{cases} \tag{5.11c}$$

$$\varrho_n^{(i)} := \begin{cases} \dfrac{\eta_{L-1}}{\eta_L} J_n'(k_L R_L) H_n^{(2)}(k_{L-1} R_L) \\ \qquad - J_n(k_L R_L) H_n^{'(2)}(k_{L-1} R_L) \,, & \text{for } i = L-1, \\ \dfrac{\eta_i}{\eta_{i+1}} \Big[J_n'(k_{i+1} R_{i+1}) H_n^{(2)}(k_{i+1} R_{i+2}) \\ \qquad - J_n(k_{i+1} R_{i+2}) H_n^{'(2)}(k_{i+1} R_{i+1}) \Big] \,, & \text{otherwise,} \end{cases} \tag{5.11d}$$

and the following for $i = 1, 2, \ldots, (L-2)$:

$$\gamma_n^{(i)} := \left[\frac{\eta_i}{\eta_{i+1}} \frac{H_n^{'(2)}(k_{i+1} R_{i+1})}{H_n^{(2)}(k_{i+1} R_{i+1})} - \frac{H_n^{'(2)}(k_i R_{i+1})}{H_n^{(2)}(k_i R_{i+1})} \right] \prod_{j=i+1}^{L-2} \frac{H_n^{(2)}(k_j R_j)}{H_n^{(2)}(k_j R_{j+1})} \,, \tag{5.11e}$$

$$\psi_n^{(i)} := \frac{H_n^{'(2)}(k_i R_{i+1})}{H_n^{(2)}(k_i R_{i+1})} \,, \tag{5.11f}$$

$$\upsilon_n^{(i)} := \begin{cases} J_n(k_L R_L) H_n^{(2)}(k_L R_L) \,, & \text{for } i = L-2, \\ \upsilon_n^{(i+1)} + \zeta_{i+2} \beta_n^{(i+2)} \varsigma_n^{(i+2)} \displaystyle\prod_{j=i+2}^{L-2} \frac{H_n^{(2)}(k_j R_j)}{H_n^{(2)}(k_j R_{j+1})} \,, & \text{otherwise.} \end{cases} \tag{5.11g}$$

We are now left with the unknown $\left\{b_n^{(L)}\right\}_{n\in\mathbb{Z}}$ to be solved by imposing the MBC on the outermost layer $\rho = R_1$. The Meixner finite condition requires that the energy contained in the innermost region L (where $\rho < R_L$) is bounded; *i.e.*,

$$W = \frac{1}{2}\int_0^{R_L}\int_{-\pi}^{\pi}\left\{\epsilon_0\epsilon_L\left|E_z^{(L)}\right|^2 + \mu_0\mu_L\left[\left|H_\phi^{(L)}\right|^2 + \left|H_\rho^{(L)}\right|^2\right]\right\}\mathrm{d}\phi\,\rho\,\mathrm{d}\rho < \infty\,. \quad (5.12)$$

Following similar steps as those in Subsection 4.3.2, (5.12) leads to the requirement that the unknown $\left\{b_n^{(L)}\right\}_{n\in\mathbb{Z}}$ satisfy the Fejér's Tauberian condition (D.4).

The CLR, as depicted in Figure 5.2, consists of a constant-K lens and (in general case) a PEC cylindrical strip separated by an air gap. When the cylindrical strip is located at some distance from the surface of the cylinder, this may be treated as a "two-layer" model with a layer of air surrounding the dielectric cylinder. The virtual air layer extends from the dielectric interface of the cylinder $\rho = R_2$ to $\rho = R_1$. The location of the cylindrical strip is described by coordinates $\Omega_{\mathrm{PEC}} = \left\{(\rho,\phi) : \rho = R_1, |\phi| < \theta^{\mathrm{PEC}}, -\infty < z < \infty\right\}$. When the cylindrical strip is attached to the cylinder, we use the limiting case of our developed code which describes the single-layer model. When there is an air-gap (*i.e.*, $\epsilon_1 = 1$ and $\mu_1 = 1$), the elimination of all unknowns except $\left\{b_n^{(2)}\right\}_{n=1}^{\infty}$ provides the following DSE:

$$\sum_{n=-\infty}^{\infty} b_n^{(2)} o_n e^{jn\phi} = 0\,, \qquad \phi \in (-\theta^{\mathrm{PEC}}, \theta^{\mathrm{PEC}}), \quad (5.13)$$

$$\sum_{n=-\infty}^{\infty}\left[b_n^{(2)} t_n + z_n\right] e^{jn\phi} = 0\,, \qquad \phi \in (-\pi, -\theta^{\mathrm{PEC}}) \cup (\theta^{\mathrm{PEC}}, \pi), \quad (5.14)$$

where $\{z_n\}_{n\in\mathbb{Z}}$ is as defined in (4.36), while the remaining coefficients are:

$$\begin{aligned} o_n :=& J_n(k_r R_2) H_n^{'(2)}(k_r R_2) + \zeta_1 H_n^{'(2)}(k_r R_2)\left[J_n(k_0 R_1) - J_n(k_0 R_2)\right] \\ &\times\left[\frac{\eta_0}{\eta_r} J_n'(k_r R_2) H_n^{(2)}(k_0 R_2) - J_n(k_r R_2) H_n^{'(2)}(k_0 R_2)\right], \quad (5.15a) \\ t_n :=& \zeta_1 \frac{H_n^{'(2)}(k_0 R_2)}{H_n^{(2)}(k_0 R_2)}\left[\frac{\eta_0}{\eta_r} J_n'(k_r R_2) H_n^{(2)}(k_0 R_2) - J_n(k_r R_2) H_n^{'(2)}(k_0 R_2)\right] \\ &\times\left\{\left[J_n'(k_0 R_1) H_n^{(2)}(k_0 R_2) - J_n(k_0 R_2) H_n^{'(2)}(k_0 R_1)\right]\right. \\ &\left. - \frac{H_n^{'(2)}(k_0 R_1)}{H_n^{(2)}(k_0 R_1)}\left[J_n(k_0 R_1) H_n^{(2)}(k_0 R_2) - J_n(k_0 R_2) H_n^{(2)}(k_0 R_1)\right]\right\}. \quad (5.15b) \end{aligned}$$

This set of DSE can be directly converted to two independent ISLAE of the second kind by using the results given in Chapter 3. Due to the normal incidence of the plane wave, the E- and H-polarizations decouple, and the above DSE can be regularized into two independent ISLAE, instead of four as in Chapter 4. The two ISLAE resulting from regularizing these DSE are the basis of this study.

5.4 Focal studies of a dielectric cylindrical lens

In this section, we consider the homogeneous dielectric cylindrical lens excited by the E-polarized plane wave. The energy density distribution, W, resulting from the plane wave scattering is studied using the classical exact series solution. The energy density distribution, W, is as defined in (2.37); *i.e.*,

$$W = \frac{1}{2}\left[\epsilon_0\epsilon_L \left|E_z^{(L)}\right|^2 + \mu_0\mu_L \left|H_\phi^{(L)}\right|^2 + \mu_0\mu_L \left|H_\rho^{(L)}\right|^2\right] . \tag{5.16}$$

When regarded as a focusing device, the homogeneous dielectric cylinder exhibits huge aberrations which are more pronounced for electrically large cylinders (*i.e.*, those described by $\frac{D}{\lambda} \gg 1$). The ray-tracing technique shows that paraxial rays are focused at the focus point, F, outside the cylinder, and location of the relative focus distance, f, is defined by an elementary formula (when $1 < \epsilon_r < 4$)

$$f = \frac{OF}{OR} = \frac{\sqrt{\epsilon_r}}{2\left(\sqrt{\epsilon_r} - 1\right)} , \tag{5.17}$$

where O is the center of the cylinder. According to (5.17), the dielectric cylinder with $\epsilon_r = 4$ collects the paraxial rays at the point $f = 1$; *i.e.*, conditional focal point lies exactly at dielectric interface ($F = R$).

Simple GO in the paraxial regime indicates that a flat or curved PEC placed exactly at the paraxial focus of the dielectric lens will produce a collimated backscattered wave from a collimated incident wave. If the PEC reflector, flat or curved, is placed away from the lens focus, then the backscattered wave becomes decollimated. In this chapter, we consider the reflector to be concentric with the dielectric lens, instead of a flat screen, not only because such structure is easily adaptable to our chosen solution method, the MoR, but also because one of the objectives for our study, as stated in Section 5.1, is the 2D analogue study of the competitiveness of spherical reflector [83] with varying incident angle.

However, the dielectric lens or the step-indexed cylindrical LL lens is not a perfect lens, non-paraxial rays always suffer aberration, and the wavelength is not zero as for

GO. The very meaning of the "focus point" at microwaves is very conditional, since, in fact, each individual ray passing the dielectric cylinder crosses the optical axis at different point inside some region called the "focal spot". The characteristic size the focal spot is comparable with the wavelength [83]. We restrict ourselves to calculation of the value W along the optical axis for the variation of intensity along the z-axis. The calculation of W gives us the necessary information for further insight into the distribution of W near the focal spot. More importantly, this defines the location of the maximum energy distribution, $W_{\max}$, across the focal spot for a fixed electrical size $\frac{D}{\lambda}$. The dB-scaled value of $W(\text{dB})$ is plotted against the relative distance $\frac{\rho}{R}$.

We examine a few constant-K lenses made of material with dielectric constant from $\epsilon_r = 2.1$ (Polytetrafluoroethylene PTFE) to $\epsilon_r = 3.5$ (fused quartz). According to (5.17), maximum intensity of the electromagnetic field, $W_{\max}$, occurs at the points $\left(\frac{\rho}{R}\right)_{\text{GO}} = 1.613$ (when $\epsilon_r = 2.1$) and 1.074 (when $\epsilon_r = 3.5$). These may be called the GO focal points.

However, at microwaves the electrical size of a constant-K lens is always finite. When the electric size $\frac{D}{\lambda}$ takes values $20, 50, 100$ and 200, the calculations reveal significant discrepancies between locations of the GO focal points and the actual values of the locations $\frac{\rho}{R}$ of the maximal intensity for each of four values $\frac{D}{\lambda}$. The chain of local maxima observed as dicussed below is actually an interference pattern observed along the axis on one side of the cusp between the caustics. For constant-K lens with $\epsilon_r = 2.1$, these values are $\frac{\rho}{R} = 1.361$, 1.437, 1.480 and 1.517, respectively, as shown in Figure 5.3 (a). Similarly, when $\epsilon_r = 2.4$ as shown in Figure 5.3 (b), the local maxima occur, respectively, at the points $\frac{\rho}{R} = 1.222$, 1.277, 1.318 and 1.340; when $\epsilon_r = 3.0$ as shown in Figure 5.3 (c), they correspond to the points $\frac{\rho}{R} = 1.081$, 1.097, 1.122 and 1.142; when $\epsilon_r = 3.5$ as shown in Figure 5.3 (d), they correspond to the points $\frac{\rho}{R} = 1.001$, 1.009, 1.026 and 1.038. Using (5.17), one can find that the estimated GO focal points lies at the point where $\left(\frac{\rho}{R}\right)_{\text{GO}} = 1.613$, 1.410, 1.183 and 1.074 for $\epsilon_r = 2.1$, 2.4, 3.0 and 3.5, respectively.

It is evident that the local maxima approaches the focus predicted by the GO concept as the electrical size increases but aberration is visible. However, the fundamental effect is achieved by the dielectric structure. Nevertheless, the local maxima locations are still far away from that predicted by the GO concept. It can be clearly seen from Figure 5.4 and Figure 5.5 that, instead of a single focal point as predicted by simplified GO concept, the actual distribution of the energy density forms a chain of local maxima of nearly equal values at higher frequencies ($\frac{D}{\lambda} = 100, 200$). We are

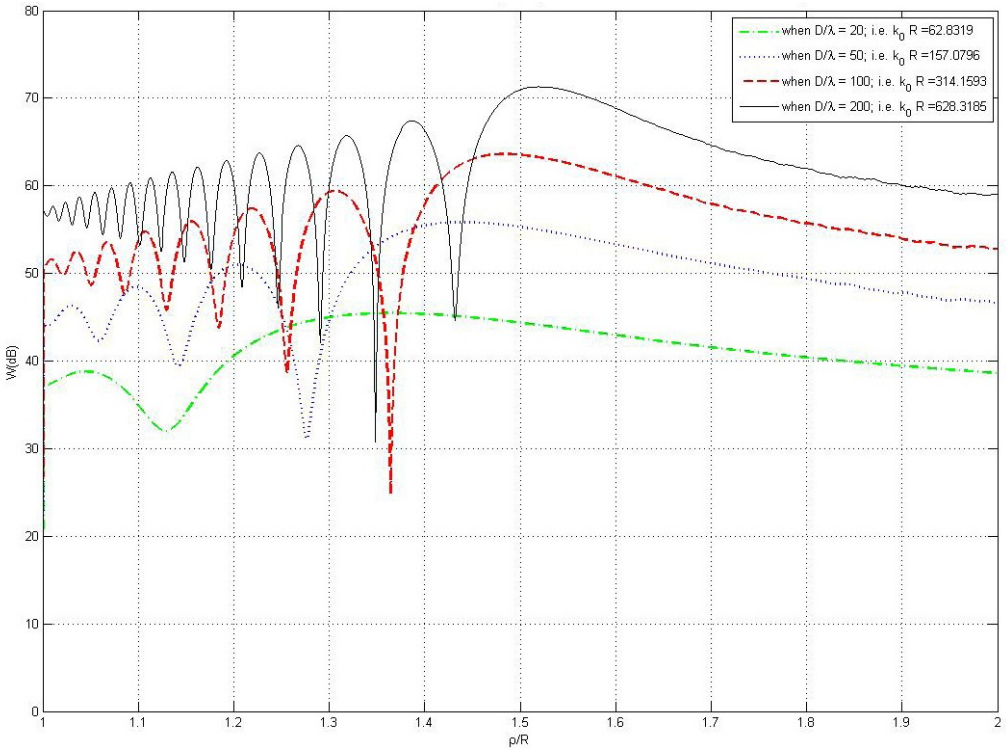

(a) $\epsilon_r = 2.1$

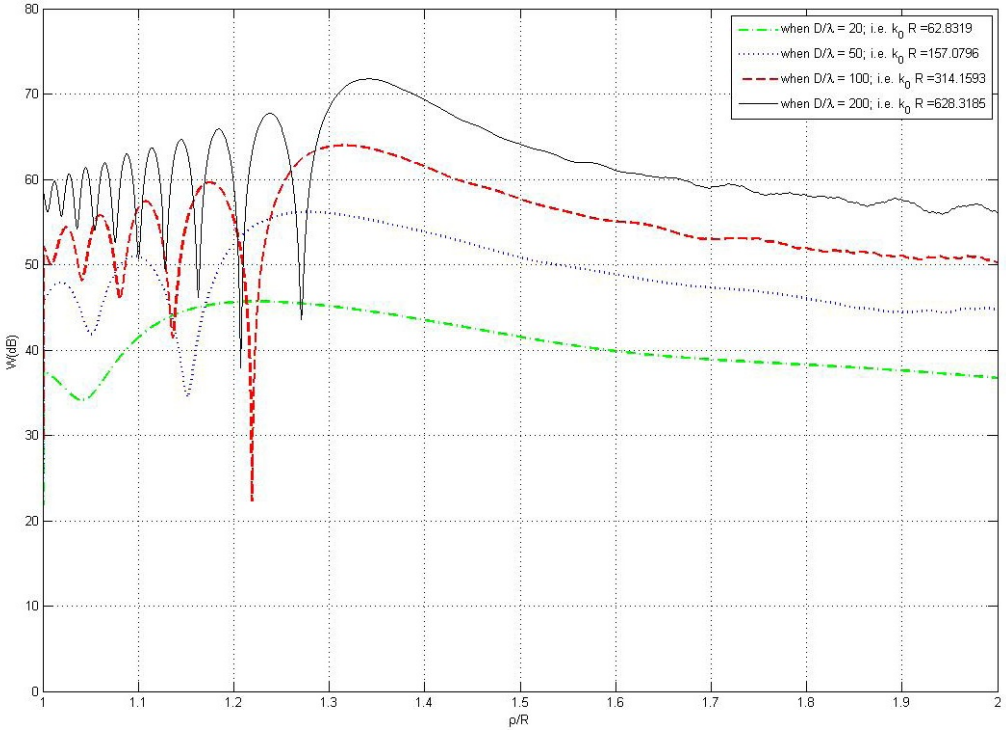

(b) $\epsilon_r = 2.4$

Figure 5.3: Continued next page.

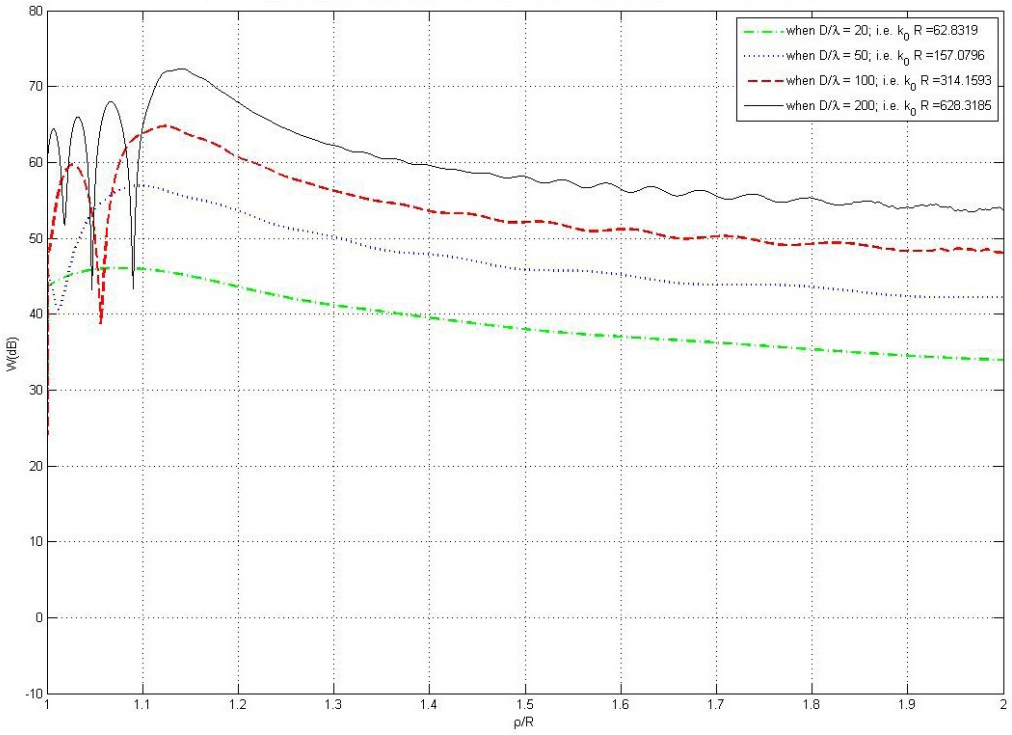

(c) $\epsilon_r = 3.0$

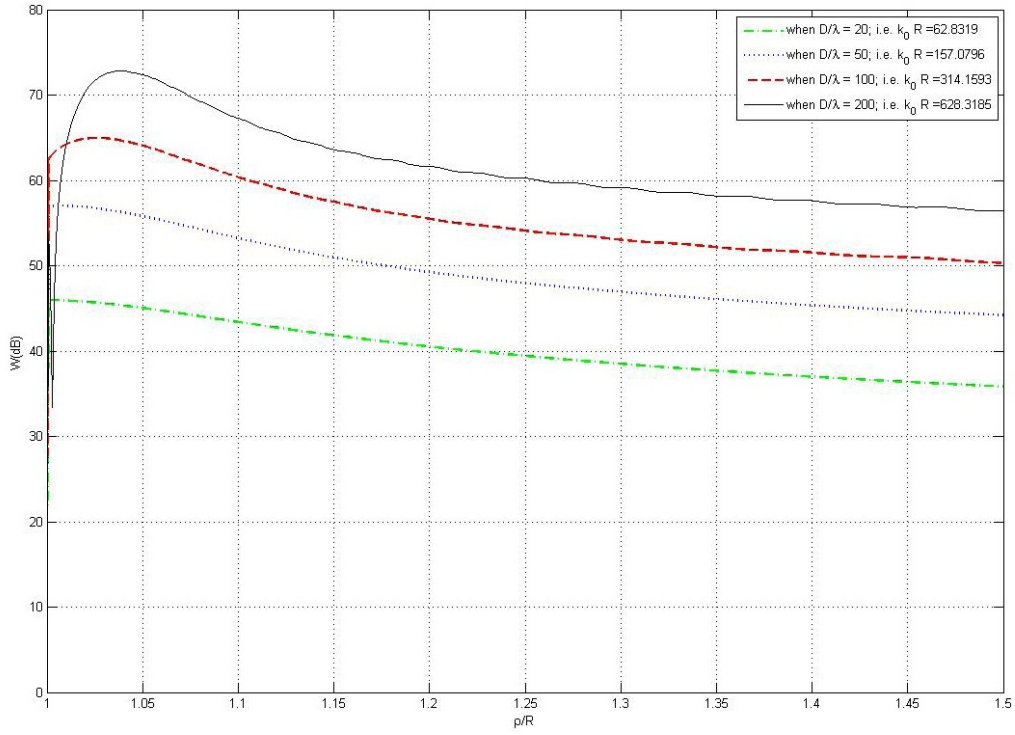

(d) $\epsilon_r = 3.5$

Figure 5.3: Comparison of W across the optical axis of the constant-K lens, when $\epsilon_r = 2.1$ (a), 2.4 (b), 3.0 (c) and 3.5 (d), while $\frac{D}{\lambda} = 20$ (dot-dashed green), 50 (dotted blue), 100 (dashed red), or 200 (solid black).

going to calculate the optimal location of the PEC strip for backscattering in next section, taking into account the discrepancies between ideal and actual structures.

Accurate knowledge of the distribution of W across the optical axis is of paramount importance for optimal location of the PEC cylindrical strip, in order to maximize the backscattering phenomenon. The optimal location is one of the necessary but sufficient prerequisites for the radiation to be effectively reflected. The optimal choice of the angular size of the reflecting strip is equally important. The simplest idea consists in overlapping of the focused beam entirely with the PEC strip, so that at least the Half Power Beam Width (HPBW) of the focused radiation would not be larger than angular size of the strip. The calculations of the spatial distribution of W, illustrated in Figure 5.4 and Figure 5.5, show that it is sufficient to have cylindrical strip of the angular half-width θ^{PEC} no less than $\frac{\pi}{36}$ (or 5°), for maximal interception of the energy in a wide range of constant-K lens with electrical size ranging from $\frac{D}{\lambda} = 5$ up to $\frac{D}{\lambda} = 200$.

5.5 Calculation of backscattering RCS

The objective of this section is to analyze the RCS behavior of a properly designed CLR in a wide frequency range. To obtain a dimensionless measurement for studies, normalized backscattering RCS, $\hat{\sigma}_b$, in dB-scale is plotted against the electric size $\frac{D}{\lambda}$. All the computations of $\hat{\sigma}_b(\mathrm{dB})$ for both the CLR and CLLR are based on solutions given by the MoR.

The values of $\hat{\sigma}_b(\mathrm{dB})$ against increasing electric size are studied in order to locate the optimal location for the reflecting PEC strip. The results from the study of paraxial energy density distribution, W, provide us with a good initial estimate of this optimal location, where the maximum backscattering is achieved. The dependences of RCS, $\hat{\sigma}_b(\mathrm{dB})$, for a CLR with reflector located in the vicinity of the focus region are computed. The computed average RCS over the range of $\frac{D}{\lambda} \in (0, 200)$ at each reflector location $\left(\frac{\rho}{R}\right)$ are compared with each other. The dependences of $\hat{\sigma}_b(\mathrm{dB})$ at three locations $\left(\frac{\rho}{R}\right)$ offering the three highest average RCS are displayed in Figure 5.6 ($\epsilon_r = 2.1$) and Figure 5.7 ($\epsilon_r = 3.5$), respectively. From these two figures, we deduce that the optimal location of the reflector is $\frac{\rho}{R} = 1.55$ ($\epsilon_r = 2.1$) and $\frac{\rho}{R} = 1.04$ ($\epsilon_r = 3.5$), as measured by maximal average RCS over this band.

It can seen from the figures that, when strip is located away from the optimal spot, more oscillations appear in the spectral dependence of $\hat{\sigma}_b(\mathrm{dB})$. This phenomenon can be seen in Figure 5.7 when $\frac{\rho}{R} = 1.02$ (the black line). The deep null indicates the

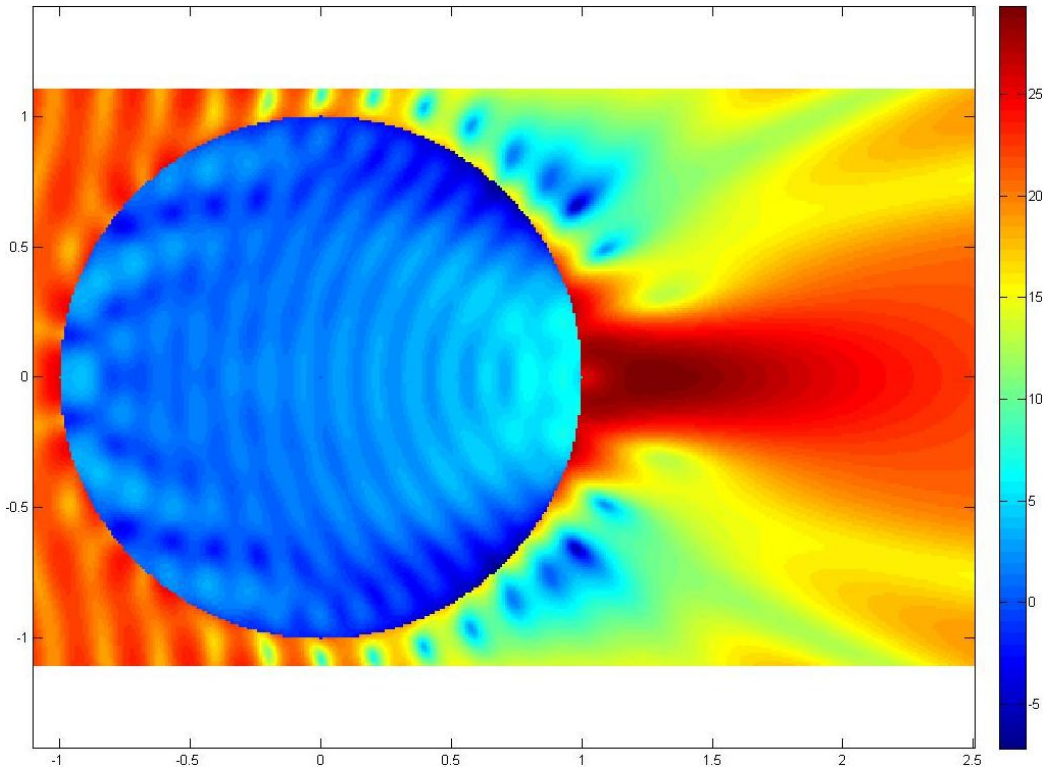

(a) $\frac{D}{\lambda} = 5$

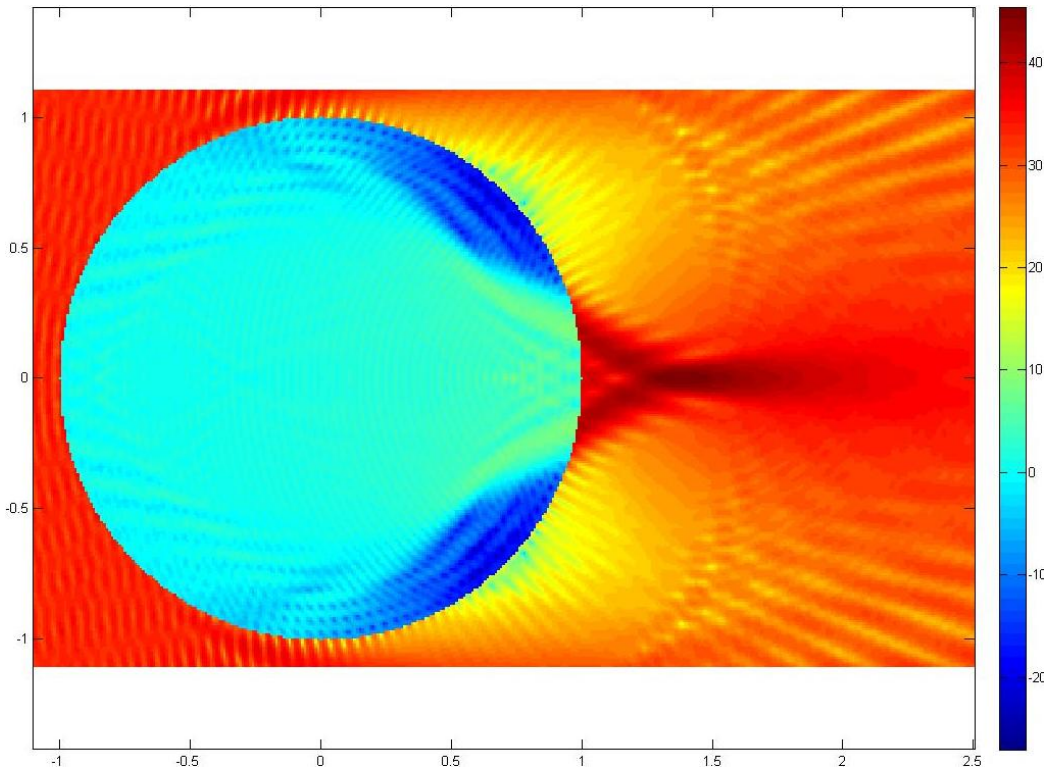

(b) $\frac{D}{\lambda} = 20$

Figure 5.4: Continued next page.

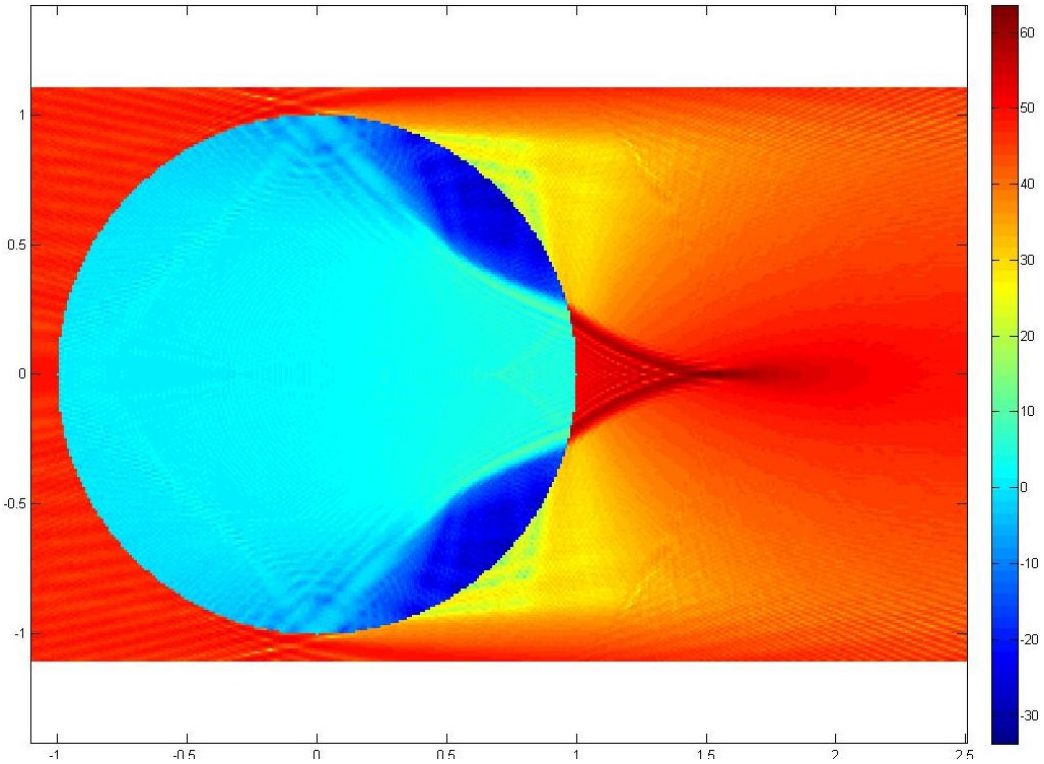

(c) $\frac{D}{\lambda} = 100$

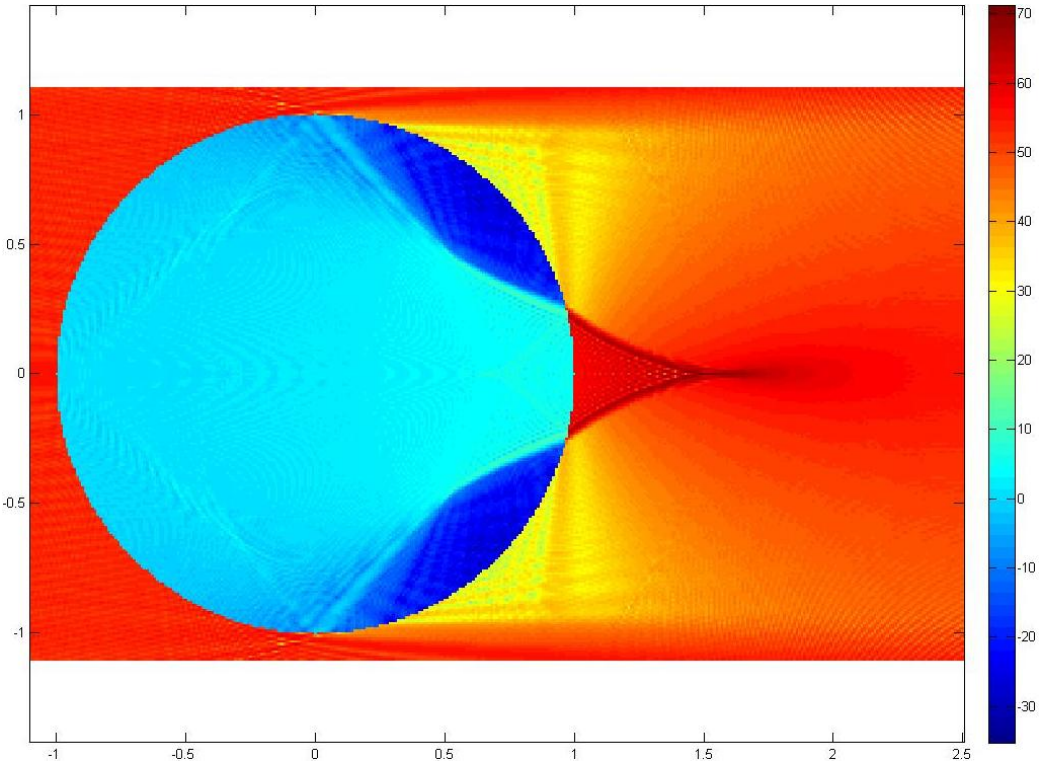

(d) $\frac{D}{\lambda} = 200$

Figure 5.4: Spatial distribution of W due to the presence of the constant-K lens with $\epsilon_r = 2.1$ of varying electrical size $\frac{D}{\lambda} = 5$ (a), 20 (b), 100 (c), and 200 (d).

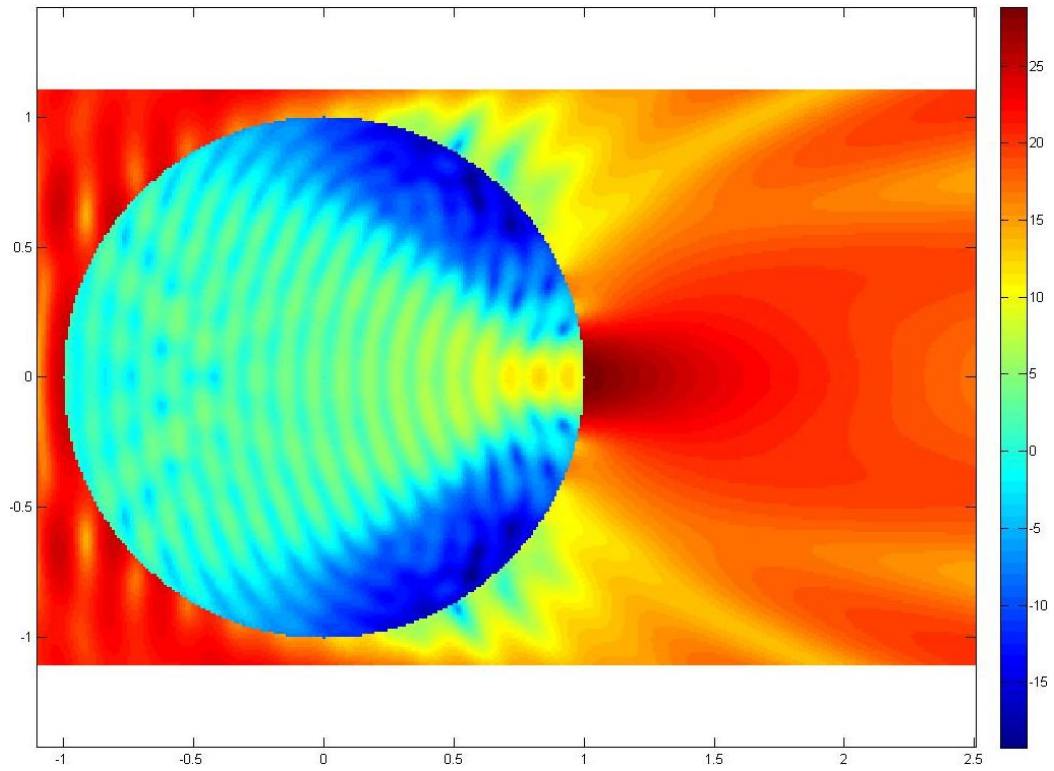

(a) $\frac{D}{\lambda} = 5$

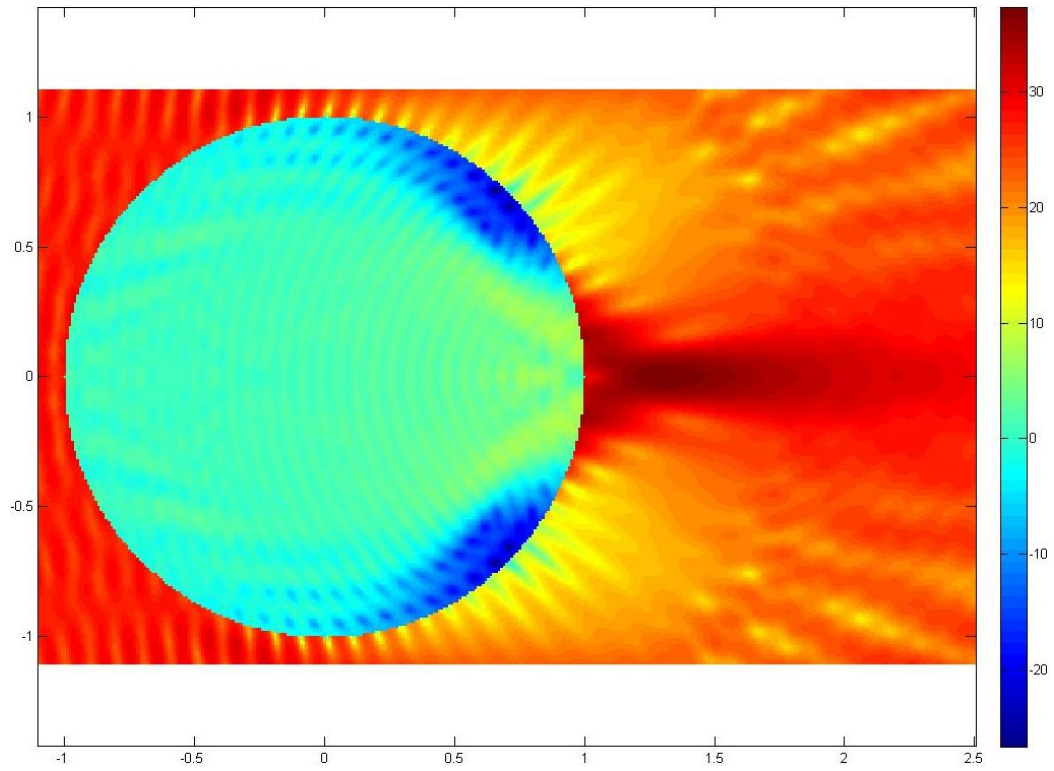

(b) $\frac{D}{\lambda} = 20$

Figure 5.5: Continued next page.

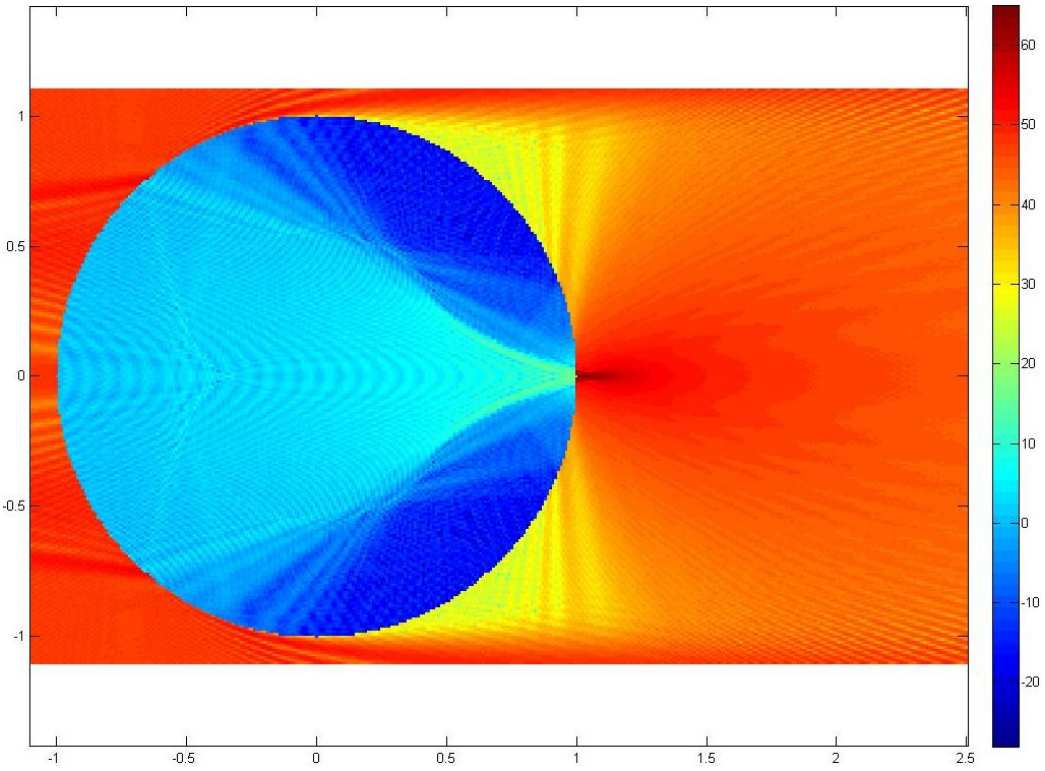

(c) $\frac{D}{\lambda} = 100$

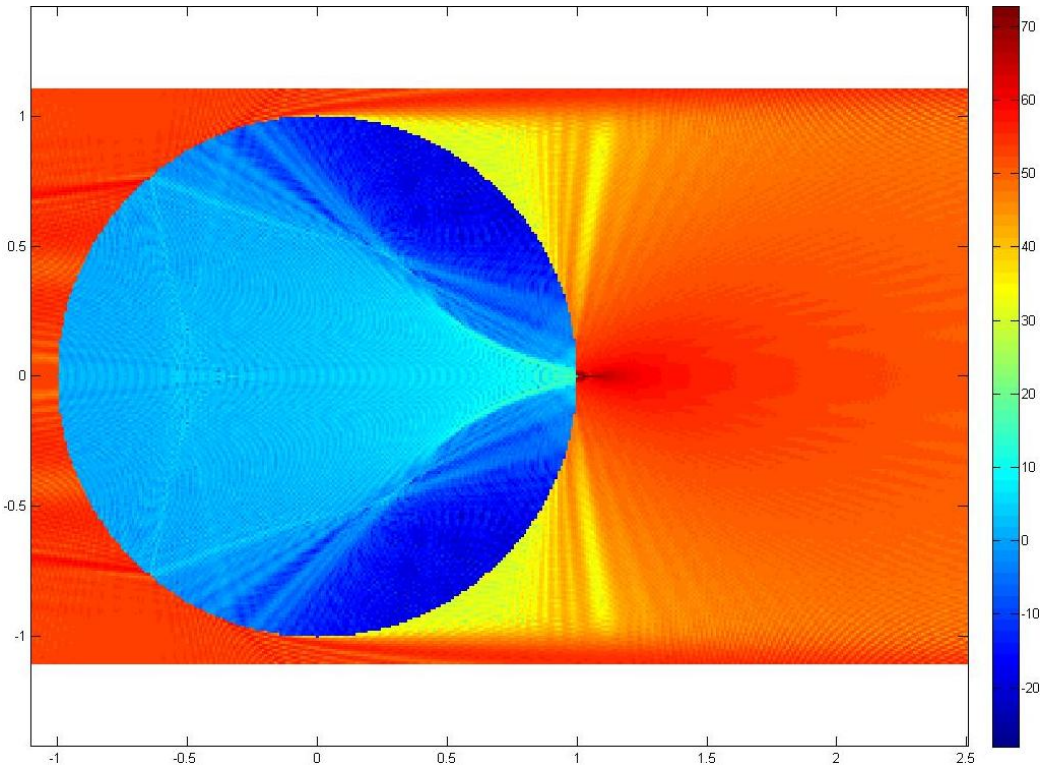

(d) $\frac{D}{\lambda} = 200$

Figure 5.5: Spatial distribution of W due to the presence of the constant-K lens with $\epsilon_r = 3.5$ of varying electrical size $\frac{D}{\lambda} = 5$ (a), 20 (b), 100 (c), and 200 (d).

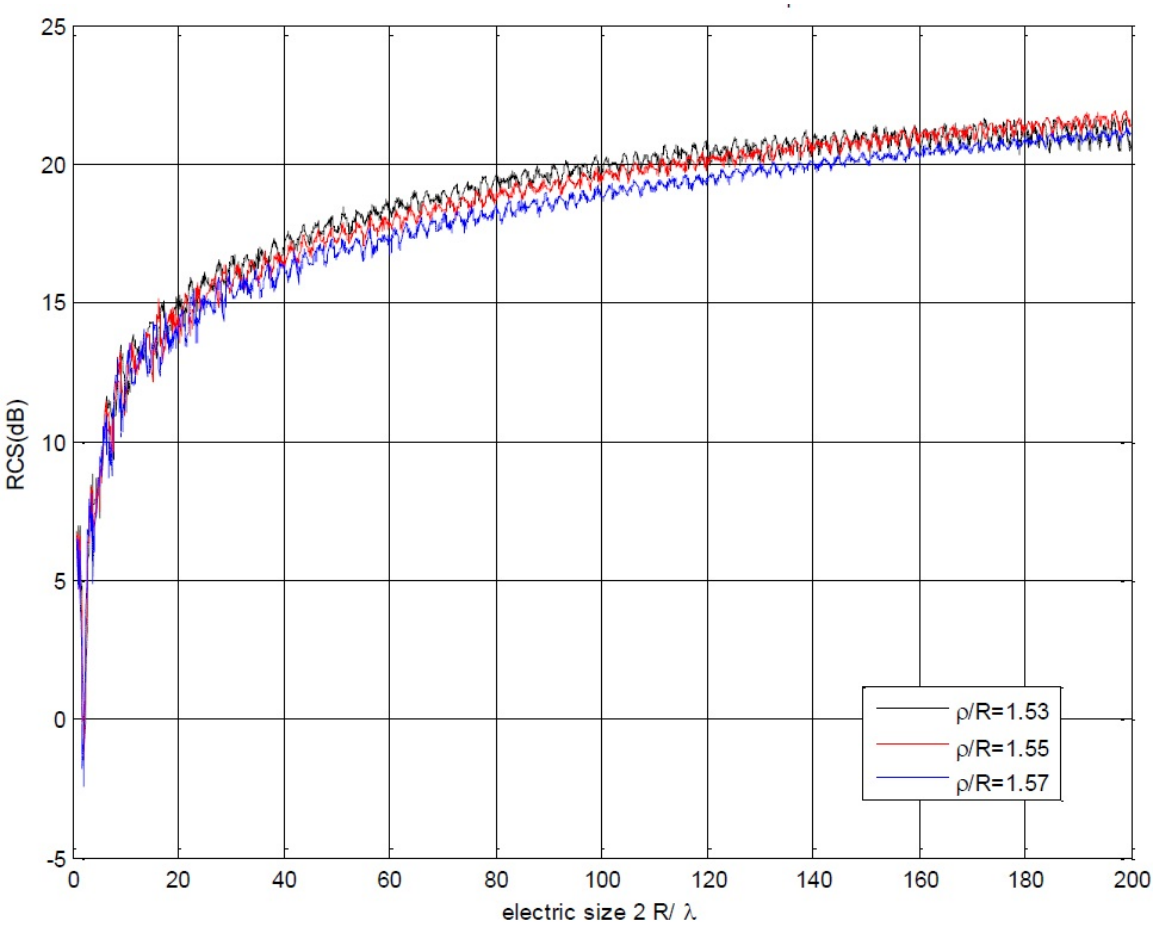

Figure 5.6: Comparison of $\hat{\sigma}_b$(dB) against electric size of a CLR with the PEC strip located at different distances: $\frac{\rho}{R} = 1.53$ (black), 1.55 (red) and 1.57 (blue). [$R_2 = 1$, $\theta^{\text{PEC}} = \frac{\pi}{36} = 5^\circ$, $\epsilon_r = 2.1$, $\mu_r = 1$, $\theta_x^{\text{pw}} = \pi = 180^\circ$]

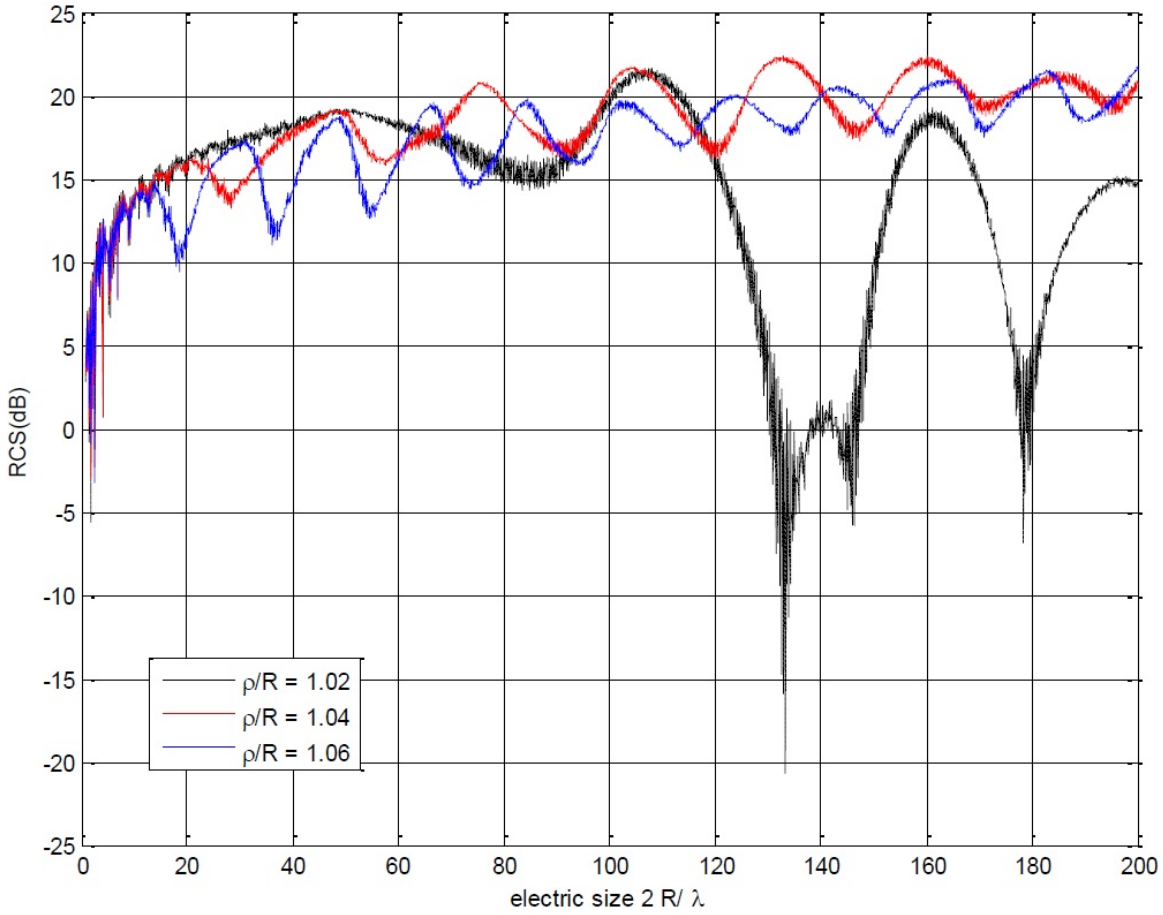

Figure 5.7: Comparison of $\hat{\sigma}_b$(dB) against electric size of a CLR with the PEC strip located at different distances: $\frac{\rho}{R} = 1.02$ (black), 1.04 (red) and 1.06 (blue). [$R_2 = 1$, $\theta^{\text{PEC}} = \frac{\pi}{36} = 5°$, $\epsilon_r = 3.5$, $\mu_r = 1$, $\theta_x^{\text{pw}} = \pi = 180°$]

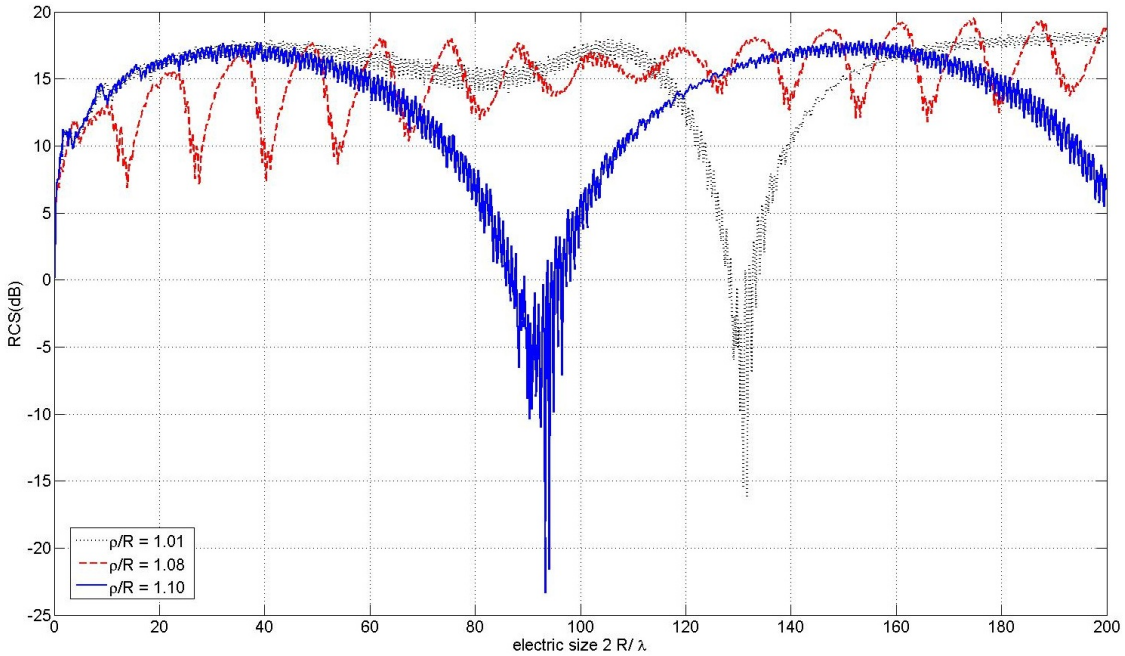

Figure 5.8: The dependences of RCS when reflector is located away from the focus region: $R_1 = 1.01R_2$ (dotted black), $R_1 = 1.08R_2$ (dashed red), $R_1 = 1.10R_1$ (solid blue). $[R_2 = 1,\ \epsilon_r = 3.5,\ \mu_r = 1,\ \theta_x^{\text{pw}} = \pi = 180°,\ \theta^{\text{PEC}} = \frac{\pi}{6} = 30°]$

complex interference between the reflector and the dielectric lens. To better illustrate this phenomenon, the dependences of $\hat{\sigma}_b(\text{dB})$ for reflector located away from this optimal location are displayed in Figure 5.8. For practical application over a relatively wide band, the oscillation in RCS values should be as small as possible relative to the average value across the band. By this reason, behavior as in Figure 5.8 is undesirable, and it reinforces the reason for choosing the optimal location to be in the vicinity of the locations specified in the last column of Table 5.1.

To obtain the maximum backscattering for a CLR, when $\epsilon_r = 2.1$, 2.4, 3.0 and 3.5, the PEC cylindrical strip is chosen to be placed at a relative distance $\frac{\rho}{R} = 1.55$, 1.35, 1.15 and 1.04, respectively. Table 5.1 provides the summary of the optimal locations for the PEC strip based on the GO concept, the computed paraxial energy intensity and the computed maximal backscattered RCS, for each of the CLR with $\epsilon_r = 2.1, 2.4, 3.0$ and 3.5.

In addition, observing Figure 5.9, we conclude that the angular width of the cylindrical PEC strip, θ^{PEC}, does not have significant effect on the reflectivity of the CLR. The comparative analysis of the spectral dependence for CLR in Figure 5.10 also shows that the performance of CLR with $\epsilon_r = 3.5$ is marginally higher than those with $\epsilon_r = 2.1$, 2.4 and 3.0. However, it is worth noting that as ϵ_r increases, there

ϵ_r	$\left(\frac{\rho}{R}\right)_{\text{GO}}$	$\left(\frac{\rho}{R}\right)_{\text{max paraxial intensity}}$	$\left(\frac{\rho}{R}\right)_{\text{max RCS}}$
2.1	1.163	1.361, 1.437, 1.480, 1.571	1.55
2.4	1.410	1.222, 1.277, 1.318, 1.340	1.35
3.0	1.183	1.081, 1.097, 1.122, 1.142	1.15
3.5	1.074	1.001, 1.009, 1.026, 1.038	1.04

Table 5.1: The optimal locations of the PEC strip according to the three different approaches, for the CLR with $\epsilon_r = 2.1, 2.4, 3.0$ and 3.5. The second column displays the focus distance calculated according to the GO concept; the third column lists the four local maximal according to the computed paraxial energy intensity; the last column gives the location of the reflector that offers maximal average RCS over the range $\frac{D}{\lambda} \in (0, 200)$.

are more oscillations in the spectral dependence of $\hat{\sigma}_b(\text{dB})$. For this reason, the CLR with dielectric material of $\epsilon_r = 2.1$ is preferred over those with higher ϵ_r.

Figure 5.11 illustrates the spectral dependence of $\hat{\sigma}_b(\text{dB})$, when a plane wave incident normally ($\theta_z^{\text{pw}} = \frac{\pi}{2} = 90^\circ$ and $\theta_x^{\text{pw}} = \pi = 180^\circ$) on a cylindrical reflector, and the PEC strip is of total width $\frac{\pi}{18} = 10^\circ$ and $\pi = 180^\circ$, respectively. They compare the performance of a CLR with $\epsilon_r = 2.1$ with those of a L-layered CLLR (constructed using stepped-index cylindrical LL). We can see from these figures that, for a minimal strip of angular size 10°, when $L = 3$, the CLR outperforms the CLLR in the range $\frac{D}{\lambda} > 20$; when $L = 5$, the CLR outperforms the CLLR in the range $\frac{D}{\lambda} > 60$; when $L = 7$, the CLR outperforms the CLLR in the range $\frac{D}{\lambda} > 115$. We have even better performance from the CLR when the strip size is increased to 10° to 180°. When $2\theta^{\text{PEC}} = 10^\circ$, the dependence of RCS against the electric size has an oscillatory character up to $N = 7$. As the strip size increases, more oscillations appear in the spectral dependence RCS for CLLR, whereas for CLR, the behavior is still overall monotonic for both sizes ($2\theta^{\text{PEC}} = 10^\circ$ and 180°). From our observations based on TM_z polarization, we draw the conclusion that the CLLR can be replaced by the cheaper alternative of the CLR, which offers reasonably high and smoother RCS against the electric size.

5.6 RCS of CLR and CLLR versus incident angle θ_x^{pw}

From a general point of view, it is evident that the case of normal incidence causes the most powerful reflection, as the incident plane wave illuminating the constant-

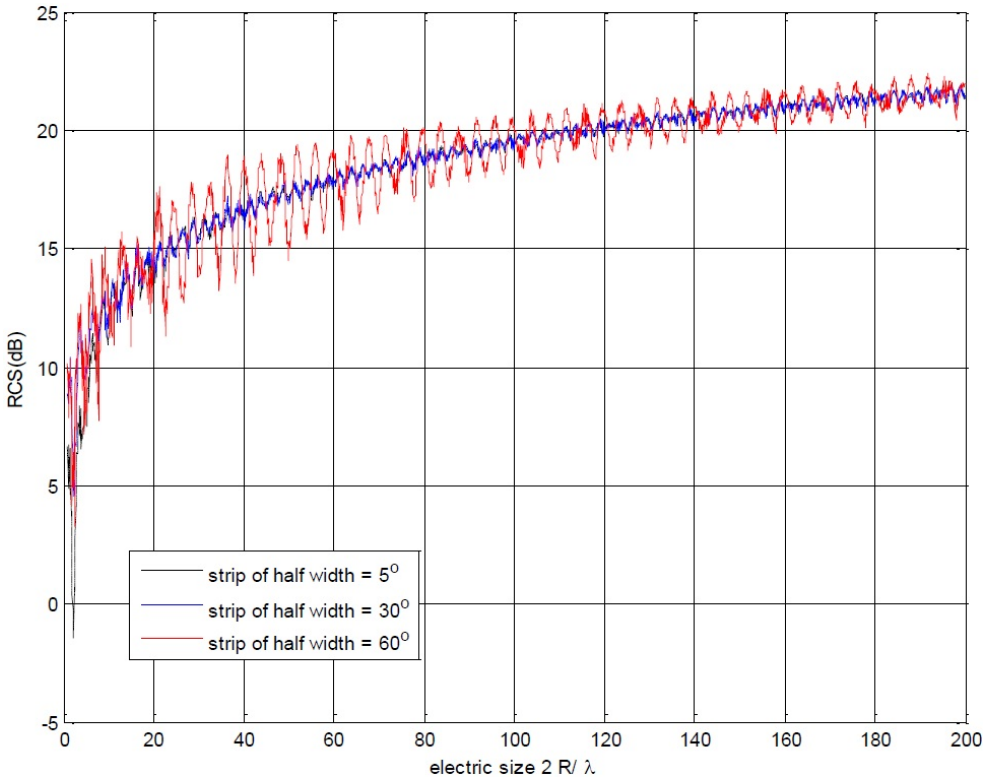

(a) $\epsilon_r = 2.1$ and $R_1 = 1.55R_2$

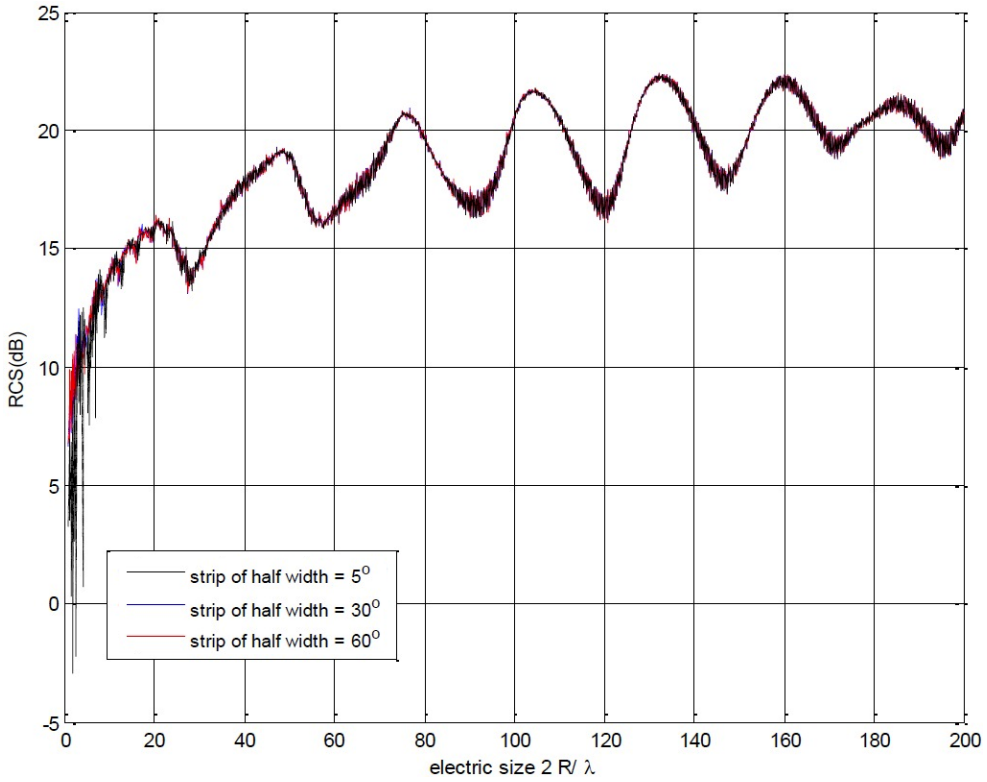

(b) $\epsilon_r = 3.5$ and $R_1 = 1.04R_2$

Figure 5.9: Comparison of $\hat{\sigma}_b$(dB) against electric size of a CLR with PEC strip of different angular widths: $\theta^{\text{PEC}} = \frac{\pi}{36} = 5°$ (black), $\frac{\pi}{6} = 30°$ (blue) and $\frac{\pi}{3} = 60°$ (red). $[R_2 = 1,\ \mu_r = 1,\ \theta_x^{\text{pw}} = \pi = 180°]$

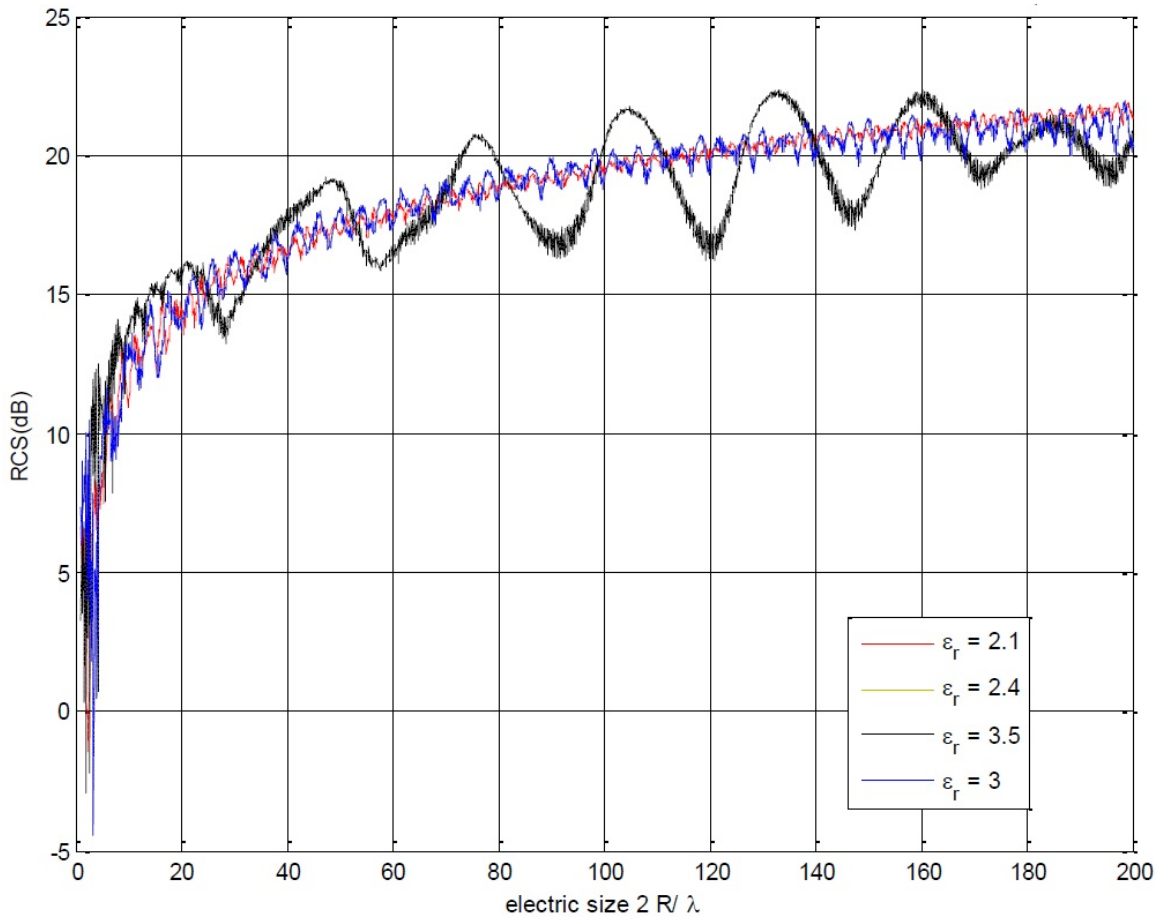

Figure 5.10: Comparison of $\hat{\sigma}_b$(dB) against electric size of a CLR composed of constant-K lens of different ϵ_r: $\epsilon_r = 2.1$ (red), 2.4 (green), 3.0 (blue) and 3.5 (black). [$R_2 = 1$, $\theta^{\text{PEC}} = \frac{\pi}{36} = 5°$, $\mu_r = 1$, $\theta_x^{\text{pw}} = \pi = 180°$, $R_1 = 1.55$, 1.35, 1.15 and 1.04 R_2, respectively]

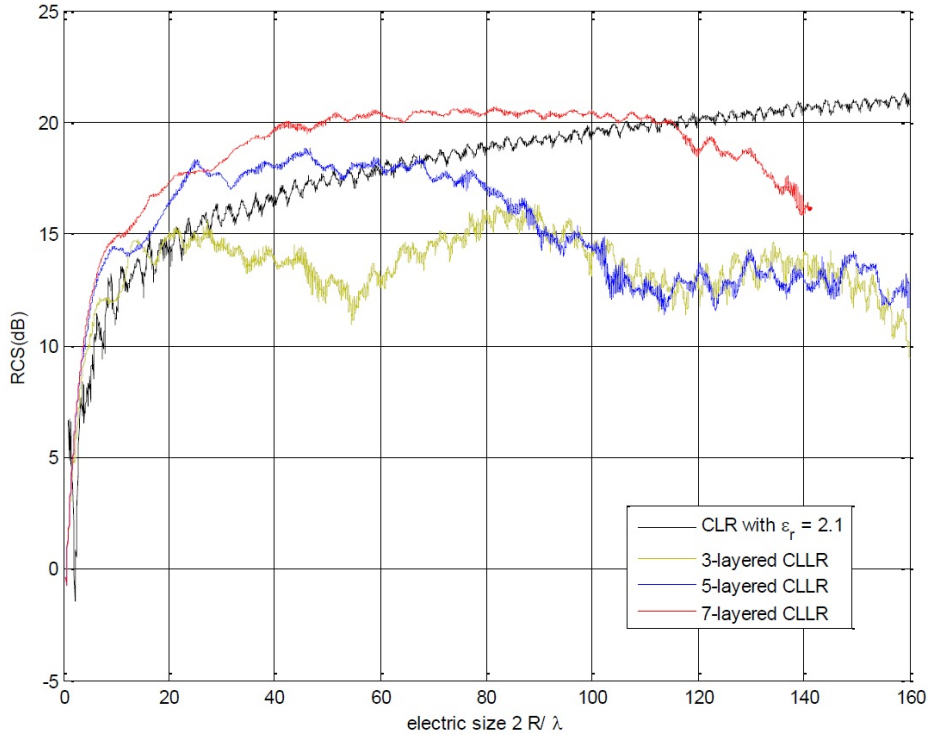

(a) $\theta^{\mathrm{PEC}} = 5°$

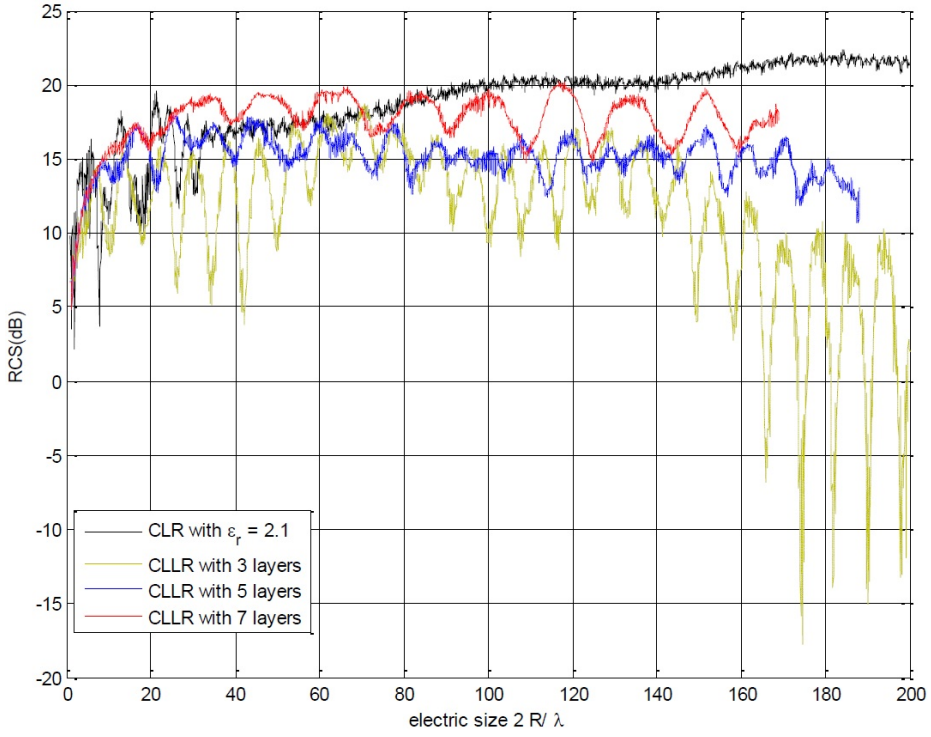

(b) $\theta^{\mathrm{PEC}} = 90°$

Figure 5.11: Comparison of the RCS of a CLR and a CLLR: CLR with $\epsilon_r = 2.1$ (solid black) versus CLLR with $L = 3$ layers (dot-dashed green), $L = 5$ (dotted blue) and $L = 7$ (dashed red).

K lens or cylidinrical LL forms a focal spot right at the central part of the PEC strip reflector. As has been shown in Section 5.4, the strip should extend over the transverse size of a focal spot to provide strong reflection. We can observe from Figure 5.4 and Figure 5.5 that the characteristic transverse size of a focal spot is about 1.0λ. Therefore, the geometrical size of the PEC strip reflector should be, at least, no less than this value. At the incidence angle θ_x^{pw} of value $\frac{\pi}{2} = 90^\circ$, there is no significant backscattering. This is because from the GO concept, the entire surface of a strip is completely shadowed. Thus, the effect of strong backscattering can be observed only in the range $0 \leq \theta_x^{\text{pw}} < \frac{\pi}{2} = 90^\circ$.

A simple physical argument predicts the existence of a cut-off incidence angle, $\theta^i_{\text{cut-off}}$, which defines the usable scanning range for the incident angle θ_x^{pw}, where $0 \leq \theta_x^{\text{pw}} < \theta^i_{\text{cut-off}}$, so that a high value of RCS is practically unchanged across the angular range. It is reasonable to suppose that $\theta^i_{\text{cut-off}}$ is that angle at which the right or left boundary (depending on θ_x^{pw}) of the focal spot lies exactly at the sharp edge of the PEC strip reflector so that whole focal spot is covered by the strip. It is also clear that the workable range $0 \leq \theta_x^{\text{pw}} < \theta^i_{\text{cut-off}}$ strongly depends on the semi-width of the reflecting strip θ^{PEC}. We assume that diffraction effects are negligible. Thus, to find the value $\theta^i_{\text{cut-off}}$, we choose at the strip surface the point at which the distance to the edge equals the angular semi-width of the focal spot; *i.e.*, 0.5λ. Elementary algebra leads to the simple formula for $\theta^i_{\text{cut-off}}$, that is

$$\theta^i_{\text{cut-off}} = \theta^{\text{PEC}} - \sin^{-1}\left(\frac{\pi}{2k_0}\right). \tag{5.18}$$

According to (5.18), when $\theta^{\text{PEC}} = \frac{\pi}{12} = 15^\circ$, $k_0 = 20\pi$ (Figure 5.12 (a)) and 100π (Figure 5.12 (b)), we have $\theta^i_{\text{cut-off}} = 13.56^\circ$ and 14.71°, respectively. It can be seen these sub-figures that these results for $\theta^i_{\text{cut-off}}$ are in good agreement with accurate numerical results. It should be noted that the CLR provides a more stable dependence of RCS (θ_x^{pw}) compared to the CLLR, even though the 5-,7- and 9-layered CLLR exhibits a higher overall level of RCS when $k_0 = 20\pi$. At higher frequency, where $k_0 = 100\pi$, the use of the CLR is preferable as its performance is superior to that of a 3-,5- or 7-layered CLLR. More strictly, our argument which led to an approximate formula for $\theta^i_{\text{cut-off}}$ is reasonable only for shallow and medium size PEC strip reflectors ($\theta^{\text{PEC}} \leq \frac{\pi}{4} = 45^\circ$), otherwise, shielding starts to occur as well as multiple reflections.

For wider PEC strip reflectors, the situation is more complicated because in a wider reflector, there are multiple reflections causing significant aberrations to the

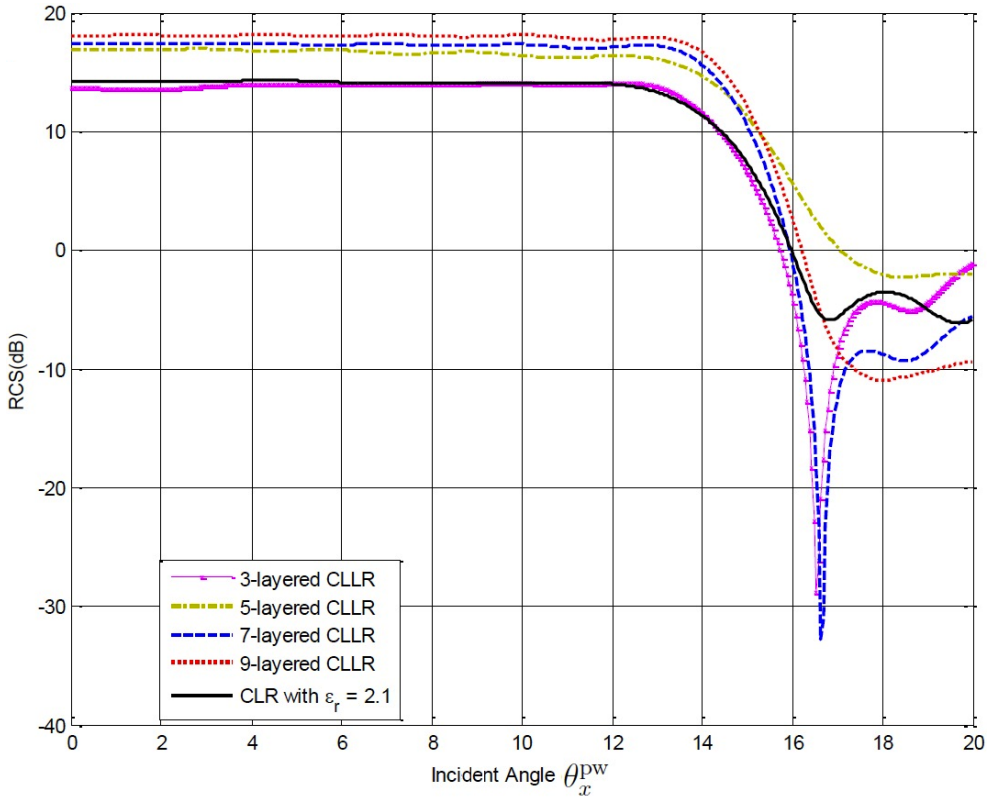

(a) $k_0 = 20\pi$

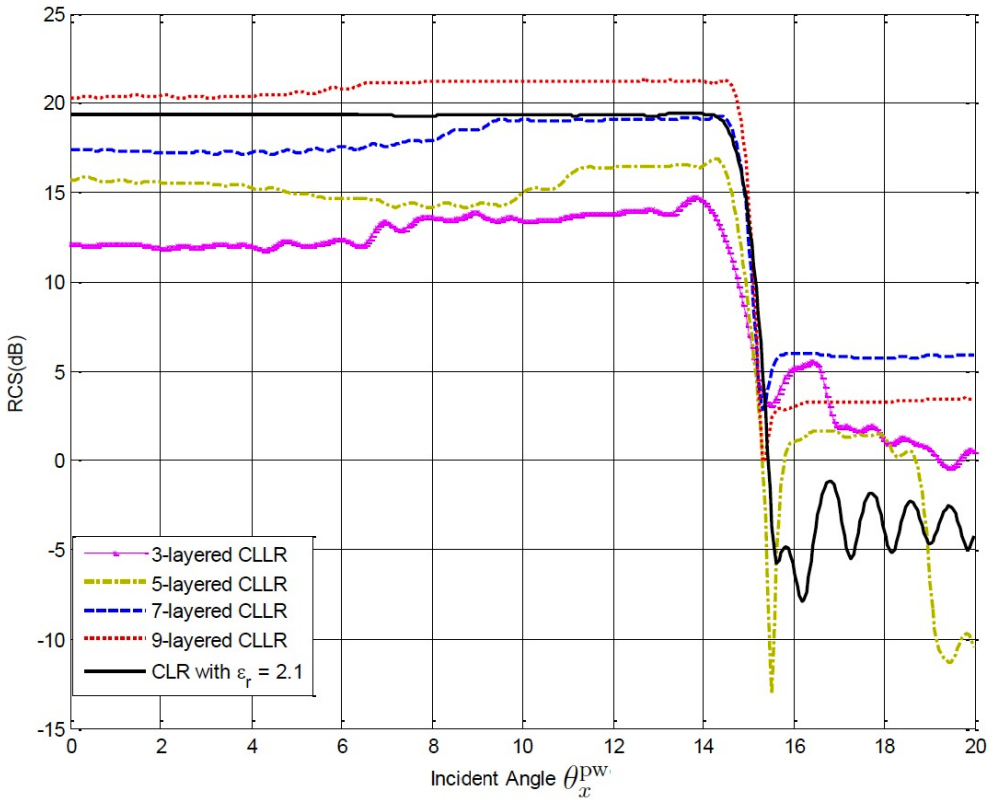

(b) $k_0 = 100\pi$

Figure 5.12: Comparison of RCS against the incident angle for a CLR ($\epsilon_r = 2.1$) with those of CLLR with different number of layers, when $\theta^{\mathrm{PEC}} = \frac{\pi}{12} = 15°$. CLR with $\epsilon_r = 2.1$ (solid black) versus CLLR with $L = 3$ layers (x-marked pink), $L = 5$ (dot-dashed green), $L = 7$ (dashed blue) and $L = 9$ (dotted red).

shape of the focal spot. This results on narrowing the range to $0 \leq \theta_x^{\text{pw}} \leq \theta^i_{\text{cut-off}}$, as shown in Figure 5.13. For example, it can be seen from Figure 5.13 (b) that, $\theta^i_{\text{cut-off}}$ lies far from the angular semi-width of the PEC strip, $\theta^{\text{PEC}} = \frac{\pi}{2} = 90°$. Again, as before the scanning performance of the CLR is preferable compare with the CLLR.

5.7 Conclusion

Accurate numerical results are computed for the RCS of both the CLR and CLLR, based on MoR, in a broad frequency band including not only the region of Rayleigh scattering ($\lambda \gg R$) and diffraction region ($\lambda \approx R$), but also the quasi-optical region ($\lambda \ll R$). With the numerical results produced, we have demonstrated competitiveness of microwave reflectors based on simple cylindrical lenses against those based on stepped-index Luneburg lenses. We also deduce from the results that CLR with lower dielectric constant ϵ_r are preferable to those with higher ϵ_r, as wavelength dependent oscillations become too strong for higher dielectric contrasts. We also observe that for higher frequencies, the scanning performance of a CLR is superior of that provided by CLLR, in the sense that the dependence of RCS has relatively less oscillations, and is of higher average value over the range of $\frac{D}{\lambda} \in (0, 200)$.

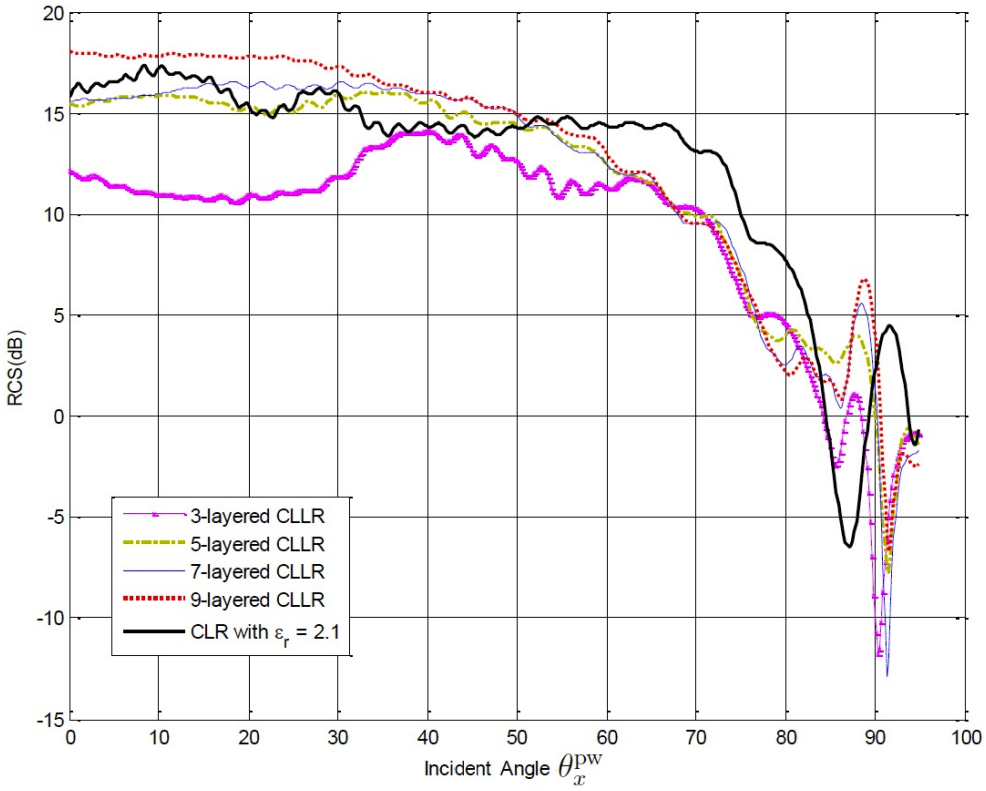

(a) $k_0 = 20\pi$

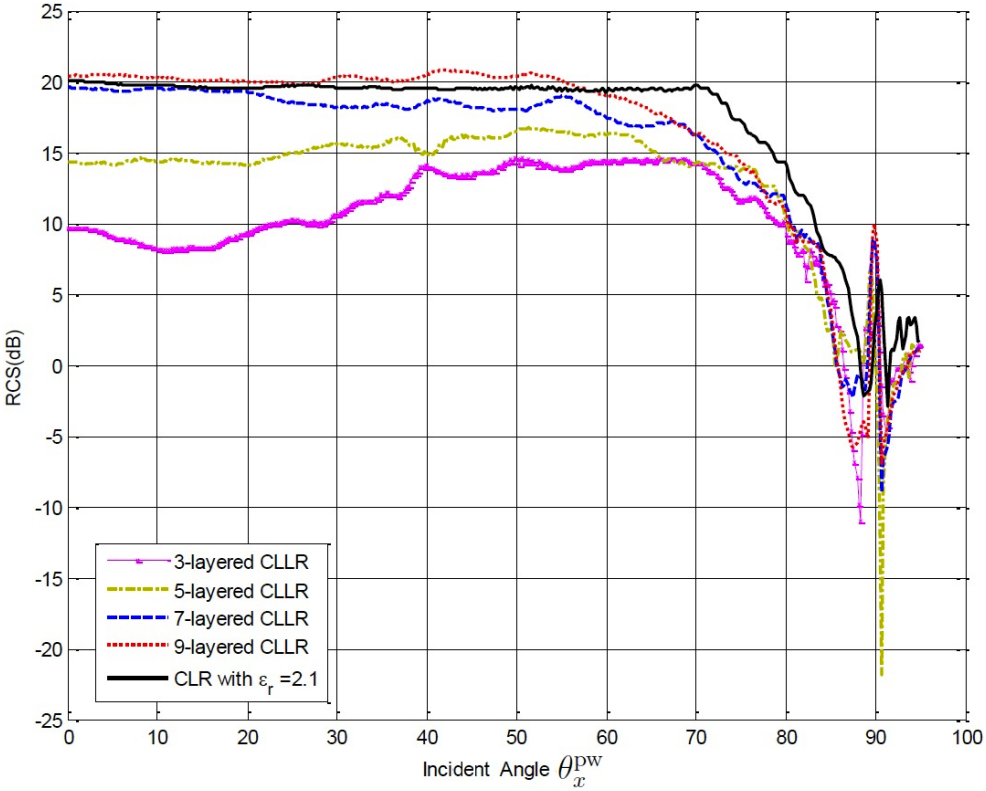

(b) $k_0 = 100\pi$

Figure 5.13: Comparison of RCS against the incident angle for a CLR ($\epsilon_r = 2.1$) with those of CLLR with different number of layers, when $\theta^{\mathrm{PEC}} = \frac{\pi}{2} = 90°$. CLR with $\epsilon_r = 2.1$ (solid black) versus CLLR with $L = 3$ layers (x-marked pink), $L = 5$ (dot-dashed green), $L = 7$ (dashed blue) and $L = 9$ (dotted red).

Chapter 6

Scattering from a finite array of CLR under normal incidence

6.1 Introduction

As a natural extension to the scattering problems of CLR considered in Chapter 4 and 5, the scattering problem of an incident plane wave by multiple CLR is considered in this chapter. A finite number M of parallel CLR (each with arbitrary size, PEC strip width and dielectric loading) are assumed located in the vicinity of one another. Consequently, the mutual interaction of the CLR cannot be ignored. Such an array is very attractive in microwave and optic wave applications, as it can be used to design for a wavelength- and polarization-selective components. It offers additional degrees of freedom for controlling the scattered fields. When the CLR are identical and equally spaced, this finite array of CLR forms a special example of gratings which are widely used in spectrum analyzers, open mesh reflectors, *etc.*

The analysis of scattering by multiple closed cylinders (either dielectric or conducting) has been studied over the years, using various techniques such as the integral equation formulation, the partial differential equation formulation, the T-matrix approach, the lattice sums approach, the source model technique, and the Green's function diakoptics approach [18, 81, 44, 91, 46, 82]. However, in all of the above literature, the surface of each of these cylinders is taken to be either purely dielectric or purely PEC. To the best of our knowledge, the analysis of multi-body scattering problem of slotted cylinders has not been done.

This chapter studies the feasibility of using of the MoR in the solving of the 2D scattering problem by a finite array of CLR under a normal plane wave excitation. The MoR has been widely used in the solution of scattering problems involving a single structure, such as a punctured spheroidal shell, a toroidal shell with slits, and

a slotted cylinder [84, 85]. The work is extended here to the investigation of the scattering problem from an arbitrary finite number M of CLR, where the CLR are of arbitrary radii, positions, dielectric loading and strip sizes.

The analysis starts in a similar approach as that of the single body problem. The scattered and transmitted fields, from each of the M CLR, are represented by series involving cylindrical harmonic functions in terms of the local coordinate system (which origin is the center of the corresponding cylinder). The sum of the scattered fields from all other CLR is then considered to be an incident wave on each of the individual cylinder. Subsequently, MBC are enforced on the surface of each of the M CLR, which leads to $2M$ sets of DSE involving the trigonometric functions. Each of the $2M$ sets of DSE are regularized to produce an ISLAE involving every unknown expansion coefficients. Therefore, the $2M$ infinite systems are interconnected, and need to be solved simultaneously for the values of all the unknown coefficients.

6.2 Problem specification

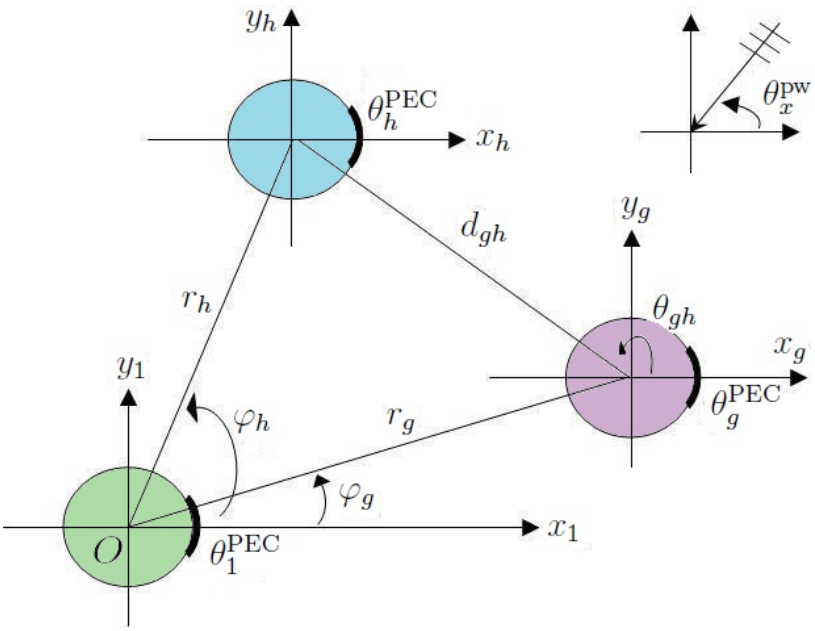

Figure 6.1: Cross-sectional view of the finite array of CLR

A cross-sectional view of the multi-body scattering problem considered is shown in Figure 6.1. Each of the CLR is as described in Chapter 4; that is, they are infinitely-long and axially-symmetric, the conducting strip on each is assumed to be infinitely thin and perfectly conducting. The CLR are assumed to be parallel to each other and

to the z-axis of the global coordinate system (ρ, ϕ, z). In addition, the PEC strips are assumed to have the same alignment. No further assumption has been made on the dimension, strip width, dielectric loading and location of each of the CLR.

We suppose the gth CLR is positioned with axial axis located at (r_g, φ_g, z) of the global polar coordinates (ρ, ϕ, z), for $g = 1, 2, \ldots, M$. Radius of this CLR is denoted as R_g. We suppose the gth CLR is constructed with a constant-K lens of relative permittivity and permeability (ϵ_g, μ_g). An infinitely thin, PEC strip of half angular size θ_g^{PEC} is placed on the surface of the gth cylinder as depicted in Figure 6.1. Without loss of generality, the surrounding homogeneous medium is taken to be free space with permittivity and permeability (ϵ_0, μ_0).

We suppose the array is excited by an E-polarized plane wave traveling in the direction making an angle θ_x^{pw} with respect to the x-axis of the global coordinate system, as illustrated in Figure 6.1. The scattering problem involving a H-polarized plane wave excitation can be treated similarly.

6.3 Derivation of the sets of DSE

The complete scattering domain is divided into $(M + 1)$ regions by the contours of the M CLR. Let region 0 denotes the surrounding medium, and region g denotes the interior of the gth CLR with $\rho_g < R_g$, for $g = 1, 2, \ldots, M$. Since the incident wave propagation direction is normal to the cylinder axis (*i.e.*, the z-axis), the problem is 2D and the induced secondary fields do not depend on z.

The analysis begins from expressing the scattered and transmitted fields by the gth CLR in terms of the local coordinate system (ρ_g, ϕ_g, z), for $g = 1, 2, \ldots, M$. To enforce the MBC on the gth CLR, the incident plane wave and the scattered fields by all other CLR have to be first expressed in terms of the gth local coordinate system, in order to take into account the interaction between the M cylinders. This is achieved by making use of the addition theorem given in (B.26).

6.3.1 Series representations for the fields

Since all of the CLR are uniform in the z-direction, and the plane wave is incident normally on the CLR, the axial components of the electric and magnetic fields are independent. For the TM_z incidence ($H_z^{\text{inc}} \equiv 0$) considered, only the components E_z, H_ϕ and H_ρ are non-vanishing, from (2.33).

In order to enforce the MBC on the surface of the gth CLR, the expression of the incident plane wave must be written in terms of the cylindrical harmonic functions

with reference to the local coordinate system (ρ_g, ϕ_g, z). This is done by application of the addition theorem given in (B.26). The series representation of the plane wave in terms of the gth local coordinate system can be obtained as

$$E_z^{\mathrm{inc}(g)}(\rho_g, \phi_g) = e^{-jk_0 r_g \cos(\varphi_g - \theta_x^{\mathrm{pw}})} \times e^{-jk_0 \rho_g \cos(\phi_g - \theta_x^{\mathrm{pw}})} \tag{6.1}$$

$$= \sum_{n=-\infty}^{\infty} (-j)^n J_n(k_0\rho_g) e^{-jk_0 r_g \cos(\varphi_g - \theta_x^{\mathrm{pw}})} e^{-jn\theta_x^{\mathrm{pw}}} e^{jn\phi_g} \,. \tag{6.2}$$

The superscript (g) is in reference to the gth local coordinate system (ρ_g, ϕ_g, z).

Suppose the series representations of the scattered and transmitted fields for the gth cylinder, in terms of the local coordinate system (ρ_g, ϕ_g) centered at (r_g, φ_g), are

$$E_z^{\mathrm{sc}(g)}(\rho_g, \phi_g) = \sum_{n=-\infty}^{\infty} a_n^{(g)} \frac{H_n^{(2)}(k_0\rho_g)}{H_n^{(2)}(k_0 R_g)} e^{jn\phi_g} \,, \tag{6.3}$$

$$E_z^{\mathrm{tr}(g)}(\rho_g, \phi_g) = \sum_{n=-\infty}^{\infty} b_n^{(g)} \frac{J_n(k_g\rho_g)}{J_n(k_g R_g)} e^{jn\phi_g} \,, \tag{6.4}$$

where $k_g = k_0\sqrt{\epsilon_g \mu_g}$ is the wave number of the dielectric material inside the gth cylinder. Here, $\left\{a_n^{(g)}, b_n^{(g)}\right\}_{n\in\mathbb{Z}}$, for $g = 1, 2, \ldots, M$, are the unknown coefficients to be determined.

Both the scattered field and the transmitted field associated with each of the cylinders are based on its local coordinate system. However, to enforce the MBC on the gth cylinder, the scattered fields of all the other cylinders need to be expressed in terms of the gth coordinate system. The addition theorem in (B.26) is used to transfer the series representation from one local coordinate system to another. The transformation from the hth local coordinate system (ρ_h, ϕ_h) to the gth local coordinate system (ρ_g, ϕ_g) of the Hankel function can be deduced from (B.26) as

$$H_n^{(2)}(k\rho_h)\, e^{jn\phi_h} = \sum_{m=-\infty}^{\infty} J_m(k\rho_g) H_{m-n}^{(2)}(kd_{g,h}) e^{-j(m-n)\theta_{g,h}} e^{jm\phi_g} \,. \tag{6.5}$$

Here, $d_{g,h}$ is the distance between the origins of the gth and h local coordinate system, $d_{g,h} = \sqrt{r_g^2 + r_h^2 - 2r_g r_h \cos(\varphi_g - \varphi_h)}$ whereas $\theta_{g,h}$ is the angle between the line joining the origins of two systems and the positive x-axis, $\theta_{g,h} = \pm\cos^{-1}\left(\frac{r_h\cos\varphi_h - r_g\cos\varphi_g}{d_{g,h}}\right)$ (where '$-$' is taken when $r_h \sin\varphi_h < r_g \sin\varphi_g$).

Having established the series representations for the longitudinal components of the electric (incident, scattered and transmitted) fields, the two non-zero transverse components of the magnetic field follows from (2.33), with $k_\rho = k$ as $k_z = 0$,

$$H_\phi = -\frac{j}{k\eta}\frac{\partial}{\partial\rho}E_z \text{ and } H_\rho = \frac{j}{k\rho\eta}\frac{\partial}{\partial\phi}E_z \,. \tag{6.6}$$

All other components, E_ϕ, E_ρ and H_z, for the incident and induced fields vanish for normal TM_z incidence.

6.3.2 Solution class

It is worth noting that the series representations given in (6.3) and (6.4) satisfy the Sommerfeld radiation condition and the finiteness of electromagnetic field at the origins of the local coordinate systems. Similar to the oblique scattering problem of a single CLR considered in Chapter 4, the Meixner finite energy condition puts an additional constraint on the unknown coefficients $\left\{a_n^{(g)}, b_n^{(g)}\right\}_{n\in\mathbb{Z}}$ by considering the electromagnetic energy per unit length of the gth CLR; that is,

$$W = \frac{1}{2}\int_0^1 \left|e^{jk_0 z}\right|^2 \mathrm{d}z \times \int_0^R \int_{-\pi}^{\pi} \Big\{\mu_0\mu_r \left|E_z^{\mathrm{tr}(g)}\left(\rho_g, \phi_g\right)\right|^2 + \epsilon_0\epsilon_r \left|H_\phi^{\mathrm{tr}(g)}\left(\rho_g, \phi_g\right)\right|^2 + \epsilon_0\epsilon_r \left|H_\rho^{\mathrm{tr}(g)}\left(\rho_g, \phi_g\right)\right|^2 \Big\} \mathrm{d}\phi_g\, \rho_g \mathrm{d}\rho_g\,. \tag{6.7}$$

Following the same integration process and arguments as that in Subsection 4.3.2, it can shown that both $\left\{a_n^{(g)}, b_n^{(g)}\right\}_{n\in\mathbb{Z}}$ satisfy the Fejér's Tauberian condition given in (D.4); *i.e.*,

$$\sum_{n=-\infty}^{\infty} |n| \left|a_n^{(g)}\right|^2 < \infty \text{ and } \sum_{n=-\infty}^{\infty} |n| \left|b_n^{(g)}\right|^2 < \infty\,. \tag{6.8}$$

6.3.3 Enforcing the MBC

The solution of the unknown coefficients $\left\{a_n^{(g)}, b_n^{(g)}\right\}_{n\in\mathbb{Z}}$ $(g = 1, 2, \ldots, M)$ can be obtained by applying the boundary conditions outlined in Subsection 2.2.1, on the surface of each of the CLR (*i.e.*, $\rho_g = R_g$, for $g = 1, 2, \ldots, M$). The boundary condition requires that the tangential components of the total electric field vanishes on the PEC surface. In this TM_z case, the electric field has only one non-zero component; *i.e.*, E_z. On the other hand, the boundary condition also requires that the tangential components of the total magnetic field varies continuously across the dielectric interface. As the axial-component of the magnetic field vanishes for E-polarization, $H_\phi = -\frac{j}{k\eta}\frac{\partial}{\partial\rho}E_z$ is the only non-vanishing tangential component of the magnetic field.

Therefore, the MBC on the surface of the gth CLR are given by

$$\lim_{\rho_g \to R_g^+} \left[E_z^{\mathrm{inc}(g)} + \sum_{h=1}^{M} E_z^{\mathrm{sc}(h)} \right] = \lim_{\rho_g \to R_g^-} E_z^{\mathrm{tr}(g)} = 0\,, \qquad \forall |\phi_g| < \theta_g^{\mathrm{PEC}}, \tag{6.9}$$

$$\lim_{\rho_g \to R_g^+} \frac{\partial}{\partial \rho} \left[E_z^{\mathrm{inc}(g)} + \sum_{h=1}^{M} E_z^{\mathrm{sc}(h)} \right] = \lim_{\rho_g \to R_g^-} \frac{1}{\mu_g} \frac{\partial}{\partial \rho} E_z^{\mathrm{tr}(g)}\,, \qquad \forall |\phi_g| > \theta_g^{\mathrm{PEC}}. \tag{6.10}$$

In addition to the MBC, the continuity of the tangential total electric field also requires that, for all $\rho_g = R_g$ and $\phi_g \in [-\pi, \pi]$,

$$\lim_{\rho_g \to R_g^+} E_z^{\mathrm{inc}(g)} + \sum_{h=1}^{M} E_z^{\mathrm{sc}(h)} = \lim_{\rho_g \to R_g^-} E_z^{\mathrm{tr}(g)}\,. \tag{6.11}$$

It is worth noting that the solution for the unknown coefficients $\left\{ a_n^{(g)}, b_n^{(g)} \right\}_{n \in \mathbb{Z}}$ related to the gth CLR, includes the effect of all interactions between the cylinders under this formulation.

There are $2M$ sequences of unknowns $\left\{ a_n^{(g)}, b_n^{(g)} \right\}_{n \in \mathbb{Z}}$ $(g = 1, 2, \ldots, M)$ to be determined from imposing the MBC on the surface of each of the CLR. The number of unknowns can be reduced by enforcing the continuity condition given in (6.11). By matching the fields across each of the surfaces, every one of the unknown $\left\{ b_n^{(g)} \right\}_{n \in \mathbb{Z}}$ $(g = 1, 2, \ldots, M)$ can be expressed as a linear combination of $\left\{ a_n^{(g)} \right\}_{n \in \mathbb{Z}}$ for $g = 1, \ldots, M$:

$$b_n^{(g)} = a_n^{(g)} + c_n^{(g)} + \sum_{h \neq g} \sum_{m=-\infty}^{\infty} a_m^{(h)} A_{n,m}^{(g,h)}\,. \tag{6.12}$$

where $c_n^{(g)} = e^{-jk_0 r_g \cos(\varphi_g - \theta_x^{\mathrm{pw}})} (-j)^n J_n(k_0 R_g) e^{-jn\theta_x^{\mathrm{pw}}}$. Here, the summation $\sum_{h \neq g}$ denotes the summation for $h = 1, \ldots, g-1, g+1, \ldots, M$.

The MBC on the gth CLR lead to the following DSE involving only the unknowns $\left\{ a_n^{(g)} \right\}_{n \in \mathbb{Z}}$ $(g = 1, \ldots, M)$:

$$\sum_{n=-\infty}^{\infty} \left[a_n^{(g)} + c_n^{(g)} + \sum_{h \neq g} \sum_{m=0}^{\infty} a_m^{(h)} A_{n,m}^{(g,h)} \right] e^{jn\phi_g} = 0\ (A)\,, \quad \forall |\phi_g| < \theta_g^{\mathrm{PEC}}. \tag{6.13}$$

$$\sum_{n=-\infty}^{\infty} \left[a_n^{(g)} p_n^{(g)} + d_n^{(g)} + q_n^{(g)} \sum_{h \neq g} \sum_{m=-\infty}^{\infty} a_m^{(h)} A_{n,m}^{(g,h)} \right] e^{jn\phi_g} = 0\ (A)\,, \quad \forall |\phi_g| > \theta_g^{\mathrm{PEC}}. \tag{6.14}$$

Recall that the notation (A) implies that the series are Abel-summable to 0 over their

corresponding intervals. The following notations are introduced for brevity:

$$d_n^{(g)} = k_0 c_n^{'(g)} - \frac{k_g}{\mu_g} c_n^{(g)} \frac{J_n^{'}(k_g R_g)}{J_n(k_g R_g)}\,, \tag{6.15a}$$

$$p_n^{(g)} = k_0 \frac{H_n^{'(2)}(k_0 R_g)}{H_n^{(2)}(k_0 R_g)} - \frac{k_g}{\mu_g} \frac{J_n^{'}(k_g R_g)}{J_n(k_g R_g)}\,, \tag{6.15b}$$

$$q_n^{(g)} = k_0 \frac{J_n^{'}(k_0 R_g)}{J_n(k_0 R_g)} - \frac{k_g}{\mu_g} \frac{J_n^{'}(k_g R_g)}{J_n(k_g R_g)}\,, \tag{6.15c}$$

$$A_{n,m}^{(g,h)} = \frac{H_{n-m}(k_0 d_{g,h}) J_n(k_0 R_g)}{H_m(k_0 R_h)} e^{j(m-n)\theta_{g,h}}\,, \tag{6.15d}$$

for $n, m \in \mathbb{Z}$.

We have M sets of DSE given in (6.13) and (6.14), for $g = 1, 2, \ldots, M$. As each of these sets of DSE involves all the unknowns $\left\{a_n^{(g)}\right\}_{n\in\mathbb{Z}}$ for $g = 1, 2, \ldots, M$, these M sets are interconnected and need to be solved simultaneously.

6.4 Regularization process

Following the similar process presented in Chapter 3, the M DSE derived in (6.13) and (6.14) are reformulated with trigonometric functions as the kernels, then regularized to $2M$ connected ISLAE. The constant unknowns $a_0^{(g)}$ $(g = 1, 2, \ldots, M)$ are removed from all the $2M$ ISLAE before matrix inversion is performed numerically to solve for the unknown coefficients. This is achieved by a simple algebraic elimination (equivalent to the application of Cramer's rule). In the final step, one single $2M$-by-$2M$ block matrix equation is obtained. The block matrix is shown to be a compact perturbation of the identity operator in ℓ_2.

6.4.1 Introducing the asymptotically small parameters

Due to the symmetry of the intervals, we can reformulate the DSE given in (6.13) and (6.14) defined over $(-\pi, \pi)$ in terms of the trigonometric functions over $(0, \pi)$. We introduce the following:

$$x_n^{(g)} := a_n^{(g)} + a_{-n}^{(g)}\,, \tag{6.16a}$$

$$y_n^{(g)} := a_n^{(g)} - a_{-n}^{(g)}\,, \tag{6.16b}$$

$$e_n^{(g)} := c_n^{(g)} + c_{-n}^{(g)}\,, \tag{6.16c}$$

$$f_n^{(g)} := \frac{d_n^{(g)} + d_{-n}^{(g)}}{n}\,, \tag{6.16d}$$

$$g_n^{(g)} := c_n^{(g)} - c_{-n}^{(g)}\,, \tag{6.16e}$$

$$h_n^{(g)} := \frac{d_n^{(g)} - d_{-n}^{(g)}}{n}\,, \tag{6.16f}$$

$$B_{n,m}^{(g,h)} := \frac{1}{2}\left[A_{n,m}^{(g,h)} + A_{-n,m}^{(g,h)} + A_{n,-m}^{(g,h)} + A_{-n,-m}^{(g,h)}\right], \tag{6.16g}$$

$$C_{n,m}^{(g,h)} := \frac{1}{2}\left[A_{n,m}^{(g,h)} + A_{-n,m}^{(g,h)} - A_{n,-m}^{(g,h)} - A_{-n,-m}^{(g,h)}\right], \tag{6.16h}$$

$$D_{n,m}^{(g,h)} := \frac{1}{2}\left[A_{n,m}^{(g,h)} - A_{-n,m}^{(g,h)} + A_{n,-m}^{(g,h)} - A_{-n,-m}^{(g,h)}\right], \tag{6.16i}$$

$$E_{n,m}^{(g,h)} := \frac{1}{2}\left[A_{n,m}^{(g,h)} - A_{-n,m}^{(g,h)} - A_{n,-m}^{(g,h)} + A_{-n,-m}^{(g,h)}\right], \tag{6.16j}$$

for $n, m = 1, 2, \ldots$

It is worth noting that $p_n^{(g)} = p_{-n}^{(g)}$ and $q_n^{(g)} = q_{-n}^{(g)}$, for all $n = 1, 2, \ldots$ By examining the asymptotic behaviors of the Bessel function and the Hankel function, the following asymptotically parameters are introduced:

$$\tilde{p}_n^{(g)} = 1 + \frac{R_g \mu_g}{1 + \mu_g} \frac{p_n^{(g)}}{|n|}\,, \tag{6.17}$$

$$\tilde{q}_n^{(g)} = \frac{q_n^{(g)}}{|n|}\,, \tag{6.18}$$

for $n = 1, 2, \ldots$ Both of the above parameters have the order of $O\left(\frac{k_g^2 R_g^2}{n^2}\right)$, as $n \to +\infty$. On the other hand, from its definition, we can see that $f_n^{(g)} = e_n^{(g)} \tilde{q}_n$, for $n = 1, 2, \ldots$

Therefore, the gth set of DSE given in (6.9) and (6.10) can be reformulated as the two sets of DSE below. The first set of DSE involving the cosine function is:

$$\begin{aligned} &a_0^{(g)} + c_0^{(g)} + \sum_{h \neq g} a_0^{(h)} A_{0,0}^{(g,h)} + \frac{1}{2} \sum_{h \neq g} \sum_{m=1}^{\infty} \left[x_m^{(h)} B_{0,m}^{(g,h)} + y_m^{(h)} C_{0,m}^{(g,h)}\right] \\ &+ \sum_{n=1}^{\infty} \left\{ e_n^{(g)} + x_n^{(g)} + \sum_{h \neq g} \left[a_0^{(h)} B_{n,0}^{(g,h)} + \sum_{m=1}^{\infty} \left(x_m^{(h)} B_{n,m}^{(g,h)} + y_m^{(h)} C_{n,m}^{(g,h)} \right) \right] \right\} \cos n\phi = 0\,, \end{aligned} \tag{6.19a}$$

for $\phi_g \in (0, \theta_g^{\mathrm{PEC}})$, and

$$\begin{aligned} &\zeta_g p_0^{(g)} a_0^{(g)} + \zeta_g d_0^{(g)} + \zeta_g q_0^{(g)} \sum_{h \neq g} a_0^{(h)} A_{0,0}^{(g,h)} \\ &+ \frac{\zeta_g q_0^{(g)}}{2} \sum_{h \neq g} \sum_{m=1}^{\infty} \left[x_m^{(h)} B_{0,m}^{(g,h)} + y_m^{(h)} C_{0,m}^{(g,h)}\right] + \sum_{n=1}^{\infty} n \left\{ \zeta_g f_n^{(g)} + x_n^{(g)} \left(1 - \tilde{p}_n^{(g)}\right) \right. \\ &\left. + \zeta_g \tilde{q}_n^{(g)} \sum_{h \neq g} \left[a_0^{(h)} B_{n,0}^{(g,h)} + \sum_{m=1}^{\infty} \left(x_m^{(h)} B_{n,m}^{(g,h)} + y_m^{(h)} C_{n,m}^{(g,h)} \right) \right] \right\} \cos n\phi = 0\,, \end{aligned} \tag{6.19b}$$

for $\phi_g \in (\theta_g^{\mathrm{PEC}}, \pi)$, where

$$\zeta_g := -\frac{R_g \mu_g}{1+\mu_g}\,. \tag{6.20}$$

The second set of DSE involving the sine function is:

$$\sum_{n=1}^{\infty} \Bigg\{ g_n^{(g)} + y_n^{(g)} \tag{6.21a}$$
$$+\sum_{h\neq g} \left[a_0^{(h)} D_{n,0}^{(g,h)} + \sum_{m=1}^{\infty} \left(x_m^{(h)} D_{n,m}^{(g,h)} + y_m^{(h)} E_{n,m}^{(g,h)} \right) \right] \Bigg\} \sin n\phi = 0\,,$$

for $\phi_g \in (0, \theta_g^{\mathrm{PEC}})$, and

$$\sum_{n=1}^{\infty} n \Bigg\{ \zeta_g h_n^{(g)} + y_n^{(g)} \left(1 - \tilde{p}_n^{(g)}\right) \tag{6.21b}$$
$$+\zeta_g \tilde{q}_n^{(g)} \sum_{h\neq g} \left[a_0^{(h)} D_{n,0}^{(g,h)} + \sum_{m=1}^{\infty} \left(x_m^{(h)} D_{n,m}^{(g,h)} + y_m^{(h)} E_{n,m}^{(g,h)} \right) \right] \Bigg\} \sin n\phi = 0\,.$$

for $\phi_g \in (\theta_g^{\mathrm{PEC}}, \pi)$.

6.4.2 Conversion to infinite system of linear algebraic equations

It may be shown with the ideas in Chapter 3, that the gth set of series equations given in (6.19) and (6.21) can be transformed to two ISLAE in terms of $\left\{ x_n^{(g)}, y_n^{(g)} \right\}_{n=1}^{\infty}$ by the MoR. The ISLAE for $x_n^{(g)}$ has the form of

$$\begin{aligned}
&\sqrt{m} x_m^{(g)} \left[1 - \tilde{p}_m^{(g)}\right] + \sum_{n=1}^{\infty} \sqrt{n} x_n^{(g)} \tilde{p}_n^{(g)} T_{m,n}^{(g)} \\
&= 2\zeta_g \left[p_0^{(g)} c_0^{(g)} - d_0^{(g)} \right] \tau_m^{(g)} - \zeta_g \sqrt{m} f_m^{(g)} + \sum_{n=1}^{\infty} \sqrt{n} \left[\zeta_g f_n^{(g)} - e_n^{(g)} \right] T_{m,n}^{(g)} \\
&\quad - \sum_{h\neq g} a_0^{(h)} H_m^{(g,h)} + \sum_{h\neq g} \sum_{n=1}^{\infty} \left[\sqrt{n} x_n^{(h)} U_{m,n}^{(g,h)} + \sqrt{n} y_n^{(h)} V_{m,n}^{(g,h)} \right]
\end{aligned} \tag{6.22}$$

The following are parameters introduced that can be explicitly calculated in terms of the geometry and physical quantities of the problem.

$$\psi_g = \cos(\theta_g^{\mathrm{PEC}}) \tag{6.23}$$

$$T_{m,n}^{(g)} = \hat{Q}_{m-1,n-1}^{(0,1)}(\psi_g) - \frac{\zeta_g p_0^{(g)} (1+\psi_g)^2}{\zeta_g p_0^{(g)} \ln\left(\frac{1-\psi_g}{2}\right) - 1} \frac{\hat{P}_{m-1}^{(0,1)}(\psi_g)}{m} \frac{\hat{P}_{n-1}^{(0,1)}(\psi_g)}{n} \tag{6.24}$$

$$\tau_n^{(g)} = \frac{(1+\psi_g)}{\sqrt{2}\left[\zeta_g p_0^{(g)} \ln\left(\frac{1-\psi_g}{2}\right) - 1\right]} \frac{\hat{P}_{n-1}^{(0,1)}(\psi_g)}{n} \tag{6.25}$$

$$\begin{aligned} H_n^{(g,h)} = & 2\zeta_g \left[q_0^{(g)} - p_0^{(g)}\right] \tau_n^{(g)} A_{0,0}^{(g,h)} + \zeta_g \tilde{q}_n^{(g)} B_{n,0}^{(g,h)} \\ & + \sum_{m=1}^{\infty} \left[1 - \zeta_g \tilde{q}_m^{(g)}\right] B_{m,0}^{(g,h)} T_{n,m}^{(g)} \end{aligned} \tag{6.26}$$

$$\begin{aligned} U_{m,n}^{(g,h)} = & \zeta_g \left[p_0^{(g)} - q_0^{(g)}\right] \tau_m^{(g)} B_{0,n}^{(g,h)} - \zeta_g \tilde{q}_m^{(g)} B_{m,n}^{(g,h)} \\ & - \sum_{k=1}^{\infty} \left[1 - \zeta_g \tilde{q}_k^{(g)}\right] T_{m,k}^{(g)} B_{k,n}^{(g,h)} \end{aligned} \tag{6.27}$$

$$\begin{aligned} V_{m,n}^{(g,h)} = & \zeta_g \left[p_0^{(g)} - q_0^{(g)}\right] \tau_m^{(g)} C_{0,n}^{(g,h)} - \zeta_g \tilde{q}_m^{(g)} C_{m,n}^{(g,h)} \\ & - \sum_{k=1}^{\infty} \left[1 - \zeta_g \tilde{q}_k^{(g)}\right] T_{m,k}^{(g)} C_{k,n}^{(g,h)} \end{aligned} \tag{6.28}$$

$$B_{m,n}^{(g,h)} = \tfrac{1}{2}\sqrt{\tfrac{m}{n}} \left[A_{m,n}^{(g,h)} + A_{-m,n}^{(g,h)} + A_{m,-n}^{(g,h)} + A_{-m,-n}^{(g,h)}\right] \tag{6.29}$$

$$C_{m,n}^{(g,h)} = \tfrac{1}{2}\sqrt{\tfrac{m}{n}} \left[A_{m,n}^{(g,h)} + A_{-m,n}^{(g,h)} - A_{m,-n}^{(g,h)} - A_{-m,-n}^{(g,h)}\right] \tag{6.30}$$

The ISLAE for $\left\{y_n^{(g)}\right\}_{n=1}^{\infty}$ is similar to that of $\left\{x_n^{(g)}\right\}_{n=1}^{\infty}$, and is omitted here for reason of space. Together with the two ISLAE obtained, an expression for $a_0^{(g)}$ is derived, which has been isolated from the ISLAE for $\left\{x_n^{(g)}\right\}_{n=1}^{\infty}$ and $\left\{y_n^{(g)}\right\}_{n=1}^{\infty}$,

$$a_0^{(g)} = -\sum_{h \neq g} a_0^{(h)} a_{g,h} + \Psi_g \,. \tag{6.31}$$

This expression is obtained by making use of the fact that $\left\{x_n^{(g)}, y_n^{(g)}\right\}_{n=1}^{\infty}$ belong to ℓ_2, and the continuity at $z = \psi_g$. The two new notations $a_{g,h}$ and Ψ_g introduced are defined as

$$a_{g,h} := \begin{cases} 1 & , g = h, \\ -\left[\gamma_g A_{0,0}^{(g,h)} + \displaystyle\sum_{n=1}^{\infty} \tau_n^{(g)} B_{n,0}^{(g,h)}\right] & , g \neq h, \end{cases} \tag{6.32}$$

$$\Psi_g := \lambda_g + \sum_{h=1}^{M} \sum_{n=1}^{\infty} \left[\sqrt{n} x_n^{(h)} F_n^{(g,h)} + \sqrt{n} y_n^{(h)} G_n^{(g,h)}\right], \tag{6.33}$$

where we have also introduced

$$\gamma_g := \frac{1 - \zeta_g q_0^{(g)} \ln\left(\frac{1-\psi_g}{2}\right)}{\zeta_g p_0^{(g)} \ln\left(\frac{1-\psi_g}{2}\right) - 1}, \tag{6.34}$$

$$\lambda_g := \frac{c_0^{(g)} - \zeta_g d_0^{(g)} \ln\left(\frac{1-\psi_g}{2}\right)}{\zeta_g p_0^{(g)} \ln\left(\frac{1-\psi_g}{2}\right) - 1} - \sum_{n=1}^{\infty} \sqrt{n} \left[\zeta_g f_n^{(g)} - e_n^{(g)}\right] \tau_n^{(g)}\,, \tag{6.35}$$

$$F_n^{(g,h)} := \begin{cases} \tau_n^{(g)} \tilde{p}_n^{(g)} & , g = h, \\ \frac{1}{2}\gamma_g B_{0,n}^{(g,h)} + \sum_{m=1}^{\infty} \left[1 - \zeta_g \tilde{q}_m^{(g)}\right] \tau_m^{(g)} B_{m,n}^{(g,h)} & , g \neq h, \end{cases} \tag{6.36}$$

$$G_n^{(g,h)} := \begin{cases} 0 & , g = h, \\ \frac{1}{2}\gamma_g C_{0,n}^{(g,h)} + \sum_{m=1}^{\infty} \left[1 - \zeta_g \tilde{q}_m^{(g)}\right] \tau_m^{(g)} C_{m,n}^{(g,h)} & , g \neq h. \end{cases} \tag{6.37}$$

For the normal incidence problem involving only single cylinder, the ISLAE for $\left\{x_n^{(1)}\right\}_{n=1}^{\infty}$ and $\left\{y_n^{(1)}\right\}_{n=1}^{\infty}$ are disjoint. They can readily and separately be solved by matrix inversion. When there are M cylinders involved, the resulting $2M$ systems are all connected to one another. Some manipulations are required before the systems can be solved numerically by the truncation method. We remove all the unknowns $a_0^{(g)}$ $(g = 1, \ldots, M)$ from each of the $2M$ systems, by analytically solving the $2M$ expressions of the form of Eqn.(6.31) by Cramer's rule or equivalent. An explicit expression for the $a_0^{(g)}$ that is independent of all the other $a_0^{(h)}$ (for $h = 1, \ldots, i-1, i+1, \ldots, M$) is obtained as

$$a_0^{(g)} = \sum_{h=1}^{M} \Psi_g \Phi_{g,h}\,, \tag{6.38}$$

where the coefficients $\Phi_{g,h}$ (for $g, h = 1, 2, \ldots, M$) can be computed from

$$\Phi_{g,h} = \frac{\begin{vmatrix} a_{1,1} & \ldots & a_{1,h-1} & a_{1,h+1} & \ldots & a_{1,M} \\ \vdots & \vdots & \vdots & \vdots & \ddots & \vdots \\ a_{g-1,1} & \ldots & a_{g-1,h-1} & a_{g-1,h+1} & \ldots & a_{g-1,M} \\ a_{g+1,1} & \ldots & a_{g+1,h-1} & a_{g+1,h+1} & \ldots & a_{g+1,M} \\ \vdots & \vdots & \vdots & \vdots & \ddots & \vdots \\ a_{M,1} & \ldots & a_{M,h-1} & a_{M,h+1} & \ldots & a_{M,M} \end{vmatrix}}{\begin{vmatrix} a_{1,1} & \ldots & a_{1,M} \\ \vdots & \vdots & \vdots \\ a_{M,1} & \ldots & a_{M,M} \end{vmatrix}}\,. \tag{6.39}$$

Therefore, once the values for the unknowns $\left\{x_n^{(g)}\right\}_{n=1}^{\infty}$ and $\left\{y_n^{(g)}\right\}_{n=1}^{\infty}$ $(g = 1, \ldots, M)$ are computed, all the unknowns $a_0^{(g)}$ (for $g = 1, \ldots, M$) can be readily calculated.

These expressions for $a_0^{(g)}$ in the form of Eqn.(6.38) are substituted back into each of the $2M$ infinite systems. For the unknown $\left\{x_n^{(g)}\right\}_{n=1}^{\infty}$, the following ISLAE is obtained

$$K_{m,n}^{(g)} = \sqrt{m} x_m^{(g)} \left[1 - \tilde{p}_m^{(g)}\right] + \sum_{h=1}^{M} \sum_{n=1}^{\infty} \left[\sqrt{n} x_n^{(h)} I_{m,n}^{(g,h)} + \sqrt{n} y_n^{(h)} J_{m,n}^{(g,h)}\right]\,, \tag{6.40}$$

where the expressions for $I_{m,n}^{(g,h)}$, $J_{m,n}^{(g,h)}$ and $K_{m,n}^{(g)}$ are defined as

$$I_{m,n}^{(g,h)} = \begin{cases} \tilde{p}_n^{(g)} T_{m,n}^{(g)} + \sum_{q=1}^{M} F_n^{(q,g)} R_m^{(g,q)} & , g = h, \\ \zeta_g \tilde{q}_m^{(g)} B_{m,n}^{(g,h)} + \sum_{q=1}^{M} F_n^{(q,h)} R_m^{(g,q)} & , g \neq h, \\ +\sum_{k=1}^{\infty} \left[1 - \zeta_g \tilde{q}_k^{(g)}\right] T_{m,k}^{(g)} B_{k,n}^{(g,h)} & \\ +\zeta_g \left[q_0^{(g)} - p_0^{(g)}\right] \tau_m^{(g)} B_{0,n}^{(g,h)} & \end{cases} \tag{6.41}$$

$$J_{m,n}^{(g,h)} = \begin{cases} \sum_{q=1}^{M} G_n^{(q,g)} R_m^{(g,q)} & , g = h, \\ \zeta_g \tilde{q}_m^{(g)} C_{m,n}^{(g,h)} + \sum_{q=1}^{M} G_n^{(q,h)} R_m^{(g,q)} & , g \neq h, \\ +\sum_{k=1}^{\infty} \left[1 - \zeta_g \tilde{q}_k^{(g)}\right] T_{m,k}^{(g)} C_{k,n}^{(g,h)} & \\ +\zeta_g \left[q_0^{(g)} - p_0^{(g)}\right] \tau_m^{(g)} C_{0,n}^{(g,h)} & \end{cases} \tag{6.42}$$

$$R_n^{(g,h)} = \sum_{p \neq g} H_n^{(g,p)} \Phi_{p,h} \,. \tag{6.43}$$

A similar ISLAE can be obtained for $\left\{y_n^{(g)}\right\}_{n=1}^{\infty}$. These ISLAE can now be written as a single matrix equation in the operator form of $(\mathcal{I} + \mathcal{H})\,\mathbf{x} = \mathbf{b}$. By truncating the infinite system of equations to N_{tr}, the problem is solved by matrix inversion. Here, $\mathcal{I}$ is the $(2N_{\text{tr}}M \times 2N_{\text{tr}}M)$ identity matrix, $\mathcal{H}$ is a compact $2M \times 2M$ block matrix in ℓ_2 where each of these block matrices is of size $N_{\text{tr}} \times N_{\text{tr}}$, $\mathbf{b}$ is a known vector, and $\mathbf{x}$ is the vector consisting of the unknowns $\left\{x_n^{(g)}\right\}_{n=1}^{\infty}$ and $\left\{y_n^{(g)}\right\}_{n=1}^{\infty}$. It is worth noting that the infinite system (for $N_{\text{tr}} \to \infty$) is a Fredholm matrix equation of the second kind. By increasing N_{tr}, the accuracy of the computed solution can be improved.

6.5 Numerical results

In this section, sample numerical results are presented to prove the validity of the developed formulation for the scattering problem involving multiple CLR. The unknown coefficients computed are substituted into the series expressions for the near field, RCS and surface current density. The properties of grating formed by an array of identical CLR are studied based on the RCS analysis. The effect of the number of CLR in the grating as well as the effect of the relative distance between each CLR have on the RCS are investigated numerically.

6.5.1 Series representations of physical quantities

For the multiple scattering problem considered in this chapter, the RCS $\sigma(\theta)$ still has the same definition as that in (2.40). However, the total scattered field by this array

of CLR is the sum of all the scattered field produced by each individual CLR. On top of that, each of this scattered field has been expressed in terms of its local coordinate system. In order to obtain a series representation for this multiple scattering problem, the far-field approximations

$$\rho_g \approx \rho - r_g \cos(\vartheta_g - \phi)\,, \tag{6.44}$$

$$\phi_g \approx \phi\,, \tag{6.45}$$

are employed, in addition to the use of the asymptotic expression of the Hankel function.

6.5.2 Numerical validation

To check the adequacy and the accuracy of the proposed formulation and the numerical algorithm, the scattering problem of five PEC cylinders as described in [18] is solved. Five closed PEC cylinders ($\theta_g^{\text{PEC}} = 180°$, for $g = 1, 2, \ldots, 5$) of the same size ($R_g = 0.1\lambda$, for $g = 1, 2, \ldots, 5$) are considered. Suppose the center of the first cylinder is located at the origin, the centers of the remaining four cylinders are located 0.5λ away; *i.e.*, at the points $(0.5\lambda, 0)$, $(0.5\lambda, 90°)$, $(0.5\lambda, 180°)$ and $(0.5\lambda, -90°)$ in relation to the global coordinate system (ρ, ϕ). The cross-sectional view of the particular problem considered is depicted in the top figure in Figure 6.2. The values of the bistatic scattering cross section computed for the problem is plotted along the entire contour, and the curve is compared directly with that in [18]. Good agreement is seen with the results calculated using the hybrid exact-method of moments technique, the iterative technique and the boundary value solution method.

As another method to check the validity of this developed formulation for slotted PEC cylinders (when $\theta_g^{\text{PEC}} \neq \pi$), the computed values of the $2M$ unknown coefficients, $\left\{x_n^{(g)}, y_n^{(g)}\right\}_{n=1}^{\infty}$ $(g = 1, \ldots, M)$, have been substituted back to the series representations given in (6.3), (6.4) and (6.6) to check the validity of MBC. For this purpose, the scattering of a TM_z plane wave incident on a pair of arbitrary chosen CLR is considered. The first CLR is assumed to have a radius of $R_1 = 2.5\lambda$, attached with a PEC strip of half angular width $\theta_1^{\text{PEC}} = 90°$ and located with center at $(0, 0)$; whereas the second CLR is assumed to take values $R_2 = 3.75\lambda$, ${\theta_2^{\text{PEC}}}_2 = 60°$, $r_2 = 10$ and $\vartheta_2 = 45°$. Both cylinders are filled with dielectric material characterized by $(\epsilon_1, \mu_1) = (\epsilon_2, \mu_2) = (2, 1)$. The computed real and imaginary values of the tangential total electric field, E_z, along the contour of the first CLR are depicted in Figure 6.3. The exterior field (sum of the scattered fields by both CLR and the incident field) is

depicted as the solid red line; while the interior field computed (the transmitted field inside the first CLR) is depicted as the dashed black line. Evidently, the total electric field is continuous across the surface and vanishes on the PEC strip. In Figure 6.4, the computed real and imaginary values of the difference between H_ϕ of the exterior and interior total fields are plotted over the entire contour. As seen from the plot, H_ϕ varies continuously across the dielectric surface. In conclusion, both of Figure 6.3 and Figure 6.4 confirm the MBC given in (6.9) and (6.10) on the surface of the first CLR. The same check has been conducted on the surface of the second CLR and excellent agreement is observed again. The figures are omitted to avoid repetition.

As another means of display for the same internal test conducted in the last paragraph, the near field distribution of the scattering problem is illustrated in the contour mesh given in Figure 6.5

6.5.3 Numerical investigation

After the problem formulation and the validation of the method, the solution can now be computed numerically and applied to actual analysis. However, there are a number of parameters to choose from. Due to the limit of space, it is not feasible to present a full range of features of the structures. Let us show a representative result. Figure 6.6 illustrates the near field distribution of a TM_z plane wave incident at $\theta_x^{\mathrm{pw}} = 180^\circ$ on a sawtooth-shaped PEC surface formed by joining CLR. Consider such a surface constructed using three cylinders of the same size, where $R_g = 2.5\lambda$, $\epsilon_g = 1$ and $\mu_g = 1$ (for $g = 1, 2, 3$).

6.6 Conclusion

A rigorous and accurate method of solving for the problem of 2D scattering from a finite array of CLR has been presented. As the CLR are open, the interior cavities of the CLR are coupled through free space. The formulation is based on the MoR, which has the advantage of a stable and convergent computed solution. The dielectric constant, strip width, radius and location of each of the cylinders can be varied to model a range of scattering problems, including a periodic array of fully- (or partially-) shielded cylinders.

The solution method described in this chapter makes no assumption nor simplication of the interaction among the multiple CLR. As the number of CLR increases, the computation cost increases significantly. One possible extension to the current work is the combination of the Green's function diakoptics approach [82] with our

method developed here. In the Green's function diakoptics approach, the configuration is decomposed into computational bricks, and the fields incident on and scattered from a computational brick are captured through the use of equivalence principles. The near-field (intricate coupling) and far-field (simple coupling) are effectively decomposed in the Green's function diakoptics approach, and thus, the computational burden is reduced.

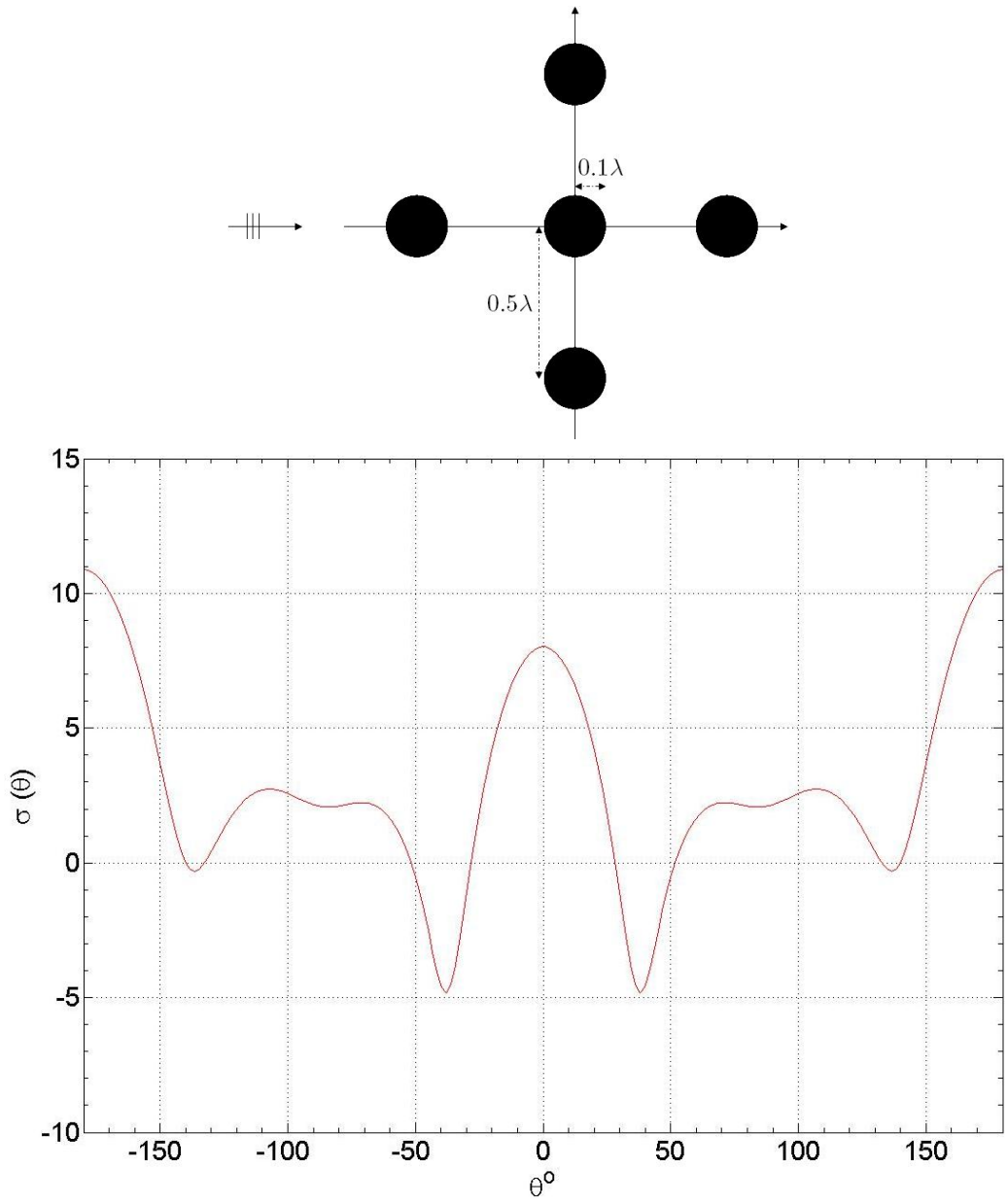

Figure 6.2: The bistatic scattering cross section of five closed PEC cylinders due to a TM_z plane wave incident at $\theta_x^{\mathrm{pw}} = 180\,^\circ$. $[R_{1,2,3,4,5} = 0.1\lambda$, $\theta_{1,2,3,4,5}^{\mathrm{PEC}} = 180^\circ$, $\epsilon_{1,2,3,4,5} = 1$, $\mu_{1,2,3,4,5} = 1$, $r_1 = 0 = \vartheta_1$, $r_{2,3,4,5} = 0.5\lambda$, $\vartheta_2 = 0$, $\vartheta_3 = 90^\circ$, $\vartheta_4 = 180^\circ$, $\vartheta_5 = -90^\circ$ and $\theta_x^{\mathrm{pw}} = 180^\circ]$

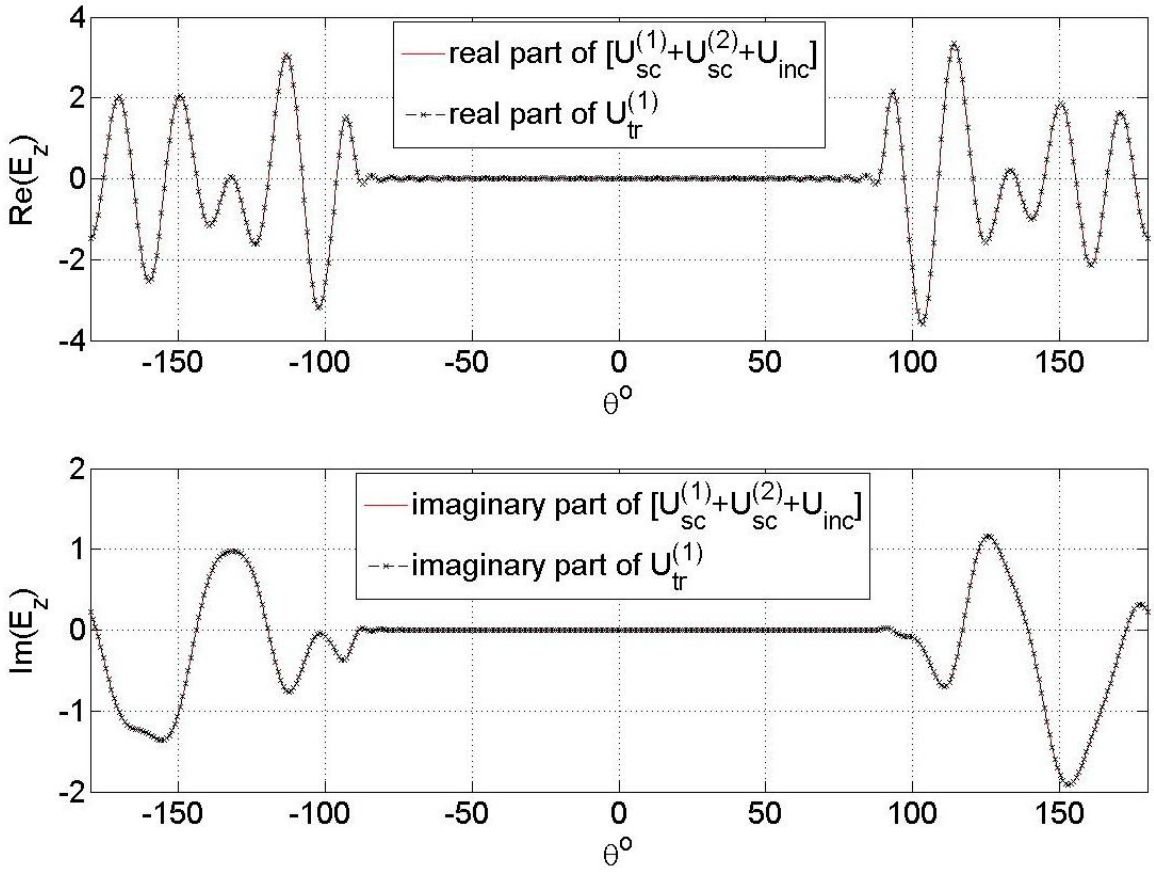

Figure 6.3: Numeric verification of boundary condition (2.9a) on the surface of the first CLR; *i.e.*, E_z vanishes on the PEC strip. [$R_1 = 2.5\lambda$, $R_2 = 3.75\lambda$, $\epsilon_{1,2} = 2$, $\mu_{1,2} = 1$, $\theta_1^{\mathrm{PEC}} = 90\circ$, $\theta_2^{\mathrm{PEC}} = 60\circ$, $r_1 = 0$, $r_2 = 10\lambda$, $\vartheta_1 = 0$, $\vartheta_2 = 45^\circ$ and $\theta_x^{\mathrm{pw}} = 180\,^\circ$]

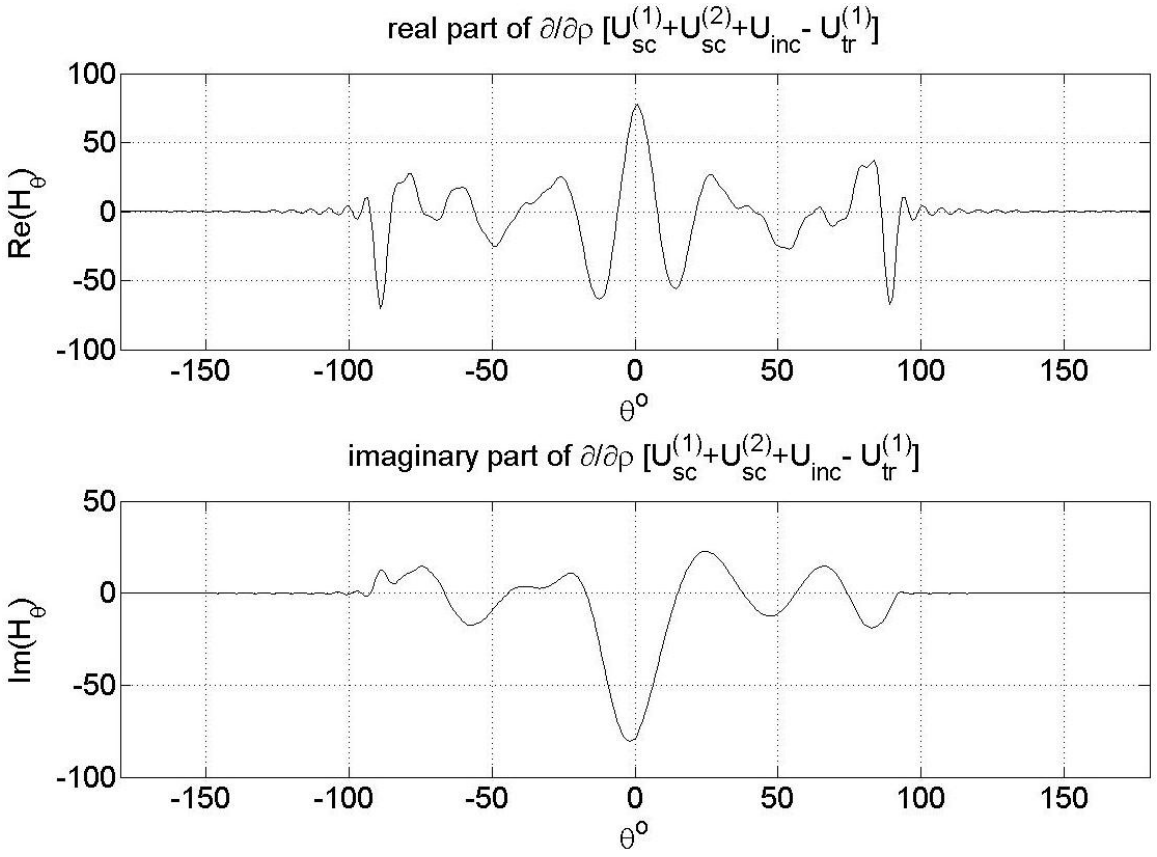

Figure 6.4: Numeric verification of (2.9b) on the surface of the first CLR; *i.e.*, H_ϕ varies continuously across the dielectric surface. [$R_1 = 2.5\lambda$, $R_2 = 3.75\lambda$, $\epsilon_{1,2} = 2$, $\mu_{1,2} = 1$, $\theta_1^{\rm PEC} = 90\circ$, $\theta_2^{\rm PEC} = 60\circ$, $r_1 = 0$, $r_2 = 10\lambda$, $\vartheta_1 = 0$, $\vartheta_2 = 45^\circ$ and $\theta_x^{\rm pw} = 180\,^\circ$]

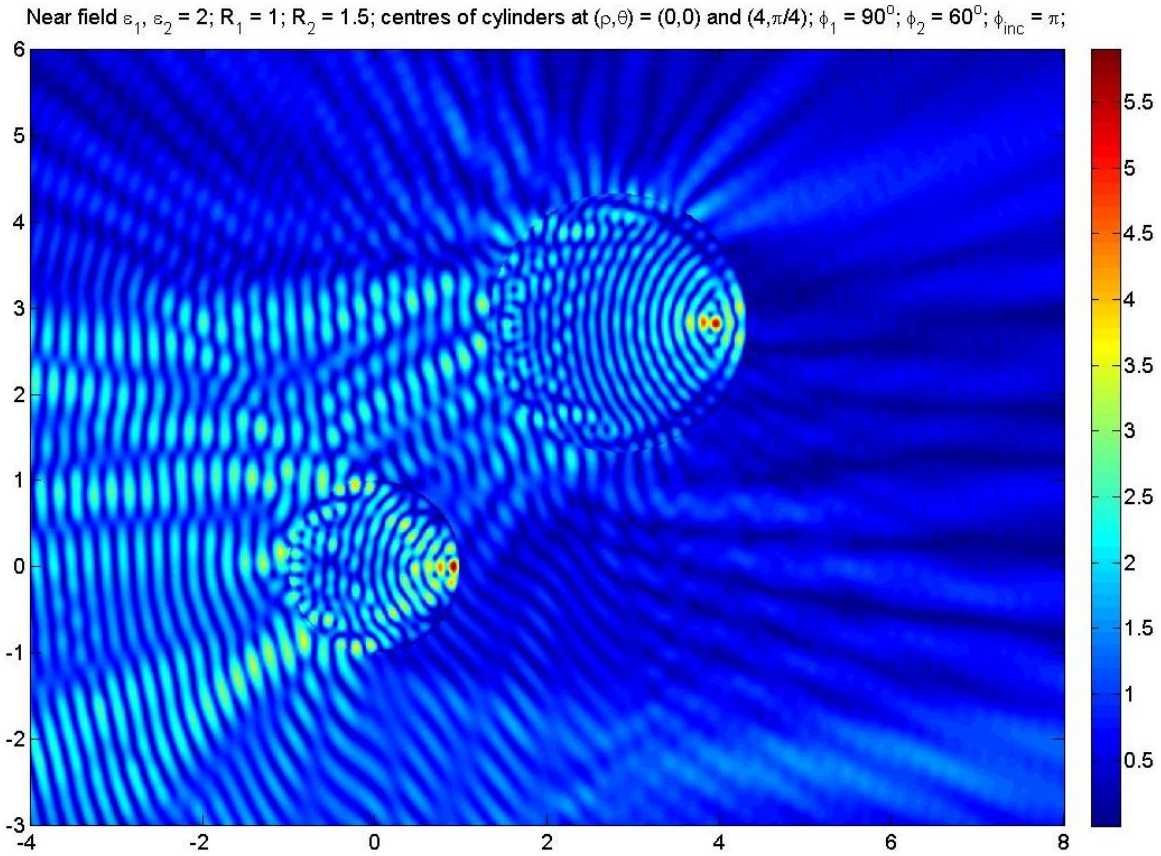

Figure 6.5: The near field distribution of a TM plane wave incident on the. [$R_1 = 2.5\lambda$, $R_2 = 3.75\lambda$, $\epsilon_{1,2} = 2$, $\mu_{1,2} = 1$, $\theta_1^{\mathrm{PEC}} = 90\circ$, $\theta_2^{\mathrm{PEC}} = 60\circ$, $r_1 = 0$, $r_2 = 10\lambda$, $\vartheta_1 = 0$, $\vartheta_2 = 45^\circ$ and $\theta_x^{\mathrm{pw}} = 180\,^\circ$]

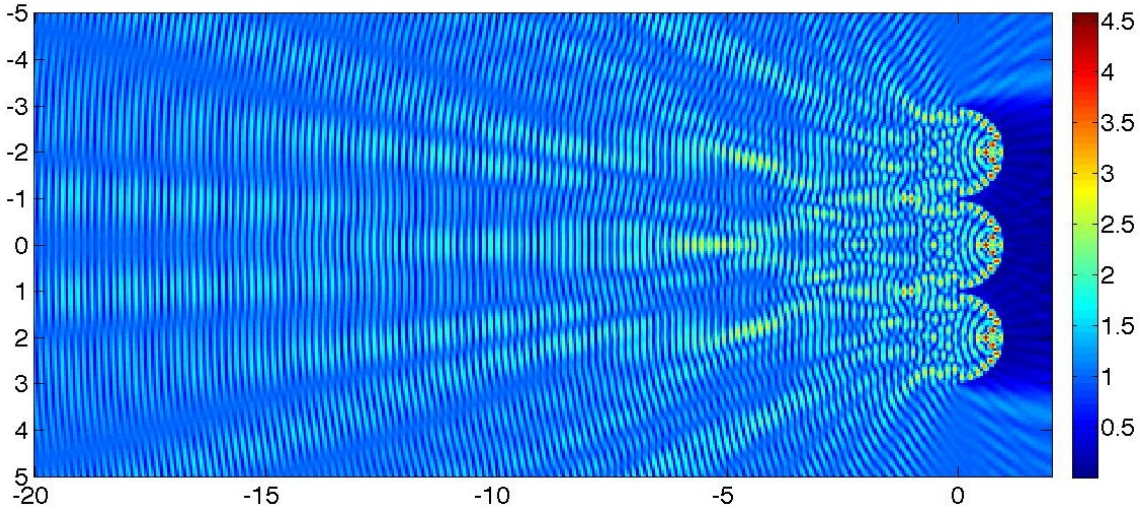

Figure 6.6: The near field distribution of a TM plane wave incident on a sawtooth-shaped surface. [$R_{1,2,3} = 2.5\lambda$, $\epsilon_{1,2,3} = 1$, $\mu_{1,2,3} = 1$, $\vartheta_{1,2,3} = 90^\circ$, $r_1 = 0$, $r_{2,3} = 5\lambda$, $\vartheta_1 = 0$, $\vartheta_2 = 90^\circ$, $\vartheta_3 = -90^\circ$, $\theta_x^{\mathrm{pw}} = 180^\circ$]

Chapter 7

Scattering from and penetration into a multi-conductor cylinder

7.1 Introduction

This chapter reports the development of a rigorous numerical algorithm for a braided cylindrical shield, based upon the MoR. The model under study is a braided cylindrical shield constructed by periodically placing an arbitrary number of PEC strips of the same width on a dielectric cylinder as depicted in Figure 7.1. Numerical code is developed to provide a prediction of the amount that an obliquely incident plane wave will penetrate through the apertures into the cavity.

The structure considered belongs to the class of nonplanar frequency selective surface (FSS) geometries. Periodic grids of PEC strips are often employed as polarization selective surfaces in applications such as improving the radiation characteristics of waveguide and antennas. In general, the PEC strips (when properly located) reflect the polarization parallel with the strips while transmitting the polarization normal to them. They have also been used to realize hard surfaces, which reflection coefficient is independent for geometrical optics ray fields. The hard surface can be used to reduce the forward scattering from the support struts in reflector antennas (which may be well modeled by a circular cylinder). The two main aspects concerning a braided cylindrical shield are that 1) the strips provides shielding for an interior cable against external disturbances, 2) the strips form a part of a transmission line with a core conductor as the cable. We consider the former aspect in this chapter, while the latter is considered in Chapter 8.

The scattering problem by such a braided cylindrical shield has been widely studied using various techniques. The literature on the problem is extensive, some examples of reported studies are given below. A resonant mode expansion has been

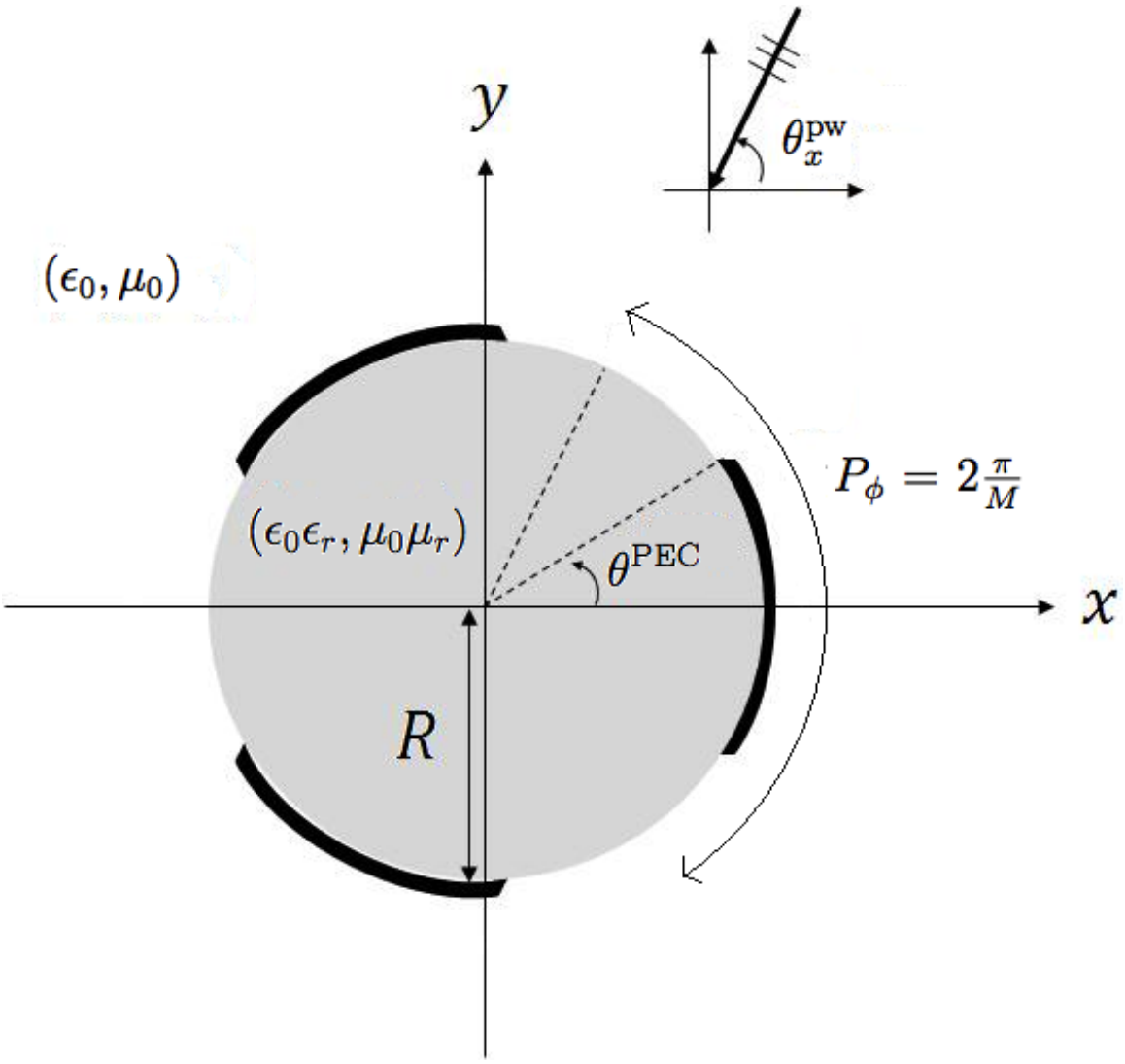

Figure 7.1: Cross-sectional view of a periodic braided cylindrical shield.

developed in [20] for the diffracted field by slit coupled cylindrical cavities with interior loading. The problem was studied in [16] using the characteristic mode theory coupled with the MoM, for a cylinder with a limited number of strips. In [35], the asymptotic strip boundary condition (ASBC), which approximates the boundary conditions directly to simplify the analysis, has been applied to study this multiconductor problem, when the distance between each strip is small enough for the approximation. Shumperts and Butler approached the penetration of both TM_z and TE_z waves through multiple slots in conducting cylinders from the MoM perspective [67, 68]. The technique of using integral equations directly has also been used extensively, many papers of the literature are listed in [92, 93]. In [22], a combined boundary conditions method is used to calculate the field inside and around a circular cavity with longitudinal slots. To the best of our knowledge, none of the reported works deal with the oblique plane wave incidence problem.

Previous study under the MoR, as detailed in [84, 85], has considered the potential problem of a toroidal shell with 2^M azimuthal cuts. The formulation for the problem with two symmetrically placed apertures involves reducing the series equations obtained from the MBC to a set of symmetrical triple series equations. The triple series equations are then transformed to two sets of DSE, each accounting for the odd and even unknown coefficients respectively. The transformation is achieved by exploiting the following symmetry property and identity of the Jacobi polynomials when $\beta = \alpha$:

$$
\begin{aligned}
P_n^{(\alpha,\alpha)}(-z) &= (-1)^n P_n^{(\alpha,\alpha)}(z)\,, \\
P_{2n+j}^{(\alpha,\alpha)}(z) &= \frac{\Gamma(n+1)\Gamma(2n+\alpha+1+j)}{\Gamma(2n+1+j)\Gamma(n+\alpha+1)} z^j P_n^{(\alpha,j-\frac{1}{2})}\left(2z^2-1\right)\,.
\end{aligned}
$$

For the problem with 2^M apertures, the process is repeatedly applied to the series equation and halving the interval at each step, until the interval is reduced that of the unit cell.

In this chapter, the MoR is extended to treat a cylindrical structure. The periodicity of the structure along the ϕ-direction allows us to restrict the analysis to only one unit cell; *i.e.*, the one limited by the cuts $\phi = -\frac{\pi}{M}$ and $\phi = \frac{\pi}{M}$. The proposed formulation makes use of the identity involving the exponential function, instead of the above two formulas, to restrict the analysis to considering only the unit cell. Under the proposed approach, the mathematical formulation is greatly reduced and we can now consider the scattering problem of a structure loaded with an arbitrary number M of strips. In subsequent sections, the formulation for the oblique TM_z problem

is presented and the series representations of the surface current and energy are obtained. As discussed in Chapter 4, the matrix operators for the scattering problem of a TE_z plane wave are the same as those for an oblique TE_z problem. Therefore, we omit the detailed derivation for the TE_z problem. The RCS, surface current and energy coupled into the cavity due to an oblique plane wave excitation are computed. The shielding effects of structure with different parameters are compared. The formulation can be readily adapted to other insightful problems, like that consisting of the same structure with a conducting core inserted or that involving a multi-layered dielectric cylinder.

7.2 Geometrical description of the problem

The structure under study in this chapter is a generalization of the CLR investigated in Chapter 4, with its cross section depicted in Figure 7.1. A finite number M of conformal strips are placed on the surface of the dielectric cylinder, which is characterized by its relative permittivity and permeability (ϵ_r, μ_r). The strips are infinitely-thin, perfectly conducting, equally-spaced and each has angular width $2\theta^{\mathrm{PEC}}$. The multi-conductor cylinder is illuminated by an obliquely incident plane wave, transverse magnetic (TM_z) to the cylinder axis. The plane wave is characterized by the polar angle θ_z^{pw} and the azimuthal angle θ_x^{pw}, as shown in Figure 2.2.

The multi-conductor cylinder has a periodicity of $P_\phi = 2\frac{\pi}{M}$, where its periodic unit cell is the interval $(-\frac{\pi}{M}, \frac{\pi}{M})$. We denote the location of the strips by Ω_{PEC} and its complement by Ω_{aper} (that is, the sections not shielded by the PEC strips). Without loss of generality, suppose the conducting strips are symmetrical with respect to the horizontal plane (*i.e.*, the x-axis). To facilitate the reduction of the analysis to only one unit cell, each of Ω_{PEC} and Ω_{aper} is expressed as a union of $2M$ subintervals as

$$\Omega_{\mathrm{PEC}} = \bigcup_{\alpha=0}^{M-1} \Theta_{\mathrm{PEC}}^{\prime\alpha} \cup \Theta_{\mathrm{PEC}}^{\prime\prime\alpha}\,, \tag{7.1a}$$

$$\Omega_{\mathrm{aper}} = \bigcup_{\alpha=0}^{M-1} \Theta_{\mathrm{aper}}^{\prime\alpha} \cup \Theta_{\mathrm{aper}}^{\prime\prime\alpha}\,, \tag{7.1b}$$

where the subintervals are defined as

$$\Theta'^{\alpha}_{\mathrm{PEC}} := \left(\alpha P_\phi, \alpha P_\phi + \theta^{\mathrm{PEC}}\right) , \tag{7.2a}$$

$$\Theta''^{\alpha}_{\mathrm{PEC}} := \left([\alpha+1] P_\phi - \theta^{\mathrm{PEC}}, [\alpha+1] P_\phi\right) , \tag{7.2b}$$

$$\Theta'^{\alpha}_{\mathrm{aper}} := \left(\alpha P_\phi + \theta^{\mathrm{PEC}}, \left[\alpha+\tfrac{1}{2}\right] P_\phi\right) , \tag{7.2c}$$

$$\Theta''^{\alpha}_{\mathrm{aper}} := \left(\left[\alpha+\tfrac{1}{2}\right] P_\phi, [\alpha+1] P_\phi - \theta^{\mathrm{PEC}}\right) , \tag{7.2d}$$

for $\alpha = 0, 1, \ldots, (M-1)$. We recall that $P_\phi = \frac{2\pi}{M}$ is the periodicity of the structure.

7.3 Problem formulation

The first part of the formulation for this multi-conductor cylinder is exactly the same as that of the single strip CLR problem reported in Chapter 4, with the only difference being Ω_{PEC} and Ω_{aper} now each made up of multiple disjoint intervals. We adopt exactly the same notations and series representations as those for the CLR problem; *i.e.*, the field components of the obliquely incident TM_z plane wave are given in (4.1), while the longitudinal-components of the scattered field in region 0 and the transmitted field in region 1 are given in (4.3) and (4.4), respectively. The transverse components of the secondary fields have expressions written in (4.5) and (4.6).

Consequently, we obtain the same set of series equations as given in (4.23), (4.24), (4.30) and (4.31) upon enforcing the MBC, except that for the current multi-conductor cylinder, the first pair is defined on the multiple disjoint intervals of Ω_{PEC} defined in (7.1a), while the second pair is defined on the multiple disjoint intervals of Ω_{aper} defined in (7.1b). In addition, the electromagnetic energy contained per unit length of the multi-conductor cylinder has the same series expression as given in (4.9) and (4.10). Therefore, the unknown expansion coefficients encountered for the multi-conductor cylinder problem belongs to the same solution class as those for the single CLR problem considered in Chapter 4; *i.e.*, they satisfy the the Fejér's Tauberian condition (D.4). To avoid repetition, we begin our analysis by looking at the series equations obtained from the MBC.

The azimuthal periodicity of the multi-conductor cylinder suggests that the regularization process can be reduced from the consideration of the series equations defined over the entire contour to those defined over the single periodic unit cell $\left(-\frac{\pi}{M}, \frac{\pi}{M}\right)$. The ordinary Floquet formulation often applied to (planar) periodic structure is not directly applicable to this scattering problem, because the oblique plane wave (or

any other incident waves usually considered) does not satisfy the azimuthal Floquet condition, which requires all the field components to satisfy $f(\phi + P_\phi) = e^{j\,C\,P_\phi} f(\phi)$, for some constant C. However, by exploiting the identity involving the exponential function, the set of series equations defined over entire contour can be decoupled into M independent sets, where each set is defined over the single periodic interval $\left(-\frac{\pi}{M}, \frac{\pi}{M}\right)$. Each of these M sets of series equations can subsequently be regularized and transformed into a pair of 2-by-2 block matrix equations of the second kind. In other words, we have decoupled the problem into $2M$ matrix equations to be solved independently. Most of all, for a predetermined accuracy of the solution computed, the truncation number $N_{\rm tr}$ required for each matrix equation is only one-Mth of that for the single CLR problem in Chapter 4. That is, the computational cost of the multi-conductor problem is independent of the number of the periodic PEC strips on the cylinder. In fact, this multi-conductor problem may even be marginally easier, since the matrix equations corresponding to different cells decouple.

7.3.1 Interval reduction due to periodicity

Similarly to Chapter 4, the four series equations are derived from the MBC on $\rho = R$. On the surface of the strips, the total tangential electric field vanishes; *i.e.*,

$$\lim_{\rho\to R^+} \left(E_z^{\rm sc} + E_z^{\rm inc}\right) = \lim_{\rho\to R^-} E_z^{\rm tr} = 0\,, \tag{7.3}$$

$$\lim_{\rho\to R^+} \left(E_\phi^{\rm sc} + E_\phi^{\rm inc}\right) = \lim_{\rho\to R^-} E_\phi^{\rm tr} = 0\,. \tag{7.4}$$

Enforcing these boundary conditions, we obtain the following two series equations:

$$\sum_{n=-\infty}^{\infty} a_n^{(1)} o_n e^{jn\phi} = 0 \quad (A)\,, \qquad \text{on } \Omega_{\rm PEC}, \tag{7.5}$$

$$\sum_{n=-\infty}^{\infty} \left\{a_n^{(1)} p_n + b_n^{(1)} q_n\right\} e^{jn\phi} = 0 \quad (A)\,, \qquad \text{on } \Omega_{\rm PEC}. \tag{7.6}$$

On the other hand, for the interface not shielded by the PEC strips, we have

$$\lim_{\rho\to R^+} \left(H_z^{\rm sc} + H_z^{\rm inc}\right) = \lim_{\rho\to R^-} H_z^{\rm tr}\,, \tag{7.7}$$

$$\lim_{\rho\to R^+} \left(H_\phi^{\rm sc} + H_\phi^{\rm inc}\right) = \lim_{\rho\to R^-} H_\phi^{\rm tr}\,, \tag{7.8}$$

which result in:

$$\sum_{n=-\infty}^{\infty} \left\{a_n^{(1)} r_n + b_n^{(1)} s_n\right\} e^{jn\phi} = 0 \quad (A)\,, \qquad \text{on } \Omega_{\rm aper}, \tag{7.9}$$

$$\sum_{n=-\infty}^{\infty} \left\{a_n^{(1)} t_n + b_n^{(1)} u_n + z_n\right\} e^{jn\phi} = 0 \quad (A)\,, \qquad \text{on } \Omega_{\rm aper}. \tag{7.10}$$

The coefficients appear in the above series equations are as defined in (4.25)–(4.27) and (4.32)–(4.36); that is,

$$o_n := J_n(\kappa_1 R) H_n^{'(2)}(\kappa_1 R)\,, \tag{7.11a}$$

$$p_n := \frac{j\cos\theta_z^{\mathrm{pw}}}{\eta_0 \mu_r \kappa_1 R}\, n\, J_n(\kappa_1 R) H_n^{'(2)}(\kappa_1 R)\,, \tag{7.11b}$$

$$q_n := J_n'(\kappa_1 R) H_n^{'(2)}(\kappa_1 R)\,, \tag{7.11c}$$

$$r_n := \frac{j\cos\theta_z^{\mathrm{pw}}}{\eta_0 \kappa_0 R}\left(1 - \frac{\kappa_0^2}{\kappa_1^2}\right) n\, J_n(\kappa_1 R) H_n^{'(2)}(\kappa_1 R) \frac{H_n^{(2)}(\kappa_0 R)}{H_n^{'(2)}(\kappa_0 R)}\,, \tag{7.11d}$$

$$s_n := J_n(\kappa_1 R) H_n^{'(2)}(\kappa_1 R) - \mu_r \frac{\kappa_0}{\kappa_1} J_n'(\kappa_1 R) H_n^{'(2)}(\kappa_1 R) \frac{H_n^{(2)}(\kappa_0 R)}{H_n^{'(2)}(\kappa_0 R)}\,, \tag{7.11e}$$

$$\begin{aligned} t_n :=& \epsilon_r \kappa_0 J_n'(\kappa_1 R) H_n^{'(2)}(\kappa_1 R) - \kappa_1 J_n(\kappa_1 R) H_n^{'(2)}(\kappa_1 R) \frac{H_n^{'(2)}(\kappa_0 R)}{H_n^{(2)}(\kappa_0 R)} \\ &+ n^2 \frac{\cos^2\theta_z^{\mathrm{pw}} \kappa_1}{\kappa_0^2 R^2}\left(1 - \frac{\kappa_0^2}{\kappa_1^2}\right) J_n(\kappa_1 R) H_n^{'(2)}(\kappa_1 R) \frac{H_n^{(2)}(\kappa_0 R)}{H_n^{'(2)}(\kappa_0 R)}\,, \end{aligned} \tag{7.11f}$$

$$\begin{aligned} u_n :=& n \frac{\eta_0 \kappa_0 \cos\theta_z^{\mathrm{pw}}}{j\kappa_1 R}\left[J_n(\kappa_1 R) H_n^{'(2)}(\kappa_1 R) \right. \\ &\left. - \mu_r \frac{\kappa_1}{\kappa_0} J_n'(\kappa_1 R) H_n^{'(2)}(\kappa_1 R) \frac{H_n^{(2)}(\kappa_0 R)}{H_n^{'(2)}(\kappa_0 R)} \right]\,, \end{aligned} \tag{7.11g}$$

$$z_n := \kappa_1 \left[c_n(\kappa_0 R) \frac{H_n^{'(2)}(\kappa_0 R)}{H_n^{(2)}(\kappa_0 R)} - c_n'(\kappa_0 R) \right]\,. \tag{7.11h}$$

We aim to reduce the set of series equations (7.5), (7.6), (7.9) and (7.10) defined over the whole contour to the sets defined over the single periodic interval $\left(-\frac{\pi}{M}, \frac{\pi}{M}\right)$. This is achieved by exploiting the periodicity in ϕ-direction, and the introduction of new variable to shift each of the subintervals to one lying in the periodic unit cell. We illustrate this manipulation by looking at the series equation (7.5) defined over the subinterval $\Theta_{\mathrm{PEC}}'^{\alpha}$, for some fixed $\alpha \in \{0, 1, \ldots, M-1\}$; *i.e.*,

$$\sum_{n=-\infty}^{\infty} a_n^{(1)} o_n\, e^{jn\phi} = 0\,, \quad \phi \in \left(\alpha P_\phi, \alpha P_\phi + \theta^{\mathrm{PEC}}\right)\,. \tag{7.12}$$

By means of new angular variable, $\phi'_\alpha = \phi - \alpha P_\phi$, (7.12) can be rewritten as

$$\sum_{n=-\infty}^{\infty} a_n^{(1)} o_n\, e^{jn\phi'_\alpha} e^{jn\alpha P_\phi} = 0\,, \quad \phi'_\alpha \in \left(0, \theta^{\mathrm{PEC}}\right)\,. \tag{7.13}$$

The series equation (7.13) holds for all values of α from 0 to $(M-1)$. On top of that, the interval of (7.13) is independent of the values of α. Consequently, we can

drop the subscript for ϕ'_α. In other words, there are M members of (7.13), each of which taking a distinct value of α from $\{0, 1, \ldots, (M-1)\}$. All these M members are defined over the same interval $\left(0, \theta^{\text{PEC}}\right)$ and are interconnected as they all involve the unknown $\left\{a_n^{(1)}\right\}_{n\in\mathbb{Z}}$.

The next step involves reformulating the M members of (7.13) to decouple them into M independent series equations, as follows. We multiply the α-th member of (7.13) by the factor $e^{-jm\alpha P_\phi}$, where m is some arbitrary real value, for each $\alpha = 0, 1, \ldots, (M-1)$. It is worth noting that this factor is non-zero and is independent of the index n. By summing over all the α-th members of (7.13) for $\alpha = 0, 1, \ldots, (M-1)$, we obtain

$$\sum_{n=-\infty}^{\infty} a_n^{(1)} o_n \, e^{jn\phi'_\alpha} \sum_{\alpha=0}^{M-1} e^{j\alpha(n-m)P_\phi} = 0\,, \quad \phi' \in \left(0, \theta^{\text{PEC}}\right). \tag{7.14}$$

Recall that $P_\phi = \frac{2\pi}{M}$, the second summation is a geometric progression with ratio $e^{j(n-m)P_\phi}$, if the value $(n-m)$ is not a multiple of M. Its sum is given by

$$\sum_{\alpha=0}^{M-1} e^{j\alpha(n-m)P_\phi} = \begin{cases} M, \text{ if } (n-m) \equiv 0 \,(\text{mod} M)\,, \\ 0, \text{ otherwise.} \end{cases} \tag{7.15}$$

As a result, the M interconnected members of (7.13) are decoupled into M of series equations in the form

$$M e^{j\alpha\phi'} \sum_{n=-\infty}^{\infty} a_{\alpha+nM}^{(1)} o_{\alpha+nM} \, e^{jnM\phi'} = 0\,, \quad \phi' \in \left(0, \theta^{\text{PEC}}\right), \tag{7.16}$$

for $\alpha = 0, 1, \ldots, (M-1)$. Each of these newly formulated series equations involves only one of the non-overlapping subsequences of the original unknown, $\left\{a_{nM+\alpha}^{(1)}\right\}_{n\in\mathbb{Z}}$ for $\alpha = 0, 1, \ldots, (M-1)$. They are therefore independent of one another. Effectively, a discrete Fourier transform has been performed on (7.12). The factor $Me^{j\alpha\phi'}$ is omitted from the following.

Similar deduction can be applied to the remaining series equations. Consequently, the analysis is reduced to the consideration of M independent sets of series equations defined over the unit cell $\left(-\frac{\pi}{M}, \frac{\pi}{M}\right)$, which α-th member is the following set:

$$\sum_{n=-\infty}^{\infty} a_{\alpha+nM}^{(1)} o_{\alpha+nM} \, e^{jnM\phi'} = 0 \; (A), \tag{7.17a}$$

$$\sum_{n=-\infty}^{\infty} \left\{ a_{\alpha+nM}^{(1)} p_{\alpha+nM} + b_{\alpha+nM}^{(1)} q_{\alpha+nM} \right\} e^{jnM\phi'} = 0 \quad (A)\,, \tag{7.17b}$$

for $\phi' \in (-\theta^{\mathrm{PEC}}, \theta^{\mathrm{PEC}})$, while

$$\sum_{n=-\infty}^{\infty} \left\{ a^{(1)}_{\alpha+nM} r_{\alpha+nM} + b^{(1)}_{\alpha+nM} s_{\alpha+nM} \right\} e^{jnM\phi'} = 0 \quad (A)\,, \tag{7.17c}$$

$$\sum_{n=-\infty}^{\infty} \left\{ a^{(1)}_{\alpha+nM} t_{\alpha+nM} + b^{(1)}_{\alpha+nM} u_{\alpha+nM} + z_{\alpha+nM} \right\} e^{jnM\phi'} = 0 \quad (A)\,, \tag{7.17d}$$

for $\phi' \in \left(-\frac{\pi}{M}, -\theta^{\mathrm{PEC}}\right) \cup \left(\theta^{\mathrm{PEC}}, \frac{\pi}{M}\right)$. These M sets of series equations are independent, as each set involves only the subsequences $\left\{ a^{(1)}_{nM+\alpha}, b^{(1)}_{nM+\alpha} \right\}_{n\in\mathbb{Z}}$, for index $\alpha = 0, 1, \ldots, (M-1)$.

These reformulated M sets of series equations can be alternatively derived by representing the incident field as a sum of M fictitious fields: $\mathbf{E}^{\mathrm{inc}} = \sum_{\alpha=0}^{M-1} \mathbf{e}^{\mathrm{inc}}_{\alpha}$, where the set $\left\{\mathbf{e}^{\mathrm{inc}}_{\alpha}\right\}_{\alpha=0}^{M-1}$ are assumed to be mutually orthogonal on $(-\pi, \pi)$ and each satisfying the condition $\mathbf{e}^{\mathrm{inc}}_{\alpha}(\rho, \phi + P_{\phi}) = \mathbf{e}^{\mathrm{inc}}_{\alpha}(\rho, \phi)\, e^{j\alpha P_{\phi}}$. Therefore, each of these fictitious fields $\mathbf{e}^{\mathrm{inc}}_{\alpha}$ satisfy the Floquet periodicity condition. We write the secondary fields induced by each $\mathbf{e}^{\mathrm{inc}}_{\alpha}$ when the fictitious field is assumed to be present by itself as $\mathbf{e}^{\mathrm{s}}_{\alpha}$ and $\mathbf{h}^{\mathrm{s}}_{\alpha}$. It has been shown in [8] that, $\mathbf{e}^{\mathrm{s}}_{\alpha}$ and $\mathbf{h}^{\mathrm{s}}_{\alpha}$ also satisfy the Floquet periodicity condition. As the secondary fields induced by the incident plane wave $\mathbf{E}^{\mathrm{inc}}$ are simplify the sum of all $\mathbf{e}^{\mathrm{s}}_{\alpha}$ and $\mathbf{h}^{\mathrm{s}}_{\alpha}$, for $\alpha = 0, 1, \ldots, (M-1)$, the scattering problem with incident field $\mathbf{E}^{\mathrm{inc}}$ can be decomposed into M independent problems, each with $\mathbf{e}^{\mathrm{inc}}_{\alpha}$ as its incident source, for some $\alpha = 0, 1, \ldots, (M-1)$.

By writing $\phi = M\phi'$ in (7.17a)–(7.17d), and $\phi_0 = M\theta^{\mathrm{PEC}}$, these series equations can be rewritten as

$$\sum_{n=-\infty}^{\infty} a^{(1)}_{\alpha+nM} o_{\alpha+nM}\, e^{jn\phi} = 0\ (A), \tag{7.18a}$$

$$\sum_{n=-\infty}^{\infty} \left\{ a^{(1)}_{\alpha+nM} p_{\alpha+nM} + b^{(1)}_{\alpha+nM} q_{\alpha+nM} \right\} e^{jn\phi} = 0 \quad (A)\,, \tag{7.18b}$$

for $\phi \in (-\phi_0, \phi_0)$, while

$$\sum_{n=-\infty}^{\infty} \left\{ a^{(1)}_{\alpha+nM} r_n + b^{(1)}_{\alpha+nM} s_{\alpha+nM} \right\} e^{jn\phi} = 0 \quad (A)\,, \tag{7.18c}$$

$$\sum_{n=-\infty}^{\infty} \left\{ a^{(1)}_{\alpha+nM} t_{\alpha+nM} + b^{(1)}_{\alpha+nM} u_{\alpha+nM} + z_{\alpha+nM} \right\} e^{jn\phi} = 0 \quad (A)\,, \tag{7.18d}$$

for $\phi \in (-\pi, -\phi_0) \cup (\phi_0, \pi)$, $\alpha = 0, 1, \ldots, (M-1)$. Therefore, each of these M sets, which are now rewritten in a same form as the set encountered in Chapter 4, can

be converted to a second kind ISLAE, upon upon the introduction of appropriate asymptotically small parameters. A single 4-by-4 block matrix equation is obtained, as opposed to the pair of 2-by-2 block matrix equations derived in Chapter 4. This is due to the fact that for $h_n \equiv \{o_n, p_n, q_n, r_n, s_n, t_n\}$, $h_{\alpha+nM} \neq h_{\alpha-nM}$, for non-trivial values of α.

7.3.2 Introducing the asymptotically small parameters

To convert the series equations to those involving the trigonometric functions and thus halving the interval to $(0, \pi)$, we introduce the following notations for $n = 1, 2, \ldots$

$$x_{\alpha n}^{(1)} := a_{\alpha+nM}^{(1)} + a_{\alpha-nM}^{(1)}\,, \qquad y_{\alpha n}^{(1)} := a_{\alpha+nM}^{(1)} - a_{\alpha-nM}^{(1)}\,, \tag{7.19a}$$

$$x_{\alpha n}^{(2)} := b_{\alpha+nM}^{(1)} + b_{\alpha-nM}^{(1)}\,, \qquad y_{\alpha n}^{(2)} := b_{\alpha+nM}^{(1)} - b_{\alpha-nM}^{(1)}\,, \tag{7.19b}$$

$$o_{\alpha n}^{(+)} := \frac{1}{2}\left(o_{\alpha+nM} + o_{\alpha-nM}\right)\,, \qquad o_{\alpha n}^{(-)} := \frac{1}{2}\left(o_{\alpha+nM} - o_{\alpha-nM}\right)\,, \tag{7.19c}$$

$$p_{\alpha n}^{(+)} := \frac{1}{2}\left(p_{\alpha+nM} + p_{\alpha-nM}\right)\,, \qquad p_{\alpha n}^{(-)} := \frac{1}{2}\left(p_{\alpha+nM} - p_{\alpha-nM}\right)\,, \tag{7.19d}$$

$$q_{\alpha n}^{(+)} := \frac{1}{2}\left(q_{\alpha+nM} + q_{\alpha-nM}\right)\,, \qquad q_{\alpha n}^{(-)} := \frac{1}{2}\left(q_{\alpha+nM} - q_{\alpha-nM}\right)\,, \tag{7.19e}$$

$$r_{\alpha n}^{(+)} := \frac{1}{2}\left(r_{\alpha+nM} + r_{\alpha-nM}\right)\,, \qquad r_{\alpha n}^{(-)} := \frac{1}{2}\left(r_{\alpha+nM} - r_{\alpha-nM}\right)\,, \tag{7.19f}$$

$$s_{\alpha n}^{(+)} := \frac{1}{2}\left(s_{\alpha+nM} + s_{\alpha-nM}\right)\,, \qquad s_{\alpha n}^{(-)} := \frac{1}{2}\left(s_{\alpha+nM} - s_{\alpha-nM}\right)\,, \tag{7.19g}$$

$$t_{\alpha n}^{(+)} := \frac{1}{2}\left(t_{\alpha+nM} + t_{\alpha-nM}\right)\,, \qquad t_{\alpha n}^{(-)} := \frac{1}{2}\left(t_{\alpha+nM} - t_{\alpha-nM}\right)\,, \tag{7.19h}$$

$$u_{\alpha n}^{(+)} := \frac{1}{2}\left(u_{\alpha+nM} + u_{\alpha-nM}\right)\,, \qquad u_{\alpha n}^{(-)} := \frac{1}{2}\left(u_{\alpha+nM} - u_{\alpha-nM}\right)\,, \tag{7.19i}$$

$$z_{\alpha n}^{(+)} := \frac{1}{2n}\left(z_{\alpha+nM} + z_{\alpha-nM}\right)\,, \qquad z_{\alpha n}^{(-)} := \frac{1}{2n}\left(z_{\alpha+nM} - z_{\alpha-nM}\right)\,. \tag{7.19j}$$

Therefore, by exploiting the symmetry of the subintervals $(-\phi_0, \phi_0)$ and $(-\pi, -\phi_0) \cup (\phi_0, \pi)$, we can reformulate (7.18a)–(7.18d) as

$$\begin{cases} x_{\alpha 0}^{(1)} o_\alpha + \displaystyle\sum_{n=1}^{\infty} \left[x_{\alpha n}^{(1)} o_{\alpha n}^{(+)} + y_{\alpha n}^{(1)} o_{\alpha n}^{(-)}\right] \cos n\phi = 0\,(A),\ \phi \in (0, \phi_0), & \text{(7.20a)} \\ x_{\alpha 0}^{(1)} t_\alpha + x_{\alpha 0}^{(2)} u_\alpha + z_\alpha + \displaystyle\sum_{n=1}^{\infty} \left[x_{\alpha n}^{(1)} t_{\alpha n}^{(+)} + y_{\alpha n}^{(1)} t_{\alpha n}^{(-)}\right. & \\ \qquad \left. + x_{\alpha n}^{(2)} u_{\alpha n}^{(+)} + y_{\alpha n}^{(2)} u_{\alpha n}^{(-)} + n z_{\alpha n}^{(+)}\right] \cos n\phi = 0\,(A),\ \phi \in (\phi_0, \pi), & \text{(7.20b)} \end{cases}$$

$$\begin{cases} \displaystyle\sum_{n=1}^{\infty} \left[x_{\alpha n}^{(1)} p_{\alpha n}^{(-)} + y_{\alpha n}^{(1)} p_{\alpha n}^{(+)} + x_{\alpha n}^{(2)} q_{\alpha n}^{(-)} + y_{\alpha n}^{(2)} q_{\alpha n}^{(+)}\right] \sin n\phi = 0\,(A),\ \phi \in (0, \phi_0), & \text{(7.21a)} \\ \displaystyle\sum_{n=1}^{\infty} \left[x_{\alpha n}^{(1)} r_{\alpha n}^{(-)} + y_{\alpha n}^{(1)} r_{\alpha n}^{(+)} + x_{\alpha n}^{(2)} s_{\alpha n}^{(-)} + y_{\alpha n}^{(2)} s_{\alpha n}^{(+)}\right] \sin n\phi = 0\,(A),\ \phi \in (\phi_0, \pi), & \text{(7.21b)} \end{cases}$$

$$\begin{cases} x_{\alpha 0}^{(1)} p_\alpha + x_{\alpha 0}^{(2)} q_\alpha + \sum\limits_{n=1}^{\infty} \big[x_{\alpha n}^{(1)} p_{\alpha n}^{(+)} + y_{\alpha n}^{(1)} p_{\alpha n}^{(-)} \\ \qquad\qquad + x_{\alpha n}^{(2)} q_{\alpha n}^{(+)} + y_{\alpha n}^{(2)} q_{\alpha n}^{(-)} \big] \cos n\phi = 0 \ (A), \qquad \phi \in (0, \phi_0), \qquad (7.22a) \\ x_{\alpha 0}^{(1)} r_\alpha + x_{\alpha 0}^{(2)} s_\alpha + \sum\limits_{n=1}^{\infty} \big[x_{\alpha n}^{(1)} r_{\alpha n}^{(+)} + y_{\alpha n}^{(1)} r_{\alpha n}^{(-)} \\ \qquad\qquad + x_{\alpha n}^{(2)} s_{\alpha n}^{(+)} + y_{\alpha n}^{(2)} s_{\alpha n}^{(-)} \big] \cos n\phi = 0 \ (A), \qquad \phi \in (\phi_0, \pi), \qquad (7.22b) \end{cases}$$

$$\begin{cases} \sum\limits_{n=1}^{\infty} \big[x_{\alpha n}^{(1)} o_{\alpha n}^{(-)} + y_{\alpha n}^{(1)} o_{\alpha n}^{(+)} \big] \sin n\phi = 0 \ (A), \qquad \phi \in (0, \phi_0), \qquad (7.23a) \\ \sum\limits_{n=1}^{\infty} \big[x_{\alpha n}^{(1)} t_{\alpha n}^{(-)} + y_{\alpha n}^{(1)} t_{\alpha n}^{(+)} + x_{\alpha n}^{(2)} u_{\alpha n}^{(-)} + y_{\alpha n}^{(2)} u_{\alpha n}^{(+)} \\ \qquad\qquad + n z_{\alpha n}^{(-)} \big] \sin n\phi = 0 \ (A), \qquad \phi \in (\phi_0, \pi). \qquad (7.23b) \end{cases}$$

Due to the reflective property of the Bessel and Hankel functions, we can see that for $n = 1, 2, \ldots$, if we have $h_n \equiv \{o_n, q_n, s_n, t_n\}$, then $h_{\alpha - nM} = h_{nM - \alpha}$. On the other hand, when $h_n \equiv \{p_n, r_n, u_n\}$, we can see that $h_{\alpha - nM} = -h_{nM-\alpha}$. From the asymptotic behaviors (when $n \to +\infty$) of $\{o_n, p_n, q_n, r_n, s_n, t_n, u_n\}_{n=1}^{\infty}$ given in (4.43a)–(4.43g), we can deduce the magnitudes of the newly introduced parameters $\left\{ o_{\alpha n}^{(\pm)}, p_{\alpha n}^{(\pm)}, q_{\alpha n}^{(\pm)}, r_{\alpha n}^{(\pm)}, s_{\alpha n}^{(\pm)}, t_{\alpha n}^{(\pm)} \right\}_{n=1}^{\infty}$, for large order n:

$$o_{\alpha n}^{(+)} = -\frac{j}{\pi \kappa_1 R} \left\{ 1 + O\left(\frac{\kappa_1^2 R^2}{M^2 n^2} \right) \right\}, \qquad (7.24a)$$

$$o_{\alpha n}^{(-)} = \begin{cases} 0, \text{ for } \alpha = 0, \\ O\left(\dfrac{\kappa_1^2 R^2}{M^2 n^2} \right), \text{ otherwise,} \end{cases} \qquad (7.24b)$$

$$p_{\alpha n}^{(+)} = \begin{cases} 0, \text{ for } \alpha = 0, \\ \dfrac{\alpha \cos \theta_z^{\text{pw}}}{\pi \eta_0 \mu_1 \kappa_1^2 R^2} \left\{ 1 + O\left(\dfrac{\kappa_1^2 R^2}{M^2 n^2} \right) \right\}, \text{ otherwise,} \end{cases} \qquad (7.24c)$$

$$p_{\alpha n}^{(-)} = \frac{Mn \cos \theta_z^{\text{pw}}}{\pi \eta_0 \mu_1 \kappa_1^2 R^2} \left\{ 1 + O\left(\frac{\kappa_1^2 R^2}{M^2 n^2} \right) \right\}, \qquad (7.24d)$$

$$q_{\alpha n}^{(+)} = -\frac{jMn}{\pi \kappa_1^2 R^2} \left\{ 1 + O\left(\frac{\kappa_1^2 R^2}{M^2 n^2} \right) \right\}, \qquad (7.24e)$$

$$q_{\alpha n}^{(-)} = \begin{cases} 0, \text{ for } \alpha = 0, \\ -\dfrac{j\alpha}{\pi \kappa_1^2 R^2} \left\{ 1 + O\left(\dfrac{\kappa_1^2 R^2}{M^2 n^2} \right) \right\}, \text{ otherwise,} \end{cases} \qquad (7.24f)$$

$$r_{\alpha n}^{(+)} = \begin{cases} 0, \text{ for } \alpha = 0, \\ O\left(\dfrac{\kappa_1^2 R^2}{M^2 n^2}\right), \text{ otherwise,} \end{cases} \tag{7.24g}$$

$$r_{\alpha n}^{(-)} = -\frac{\cos\theta_z^{\mathrm{pw}}}{\pi\eta_0\kappa_1 R}\left(1 - \frac{\kappa_0^2}{\kappa_1^2}\right)\left\{1 + O\left(\frac{\kappa_1^2 R^2}{M^2 n^2}\right)\right\}, \tag{7.24h}$$

$$s_{\alpha n}^{(+)} = -\frac{j}{\pi\kappa_1 R}\left(1 + \mu_1\frac{\kappa_0^2}{\kappa_1^2}\right)\left\{1 + O\left(\frac{\kappa_1^2 R^2}{M^2 n^2}\right)\right\}, \tag{7.24i}$$

$$s_{\alpha n}^{(-)} = \begin{cases} 0, \text{ for } \alpha = 0, \\ O\left(\dfrac{\kappa_1^2 R^2}{M^2 n^2}\right), \text{ otherwise,} \end{cases} \tag{7.24j}$$

$$t_{\alpha n}^{(+)} = -\frac{j\zeta Mn}{\pi\kappa_0 R^2}\left\{1 + O\left(\frac{\kappa_1^2 R^2}{M^2 n^2}\right)\right\}, \tag{7.24k}$$

$$t_{\alpha n}^{(-)} = \begin{cases} 0, \text{ for } \alpha = 0, \\ -\dfrac{j\zeta\alpha}{\pi\kappa_0 R^2} O\left(\dfrac{\kappa_1^2 R^2}{M^2 n^2}\right), \text{ otherwise,} \end{cases} \tag{7.24l}$$

$$u_{\alpha n}^{(+)} = \begin{cases} 0, \text{ for } \alpha = 0, \\ -\dfrac{\alpha\cos\theta_z^{\mathrm{pw}}\eta_0\kappa_0\left(1+\mu_1\right)}{\pi\kappa_1^2 R^2}\left\{1 + O\left(\dfrac{\kappa_1^2 R^2}{M^2 n^2}\right)\right\}, \text{ otherwise,} \end{cases} \tag{7.24m}$$

$$u_{\alpha n}^{(-)} = -\frac{nM\cos\theta_z^{\mathrm{pw}}\eta_0\kappa_0\left(1+\mu_1\right)}{\pi\kappa_1^2 R^2}\left\{1 + O\left(\frac{\kappa_1^2 R^2}{M^2 n^2}\right)\right\}, \tag{7.24n}$$

where $\zeta := 1 + \epsilon_1\frac{\kappa_0^2}{\kappa_1^2} - \cos^2\theta_z^{\mathrm{pw}}\left(1 - \frac{\kappa_0^2}{\kappa_1^2}\right)$, as defined in (4.44). Correspondingly, the following asymptotically small parameters are introduced, where we use an accent ($\tilde{}$) to distinguish these asymptotically small parameters from their corresponding coefficients:

$$\tilde{o}_{\alpha n}^{(+)} = 1 - j\pi\kappa_1 R\, o_{\alpha n}^{(+)}, \tag{7.25a}$$

$$\tilde{o}_{\alpha n}^{(-)} = \begin{cases} 0, \text{ for } \alpha = 0, \\ j\pi\kappa_1 R\, o_{\alpha n}^{(-)}, \text{ otherwise,} \end{cases} \tag{7.25b}$$

$$\tilde{p}_{\alpha n}^{(+)} = \begin{cases} 1, \text{ for } \alpha = 0, \\ 1 - \dfrac{\pi\mu_1\eta_0\kappa_1^2 R^2}{\alpha\cos\theta_z^{\mathrm{pw}}} p_{\alpha n}^{(+)}, \text{ otherwise,} \end{cases} \tag{7.25c}$$

$$\tilde{p}_{\alpha n}^{(-)} = 1 - \frac{\pi\mu_1\eta_0\kappa_1^2 R^2}{Mn\cos\theta_z^{\mathrm{pw}}} p_{\alpha n}^{(-)}, \tag{7.25d}$$

$$\tilde{q}_{\alpha n}^{(+)} = 1 - \frac{j\pi\kappa_1^2 R^2}{Mn} q_{\alpha n}^{(+)}, \tag{7.25e}$$

$$\tilde{q}_{\alpha n}^{(-)} = \begin{cases} 1, \text{ for } \alpha = 0, \\ 1 - \dfrac{j\pi\kappa_1^2 R^2}{\alpha} q_{\alpha n}^{(-)}, \text{ otherwise,} \end{cases} \tag{7.25f}$$

$$\tilde{r}_{\alpha n}^{(+)} = \begin{cases} 0, \text{ for } \alpha = 0, \\ \dfrac{j\pi\kappa_1 R}{1+\mu_1\frac{\kappa_0^2}{\kappa_1^2}} r_{\alpha n}^{(+)}, \text{ otherwise}, \end{cases} \tag{7.25g}$$

$$\tilde{r}_{\alpha n}^{(-)} = 1 + \frac{\pi\eta_0\kappa_1 R}{\cos\theta_z^{\mathrm{pw}}\left(1-\frac{\kappa_0^2}{\kappa_1^2}\right)} r_{\alpha n}^{(-)}, \tag{7.25h}$$

$$\tilde{s}_{\alpha n}^{(+)} = 1 - \frac{j\pi\kappa_1 R}{1+\mu_1\frac{\kappa_0^2}{\kappa_1^2}} s_{\alpha n}^{(+)}, \tag{7.25i}$$

$$\tilde{s}_{\alpha n}^{(-)} = \begin{cases} 0, \text{ for } \alpha = 0, \\ \dfrac{j\pi\kappa_1 R}{1+\mu_1\frac{\kappa_0^2}{\kappa_1^2}} s_{\alpha n}^{(-)}, \text{ otherwise}, \end{cases} \tag{7.25j}$$

$$\tilde{t}_{\alpha n}^{(+)} = 1 - \frac{j\pi\kappa_0 R^2}{\zeta M n} t_{\alpha n}^{(+)}, \tag{7.25k}$$

$$\tilde{t}_{\alpha n}^{(-)} = \begin{cases} 1, \text{ for } \alpha = 0, \\ 1 - \dfrac{j\pi\kappa_0 R^2}{\zeta\alpha} t_{\alpha n}^{(-)}, \text{ otherwise}, \end{cases} \tag{7.25l}$$

$$\tilde{u}_{\alpha n}^{(+)} = \begin{cases} 1, \text{ for } \alpha = 0, \\ 1 + \dfrac{\pi\kappa_1^2 R^2}{\eta_0\kappa_0\alpha\left(1+\mu_1\right)\cos\theta_z^{\mathrm{pw}}} u_{\alpha n}^{(+)}, \text{ otherwise}, \end{cases} \tag{7.25m}$$

$$\tilde{u}_{\alpha n}^{(-)} = 1 + \frac{\pi\kappa_1^2 R^2}{\eta_0\kappa_0\left(1+\mu_1\right) M n\cos\theta_z^{\mathrm{pw}}} u_{\alpha n}^{(-)}. \tag{7.25n}$$

Each of these newly introduced parameters has an order of $O\left(\frac{\kappa_1^2 R^2}{M^2 n^2}\right)$, as $n \to +\infty$. By substitution of them into the four sets of DSE given in (7.20)–(7.23), the sets have a similar form to those given in Chapter 4.

$$\begin{cases} x_{\alpha 0}^{(1)}\tilde{o}_\alpha + \sum_{n=1}^{\infty}\left[x_{\alpha n}^{(1)}\left(1-\tilde{o}_{\alpha n}^{(+)}\right) + y_{\alpha n}^{(1)}\tilde{o}_{\alpha n}^{(-)}\right]\cos n\phi = 0\,, & \phi\in(0,\phi_0), \quad (7.26a) \\ x_{\alpha 0}^{(1)}\tilde{t}_\alpha + x_{\alpha 0}^{(2)}\tilde{u}_\alpha + \tilde{z}_\alpha + \sum_{n=1}^{\infty} n\left[x_{\alpha n}^{(1)}\left(1-\tilde{t}_{\alpha n}^{(+)}\right)\right. & \\ \quad + y_{\alpha n}^{(1)}\left(1-\tilde{t}_{\alpha n}^{(-)}\right)\frac{\alpha}{Mn} + x_{\alpha n}^{(2)}\left(1-\tilde{u}_{\alpha n}^{(+)}\right)\frac{\alpha}{Mn}\varsigma & \\ \quad \left. + y_{\alpha n}^{(2)}\left(1-\tilde{u}_{\alpha n}^{(-)}\right)\varsigma + \tilde{z}_{\alpha n}^{(+)}\right]\cos n\phi = 0\,, & \phi\in(\phi_0,\pi), \quad (7.26b) \end{cases}$$

$$\begin{cases} \sum_{n=1}^{\infty} n \Big[x_{\alpha n}^{(1)} \left(1-\tilde{p}_{\alpha n}^{(-)}\right) \tau + y_{\alpha n}^{(1)} \left(1-\tilde{p}_{\alpha n}^{(+)}\right) \dfrac{\alpha}{Mn} \tau \\ \qquad + x_{\alpha n}^{(2)} \left(1-\tilde{q}_{\alpha n}^{(-)}\right) \dfrac{\alpha}{Mn} + y_{\alpha n}^{(2)} \left(1-\tilde{q}_{\alpha n}^{(+)}\right) \Big] \sin n\phi = 0 \,, & \phi \in (0, \phi_0), \quad (7.27a) \\ \sum_{n=1}^{\infty} \left[x_{\alpha n}^{(1)} \left(1-\tilde{r}_{\alpha n}^{(-)}\right) \upsilon + y_{\alpha n}^{(1)} \tilde{r}_{\alpha n}^{(+)} + x_{\alpha n}^{(2)} \tilde{s}_{\alpha n}^{(-)} + y_{\alpha n}^{(2)} \left(1-\tilde{s}_{\alpha n}^{(+)}\right) \right] \\ \qquad \times \sin n\phi = 0 \,, & \phi \in (\phi_0, \pi), \quad (7.27b) \end{cases}$$

$$\begin{cases} x_{\alpha 0}^{(1)} \tilde{p}_{\alpha} + x_{\alpha 0}^{(2)} \tilde{q}_{\alpha} + \sum_{n=1}^{\infty} n \Big[x_{\alpha n}^{(1)} \left(1-\tilde{p}_{\alpha n}^{(+)}\right) \dfrac{\alpha}{Mn} \tau \\ \qquad + y_{\alpha n}^{(1)} \left(1-\tilde{p}_{\alpha n}^{(-)}\right) \tau + x_{\alpha n}^{(2)} \left(1-\tilde{q}_{\alpha n}^{(+)}\right) \\ \qquad + y_{\alpha n}^{(2)} \left(1-\tilde{q}_{\alpha n}^{(-)}\right) \dfrac{\alpha}{Mn} \Big] \cos n\phi = 0 \,, & \phi \in (0, \phi_0), \quad (7.28a) \\ x_{\alpha 0}^{(1)} \tilde{r}_{\alpha} + x_{\alpha 0}^{(2)} \tilde{s}_{\alpha} + \sum_{n=1}^{\infty} \left[x_{\alpha n}^{(1)} \tilde{r}_{\alpha n}^{(+)} + y_{\alpha n}^{(1)} \left(1-\tilde{r}_{\alpha n}^{(-)}\right) \upsilon \right. \\ \qquad \left. + x_{\alpha n}^{(2)} \left(1-\tilde{s}_{\alpha n}^{(+)}\right) + y_{\alpha n}^{(2)} \tilde{s}_{\alpha n}^{(-)} \right] \cos n\phi = 0 \,, & \phi \in (\phi_0, \pi), \quad (7.28b) \end{cases}$$

$$\begin{cases} \sum_{n=1}^{\infty} \left[x_{\alpha n}^{(1)} \tilde{o}_{\alpha n}^{(-)} + y_{\alpha n}^{(1)} \left(1-\tilde{o}_{\alpha n}^{(+)}\right) \right] \sin n\phi = 0 \,, & \phi \in (0, \phi_0), \quad (7.29a) \\ \sum_{n=1}^{\infty} n \Big[x_{\alpha n}^{(1)} \left(1-\tilde{t}_{\alpha n}^{(-)}\right) \dfrac{\alpha}{Mn} + y_{\alpha n}^{(1)} \left(1-\tilde{t}_{\alpha n}^{(+)}\right) + x_{\alpha n}^{(2)} \left(1-\tilde{u}_{\alpha n}^{(-)}\right) \varsigma \\ \qquad + y_{\alpha n}^{(2)} \left(1-\tilde{u}_{\alpha n}^{(+)}\right) \dfrac{\alpha}{Mn} \varsigma + \tilde{z}_{\alpha n}^{(-)} \Big] \sin n\phi = 0 \,, & \phi \in (\phi_0, \pi). \quad (7.29b) \end{cases}$$

In the above series equations, ς, τ and υ are as defined in (4.50a); *i.e.*,

$$\varsigma := \frac{\eta_0 \cos\theta_z^{\mathrm{pw}} (1+\mu_r) \kappa_0^2}{j\zeta\kappa_1^2} \,, \qquad \tau := \frac{j \cos\theta_z^{\mathrm{pw}}}{\eta_0 \mu_r} \,, \qquad \upsilon := \frac{(\kappa_1^2 - \kappa_0^2) \cos\theta_z^{\mathrm{pw}}}{j\eta_0 \left(\kappa_1^2 + \mu_r \kappa_0^2\right)} \,, \tag{7.30a}$$

while $\tilde{o}_{\alpha}, \tilde{p}_{\alpha}, \tilde{q}_{\alpha}, \tilde{r}_{\alpha}, \tilde{s}_{\alpha}, \tilde{t}_{\alpha}, \tilde{u}_{\alpha}, \tilde{z}_{\alpha}$ and $\left\{ z_{\alpha n}^{(\pm)} \right\}_{n=1}^{\infty}$ are defined as:

$$\tilde{o}_{\alpha} := j\pi\kappa_1 R \, o_{\alpha} \,, \qquad \tilde{p}_{\alpha} := \frac{j\pi\kappa_1^2 R^2}{M} \, p_{\alpha} \,, \qquad \tilde{q}_{\alpha} := \frac{j\pi\kappa_1^2 R^2}{M} \, q_{\alpha} \,, \tag{7.30b}$$

$$\tilde{r}_{\alpha} := \frac{j\pi\kappa_1^3 R}{\kappa_1^2 + \mu_r \kappa_0^2} \, r_{\alpha} \,, \qquad \tilde{s}_{\alpha} := \frac{j\pi\kappa_1^3 R}{\kappa_1^2 + \mu_r \kappa_0^2} \, s_{\alpha} \,, \qquad \tilde{t}_{\alpha} := \frac{j\pi\kappa_0 R^2}{\zeta M} \, t_{\alpha} \,, \tag{7.30c}$$

$$\tilde{u}_{\alpha} := \frac{j\pi\kappa_0 R^2}{\zeta M} \, u_{\alpha} \,, \qquad \tilde{z}_{\alpha} := \frac{j\pi\kappa_0 R^2}{\zeta M} \, z_{\alpha} \,, \qquad \tilde{z}_n^{(\pm)} := \frac{j\pi\kappa_0 R^2}{\zeta M} \, z_n^{(\pm)} \,. \tag{7.30d}$$

We can see that, each α-th set of these series equations in (7.26)–(7.29) involves only the subsequences $\left\{ x_{\alpha n}^{(i)}, y_{\alpha n}^{(i)} \right\}_{n=1}^{\infty}$, for $i = 1, 2$. Therefore, each of these M sets are independent for different values of α, and are solved separately by the MoR detailed in Chapter 3.

7.3.3 Regularization process and the ISLAE

For each fixed value of $\alpha = 0, 1, \ldots, (M-1)$, we have the above four sets of DSE to solve simultaneously for the unknowns $\left\{x_{\alpha n}^{(i)}, y_{\alpha n}^{(i)}\right\}_{n=1}^{\infty}$. Each of these four sets of DSE are converted to a second kind ISLAE by the MoR. As all four of these DSE involve the same unknowns $\left\{x_{\alpha n}^{(i)}, y_{\alpha n}^{(i)}\right\}_{n=1}^{\infty}$, the four ISLAE obtained separately are interconnected, and can be written as one 4-by-4 block matrix equation of the second kind.

We begin by considering the first pair of DSE given in (7.26). By making the following replacement in (3.27): $x_0 \mapsto x_{\alpha 0}^{(1)}$, $x_n \mapsto x_{\alpha n}^{(1)}$, $a \mapsto \tilde{o}_\alpha$, $b \mapsto \tilde{t}_\alpha$, $c \mapsto 0$, $d \mapsto \tilde{u}_\alpha x_{\alpha 0}^{(2)} + \tilde{z}_\alpha$, $s_n \mapsto \tilde{o}_{\alpha n}^{(+)}$, $t_n \mapsto \tilde{t}_{\alpha n}^{(+)}$, $e_n \mapsto \tilde{o}_{\alpha n}^{(-)} y_{\alpha n}^{(1)}$, $f_n \mapsto \frac{\alpha}{nM} y_{\alpha n}^{(1)} \left(1 - \tilde{t}_{\alpha n}^{(-)}\right) + y_{\alpha n}^{(2)} \left(1 - \tilde{u}_{\alpha n}^{(-)}\right) \varsigma + \frac{\alpha}{nM} x_{\alpha n}^{(2)} \left(1 - \tilde{u}_{\alpha n}^{(+)}\right) \varsigma + \tilde{z}_{\alpha n}^{(+)}$, and $\psi_0 \mapsto \cos\phi_0 = \cos M\theta^{\mathrm{PEC}}$, the equation for the unknown $x_{\alpha 0}^{(1)}$ is obtained as:

$$
\begin{aligned}
x_{\alpha 0}^{(1)} = & - \frac{\left(\tilde{u}_\alpha x_{\alpha 0}^{(2)} + \tilde{z}_\alpha\right) \ln\left(\frac{1-\psi_0}{2}\right)}{\tilde{t}_\alpha \ln\left(\frac{1-\psi_0}{2}\right) - \tilde{o}_\alpha} + \frac{1+\psi_0}{\sqrt{2}\left[\tilde{t}_\alpha \ln\left(\frac{1-\psi_0}{2}\right) - \tilde{o}_\alpha\right]} \\
& \times \sum_{n=1}^{\infty} \left\{ x_{\alpha n}^{(1)} \left(\tilde{t}_{\alpha n}^{(+)} - \tilde{o}_{\alpha n}^{(+)}\right) + y_{\alpha n}^{(1)} \left[\tilde{o}_{\alpha n}^{(-)} - \frac{\alpha}{Mn}\left(1 - \tilde{t}_{\alpha n}^{(-)}\right]\right) \right. \\
& \left. - y_{\alpha n}^{(2)} \left(1 - \tilde{u}_{\alpha n}^{(-)}\right) \varsigma - x_{\alpha n}^{(2)} \frac{\alpha}{Mn} \left(1 - \tilde{u}_{\alpha n}^{(+)}\right) \varsigma - z_{\alpha n}^{(+)} \right\} \frac{\hat{P}_{n-1}^{(0,1)}(\psi_0)}{\sqrt{n}} \, .
\end{aligned}
\tag{7.31}
$$

Similarly, from the other DSE involving cosine functions (7.28), we make the following replacement in (3.39): $x_0 \mapsto x_{\alpha 0}^{(2)}$, $x_n \mapsto x_{\alpha n}^{(2)}$, $a \mapsto \tilde{s}_\alpha$, $b \mapsto \tilde{q}_\alpha$, $c \mapsto \tilde{r}_\alpha x_{\alpha 0}^{(1)}$, $d \mapsto \tilde{p}_\alpha x_{\alpha 0}^{(1)}$, $s_n \mapsto \tilde{s}_{\alpha n}^{(+)}$, $t_n \mapsto \tilde{q}_{\alpha n}^{(+)}$, $e_n \mapsto \left(1 - \tilde{r}_{\alpha n}^{(-)}\right) y_{\alpha n}^{(1)} \upsilon + \tilde{r}_{\alpha n}^{(+)} x_{\alpha n}^{(1)} + \tilde{s}_{\alpha n}^{(-)} y_{\alpha n}^{(2)}$, $f_n \mapsto \left(1 - \tilde{p}_{\alpha n}^{(-)}\right) y_{\alpha n}^{(1)} \tau + \frac{\alpha}{Mn} \left(1 - \tilde{p}_{\alpha n}^{(+)}\right) x_{\alpha n}^{(1)} \tau + \frac{\alpha}{Mn} \left(1 - \tilde{q}_{\alpha n}^{(-)}\right) y_{\alpha n}^{(2)}$, and $\psi_0 \mapsto \cos\phi_0 = \cos M\theta^{\mathrm{PEC}}$, the equation for the unknown $x_{\alpha 0}^{(2)}$ is obtained as:

$$
\begin{aligned}
x_{\alpha 0}^{(2)} = & \frac{\tilde{r}_\alpha - \tilde{p}_\alpha \ln\left(\frac{1+\psi_0}{2}\right)}{\tilde{q}_\alpha \ln\left(\frac{1+\psi_0}{2}\right) - \tilde{s}_\alpha} x_{\alpha 0}^{(1)} - \frac{1-\psi_0}{\sqrt{2}\left[\tilde{q}_\alpha \ln\left(\frac{1+\psi_0}{2}\right) - \tilde{s}_\alpha\right]} \\
& \times \sum_{n=1}^{\infty} \left\{ x_{\alpha n}^{(2)} \left(\tilde{q}_{\alpha n}^{(+)} - \tilde{s}_{\alpha n}^{(+)}\right) + y_{\alpha n}^{(1)} \left[\left(1 - \tilde{r}_{\alpha n}^{(-)}\right) \upsilon - \left(1 - \tilde{p}_{\alpha n}^{(-)}\right) \tau\right] \right. \\
& \left. + x_{\alpha n}^{(1)} \left[\tilde{r}_{\alpha n}^{(+)} - \frac{\alpha}{Mn}\left(1 - \tilde{p}_{\alpha n}^{(+)}\right) \tau\right] + y_{\alpha n}^{(2)} \left[\tilde{s}_{\alpha n}^{(-)} - \frac{\alpha}{Mn}\left(1 - \tilde{q}_{\alpha n}^{(-)}\right)\right] \right\} \frac{\hat{P}_{n-1}^{(1,0)}(\psi_0)}{\sqrt{n}} \, .
\end{aligned}
\tag{7.32}
$$

The two expressions above; *i.e.*, (7.31) and (7.32), are related as they both involve the two of $x_{\alpha 0}^{(1,2)}$. By substitution of (7.31) into (7.32), we can obtain an expression for $x_{\alpha 0}^{(2)}$ that is independent from $x_{\alpha 0}^{(1)}$. With this expression, an expression for $x_{\alpha 0}^{(1)}$

in terms of only $\left\{x_{\alpha n}^{(i)}, y_{\alpha n}^{(i)}\right\}_{n=1}^{\infty}$ (for $i = 1, 2$) can be derived subsequently by back substitution. These two expressions are:

$$\begin{aligned}
x_{\alpha 0}^{(1)} =& -\frac{1}{\varrho}\tilde{z}_{\alpha}\ln\left(\frac{1-\phi_0}{2}\right)\left[\tilde{q}_{\alpha}\ln\left(\frac{1+\phi_0}{2}\right)-\tilde{s}_{\alpha}\right]\frac{\hat{P}_{m-1}^{(0,1)}(\psi_0)}{m} \\
&+\sum_{n=1}^{\infty}\Bigg(x_{\alpha n}^{(1)}\left\{\left(\tilde{t}_{\alpha n}^{(+)}-\tilde{o}_{\alpha n}^{(+)}\right)v_{\alpha n}^{(1)}+\left[\tilde{r}_{\alpha n}^{(+)}-\frac{\alpha}{Mn}\left(1-\tilde{p}_{\alpha n}^{(+)}\right)\right]w_{\alpha n}^{(1)}\right\} \\
&\quad +y_{\alpha n}^{(1)}\left\{\left[\tilde{o}_{\alpha n}^{(-)}-\frac{\alpha}{Mn}\left(1-\tilde{t}_{\alpha n}^{(-)}\right)\right]v_{\alpha n}^{(1)}+\left[\left(1-\tilde{r}_{\alpha n}^{(-)}\right)\upsilon-\left(1-\tilde{p}_{\alpha n}^{(-)}\right)\tau\right]w_{\alpha n}^{(1)}\right\} \\
&\quad +x_{\alpha n}^{(2)}\left\{-\frac{\alpha}{Mn}\left(1-\tilde{u}_{\alpha n}^{(+)}\right)\varsigma v_{\alpha n}^{(1)}+\left(\tilde{q}_{\alpha n}^{(+)}-\tilde{s}_{\alpha n}^{(+)}\right)w_{\alpha n}^{(1)}\right\} \\
&\quad +y_{\alpha n}^{(2)}\left\{-\left(1-\tilde{u}_{\alpha n}^{(-)}\right)\varsigma v_{\alpha n}^{(1)}+\left[\tilde{s}_{\alpha n}^{(-)}-\frac{\alpha}{Mn}\left(1-\tilde{q}_{\alpha n}^{(-)}\right)\right]w_{\alpha n}^{(1)}\right\} \\
&\quad -\tilde{z}_{\alpha n}^{(+)}v_{\alpha n}^{(1)}\Bigg)\ ,
\end{aligned} \tag{7.33a}$$

$$\begin{aligned}
x_{\alpha 0}^{(2)} =& \frac{1}{\varrho}\tilde{z}_{\alpha}\ln\left(\frac{1-\phi_0}{2}\right)\left[\tilde{p}_{\alpha}\ln\left(\frac{1+\phi_0}{2}\right)-\tilde{r}_{\alpha}\right]\frac{\hat{P}_{m-1}^{(0,1)}(\psi_0)}{m} \\
&+\sum_{n=1}^{\infty}\Bigg(x_{\alpha n}^{(1)}\left\{\left(\tilde{t}_{\alpha n}^{(+)}-\tilde{o}_{\alpha n}^{(+)}\right)v_{\alpha n}^{(2)}+\left[\tilde{r}_{\alpha n}^{(+)}-\frac{\alpha}{Mn}\left(1-\tilde{p}_{\alpha n}^{(+)}\right)\right]w_{\alpha n}^{(2)}\right\} \\
&\quad +y_{\alpha n}^{(1)}\left\{\left[\tilde{o}_{\alpha n}^{(-)}-\frac{\alpha}{Mn}\left(1-\tilde{t}_{\alpha n}^{(-)}\right)\right]v_{\alpha n}^{(2)}+\left[\left(1-\tilde{r}_{\alpha n}^{(-)}\right)\upsilon-\left(1-\tilde{p}_{\alpha n}^{(-)}\right)\tau\right]w_{\alpha n}^{(2)}\right\} \\
&\quad +x_{\alpha n}^{(2)}\left\{-\frac{\alpha}{Mn}\left(1-\tilde{u}_{\alpha n}^{(+)}\right)\varsigma v_{\alpha n}^{(2)}+\left(\tilde{q}_{\alpha n}^{(+)}-\tilde{s}_{\alpha n}^{(+)}\right)w_{\alpha n}^{(2)}\right\} \\
&\quad +y_{\alpha n}^{(2)}\left\{-\left(1-\tilde{u}_{\alpha n}^{(-)}\right)\varsigma v_{\alpha n}^{(2)}+\left[\tilde{s}_{\alpha n}^{(-)}-\frac{\alpha}{Mn}\left(1-\tilde{q}_{\alpha n}^{(-)}\right)\right]w_{\alpha n}^{(2)}\right\} \\
&\quad +\tilde{z}_{\alpha n}^{(+)}v_{\alpha n}^{(2)}\Bigg)\ .
\end{aligned} \tag{7.33b}$$

In the above expressions, the parameters $\left\{v_{\alpha n}^{(i)}, w_{\alpha n}^{(i)}\right\}_{n=1}^{\infty}$ (for $i = 1, 2$) are introduced to simplify the expressions

$$v_{\alpha n}^{(1)} := \frac{1+\phi_0}{\sqrt{2}\,\varrho}\left[\tilde{q}_{\alpha}\ln\left(\frac{1+\phi_0}{2}\right)-\tilde{s}_{\alpha}\right]\frac{\hat{P}_{n-1}^{(0,1)}(\psi_0)}{\sqrt{n}}\,, \tag{7.34a}$$

$$v_{\alpha n}^{(2)} := -\frac{1+\phi_0}{\sqrt{2}\,\varrho}\left[\tilde{p}_{\alpha}\ln\left(\frac{1+\phi_0}{2}\right)-\tilde{r}_{\alpha}\right]\frac{\hat{P}_{n-1}^{(0,1)}(\psi_0)}{\sqrt{n}}\,, \tag{7.34b}$$

$$w_{\alpha n}^{(1)} := \frac{1-\phi_0}{\sqrt{2}\,\varrho}\tilde{u}_{\alpha}\ln\left(\frac{1-\phi_0}{2}\right)\frac{\hat{P}_{n-1}^{(1,0)}(\psi_0)}{\sqrt{n}}\,, \tag{7.34c}$$

$$w_{\alpha n}^{(2)} := -\frac{1-\phi_0}{\sqrt{2}\,\varrho}\left[\tilde{t}_\alpha \ln\left(\frac{1-\phi_0}{2}\right) - \tilde{o}_\alpha\right]\frac{\hat{P}_{n-1}^{(1,0)}(\psi_0)}{\sqrt{n}}\,, \tag{7.34d}$$

where the constant ϱ is defined as:

$$\begin{aligned}\varrho := &\left[\tilde{t}_\alpha \ln\left(\frac{1-\phi_0}{2}\right) - \tilde{o}_\alpha\right] \times \left[\tilde{q}_\alpha \ln\left(\frac{1+\phi_0}{2}\right) - \tilde{s}_\alpha\right] \\ &- \tilde{u}_\alpha \ln\left(\frac{1-\phi_0}{2}\right) \times \left[\tilde{p}_\alpha \ln\left(\frac{1+\phi_0}{2}\right) - \tilde{r}_\alpha\right]\,. \end{aligned} \tag{7.35}$$

We have obtained series expressions for the two unknowns $x_{\alpha 0}^{(i)}$ in terms of $\left\{x_{\alpha n}^{(i)}, y_{\alpha n}^{(i)}\right\}_{n=1}^{\infty}$ (for $i = 1, 2$). Therefore, the values of $x_{\alpha 0}^{(i)}$ can be calculated once the values of $\left\{x_{\alpha n}^{(i)}, y_{\alpha n}^{(i)}\right\}_{n=1}^{\infty}$ (for $i = 1, 2$) are known. We obtain the first infinite system involving only these unknowns $\left\{x_{\alpha n}^{(i)}, y_{\alpha n}^{(i)}\right\}_{n=1}^{\infty}$ (for $i = 1, 2$) from the first pair of DSE given in (7.26), by making the following replacement in (3.28): $x_0 \mapsto x_{\alpha 0}^{(1)}$, $x_n \mapsto x_{\alpha n}^{(1)}$, $a \mapsto \tilde{o}_\alpha$, $b \mapsto \tilde{t}_\alpha$, $c \mapsto 0$, $d \mapsto \tilde{u}_\alpha x_{\alpha 0}^{(2)} + \tilde{z}_\alpha$, $s_n \mapsto \tilde{o}_{\alpha n}^{(+)}$, $t_n \mapsto \tilde{t}_{\alpha n}^{(+)}$, $e_n \mapsto \tilde{o}_{\alpha n}^{(-)} y_{\alpha n}^{(1)}$, $f_n \mapsto \frac{\alpha}{nM} y_{\alpha n}^{(1)}\left(1 - \tilde{t}_{\alpha n}^{(-)}\right) + y_{\alpha n}^{(2)}\left(1 - \tilde{u}_{\alpha n}^{(-)}\right)\varsigma + \frac{\alpha}{nM} x_{\alpha n}^{(2)}\left(1 - \tilde{u}_{\alpha n}^{(+)}\right)\varsigma + \tilde{z}_{\alpha n}^{(+)}$, and $\psi_0 \mapsto \cos\phi_0 = \cos M\theta^{\mathrm{PEC}}$, as well as substitution of (7.33a) and (7.33b), which leads to

$$\begin{aligned}
&\sqrt{m} x_{\alpha m}^{(1)}\left(1 - \tilde{t}_m^{(+)}\right) + \frac{\alpha}{Mm}\sqrt{m} y_{\alpha m}^{(1)}\left(1 - \tilde{t}_m^{(-)}\right) \\
&+ \frac{\alpha}{Mm}\sqrt{m} x_{\alpha m}^{(2)}\left(1 - \tilde{u}_m^{(+)}\right)\varsigma + \sqrt{m} y_{\alpha m}^{(2)}\left(1 - \tilde{u}_m^{(-)}\right)\varsigma \\
&+ \sum_{n=1}^{\infty}\sqrt{n}\left(x_{\alpha n}^{(1)}\left\{\left(\tilde{t}_{\alpha n}^{(+)} - \tilde{o}_{\alpha n}^{(+)}\right)\hat{T}_{m-1,n-1} + \left[\tilde{r}_{\alpha n}^{(+)} - \frac{\alpha}{Mn}\left(1 - \tilde{p}_{\alpha n}^{(+)}\right)\right]\hat{U}_{m-1,n-1}\right\}\right. \\
&\qquad + y_{\alpha n}^{(1)}\left\{\left[\tilde{o}_{\alpha n}^{(-)} - \frac{\alpha}{Mn}\left(1 - \tilde{t}_{\alpha n}^{(-)}\right)\right]\hat{T}_{m-1,n-1} + \left[\left(1 - \tilde{r}_{\alpha n}^{(-)}\right)\upsilon - \left(1 - \tilde{p}_{\alpha n}^{(-)}\right)\tau\right]\hat{U}_{m-1,n-1}\right\} \\
&\qquad + x_{\alpha n}^{(2)}\left\{-\frac{\alpha}{Mn}\left(1 - \tilde{u}_{\alpha n}^{(+)}\right)\varsigma\hat{T}_{m-1,n-1} + \left(\tilde{q}_{\alpha n}^{(+)} - \tilde{s}_{\alpha n}^{(+)}\right)\hat{U}_{m-1,n-1}\right\} \\
&\qquad \left. + y_{\alpha n}^{(2)}\left\{-\left(1 - \tilde{u}_{\alpha n}^{(-)}\right)\varsigma\hat{T}_{m-1,n-1} + \left[\tilde{s}_{\alpha n}^{(-)} - \frac{\alpha}{Mn}\left(1 - \tilde{q}_{\alpha n}^{(-)}\right)\right]\hat{U}_{m-1,n-1}\right\}\right) \\
&= -\frac{\sqrt{2}(1+\psi_0)\tilde{o}_\alpha\tilde{z}_\alpha}{\tilde{t}_\alpha \ln\left(\frac{1-\psi_0}{2}\right) - \tilde{o}_\alpha}\left[1 + \frac{1}{\varrho}\tilde{u}_\alpha \ln\left(\frac{1-\psi_0}{2}\right)(\tilde{p}_\alpha - \tilde{r}_\alpha)\right]\frac{\hat{P}_{m-1}^{(0,1)}(\psi_0)}{m} \\
&\quad - \sqrt{m}\tilde{z}_{\alpha m}^{(+)} + \sum_{n=1}^{\infty}\sqrt{n}\tilde{z}_{\alpha n}^{(+)}\hat{T}_{m-1,n-1}\,,
\end{aligned} \tag{7.36}$$

for $m = 1, 2, 3, \ldots$, where

$$\hat{T}_{m-1,n-1} := \hat{Q}_{m-1,n-1}^{(1,0)}(\psi_0) - \frac{(1+\psi_0)^2}{\tilde{t}_\alpha \ln\left(\frac{1-\psi_0}{2}\right) - \tilde{o}_\alpha}\left\{\frac{1}{\varrho}\tilde{o}_\alpha\tilde{u}_\alpha\left[\tilde{p}_\alpha \ln\left(\frac{1+\psi_0}{2}\right) - \tilde{r}_\alpha\right] + \tilde{t}_\alpha\right\}$$

$$\times \frac{\hat{P}_{m-1}^{(0,1)}(\psi_0)}{m} \frac{\hat{P}_{n-1}^{(0,1)}(\psi_0)}{n}\,, \tag{7.37}$$

$$\hat{U}_{m-1,n-1} := \frac{\tilde{o}_\alpha \tilde{u}_\alpha (1-\psi_0)^2}{\varrho} \frac{\hat{P}_{m-1}^{(0,1)}(\psi_0)}{m} \frac{\hat{P}_{n-1}^{(1,0)}(\psi_0)}{n}\,. \tag{7.38}$$

For the second ISLAE, we consider the DSE given in (7.29). By making the following replacement in (3.28): $y_n \mapsto y_{\alpha n}^{(1)}$, $s_n \mapsto \tilde{o}_{\alpha n}^{(+)}$, $t_n \mapsto \tilde{t}_{\alpha n}^{(+)}$, $g_n \mapsto \tilde{o}_{\alpha n}^{(-)} x_{\alpha n}^{(1)}$, $h_n \mapsto \frac{\alpha}{nM} x_{\alpha n}^{(1)} \left(1 - \tilde{t}_{\alpha n}^{(-)}\right) + \frac{\alpha}{nM} y_{\alpha n}^{(2)} \left(1 - \tilde{u}_{\alpha n}^{(+)}\right) \varsigma + x_{\alpha n}^{(2)} \left(1 - \tilde{u}_{\alpha n}^{(-)}\right) \varsigma + \tilde{z}_{\alpha n}^{(-)}$, and $\psi_0 \mapsto \cos\phi_0 = \cos M\theta^{\mathrm{PEC}}$, we obtain for $m = 1, 2, 3, \ldots$

$$\begin{aligned}
&\frac{\alpha}{Mm} \sqrt{m} x_{\alpha m}^{(1)} \left(1 - \tilde{t}_m^{(-)}\right) + \sqrt{m} y_{\alpha m}^{(1)} \left(1 - \tilde{t}_m^{(+)}\right) \\
&+ \sqrt{m} x_{\alpha m}^{(2)} \left(1 - \tilde{u}_m^{(-)}\right) \varsigma + \frac{\alpha}{Mm} \sqrt{m} y_{\alpha m}^{(2)} \left(1 - \tilde{u}_m^{(+)}\right) \varsigma \\
&+ \sum_{n=1}^{\infty} \sqrt{n} \Big\{ x_{\alpha n}^{(1)} \left[\tilde{o}_{\alpha n}^{(-)} - \frac{\alpha}{Mn} \left(1 - \tilde{t}_{\alpha n}^{(-)}\right)\right] + y_{\alpha n}^{(1)} \left(\tilde{t}_{\alpha n}^{(+)} - \tilde{o}_{\alpha n}^{(+)}\right) - x_{\alpha n}^{(2)} \left(1 - \tilde{u}_{\alpha n}^{(-)}\right) \varsigma \\
&\qquad - y_{\alpha n}^{(2)} \frac{\alpha}{Mn} \left(1 - \tilde{u}_{\alpha n}^{(+)}\right) \varsigma \Big\} \hat{Q}_{m-1,n-1}^{(0,1)}(\phi_0) \\
&= -\sqrt{m} \tilde{z}_{\alpha m}^{(-)} + \sum_{n=1}^{\infty} \sqrt{n} \tilde{z}_{\alpha n}^{(-)} \hat{Q}_{m-1,n-1}^{(0,1)}(\phi_0)\,.
\end{aligned} \tag{7.39}$$

From the DSE given in (7.28), we can obtain the third ISLAE by making the following replacement in (3.37): $x_0 \mapsto x_{\alpha 0}^{(2)}$, $x_n \mapsto x_{\alpha n}^{(2)}$, $a \mapsto \tilde{s}_\alpha$, $b \mapsto \tilde{q}_\alpha$, $c \mapsto \tilde{r}_\alpha x_{\alpha 0}^{(1)}$, $d \mapsto \tilde{p}_\alpha x_{\alpha 0}^{(1)}$, $s_n \mapsto \tilde{s}_{\alpha n}^{(+)}$, $t_n \mapsto \tilde{q}_{\alpha n}^{(+)}$, $e_n \mapsto \left(1 - \tilde{r}_{\alpha n}^{(-)}\right) y_{\alpha n}^{(1)} \upsilon + \tilde{r}_{\alpha n}^{(+)} x_{\alpha n}^{(1)} + \tilde{s}_{\alpha n}^{(-)} y_{\alpha n}^{(2)}$, $f_n \mapsto \left(1 - \tilde{p}_{\alpha n}^{(-)}\right) y_{\alpha n}^{(1)} \tau + \frac{\alpha}{Mn} \left(1 - \tilde{p}_{\alpha n}^{(+)}\right) x_{\alpha n}^{(1)} \tau + \frac{\alpha}{Mn} \left(1 - \tilde{q}_{\alpha n}^{(-)}\right) y_{\alpha n}^{(2)}$, and $\psi_0 \mapsto \cos\phi_0 = \cos M\theta^{\mathrm{PEC}}$, as well as substitution of (7.33a) and (7.33b), which leads to

$$\begin{aligned}
&\sqrt{m} x_{\alpha m}^{(1)} \tilde{r}_m^{(+)} + \sqrt{m} y_{\alpha m}^{(1)} \left(1 - \tilde{r}_m^{(-)}\right) \upsilon + \sqrt{m} x_{\alpha m}^{(2)} \left(1 - \tilde{s}_m^{(+)}\right) + \sqrt{m} y_{\alpha m}^{(2)} \tilde{s}_m^{(-)} \\
&+ \sum_{n=1}^{\infty} \sqrt{n} \Big(x_{\alpha n}^{(1)} \Big\{ \left(\tilde{t}_{\alpha n}^{(+)} - \tilde{o}_{\alpha n}^{(+)}\right) \hat{W}_{m-1,n-1} + \left[\tilde{r}_{\alpha n}^{(+)} - \frac{\alpha}{Mn} \left(1 - \tilde{p}_{\alpha n}^{(+)}\right)\right] \hat{V}_{m-1,n-1} \Big\} \\
&\qquad + y_{\alpha n}^{(1)} \Big\{ \left[\tilde{o}_{\alpha n}^{(-)} - \frac{\alpha}{Mn} \left(1 - \tilde{t}_{\alpha n}^{(-)}\right)\right] \hat{W}_{m-1,n-1} + \left[\left(1 - \tilde{r}_{\alpha n}^{(-)}\right) \upsilon - \left(1 - \tilde{p}_{\alpha n}^{(-)}\right) \tau\right] \hat{V}_{m-1,n-1} \Big\} \\
&\qquad + x_{\alpha n}^{(2)} \Big\{ -\frac{\alpha}{Mn} \left(1 - \tilde{u}_{\alpha n}^{(+)}\right) \varsigma \hat{W}_{m-1,n-1} + \left(\tilde{q}_{\alpha n}^{(+)} - \tilde{s}_{\alpha n}^{(+)}\right) \hat{V}_{m-1,n-1} \Big\} \\
&\qquad + y_{\alpha n}^{(2)} \Big\{ -\left(1 - \tilde{u}_{\alpha n}^{(-)}\right) \varsigma \hat{W}_{m-1,n-1} + \left[\tilde{s}_{\alpha n}^{(-)} - \frac{\alpha}{Mn} \left(1 - \tilde{q}_{\alpha n}^{(-)}\right)\right] \hat{V}_{m-1,n-1} \Big\} \Big) \\
&= \frac{1}{\varrho} \sqrt{2} (1 - \psi_0) \tilde{z}_\alpha \ln\left(\frac{1 - \psi_0}{2}\right) \left(\tilde{q}_\alpha \tilde{r}_\alpha - \tilde{s}_\alpha \tilde{p}_\alpha\right) \frac{\hat{P}_{m-1}^{(1,0)}(\psi_0)}{m}
\end{aligned}$$

$$+\sum_{n=1}^{\infty}\sqrt{n}\tilde{z}_{\alpha n}^{(+)}\hat{W}_{m-1,n-1}\,, \tag{7.40}$$

for $m=1,2,3,\ldots$, where

$$\begin{aligned}\hat{V}_{m-1,n-1}:=&\frac{(1-\psi_0)^2}{\tilde{q}_\alpha\ln\left(\frac{1+\psi_0}{2}\right)-\tilde{s}_\alpha}\left\{\frac{1}{\varrho}\tilde{u}_\alpha\ln\left(\frac{1-\psi_0}{2}\right)(\tilde{r}_\alpha\tilde{q}_\alpha-\tilde{s}_\alpha\tilde{p}_\alpha)-\tilde{q}_\alpha\right\}\\&\times\frac{\hat{P}_{m-1}^{(1,0)}(\psi_0)}{m}\frac{\hat{P}_{n-1}^{(1,0)}(\psi_0)}{n}-\hat{Q}_{m-1,n-1}^{(0,1)}(\psi_0)\,,\end{aligned} \tag{7.41}$$

$$\hat{W}_{m-1,n-1}:=\frac{(\tilde{r}_\alpha\tilde{q}_\alpha-\tilde{s}_\alpha\tilde{p}_\alpha)\,(1-\psi_0)^2}{\varrho}\frac{\hat{P}_{m-1}^{(1,0)}(\psi_0)}{m}\frac{\hat{P}_{n-1}^{(0,1)}(\psi_0)}{n}\,. \tag{7.42}$$

For the final ISLAE, we consider the DSE given in (7.27). By making the following replacement in (3.51): $y_n\mapsto y_{\alpha n}^{(2)}$, $s_n\mapsto\tilde{s}_{\alpha n}^{(+)}$, $t_n\mapsto\tilde{q}_{\alpha n}^{(+)}$, $g_n\mapsto\tilde{r}_{\alpha n}^{(+)}y_{\alpha n}^{(1)}+\left(1-\tilde{r}_{\alpha n}^{(-)}\right)\upsilon x_{\alpha n}^{(1)}+\tilde{s}_{\alpha n}^{(+)}x_{\alpha n}^{(2)}$, $h_n\mapsto\frac{\alpha}{nM}y_{\alpha n}^{(1)}\left(1-\tilde{p}_{\alpha n}^{(+)}\right)\tau+x_{\alpha n}^{(1)}\left(1-\tilde{p}_{\alpha n}^{(-)}\right)\tau+\frac{\alpha}{nM}x_{\alpha n}^{(2)}\left(1-\tilde{q}_{\alpha n}^{(-)}\right)$, and $\psi_0\mapsto\cos\phi_0=\cos M\theta^{\mathrm{PEC}}$, we obtain for $m=1,2,3,\ldots$

$$\begin{aligned}&\sqrt{m}x_{\alpha m}^{(1)}\left(1-\tilde{r}_m^{(-)}\right)\upsilon+\sqrt{m}y_{\alpha m}^{(1)}\tilde{r}_m^{(+)}+\sqrt{m}x_{\alpha m}^{(2)}\tilde{s}_m^{(-)}+\sqrt{m}y_{\alpha m}^{(2)}\left(1-\tilde{s}_m^{(+)}\right)\\&+\sum_{n=1}^{\infty}\sqrt{n}\left\{x_{\alpha n}^{(1)}\left[\left(1-\tilde{r}_{\alpha n}^{(-)}\right)\upsilon-\left(1-\tilde{p}_{\alpha n}^{(-)}\right)\tau\right]+y_{\alpha n}^{(1)}\left[\tilde{r}_{\alpha n}^{(+)}-\frac{\alpha}{Mn}\left(1-\tilde{p}_{\alpha n}^{(+)}\right)\tau\right]\right.\\&\qquad\left.+x_{\alpha n}^{(2)}\left[\tilde{s}_{\alpha n}^{(-)}-\frac{\alpha}{Mn}\left(1-\tilde{q}_{\alpha n}^{(-)}\right)\right]+y_{\alpha n}^{(2)}\left(\tilde{q}_{\alpha n}^{(+)}-\tilde{s}_{\alpha n}^{(+)}\right)\right\}\hat{Q}_{m-1,n-1}^{(1,0)}(\phi_0)\\&=0.\end{aligned} \tag{7.43}$$

7.3.4 Matrix operator form

In this subsection, we write the four interconnected ISLAE in matrix operator form, for each $\alpha\in\{0,1,\ldots,M-1\}$. The resulting 4-by-4 block matrix operator can be written as:

$$\left[\mathcal{I}+\varsigma\,\mathcal{I}^t-\mathcal{C}_1+\mathcal{H}\,\mathcal{C}_2\right]\begin{pmatrix}\mathbf{x}_1\\\mathbf{y}_1\\\mathbf{x}_2\\\mathbf{y}_2\end{pmatrix}=\begin{pmatrix}\mathbf{z}_1\\\mathbf{z}_2\\\mathbf{z}_3\\0\end{pmatrix}. \tag{7.44}$$

The following matrix operators have been introduced in the above equation:

$$\mathcal{C}_1:=\left(\begin{array}{c|c|c|c}\mathcal{T}^{(+)}&-\mathcal{T}^{(-)}&-\varsigma\mathcal{U}^{(+)}&\varsigma\mathcal{U}^{(-)}\\\hline-\mathcal{R}^{(+)}&\upsilon\mathcal{R}^{(-)}&\mathcal{S}^{(+)}&-\mathcal{S}^{(-)}\\\hline-\mathcal{T}^{(-)}&\mathcal{T}^{(+)}&\varsigma\mathcal{U}^{(-)}&-\varsigma\mathcal{U}^{(+)}\\\hline\upsilon\mathcal{R}^{(-)}&-\mathcal{R}^{(+)}&-\mathcal{S}^{(-)}&\mathcal{S}^{(+)}\end{array}\right), \tag{7.45a}$$

$$\mathcal{H} := \left(\begin{array}{c:c:c:c} \mathcal{H}_1 & \mathcal{H}_2 & 0 & 0 \\ \hdashline \mathcal{H}_3 & \mathcal{H}_4 & 0 & 0 \\ \hdashline 0 & 0 & \mathcal{H}_5 & 0 \\ \hdashline 0 & 0 & 0 & \mathcal{H}_6 \end{array}\right) , \tag{7.45b}$$

$$\mathcal{C}_2 := \left(\begin{array}{c:c:c:c} \mathcal{T}^{(+)} - \mathcal{O}^{(+)} & \mathcal{R}^{(+)} - \mathcal{P}^{(+)} & \mathcal{O}^{(-)} - \mathcal{T}^{(-)} & \upsilon\left(\mathcal{I} - \mathcal{R}^{(-)}\right) \\ & & & +\tau\left(\mathcal{I} - \mathcal{P}^{(-)}\right) \\ \hdashline \mathcal{O}^{(-)} - \mathcal{T}^{(-)} & \upsilon\left(\mathcal{I} - \mathcal{R}^{(-)}\right) & \mathcal{T}^{(+)} - \mathcal{O}^{(+)} & \mathcal{R}^{(+)} - \mathcal{P}^{(+)} \\ & +\tau\left(\mathcal{I} - \mathcal{P}^{(-)}\right) & & \\ \hdashline -\varsigma\mathcal{U}^{(+)} & \mathcal{Q}^{(+)} - \mathcal{S}^{(+)} & -\varsigma\left(\mathcal{I} - \mathcal{U}^{(-)}\right) & \mathcal{S}^{(-)} - \mathcal{Q}^{(-)} \\ \hdashline -\varsigma\left(\mathcal{I} - \mathcal{U}^{(-)}\right) & \mathcal{S}^{(-)} - \mathcal{Q}^{(-)} & -\varsigma\mathcal{U}^{(+)} & \mathcal{Q}^{(+)} - \mathcal{S}^{(+)} \end{array}\right) . \tag{7.45c}$$

To simplify the above, we introduce the following diagonal sub-matrices involving the asymptotically small parameters:

$$\mathcal{O}^{(+)} := \text{diag}\left(o_{\alpha n}^{(+)}\right) , \qquad \mathcal{O}^{(-)} := \text{diag}\left(o_{\alpha n}^{(-)}\right) , \tag{7.46a}$$

$$\mathcal{P}^{(+)} := \frac{\alpha}{M}\text{diag}\left(\frac{1 - p_{\alpha n}^{(+)}}{n}\right) , \qquad \mathcal{P}^{(-)} := \text{diag}\left(p_{\alpha n}^{(-)}\right) , \tag{7.46b}$$

$$\mathcal{Q}^{(+)} := \text{diag}\left(q_{\alpha n}^{(+)}\right) , \qquad \mathcal{Q}^{(-)} := \frac{\alpha}{M}\text{diag}\left(\frac{1 - q_{\alpha n}^{(-)}}{n}\right) , \tag{7.46c}$$

$$\mathcal{R}^{(+)} := \text{diag}\left(r_{\alpha n}^{(+)}\right) , \qquad \mathcal{R}^{(-)} := \text{diag}\left(r_{\alpha n}^{(-)}\right) , \tag{7.46d}$$

$$\mathcal{S}^{(+)} := \text{diag}\left(s_{\alpha n}^{(+)}\right) , \qquad \mathcal{S}^{(-)} := \text{diag}\left(s_{\alpha n}^{(-)}\right) , \tag{7.46e}$$

$$\mathcal{T}^{(+)} := \text{diag}\left(t_{\alpha n}^{(+)}\right) , \qquad \mathcal{T}^{(-)} := \frac{\alpha}{M}\text{diag}\left(\frac{1 - t_{\alpha n}^{(-)}}{n}\right) , \tag{7.46f}$$

$$\mathcal{U}^{(+)} := \frac{\alpha}{M}\text{diag}\left(\frac{1 - u_{\alpha n}^{(+)}}{n}\right) , \qquad \mathcal{U}^{(-)} := \text{diag}\left(u_{\alpha n}^{(-)}\right) . \tag{7.46g}$$

The remaining symmetric and bounded sub-matrices are defined as:

$$[\mathcal{H}_1]_{n,m} := \hat{T}_{m-1,n-1} , \qquad [\mathcal{H}_2]_{n,m} := \hat{U}_{m-1,n-1} , \tag{7.47a}$$

$$[\mathcal{H}_3]_{n,m} := \hat{W}_{m-1,n-1} , \qquad [\mathcal{H}_4]_{n,m} := \hat{V}_{m-1,n-1} , \tag{7.47b}$$

$$[\mathcal{H}_5]_{n,m} := \hat{Q}_{m-1,n-1}^{(0,1)}(\phi_0) , \qquad [\mathcal{H}_6]_{n,m} := \hat{Q}_{m-1,n-1}^{(1,0)}(\phi_0) , \tag{7.47c}$$

for $n, m = 1, 2, \ldots$ The column vectors $\mathbf{x}_i$ and $\mathbf{y}_i$ denote $\left\{\sqrt{n}x_n^{(i)}, \sqrt{n}y_n^{(i)}\right\}_{n=1}^{\infty}$, respectively (for $i = 1, 2$). The right hand vector of (7.44) is made up of the column vectors $\mathbf{z}_1$, $\mathbf{z}_2$ and $\mathbf{z}_3$, which denote the right side of (7.36), (7.40), and (7.39), respectively; *i.e.*,

$$[\mathbf{z}_1]_n := -\frac{\sqrt{2}(1 + \psi_0)\tilde{o}_\alpha \tilde{z}_\alpha}{\tilde{t}_\alpha \ln\left(\frac{1-\psi_0}{2}\right) - \tilde{o}_\alpha}\left[1 + \frac{1}{\varrho}\tilde{u}_\alpha \ln\left(\frac{1 - \psi_0}{2}\right)(\tilde{p}_\alpha - \tilde{r}_\alpha)\right]\frac{\hat{P}_{m-1}^{(0,1)}(\psi_0)}{m}$$

$$- \sqrt{m}\tilde{z}_{\alpha m}^{(+)} + \sum_{n=1}^{\infty} \sqrt{n}\tilde{z}_{\alpha n}^{(+)} \hat{T}_{m-1,n-1} \,, \tag{7.48a}$$

$$[\mathbf{z}_2]_n := \frac{1}{\varrho}\sqrt{2}(1-\psi_0)\tilde{z}_\alpha \ln\left(\frac{1-\psi_0}{2}\right)(\tilde{q}_\alpha \tilde{r}_\alpha - \tilde{s}_\alpha \tilde{p}_\alpha)\frac{\hat{P}_{m-1}^{(1,0)}(\psi_0)}{m} + \sum_{n=1}^{\infty} \sqrt{n}\tilde{z}_{\alpha n}^{(+)} \hat{W}_{m-1,n-1} \,, \tag{7.48b}$$

$$[\mathbf{z}_3]_n := - \sqrt{m}\tilde{z}_{\alpha m}^{(-)} + \sum_{n=1}^{\infty} \sqrt{n}\tilde{z}_{\alpha n}^{(-)} \hat{Q}_{m-1,n-1}^{(0,1)}(\phi_0) \,. \tag{7.48c}$$

Following similar arguments as those given in Subsection 4.4.2, we can show that (7.44) is a second kind Fredholm equation, and hence enjoys the same advantages as those discussed in Chapter 3. The distinct feature of current problem, when compared with that of the oblique scattering problem of CLR in Chapter 4 (where only a single strip is included), is that in the final form of solution there are M infinite systems to be solved separately. Each of these M systems is accountable for the unknowns $\left\{x_{\alpha n}^{(i)}, y_{\alpha n}^{(i)}\right\}_{n=1}^{\infty}$ $(i = 1, 2)$, for a fixed value of $\alpha \in \{0, 1, \ldots, M-1\}$. As the asymptotically small parameters all have magnitude of order $\left(\frac{\kappa_1^2 R^2}{M^2 n^2}\right)$, as $n \to +\infty$, we can see that the truncation number N_{tr} required to achieve a desired accuracy for $\left\{x_{\alpha n}^{(i)}, y_{\alpha n}^{(i)}\right\}_{n=1}^{\infty}$ $(i = 1, 2)$ is only one-Mth of that for the problem involving only a single reflecting strip ($M = 1$). In other words, for a predetermined accuracy of the computed solutions, the total number of series equations required (*i.e.*, $M \times N_{\text{tr}}$) is independent of the number of PEC strips M.

7.4 Numerical results and discussion

7.4.1 Numerical validation

With the knowledge of the expansion coefficients $\left\{x_{\alpha n}^{(i)}, y_{\alpha n}^{(i)}\right\}_{n=1}^{\infty}$ for $i = 1, 2$ and $\alpha = 0, 1, \ldots, (M-1)$, the near field, surface current density and RCS can be determined and compared for the numerical checks of the algorithm.

Some internal checks have been conducted on the scattering problem by a multi-conductor cylinder with three strips ($M = 3$). The tangential components of the total electric field, E_z^{tot} (recall that E_ϕ vanishes for normally incident TM_z plane wave), along the contour of the cylinder are plotted in the top figure in Figure 7.2. Evidently, the z-components of the interior (solid red line) and exterior (dotted black line) electric fields match perfectly over the entire surface of the cylinder, and vanish on the PEC strips, which are located at the intervals $(-30°, 30°)$, $(90°, 150°)$ and

$(-150°, -90°)$. On the other hand, the bottom figure depicts the difference between the ϕ-components of the magnetic field across the structure's contour. The boundary condition on dielectric surface is confirmed here, as the difference is seen oscillating around the value zero. The oscillation seen is a result of the Gibbs phenomenon, which can be reduced by increasing the truncation number or by some series manipulation to speed up the rate of convergence. As mentioned previously, there are various different approaches applicable to suppress the Gibbs phenomenon: they include Fejér's method of summing Cesàro sums, ϵ-algorithm extrapolation method, and by extracting the square root singularities at the two edges of the strip at $\phi = \pm\theta^{\text{PEC}}$, explicitly. Alternatively, we can follow the approach described in Section 4.7 to obtain a series expression with faster convergence rate than the original one. Here, truncation number N_{tr} of 50 is used.

Several external tests have also been conducted. To examine the accuracy of the solution over the boundary of CLR, the tangential components of the total electric field E_z, are computed for a multi-conductor cylinder with two PEC strips, each of angular width 80° (*i.e.*, $\theta^{\text{PEC}} = 40°$). The absolute magnitude of E_z^{tot} are computed for the problem characterized by parameters $R = 1$, $\epsilon_r = 1$, $\mu_r = 1$, $\theta^{\text{PEC}} = 40°$, $M = 2$, $k_0 = 2\pi$ and $\theta_x^{\text{pw}} = 90°$. It is worth noting that the total tangential electric field vanishes at the two PEC strips as dictated by the boundary condition. The curve is compared directly with Figure 2 in [28] which results were calculated using MoM and boundary value method.

7.4.2 Numerical investigation

For the problem involving a multi-conductor scattered by plane wave, suppose each of the ISLAE is truncated to N_{tr} equations. As a result, each of the 4-by-4 block matrix equations has a dimension of $4N_{\text{tr}}$-by-$4N_{\text{tr}}$. We can see that, for $N_{\text{tr}} > \kappa_1 R/4$, the relative error of the unknown coefficients decreases as N_{tr} increases. Therefore, it is only sensible to choose a truncation number of at least $\kappa_1 R/4$, for a converging solution. We can also see that this total number of equations, $M \times 4N_{\text{tr}}$, required for a specific accuracy has about the same magnitude as that for the structure with only one conducting strip (*i.e.*, $M = 1$). However, a comparison of the condition number for the ISLAE, when $M = 1, 2$ and 4 in Figure 7.4 reveals that the system has a higher condition number as M increases.

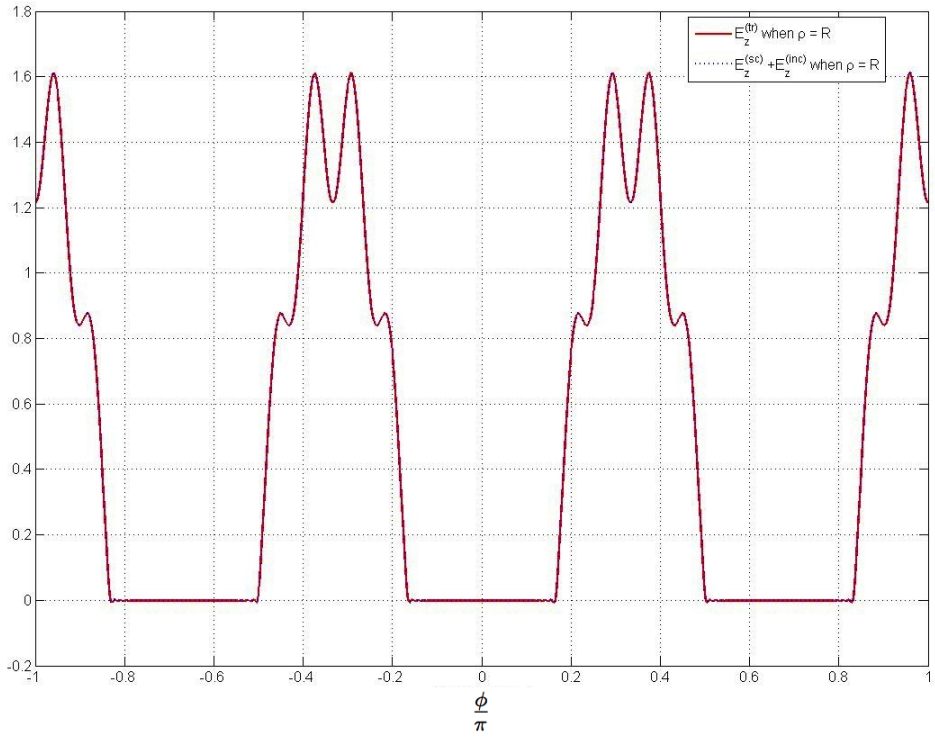

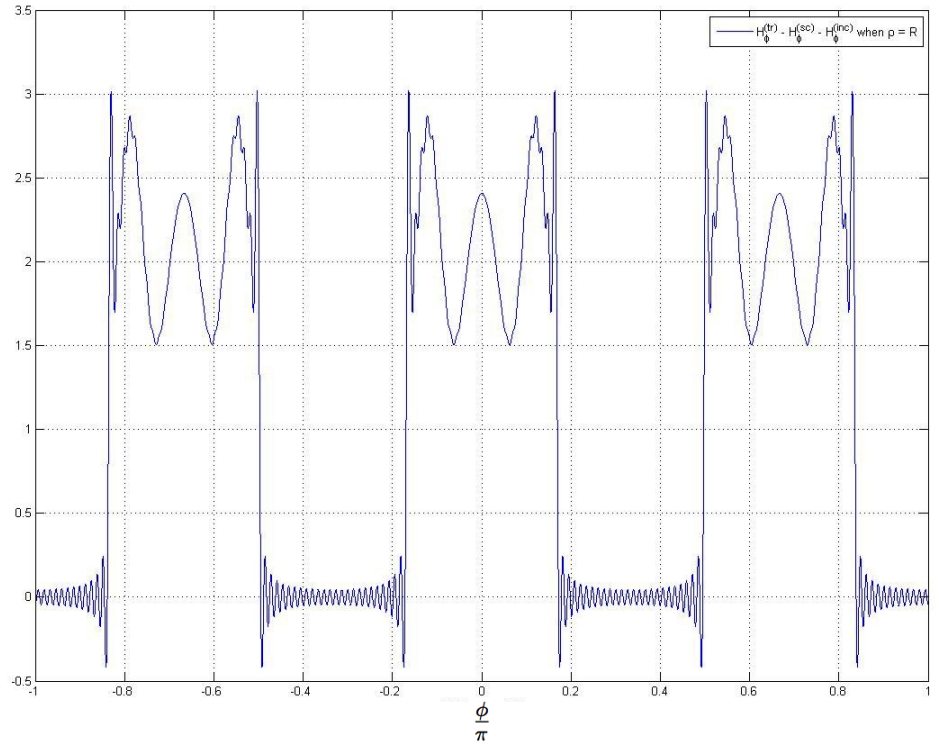

Figure 7.2: MBC check for the scattering problem by a multi-conductor cylinder with three strips when excited by a line source at the origin. [$R = 1$, $M = 3$, $\epsilon_r = 2$, $\mu_r = 1$, $\theta^{\text{PEC}} = 30°$, $k_0 = 20$, $\theta_{\text{ls}} = 0$, $\psi_{\text{ls}} = 0$ and $N_{\text{tr}} = 50$]

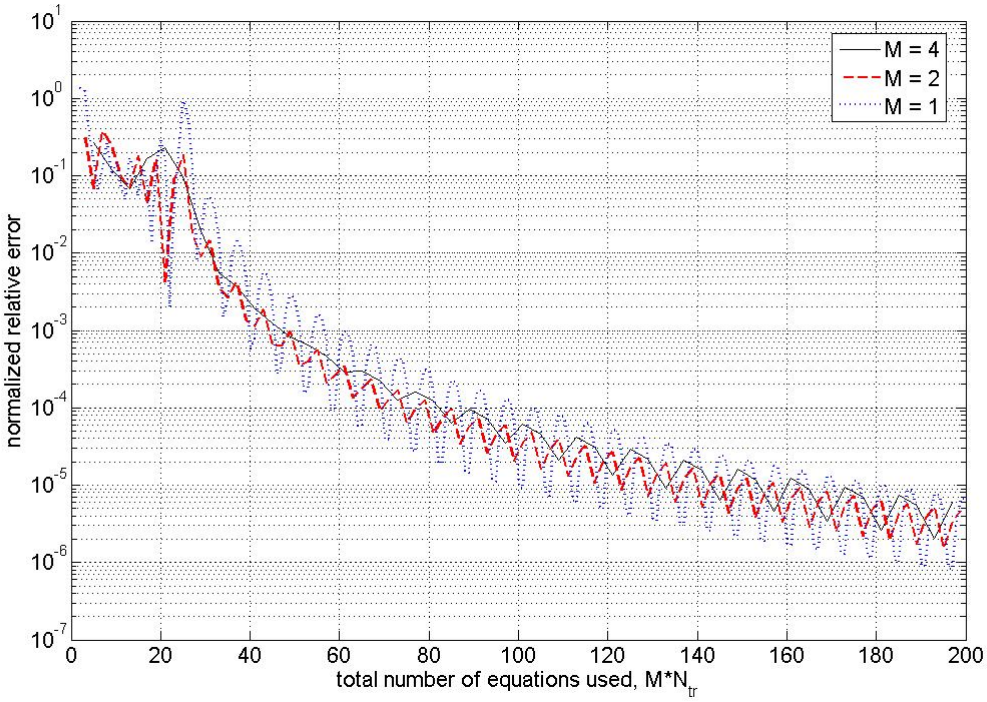

Figure 7.3: Comparison of the relative error of the ISLAE for different M, as the total (truncated) number of equations $M * N_{\text{tr}}$ increases. $\left[k_0 R = 20, \epsilon_r = 2, \mu_r = 1, \theta^{\text{PEC}} = \pi/6\right]$

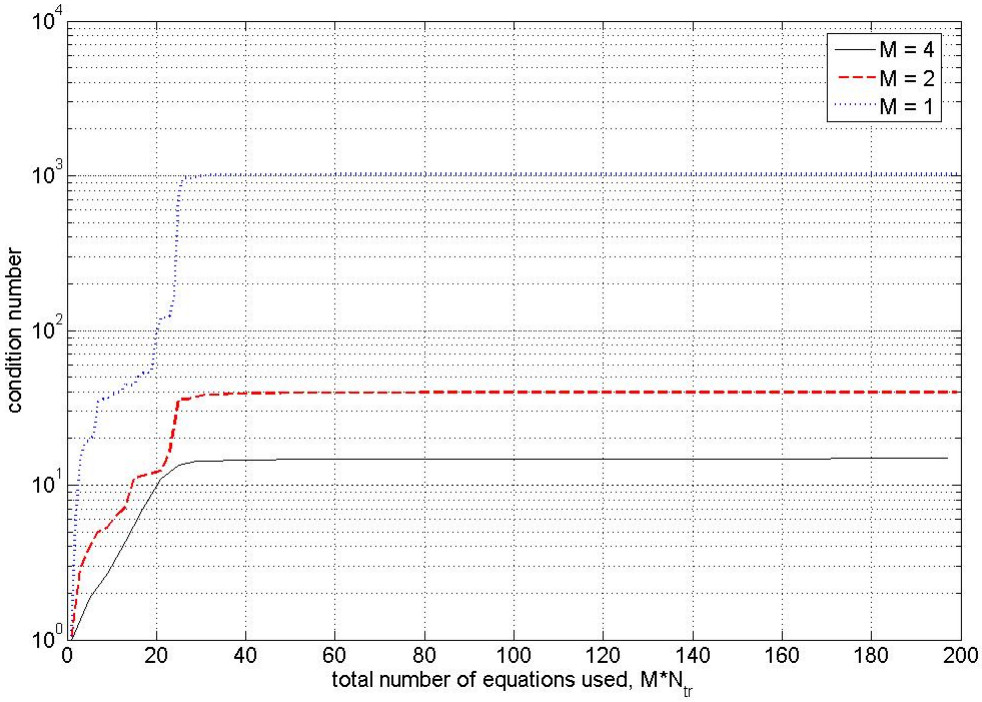

Figure 7.4: Comparison of the condition number of the matrix operator for different M, as the total (truncated) number of equations $M \times N_{\mathrm{tr}}$ increases. $\left[k_0 R = 20, \epsilon_r = 2, \mu_r = 1, \theta^{\mathrm{PEC}} = \pi/6\right]$

7.5 Conclusion

The problem of a braided cylindrical shield with periodic apertures and dielectric loading under the excitation of an oblique plane wave is considered. An algorithm based upon the MoR is formulated, by making use of the periodicity of the structure to reduce the formulation to one defined over the periodic unit cell. In the final step, M non-interconnected systems of equations of the second kind are obtained, where M is the number of strips. Each of these M ISLAE can be written as a 4-by-4 block matrix equations and is subsequently solved numerically by truncation method. The computed solution provides a rigorous analysis of the shielding effect of the braided cylindrical shield.

The numerical analysis first deals with the verification of the algorithm. The tangential components of the electric and magnetic fields on the surface of the scatterer are computed to verify the satisfaction of the MBC. The solution computed is also shown to be convergent and stable. To examine the effectiveness of the braided cylindrical shield, the transmitted field inside the structure is calculated as a function of the number and width of the strips as well as the dielectric constant.

Chapter 8

Hybrid mode analysis of a multi-conductor microstrip line

8.1 Introduction

The shielding effect of a braided cylindrical shield exposed to an external excitation has been investigated in previous chapter, Chapter 7. It is our goal in this chapter to study the aspect of a braided cylindrical shield as a part of a transmission line (thus forming a cylindrical multi-conductor microstrip line). The MBVP associated with a double-layered, shielded transmission line, which inner interface consists an arbitrary number M of PEC strips, is formulated in terms of a rigorous hybrid electromagnetic mode (HEM) representation.

From substrate permittivity measurements to microwave filters, splitters, baluns, transition adapters, and impedance transformers, the applications of multi-conductor transmission line are vast. The investigations on multi-conductor transmission lines have been a topic of interest for a few decades, and have used a variety of techniques including the conformal mapping approach [26, 48, 60, 95], the MoM [3, 54, 72], the FDM [19, 13, 64], the iterative approach [10], the FEM [39, 38], *etc.* Reported work on this subject can be classified into two categories: quasi-TEM approximation and hybrid-mode analyses. The quasi-TEM assumption provides acceptable approximate results only in some circumstances, *e.g.*, when the structure dimension is a lot smaller than half a wavelength. For higher frequency bands (*e.g.*, millimeter wave bands), hybrid-mode analyses is needed to provide accurate prediction of the dispersion characteristics. However, due to its complexity, there are a lot less reported hybrid-mode analysis of this type of multi-conductor transmission line.

As opposed to many of the approaches mentioned above (which are purely numerical), the analysis presented in this chapter is based on the MoR without any

a priori simplifications. Following a similar formulation to that for the scattering problem of a multi-conductor cylinder considered in Chapter 7, the spectral problem of the multi-conductor transmission line problem can be equivalently reduced to the problem of determination of the propagation constant k_z from the M resulting matrix equations by solving for the eigenvalues of the following characteristic equation

$$[\mathcal{A}_\alpha(k_z)]\,\mathbf{x}(k_z) = \mathbf{0}\,, \tag{8.1}$$

for $\alpha = 0, 1, \ldots, (M-1)$. Here, $\mathbf{x}$ is the corresponding characteristic vector, and $\mathcal{A}_\alpha$ is the α-th matrix operator derived from using the MoR on the ill-conditioned series equations. It is worth noting that each matrix operator, $\mathcal{A}_\alpha$ for $\alpha = 0, 1, \ldots, (M-1)$, is a compact perturbation of the identity matrix operator. As has been discussed in preceding chapters, due to this, the accuracy of the results computed is guaranteed and the numerical algorithm is well-conditioned. The numerical analysis concentrates on the finding of the cutoff frequency (the lowest frequency for which the unattenuated propagation occurs) of such a line. Numerical results of frequency-dependent effective dielectric constants are given for different number of strips, relative dimension of the interior cylinder and dielectric constants of substrates. A shielded transmission line is assumed in the problem formulation for simplicity, although the approach can be extended to the open waveguide problem.

8.2 Geometrical description of the problem

The cross-section of the multi-conductor transmission line considered is shown in Figure 8.1. The outer circle represents a cross-section of a PEC cylinder of radius R_0, while the interior circle represents the contour of a multi-conductor cylinder of radius R_1. Both cylinders are assumed to be parallel to the z-axis and uniform in the z direction. On the surface of the interior cylinder, a finite number M of conformal PEC strips are placed. Similar to the assumptions made in Chapter 7, the strips are assumed to be equally-spaced, infinitesimally-thin, and each has the same angular width of $2\theta^{\mathrm{PEC}}$.

We denote the region between the outer and inner cylinders as region 1, while the region inside the interior cylinder as region 2. Although it offers great advantage of low dielectric loss, an air-filled version of the line is difficult to construct as the inner cylinder (which consists multiple PEC strips) will then have to be suspended. Therefore, unlike the scattering problem in previous chapter, where the outer region is supposed to be free space, we do not assume that region 1 is air-filled here. The

dielectric materials in region 1 and 2 are assumed to be lossless, isotropic and homogeneous. We denote the relative permittivity and permeability of region 1 and 2 as (ϵ_1, μ_1) and (ϵ_2, μ_2), respectively. Due to the presence of different dielectrics, the field distribution is a combination of TE and TM modes, which is referred to as hybrid electromagnetic mode (HEM). The electric and magnetic field components are denoted with superscript (1) inside the cladding (region 1), and with superscript (2) inside the inner core (region 2). The superscripts (1) and (2) are used, instead of (0) and (1) adopted in Chapter 7, to avoid confusion with free space parameters.

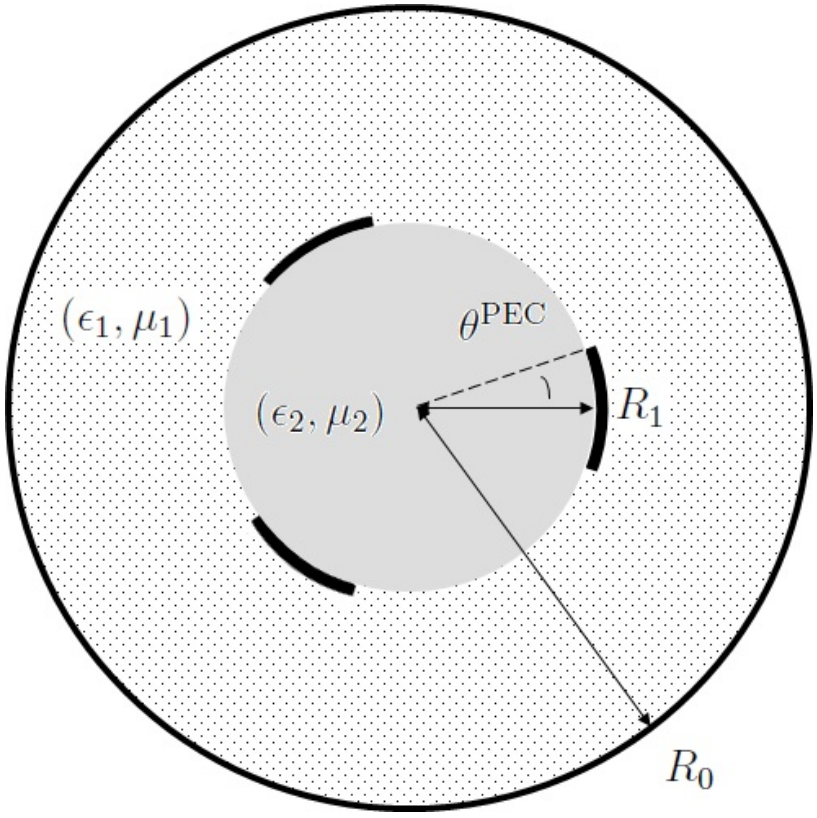

Figure 8.1: Cross-sectional view of a multi-conductor transmission line.

8.3 Problem formulation

Due to the periodicity of this multi-conductor transmission line, the Floquet formulation can be applied directly to the series representations of the field components. However, as there is great structural similarity between the line considered in this chapter and the scatterer studied in Chapter 7, we have chosen to adopt the same approach as that in previous chapter for consistency; *i.e.*, by making use of the identity

for exponential functions. We have adopted the same notations and series representations as those employed in previous chapter, where possible, in our formulation here. The series equations derived from the MBC, and the final matrix equations derived from the application of the MoR are the homogeneous forms of those obtained in the scattering problem in Chapter 7, with some of the asymptotically small parameters redefined. To avoid repetition, the detailed derivation of the final block matrix equation is omitted.

For this shielded transmission line, we denote the z-components of the fields in each region as:

$$E_z^{(1)}(\rho,\phi) = \sum_{n=-\infty}^{\infty} \left[a_n^{(1)} \frac{H_n^{(2)}(\kappa_1\rho)}{H_n^{(2)}(\kappa_1 R_1)} + c_n J_n(\kappa_1\rho) H_n^{\prime(2)}(\kappa_1 R_0) \right] e^{jn\phi}\,, \tag{8.2a}$$

$$H_z^{(1)}(\rho,\phi) = \sum_{n=-\infty}^{\infty} \left[b_n^{(1)} \frac{H_n^{(2)}(\kappa_1\rho)}{H_n^{(2)}(\kappa_1 R_1)} + d_n J_n(\kappa_1\rho) H_n^{\prime(2)}(\kappa_1 R_0) \right] e^{jn\phi}\,, \tag{8.2b}$$

$$E_z^{(2)}(\rho,\phi) = \sum_{n=-\infty}^{\infty} a_n^{(2)} J_n(\kappa_1\rho) H_n^{\prime(2)}(\kappa_1 R_0) e^{jn\phi}\,, \tag{8.2c}$$

$$H_z^{(2)}(\rho,\phi) = \sum_{n=-\infty}^{\infty} b_n^{(2)} J_n(\kappa_1\rho) H_n^{\prime(2)}(\kappa_1 R_0) e^{jn\phi}\,. \tag{8.2d}$$

The unknowns $\left\{ a_n^{(i)}, b_n^{(i)}, c_n, d_n \right\}_{n\in\mathbb{Z}}$ $(i = 1, 2)$ are evaluated by applying the boundary conditions on the contours of both cylinders (where $\rho = R_0$ or R_1).

As the transmission line is shielded, the tangential components of the electric field vanish on on the contour of the outer cylinder; *i.e.*,

$$\lim_{\rho\to R_0^-} E_z^{(1)}(\rho,\phi) = 0\,, \qquad \phi \in (-\pi,\pi), \tag{8.3a}$$

$$\lim_{\rho\to R_0^-} E_\phi^{(1)}(\rho,\phi) = 0\,, \qquad \phi \in (-\pi,\pi). \tag{8.3b}$$

At the same time, the tangential components of the electric field are continuous across the contour of the inner cylinder; *i.e.*,

$$\lim_{\rho\to R_1^+} E_z^{(1)}(\rho,\phi) = \lim_{\rho\to R_1^-} E_z^{(2)}(\rho,\phi)\,, \qquad \phi \in (-\pi,\pi), \tag{8.4a}$$

$$\lim_{\rho\to R_1^+} E_\phi^{(1)}(\rho,\phi) = \lim_{\rho\to R_1^-} E_\phi^{(2)}(\rho,\phi)\,, \qquad \phi \in (-\pi,\pi). \tag{8.4b}$$

We can eliminate four out of six unknown coefficients by substituting the series representations given in (8.2) into (8.3) and (8.4), then equating termwise; *i.e.*,

$\left\{a_n^{(1)}, b_n^{(1)}, c_n, d_n\right\}_{n\in\mathbb{Z}}$ can be written in terms of $\left\{a_n^{(2)}, b_n^{(2)}\right\}_{n\in\mathbb{Z}}$. From these continuity conditions, we derive the following relations:

$$a_n^{(1)} = - c_n^{(1)} J_n(\kappa_1 R_0) H_n^{(2)}(\kappa_1 R_1) H_n^{'(2)}(\kappa_1 R_0) \big/ H_n^{(2)}(\kappa_1 R_0) \ , \tag{8.5a}$$

$$b_n^{(1)} = - d_n^{(1)} J_n'(\kappa_1 R_0) H_n^{(2)}(\kappa_1 R_1) \, . \tag{8.5b}$$

$$c_n = a_n^{(2)} \frac{J_n(\kappa_2 R_1) H_n^{'(2)}(\kappa_2 R_1) H_n^{(2)}(\kappa_1 R_0)}{\vartheta_n^{(1)} H_n^{'(2)}(\kappa_1 R_0)} \, , \tag{8.5c}$$

$$d_n = \left[\frac{n a_n^{(2)} \beta_z}{j\eta_0 \mu_1 \kappa_1 R_1} \left(1 - \frac{\kappa_1^2}{\kappa_2^2}\right) J_n(\kappa_2 R_1) + b_n^{(2)} \frac{\mu_2 \kappa_1}{\mu_1 \kappa_2} J_n'(\kappa_2 R_1) \right] \frac{H_n^{'(2)}(\kappa_2 R_1)}{\vartheta_n^{(2)}} \, , \tag{8.5d}$$

where the denominators $\vartheta_n^{(1)}$ and $\vartheta_n^{(2)}$ are defined as

$$\vartheta_n^{(1)} = J_n(\kappa_1 R_1) H_n^{(2)}(\kappa_1 R_0) - J_n(\kappa_1 R_0) H_n^{(2)}(\kappa_1 R_1) \, , \tag{8.6}$$

$$\vartheta_n^{(2)} = J_n'(\kappa_1 R_1) H_n^{'(2)}(\kappa_1 R_0) - J_n'(\kappa_1 R_0) H_n^{'(2)}(\kappa_1 R_1) \, . \tag{8.7}$$

In the above equations, we have introduced the normalized propagation constant $\beta_z = k_z/k_0$[1]. The unknowns $\left\{a_n^{(1)}, b_n^{(1)}\right\}_{n\in\mathbb{Z}}$ can be expressed in terms of $\left\{a_n^{(2)}, b_n^{(2)}\right\}_{n\in\mathbb{Z}}$ as well by substitution of (8.5c) and (8.5d) into (8.5a) and (8.5b):

$$a_n^{(1)} = - a_n^{(2)} \ J_n(\kappa_1 R_0) H_n^{(2)}(\kappa_1 R_1) J_n(\kappa_2 R_1) H_n^{'(2)}(\kappa_2 R_1) \Big/ \vartheta_n^{(1)} \, , \tag{8.8a}$$

$$\begin{aligned} b_n^{(1)} = & - \left[\frac{n a_n^{(2)} \beta_z}{j\eta_0 \mu_1 \kappa_1 R_1} \left(1 - \frac{\kappa_1^2}{\kappa_2^2}\right) J_n(\kappa_2 R_1) + b_n^{(2)} \frac{\mu_2 \kappa_1}{\mu_1 \kappa_2} J_n'(\kappa_2 R_1) \right] \\ & \times \frac{H_n^{'(2)}(\kappa_2 R_1) J_n'(\kappa_1 R_0) H_n^{(2)}(\kappa_1 R_1)}{\vartheta_n^{(2)}} \, . \end{aligned} \tag{8.8b}$$

The above representations (8.5c), (8.5d), (8.8a) and (8.8b) hold when both of the denominators, $\vartheta_n^{(1)}$ and $\vartheta_n^{(2)}$, are non-zero for all integer values of n. When either of them vanishes for some $n \in \mathbb{Z}$, the representations above take slightly different forms, and are considered in next section. It is worth noting that the conditions

$$\vartheta_n^{(1)} = 0 \, , \tag{8.9}$$

$$\vartheta_n^{(2)} = 0 \, , \tag{8.10}$$

are, respectively, the characteristic equations for the TM_z and TE_z modes for the coaxial line which consists of a central conductor of radius R_1, surrounded by grounded one of radius R_0, and filled with dielectric material of relative parameters (ϵ_1, μ_1) (see the left figure in Figure 8.2).

[1]For the scattering problem with an obliquely incident plane wave, $\beta_z = \cos\theta_z^{\mathrm{pw}}$.

Therefore, similar to the previous scattering problem, we have only the unknowns $\left\{a_n^{(2)}, b_n^{(2)}\right\}_{n\in\mathbb{Z}}$ left to be determined from the MBC given below:

$$\lim_{\rho\to R_1^-} E_z^{(2)}(\rho,\phi) = 0\,, \qquad \phi\in\Omega_{\text{PEC}}, \tag{8.11a}$$

$$\lim_{\rho\to R_1^-} E_\phi^{(2)}(\rho,\phi) = 0\,, \qquad \phi\in\Omega_{\text{PEC}}, \tag{8.11b}$$

$$\lim_{\rho\to R_1^+} H_z^{(1)}(\rho,\phi) = \lim_{\rho\to R_1^-} H_z^{(2)}(\rho,\phi)\,, \qquad \phi\in\Omega_{\text{aper}}, \tag{8.11c}$$

$$\lim_{\rho\to R_1^+} H_\phi^{(1)}(\rho,\phi) = \lim_{\rho\to R_1^-} H_\phi^{(2)}(\rho,\phi)\,, \qquad \phi\in\Omega_{\text{aper}}, \tag{8.11d}$$

where Ω_{PEC} and Ω_{aper} are portions of the boundary Ω of the inner cylinder as defined in (7.1a) and (7.1b).

The set of series equations derived from the MBC for this transmission line bears great similarity to those obtained in Chapter 7 with β_z replacing $\cos\theta_z^{\text{pw}}$ and R_1 replacing R. The main differences between the two problems lies in the definitions of the parameters $\{r_n, s_n, t_n, u_n\}_{n\in\mathbb{Z}}$, and the absence of external excitation (which is summarized in the parameter $\{z_n\}_{n\in\mathbb{Z}}$ previously). From (8.11a) and (8.11b), we have

$$\sum_{n=-\infty}^{\infty} a_n^{(2)} o_n e^{jn\phi} = 0 \quad (A)\,, \tag{8.12}$$

$$\sum_{n=-\infty}^{\infty} \left\{a_n^{(2)} p_n + b_n^{(2)} q_n\right\} e^{jn\phi} = 0 \quad (A)\,, \tag{8.13}$$

for $\phi\in\Omega_{\text{PEC}}$; while from (8.11c) and (8.11d), we have

$$\sum_{n=-\infty}^{\infty} \left\{a_n^{(2)} r_n + b_n^{(2)} s_n\right\} e^{jn\phi} = 0 \quad (A)\,, \tag{8.14}$$

$$\sum_{n=-\infty}^{\infty} \left\{a_n^{(2)} t_n + b_n^{(2)} u_n\right\} e^{jn\phi} = 0 \quad (A)\,, \tag{8.15}$$

for $\phi\in\Omega_{\text{aper}}$. The coefficients $\{o_n, p_n, q_n\}_{n\in\mathbb{Z}}$ are as defined in (4.25)–(4.27); that is, for all $n\in\mathbb{Z}$,

$$o_n := J_n(\kappa_2 R_1) H_n^{\prime(2)}(\kappa_2 R_1)\,, \tag{8.16}$$

$$p_n := \frac{jn\beta_z}{\eta_0\mu_2\kappa_2 R_1} J_n(\kappa_2 R_1) H_n^{\prime(2)}(\kappa_2 R_1)\,, \tag{8.17}$$

$$q_n := J_n'(\kappa_2 R_1) H_n^{\prime(2)}(\kappa_2 R_1)\,, \tag{8.18}$$

whereas the coefficients $\{r_n, s_n, t_n, u_n\}_{n\in\mathbb{Z}}$ are redefined as

$$r_n := \frac{jn\beta_z}{\eta_0\mu_1\kappa_1 R_1}\left(1-\frac{\kappa_1^2}{\kappa_2^2}\right) J_n(\kappa_2 R_1) H_n^{'(2)}(\kappa_2 R_1)\,\gamma_n^{(1)}\,, \tag{8.19}$$

$$s_n := J_n(\kappa_2 R_1) H_n^{'(2)}(\kappa_2 R_1) - \frac{\mu_2\,\kappa_1}{\mu_1\,\kappa_2} J_n'(\kappa_2 R_1) H_n^{'(2)}(\kappa_2 R_1)\,\gamma_n^{(1)}\,, \tag{8.20}$$

$$\begin{aligned} t_n :=& \epsilon_2\kappa_1 J_n'(\kappa_2 R_1) H_n^{'(2)}(\kappa_2 R_1) - \epsilon_1\kappa_2 J_n(\kappa_2 R_1) H_n^{'(2)}(\kappa_2 R_1)\,\gamma_n^{(2)} \\ &+ \frac{n^2\beta_z^2\kappa_2}{\mu_1\kappa_1^2 R_1^2}\left(1-\frac{\kappa_1^2}{\kappa_2^2}\right) J_n(\kappa_2 R_1) H_n^{'(2)}(\kappa_2 R_1)\,\gamma_n^{(1)}\,, \end{aligned} \tag{8.21}$$

$$u_n := \frac{n\beta_z\eta_0\kappa_1}{j\kappa_2 R_1}\left[J_n(\kappa_2 R_1) H_n^{'(2)}(\kappa_2 R_1) - \frac{\mu_2\,\kappa_2}{\mu_1\,\kappa_1} J_n'(\kappa_2 R_1) H_n^{'(2)}(\kappa_2 R_1)\,\gamma_n^{(1)}\right]. \tag{8.22}$$

In the above, we have introduced the following for neater expressions

$$\gamma_n^{(1)} = \frac{J_n(\kappa_1 R_1) H_n^{'(2)}(\kappa_1 R_0) - J_n'(\kappa_1 R_0) H_n^{(2)}(\kappa_1 R_1)}{J_n'(\kappa_1 R_1) H_n^{'(2)}(\kappa_1 R_0) - J_n'(\kappa_1 R_0) H_n^{'(2)}(\kappa_1 R_1)}\,, \tag{8.23}$$

$$\gamma_n^{(2)} = \frac{J_n'(\kappa_1 R_1) H_n^{(2)}(\kappa_1 R_0) - J_n(\kappa_1 R_0) H_n^{'(2)}(\kappa_1 R_1)}{J_n(\kappa_1 R_1) H_n^{(2)}(\kappa_1 R_0) - J_n(\kappa_1 R_0) H_n^{(2)}(\kappa_1 R_1)}\,. \tag{8.24}$$

That is, to incorporate the effect of the external shield, we have replaced the ratios $\frac{H_n^{(2)}(\kappa_1 R)}{H_n^{'(2)}(\kappa_1 R)}$ and $\frac{H_n^{'(2)}(\kappa_1 R)}{H_n^{(2)}(\kappa_1 R)}$ (which occur in the unbounded scattering problem in Chapter 4 and Chapter 7) with $\gamma_n^{(1)}$ and $\gamma_n^{(2)}$, respectively, provided $\vartheta_n^{(1)}, \vartheta_n^{(2)} \neq 0$, for all $n \in \mathbb{Z}$. The circumstances when at least one of $\vartheta_n^{(1)}, \vartheta_n^{(2)}$ vanishes, for some integer n, are considered in the next section.

The series equations obtained from the MBC, as given in (8.12)–(8.15), are defined over Ω_{PEC} and Ω_{aper}. Following the same approach as that in Chapter 7, this set of series equations can be reformulated as M independent sets defined over the periodic unit cell $\left(-\frac{\pi}{M}, \frac{\pi}{M}\right)$, which are subsequently regularized individually to an ISLAE of the second kind. Before giving the mathematical formulation to arrive at this final matrix equation, we will first look the circumstances when β_z permits propagating (TM_z or TE_z) modes in this multi-conductor transmission line that are closely related to those of a coaxial transmission line and those of a metallic waveguide. These propagating modes are present when β_z permits coexistence of the TM_z (or TE_z) modes for the two closely related fundamental waveguides, at a particular wavelength λ. The eigenvalues of these modes are independent of the number and angular size of the strips, which affects only the set of series equations given in (8.12)–(8.15). We first outline the eigenvalues corresponding to these modes in next section, then the M infinite systems of the second kind derived from (8.12)–(8.15) are numerically solved for the additional eigenvalues of the problem.

8.4 Relationship with the coaxial line and circular metallic waveguide

We observe in this section, the connection between the eigenvalues for the considered inhomogeneous, multi-conductor transmission line to those of the closely related (homogeneous) coaxial line and dielectric-filled metallic waveguide. The geometry description of these two basic waveguides are given in Figure 8.2. The coaxial line, depicted on the left hand side of Figure 8.2, is formed by two PEC cylinders of radii R_0 and R_1 (where $R_0 > R_1$), and is filled with the same material as that in region (1) of the multi-conductor line; *i.e.*, dielectric loading with relative parameters (ϵ_1, μ_1). The metallic waveguide, depicted on the right hand side of Figure 8.2, is a closed circular waveguide of radius R_1, the interior of which is loaded with the same material as that in region (2) of the multi-conductor line; *i.e.*, dielectric loading with (ϵ_2, μ_2).

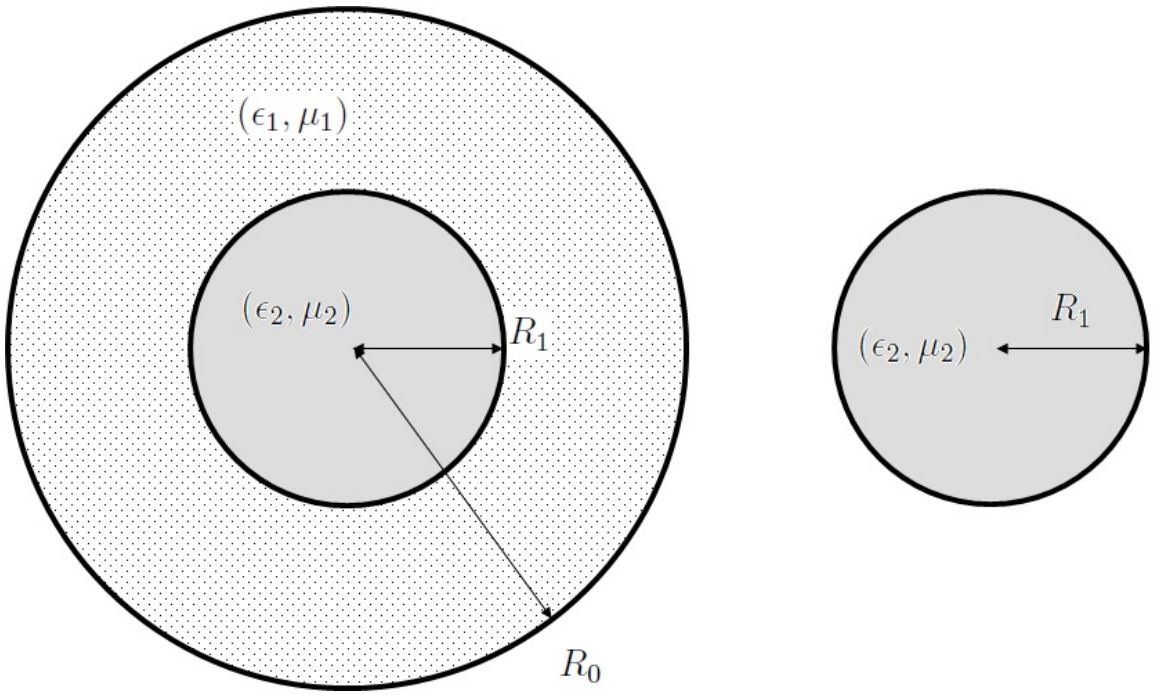

Figure 8.2: Geometry description of the corresponding coaxial line and homogeneous metallic waveguide.

For fixed wavelength λ and some specified problem parameters $R_{0,1}$, $\epsilon_{1,2}$ and $\mu_{1,2}$, and when β_z is such that one of the two separate circumstances below takes place, the fields do not vanish in the multi-conductor line:

1. both $\vartheta_{n_0}^{(1)}$ and $J_{n_0}(\kappa_2 R_1)$ vanishes, for some integer n_0,

2. both $\vartheta_{n_0}^{(2)}$ and $J'_{n_0}(\kappa_2 R_1)$ vanishes, for some integer n_0, when at least one of the following holds:

   (a) $\epsilon_1\mu_1 = \epsilon_2\mu_2$,

   (b) $\beta_z = 0$,

   (c) $n_0 = 0$,

   (d) $\vartheta_{n_0}^{(1)} = 0$,

3. $\det\left[\mathcal{A}_\alpha(\beta_z)\right] = 0$, for at least one of $\alpha \in \{0, 1, \ldots, M-1\}$, where $\mathcal{A}_\alpha$ is the matrix operator derived by the MoR from the α-th member of the set of series equations (8.12)–(8.15).

We examine next the existence of non-trivial solutions to the multi-conductor transmission line problem, corresponding to each of the above mentioned cases. The two cases, (1) and (2), are mutually exclusive as only one of $J_{n_0}(\kappa_2 R_1)$ and $J'_{n_0}(\kappa_2 R_1)$ can vanish at a time. It is also worth noting that the conditions

$$J_{n_0}(\kappa_2 R_1) = 0\,, \tag{8.25}$$

$$J'_{n_0}(\kappa_2 R_1) = 0\,, \tag{8.26}$$

are the characteristic equations of the TM_z and TE_z modes of the metallic waveguide in Figure 8.2.

We begin by considering case (1). From (8.4a) and substituting of the series representation, we arrive at the relationship

$$c_n \vartheta_n^{(1)} \frac{H_n^{'(2)}(\kappa_1 R_0)}{H_n^{(2)}(\kappa_1 R_0)} = a_n^{(2)} J_n(\kappa_2 R_1) H_n^{'(2)}(\kappa_2 R_1)\,. \tag{8.27}$$

For $n = n_0$, as $\vartheta_{n_0}^{(1)} = J_{n_0}(\kappa_2 R_1) = 0$, the dependence of c_{n_0} on $a_{n_0}^{(2)}$ given in (8.5c) no longer holds, and the unknown c_{n_0} becomes a free variable as we now have one less equation. It is worth noting that the set of permissible values of β_z for case (1) to occur is the values of β_z that permit TM_{n_0} modes for both the coaxial line and the metallic waveguide. The coexistence can be planted or removed by careful selection of the dielectric loadings. For example, for $R_0 = \lambda$, $R_1 = 0.5\lambda$, $\epsilon_1 = 2.1$, $\epsilon_2 = 1$, $\mu_{1,2} = 1$, and $n_0 = 0$, the coexistence occurs at $\beta_z = 0.2206$.

When $\vartheta_{n_0}^{(2)}$ and $J'_{n_0}(\kappa_2 R_1)$ vanish, we can derive from (8.4b) that

$$\frac{n_0 k_z}{R_1}\left(\frac{1}{\kappa_1^2} - \frac{1}{\kappa_2^2}\right) a_{n_0}^{(2)} J_{n_0}(\kappa_2 R_1) H_{n_0}^{'(2)}(\kappa_2 R_1) = 0\,. \tag{8.28}$$

When none of case (2a) to (2c) applies, the above equation leads to $a_{n_0}^{(2)} = 0$. We recall that $\kappa_i^2 = k_i^2 - k_z^2$ for $i = 1, 2$, therefore when $\epsilon_1\mu_1 = \epsilon_2\mu_2$, the factor $\left(\frac{1}{\kappa_1^2} - \frac{1}{\kappa_2^2}\right)$ vanishes, and we have one less equation to solve for the unknowns. It is worth noting that, case (2a) corresponds to the homogeneous multi-conductor transmission line, if we consider non-magnetic material where $\mu_{1,2} = 1$. In other words, the coexistence of the TE_{n_0} modes for the coaxial line and metallic waveguide also implies a propagating mode in the homogeneous multi-conductor line. When $\epsilon_1 = \epsilon_2$ is considered, the condition $\vartheta_{n_0}^{(2)} = 0$ reduces to requiring $J_{n_0}(\kappa_1 R_0) = 0$. Therefore, by varying the relative size of the radii R_0 and R_1, the propagating mode corresponding to this situation can be postponed or brought forward. On the other hand, in case (2b), where $\beta_z = 0$, we are considering pure TE_z modes for the multi-conductor line; while in case (2c), where $n_0 = 0$, the lowest order TE_0 modes for the coaxial line and metallic waveguide are considered. In all of cases (2a)–(2c), the unknown c_{n_0} becomes a free variable for the multi-conductor line problem. When no assumption is made on the dielectric loadings and propagation constant β_z, propagating modes exist for the multi-conductor line when we also have $\vartheta_{n_0}^{(1)} = 0$; *i.e.*, the coexistence of the TM_z and TE_z modes for the coaxial line. Under this case, we have $a_{n_0}^{(2)} = 0$ from both of (8.4a) and (8.4b), when $n = n_0$. Therefore, we have at least one less equation than the number of unknowns coefficients (if $\det[\mathcal{A}_\alpha(\beta_z)] \neq 0$, we have exactly one free variable).

The existence of all the propagating modes corresponding to cases (1) and (2) are independent of the MBC on $\rho = R_1$. The most difficult modes to determine are of course those of case (3). At the values of β_z such that none of the cases (1) and (2) occurs, the series equations (8.12)–(8.15) can be transformed into M infinite systems of equations of the following form:

$$[\mathcal{A}_\alpha(\beta_z)]\,\mathbf{x}(\beta_z) = 0\,, \tag{8.29}$$

where $\alpha = 0, 1, \ldots, (M-1)$, $\mathbf{x}$ is the vector consisting the unknown coefficients , $\mathcal{A}_\alpha$ is the α-th matrix operator derived by using the approach detailed in Chapter 7 and the MoR. This matrix equation has non-trivial solutions only for those values of β_z that make the matrix determinant vanish. These values of β_z can be computed by using a root-finding procedure such as Newton's method. In our computation regime, the values of β_z that correspond to case (1) and (2) are predetermined, and subsequently excluded in the root-finding calculation for $\det[\mathcal{A}_\alpha(\beta_z)] = 0$. We will derive in the next section the modifications to problem formulation that are required,

when at least one of the denominators $\vartheta_{n_0}^{(1)}$ and $\vartheta_{n_0}^{(2)}$ vanishes but none of the cases in (1) and (2) applies.

8.4.1 Modifications to the problem formulation

The series equations (8.12)–(8.15) and their parameter definitions given in (8.16)–(8.24) are only valid if $\vartheta_n^{(1)}, \vartheta_n^{(2)} \neq 0$, for all $n \in \mathbb{Z}$. Modifications to these equations when $n = n_0$ are required if $\vartheta_{n_0}^{(i)} = 0$ (for $i = 1, 2$), where n_0 is some integer. We consider the following three cases separately:

1. both $\vartheta_{n_0}^{(1,2)} = 0$, and none of $J_{n_0}(\kappa_2 R_1)$ and $J'_{n_0}(\kappa_2 R_1)$ vanishes;
2. $\vartheta_{n_0}^{(1)} = 0$, and both $\vartheta_{n_0}^{(2)}$, $J_{n_0}(\kappa_2 R_1) \neq 0$; or
3. $\vartheta_{n_0}^{(2)} = 0$, $\vartheta_{n_0}^{(1)} \neq 0$ and none of the cases in (2a)–(2c) in previous subsection applies.

In case (1), from (8.4b), we have $a_{n_0}^{(2)} = 0$ as $\vartheta_{n_0}^{(1)} = 0$, and c_{n_0} is an unknown yet to be determined from the MBC. Similarly, from (8.4a), we have $b_{n_0}^{(2)} = 0$ as $\vartheta_{n_0}^{(2)} = 0$ and $a_{n_0}^{(2)} = 0$, while d_{n_0} is an unknown to be determined from the MBC. Therefore, we replace $a_{n_0}^{(2)}$ and $b_{n_0}^{(2)}$ in the unknown vector $\mathbf{x}$ of the final matrix equation by c_{n_0} and d_{n_0}. The following amendments are made to the parameters of (8.12)–(8.15) to incorporate the changes:

$$o_{n_0} = p_{n_0} = q_{n_0} = r_{n_0} = 0\,, \tag{8.30}$$

while redefining the parameters below:

$$s_{n_0} = J_{n_0}(\kappa_1 R_1) H_{n_0}^{'(2)}(\kappa_1 R_0) - J'_{n_0}(\kappa_1 R_0) H_{n_0}^{(2)}(\kappa_1 R_1)\,, \tag{8.31}$$

$$t_{n_0} = -\epsilon_1 \kappa_2 \frac{H_{n_0}^{'(2)}(\kappa_1 R_0)}{H_{n_0}^{(2)}(\kappa_1 R_0)} \left[J'_{n_0}(\kappa_1 R_1) H_{n_0}^{(2)}(\kappa_1 R_0) - J_{n_0}(\kappa_1 R_0) H_{n_0}^{'(2)}(\kappa_1 R_1) \right]\,, \tag{8.32}$$

$$u_{n_0} = -\frac{n_0 \beta_z \eta_0 \kappa_2}{\kappa_1 R_1} \left[J_{n_0}(\kappa_1 R_1) H_{n_0}^{'(2)}(\kappa_1 R_0) - J'_{n_0}(\kappa_1 R_0) H_{n_0}^{(2)}(\kappa_1 R_1) \right]\,. \tag{8.33}$$

In case (2), similar to the argument given above, as $\vartheta_{n_0}^{(1)} = 0$, we derive from (8.4b) that $a_{n_0}^{(2)} = 0$, and replace $a_{n_0}^{(2)}$ in the unknown vector $\mathbf{x}$ by c_{n_0}. Consequently, from (8.4b), we have

$$d_{n_0} = b_{n_0}^{(2)} \frac{\mu_2 \kappa_1}{\mu_1 \kappa_2} \frac{J'_{n_0}(\kappa_2 R_1) H_{n_0}^{'(2)}(\kappa_2 R_1)}{\vartheta_{n_0}^{(2)}}\,. \tag{8.34}$$

The amendments to case (3) follow in exactly the same manner.

8.5 Regularized systems

Following the same approach as in Chapter 7 and utilizing the identity for the exponential function, these series equations can be equivalently reduced to M independent sets of series equations defined over the unit cell $\left(-\frac{\pi}{M}, \frac{\pi}{M}\right)$. Each of these series equations can subsequently be rewritten in terms of the trigonometric functions to halve the interval of consideration, as outlined in Subsection 7.3.2. The details of these steps are omitted to avoid repetition.

The definitions for the parameters $\{o_n, p_n, q_n\}_{n\in\mathbb{Z}}$ are exactly the same as those in Chapter 4 and Chapter 7. Therefore, we only look at the asymptotic behaviors of the parameters $\left\{r_{\alpha n}^{(\pm)}, s_{\alpha n}^{(\pm)}, t_{\alpha n}^{(\pm)}, u_{\alpha n}^{(\pm)}\right\}_{n=1}^{\infty}$ (defined in (7.19)). As $n \to \infty$, these parameters have the following magnitudes

$$r_{\alpha n}^{(+)} = \begin{cases} 0, \text{ for } \alpha = 0 \\ \dfrac{j\beta_z}{\eta_0}\left(1 - \dfrac{\kappa_1^2}{\kappa_2^2}\right) O\left(\dfrac{\kappa_2^2 R_1^2}{n^2}\right), \text{ otherwise,} \end{cases} \tag{8.35}$$

$$r_{\alpha n}^{(-)} = \frac{j\beta_z}{\eta_0}\left(1 - \frac{\kappa_1^2}{\kappa_2^2}\right)\left\{1 + O\left(\frac{\kappa_2^2 R_1^2}{n^2}\right)\right\}, \tag{8.36}$$

$$s_{\alpha n}^{(+)} = \left(1 + j\mu_1 \frac{\kappa_1^2}{\kappa_2^2}\right)\left\{1 + O\left(\frac{\kappa_2^2 R_1^2}{n^2}\right)\right\}, \tag{8.37}$$

$$s_{\alpha n}^{(-)} = \begin{cases} 0, \text{ for } \alpha = 0, \\ \left(j - \mu_1 \dfrac{\kappa_1^2}{\kappa_2^2}\right) O\left(\dfrac{\kappa_2^2 R_1^2}{n^2}\right), \text{ otherwise,} \end{cases} \tag{8.38}$$

$$t_{\alpha n}^{(+)} = \frac{\zeta M n}{\beta_z \eta_0}\left\{1 + O\left(\frac{\kappa_2^2 R_1^2}{n^2}\right)\right\}, \tag{8.39}$$

$$t_{\alpha n}^{(-)} = \begin{cases} 0, \text{ for } \alpha = 0, \\ \dfrac{\zeta\alpha}{\beta_z\eta_0} O\left(\dfrac{\kappa_2^2 R_1^2}{n^2}\right), \text{ otherwise,} \end{cases} \tag{8.40}$$

$$u_{\alpha n}^{(+)} = \begin{cases} 0, \text{ for } \alpha = 0, \\ \alpha\left(1 + j\mu_1\right)\left\{1 + O\left(\dfrac{\kappa_2^2 R_1^2}{n^2}\right)\right\}, \text{ otherwise,} \end{cases} \tag{8.41}$$

$$u_{\alpha n}^{(-)} = Mn\left(1 + j\mu_1\right)\left\{1 + O\left(\frac{\kappa_2^2 R_1^2}{n^2}\right)\right\}, \tag{8.42}$$

where

$$\zeta := -j + \epsilon_r \frac{\kappa_1^2}{\kappa_2^2} - j\beta_z^2\left(1 - \frac{\kappa_1^2}{\kappa_2^2}\right). \tag{8.43}$$

From the above observations, we can introduce the following asymptotically small

parameters:

$$\tilde{r}_{\alpha n}^{(+)} = \begin{cases} 0, \text{ for } \alpha = 0, \\ \dfrac{j\pi\kappa_2 R_1}{1 + j\frac{\mu_2\kappa_1^2}{\mu_1\kappa_2^2}} r_{\alpha n}^{(+)}, \text{ otherwise,} \end{cases} \tag{8.44a}$$

$$\tilde{r}_{\alpha n}^{(-)} = 1 + \frac{\pi\eta_1\kappa_2 R_1}{j\beta_z\left(1 - \frac{\kappa_1^2}{\kappa_2^2}\right)} r_{\alpha n}^{(-)}, \tag{8.44b}$$

$$\tilde{s}_{\alpha n}^{(+)} = 1 - \frac{j\pi\kappa_2 R_1}{1 + j\frac{\mu_2\kappa_1^2}{\mu_1\kappa_2^2}} s_{\alpha n}^{(+)}, \tag{8.44c}$$

$$\tilde{s}_{\alpha n}^{(-)} = \begin{cases} 0, \text{ for } \alpha = 0, \\ \dfrac{j\pi\kappa_2 R_1}{1 + j\frac{\mu_2\kappa_1^2}{\mu_1\kappa_2^2}} s_{\alpha n}^{(-)}, \text{ otherwise,} \end{cases} \tag{8.44d}$$

$$\tilde{t}_{\alpha n}^{(+)} = 1 - \frac{j\pi\kappa_1 R_1^2}{\zeta M n} t_{\alpha n}^{(+)}, \tag{8.44e}$$

$$\tilde{t}_{\alpha n}^{(-)} = \begin{cases} 1, \text{ for } \alpha = 0, \\ 1 - \dfrac{j\pi\kappa_1 R_1^2}{\zeta\alpha} t_{\alpha n}^{(-)}, \text{ otherwise,} \end{cases} \tag{8.44f}$$

$$\tilde{u}_{\alpha n}^{(+)} = \begin{cases} 1, \text{ for } \alpha = 0, \\ 1 + \dfrac{\pi\kappa_2^2 R_1^2}{\eta_0\kappa_1\alpha\left(1 + j\frac{\mu_2}{\mu_1}\right)\beta_z} u_{\alpha n}^{(+)}, \text{ otherwise,} \end{cases} \tag{8.44g}$$

$$\tilde{u}_{\alpha n}^{(-)} = 1 + \frac{\pi\kappa_2^2 R_1^2}{\eta_1\kappa_1\left(1 + j\frac{\mu_2}{\mu_1}\right) M n\beta_z} u_{\alpha n}^{(-)}. \tag{8.44h}$$

For each fixed α, four sets of DSE involving $\left\{x_n^{(i)}, y_n^{(i)}\right\}_{n=1}^{\infty}$ $(i = 0, 1)$ of the following form are derived upon the substitution of the introduced asymptotically small parameters:

$$\begin{cases} x_{\alpha 0}^{(1)}\tilde{o}_\alpha + \sum\limits_{n=1}^{\infty}\left[x_{\alpha n}^{(1)}\left(1 - \tilde{o}_{\alpha n}^{(+)}\right) + y_{\alpha n}^{(1)}\tilde{o}_{\alpha n}^{(-)}\right]\cos n\phi = 0\,(A), \quad \phi \in (0, \phi_0), & (8.45a) \\ x_{\alpha 0}^{(1)}\tilde{t}_{\alpha 0} + x_{\alpha 0}^{(2)}\tilde{u}_{\alpha 0} + \tilde{z}_{\alpha 0} + \sum\limits_{n=1}^{\infty}\Big[nx_{\alpha n}^{(1)}\left(1 - \tilde{t}_{\alpha n}^{(+)}\right) + y_{\alpha n}^{(1)}\left(1 - \tilde{t}_{\alpha n}^{(-)}\right)\frac{\alpha}{M} \\ \quad + x_{\alpha n}^{(2)}\left(1 - u_{\alpha n}^{(+)}\right)\frac{\alpha}{M}\varsigma + ny_{\alpha n}^{(2)}\left(1 - u_{\alpha n}^{(-)}\right)\varsigma\Big]\cos n\phi = 0\,(A), \quad \phi \in (\phi_0, \pi), & (8.45b) \end{cases}$$

$$
\begin{cases}
\displaystyle\sum_{n=1}^{\infty}\Big[nx_{\alpha n}^{(1)}\left(1-\tilde{p}_{\alpha n}^{(-)}\right)\xi+y_{\alpha n}^{(1)}\left(1-\tilde{p}_{\alpha n}^{(+)}\right)\frac{\alpha}{M}\xi \\
\quad +x_{\alpha n}^{(2)}\left(1-\tilde{q}_{\alpha n}^{(-)}\right)\frac{\alpha}{M}+ny_{\alpha n}^{(2)}\left(1-\tilde{q}_{\alpha n}^{(+)}\right)\Big]\sin n\phi=0\,(A), \quad \phi\in(0,\phi_0), & (8.46a)\\
\displaystyle\sum_{n=1}^{\infty}\left[x_{\alpha n}^{(1)}\left(1-\tilde{r}_{\alpha n}^{(-)}\right)\tau+y_{\alpha n}^{(1)}\tilde{r}_{\alpha n}^{(+)}\right. \\
\quad \left.+x_{\alpha n}^{(2)}\tilde{s}_{\alpha n}^{(-)}+y_{\alpha n}^{(2)}\left(1-\tilde{s}_{\alpha n}^{(+)}\right)\right]\sin n\phi=0\,(A), \quad \phi\in(\phi_0,\pi), & (8.46b)
\end{cases}
$$

$$
\begin{cases}
x_{\alpha 0}^{(1)}\tilde{p}_{\alpha 0}+x_{\alpha 0}^{(2)}\tilde{q}_{\alpha 0}+\displaystyle\sum_{n=1}^{\infty}\Big[x_{\alpha n}^{(1)}\left(1-\tilde{p}_{\alpha n}^{(+)}\right)\frac{\alpha}{M}\xi+ny_{\alpha n}^{(1)}\left(1-\tilde{p}_{\alpha n}^{(-)}\right)\xi \\
\quad +nx_{\alpha n}^{(2)}\left(1-q_{\alpha n}^{(+)}\right)+y_{\alpha n}^{(2)}\left(1-q_{\alpha n}^{(-)}\right)\frac{\alpha}{M}\Big]\cos n\phi=0\;(A), \quad \phi\in(0,\phi_0), & (8.47a)\\
x_{\alpha 0}^{(1)}\tilde{r}_{\alpha 0}+\tilde{x}_{\alpha 0}^{(2)}s_{\alpha 0}+\displaystyle\sum_{n=1}^{\infty}\left[x_{\alpha n}^{(1)}\tilde{r}_{\alpha n}^{(+)}+y_{\alpha n}^{(1)}\left(1-\tilde{r}_{\alpha n}^{(-)}\right)\tau\right. \\
\quad \left.+x_{\alpha n}^{(2)}\left(1-\tilde{s}_{\alpha n}^{(+)}\right)+y_{\alpha n}^{(2)}\tilde{s}_{\alpha n}^{(-)}\right]\cos n\phi=0\;(A), \quad \phi\in(\phi_0,\pi), & (8.47b)
\end{cases}
$$

$$
\begin{cases}
\displaystyle\sum_{n=1}^{\infty}\left[x_{\alpha n}^{(1)}\tilde{o}_{\alpha n}^{(-)}+y_{\alpha n}^{(1)}\left(1-\tilde{o}_{\alpha n}^{(+)}\right)\right]\sin n\phi=0\;(A), \quad \phi\in(0,\phi_0), & (8.48a)\\
\displaystyle\sum_{n=1}^{\infty}\Big[x_{\alpha n}^{(1)}\left(1-\tilde{t}_{\alpha n}^{(-)}\right)\frac{\alpha}{M}+ny_{\alpha n}^{(1)}\left(1-\tilde{t}_{\alpha n}^{(+)}\right)+nx_{\alpha n}^{(2)}\left(1-\tilde{u}_{\alpha n}^{(-)}\right)\varsigma \\
\quad +y_{\alpha n}^{(2)}\left(1-\tilde{u}_{\alpha n}^{(+)}\right)\frac{\alpha}{M}\varsigma\Big]\sin n\phi=0\;(A), \quad \phi\in(\phi_0,\pi), & (8.48b)
\end{cases}
$$

where $\{\tilde{o}_\alpha,\tilde{p}_\alpha,\tilde{q}_\alpha\}$ are as defined in (7.30b), while $\left\{\tilde{t}_\alpha,\tilde{u}_\alpha,\tilde{z}_\alpha\right\}$ are defined as in (7.30c) and (7.30d) with the redefined ζ value in (8.43). On the other hand, we redefine $\tilde{r}_\alpha$ and $\tilde{s}_\alpha$ as

$$
\tilde{r}_\alpha := \frac{j\pi\kappa_2^3 R_1}{\kappa_2^2+j\frac{\mu_1}{\mu_2}\kappa_1^2}\,r_\alpha\,, \tag{8.49a}
$$

$$
\tilde{s}_\alpha := \frac{j\pi\kappa_2^3 R_1}{\kappa_2^2+j\frac{\mu_1}{\mu_2}\kappa_1^2}\,s_\alpha\,. \tag{8.49b}
$$

Due to the great similarity, the ISLAE obtained after the regularization process is the same as that in Chapter 7, and we omit the details to avoid repetition. The ISLAE derived can be written in the following matrix operator form. The resulting 4-by-4 block matrix operator is the homogenous form of that in (7.44); *i.e.*,

$$
\left[\mathcal{I}+\varsigma\,\mathcal{I}^t-\mathcal{C}_1+\mathcal{H}\,\mathcal{C}_2\right]\begin{pmatrix}\mathbf{x}_1\\ \mathbf{y}_1\\ \mathbf{x}_2\\ \mathbf{y}_2\end{pmatrix}=\mathbf{0}\,. \tag{8.50}
$$

The matrix operators $\mathcal{C}_1, \mathcal{C}_2$ and $\mathcal{H}$ are as defined in (7.45), where the only difference lying in the definitions of the asymptotically small parameters $\left\{\tilde{r}_{\alpha n}^{(\pm)}, \tilde{s}_{\alpha n}^{(\pm)}, \tilde{t}_{\alpha n}^{(\pm)}, \tilde{u}_{\alpha n}^{(\pm)}\right\}_{n=1}^{\infty}$ involved in $\mathcal{C}_1$ and $\mathcal{C}_2$.

8.6 Evaluation of the cutoff wavenumbers

The cutoff wavenumbers $\kappa_{1,2}$ occur as arguments to the Bessel and Hankel functions. As for a given wavelength (or frequency), the cutoff wavenumber is defined as $\kappa_i^2 = k_0^2\left(\epsilon_i\mu_i - \beta_z^2\right)$, for $i = 1, 2$. The problem therefore reduces to finding the values of β_z, at which at least one of the matrix operators $\mathcal{A}_\alpha$ for $\alpha = 0, 1, \ldots, (M-1)$ is singular. As each of the matrices $\mathcal{A}_\alpha$ for $\alpha = 0, 1, \ldots, (M-1)$ is non-symmetric and complex-valued, the determinant of each is thus complex-valued.

The values of β_z corresponding to non-trivial solution of the systems are given in Figure 8.3. In the figure, a multi-conductor transmission line of the following characteristics is considered: $M = 2$, $\theta^{\text{PEC}} = \frac{\pi}{6}$, $R_0 = 1$, $R_1 = 0.5$, $k_0 = 10$, $\epsilon_1 = 1$, $\mu_1 = 1$, $\epsilon_2 = 2.1$ and $\mu_2 = 1$. The determinant of the two block matrices are computed for increasing values of β_z, for $\alpha = 0, 1$. We have used the truncation number of $N_{\text{tr}} = 50$ in our computation. When one of the determinant values vanishes, a propagating mode is said to be present at that particular value of β_z.

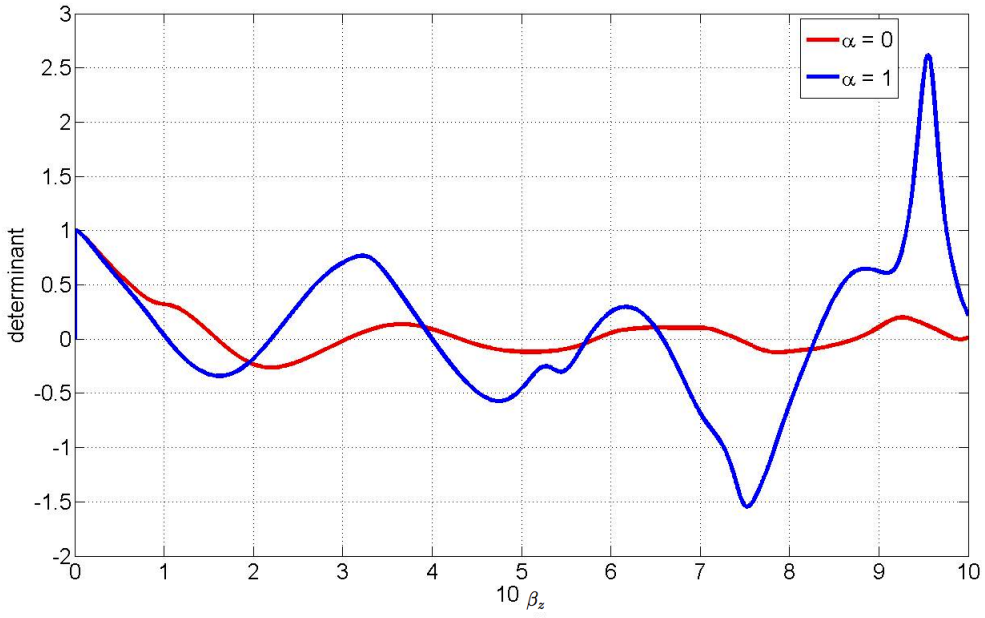

Figure 8.3: The determinant values of the matrix operators for $\alpha = 0$ (red) and 1 (blue), for the microstrip line with two conductors ($M = 2$) each of width $\frac{\pi}{3}$.

To find the cutoff wavenumber for this structure, we have also plotted the absolute values of $\vartheta_n^{(1,2)}$, $J_n(\kappa_2 R_1)$ and $J_n'(\kappa_2 R_1)$, for $n = 0, 1, \ldots, 2N_{\text{tr}}$. The minimum absolute values of these functions are plotted against β_z, with step size of 0.0001 in β_z. From Figure 8.4, we can see that the possible cutoff wavenumber β_z is less than 1. We take a closer look at these functions in order to find the values of β_z such that either of the pairs: "$\vartheta_{n_0}^{(1)}$ and $J_{n_0}(\kappa_2 R_1)$" or "$\vartheta_{n_0}^{(2)}$ and $J_{n_0}'(\kappa_2 R_1)$" vanish together for the some $n_0 = 0, 1, \ldots, 2N_{\text{tr}}$ We can see that, for $n = 0, 1, \ldots, 100$, $\vartheta_n^{(1)}$ vanishes when $\beta_z = 0.3942$, 0.5627, 0.6662, 0.7319, 0.7689 and 0.7809; while $J_n(\kappa_2 R_1)$ may be vanishing at $\beta_z = 0.7863$. These values are read from the top and bottom figures in Figure 8.5, respectively. As none of these values coincide, we do not need to proceed to checking that the eigenvalues actually correspond to the same order n of both $\vartheta_n^{(1)}$ and $J_n(\kappa_2 R_1)$. On the other hand, $\vartheta_n^{(2)}$ vanishes when $\beta_z = 0.2666$, 0.4681, 0.6207, 0.6657, 0.708, 0.7544, 0.7734, 0.8557, 0.9184, 0.9634 and 0.9908; while $J_n'(\kappa_2 R_1)$ may be vanishing around $\beta_z = 0.4533$ and 0.909. These values are read from the top and bottom figures in Figure 8.6, respectively. After having a closer look at the values of β_z in the intervals $(0.4533, 0.4681)$ and $(0.9090, 0.9184)$, we conclude that, in these intervals, $\vartheta_{n_0}^{(2)}$ and $J_{n_0}'(\kappa_2 R_1)$ never vanish at the same time, for all of $n_0 = 0, 1, \ldots$ Therefore, the cutoff wavenumber of this line comes from the eigenvalue of $[\mathcal{I} + \varsigma \mathcal{I}^t - \mathcal{C}_1 + \mathcal{H}\mathcal{C}_2]$.

8.7 Comments and conclusion

An accurate and mathematical rigorous analysis method for the multi-conductor transmission line with periodic strip has been proposed in this chapter. The hybrid mode case has been considered. The solution computed with the use of the MoR enjoys the benefits of guaranteed convergence, as well as numerical and theoretical stability.

In this chapter, the analysis is carried out on the assumption that $\epsilon_{r1}\mu_{r1} < \epsilon_{r2}\mu_{r2}$, and thus, the dominant mode has normalized propagation coefficient $\beta_z = \frac{k_z}{k_0}$ in the interval $(\epsilon_{r1}\mu_{r1}, \epsilon_{r2}\mu_{r2})$. We wish to extend the analysis of the roots of the characteristic equation for β_z from the interval $(0, \epsilon_{r1}\mu_{r1})$ to the interval $(0, \epsilon_{r2}\mu_{r2})$ in the future.

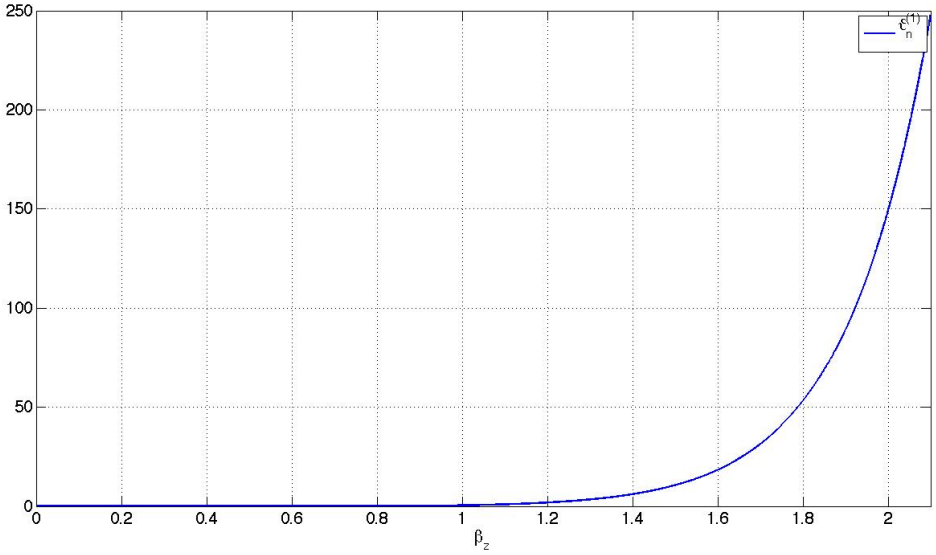

(a) $\vartheta_n^{(1)}$

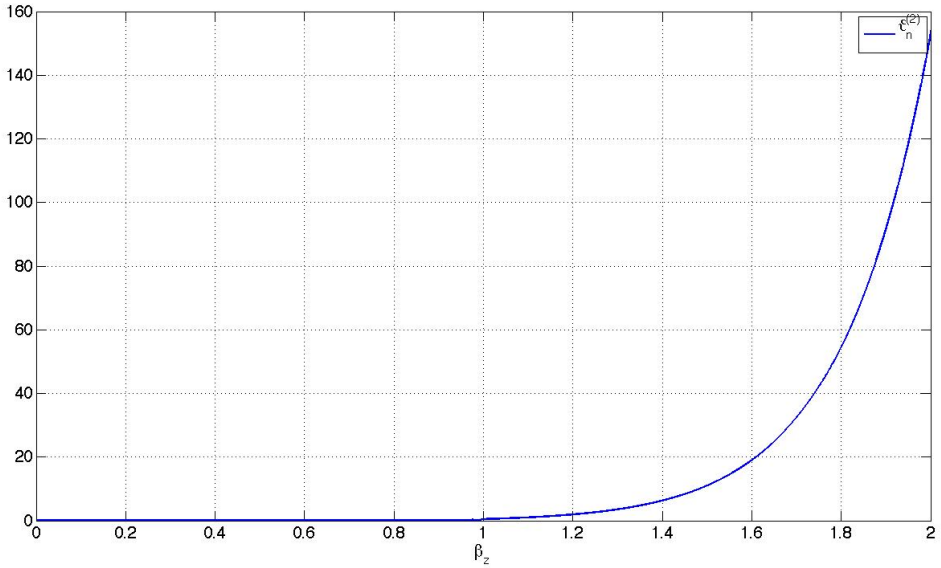

(b) $\vartheta_n^{(2)}$

Figure 8.4: The minimum absolute values of $\vartheta_n^{(1)}$ and $\vartheta_n^{(2)}$, for $n = 0, 1, \ldots, MN_{\text{tr}}$.

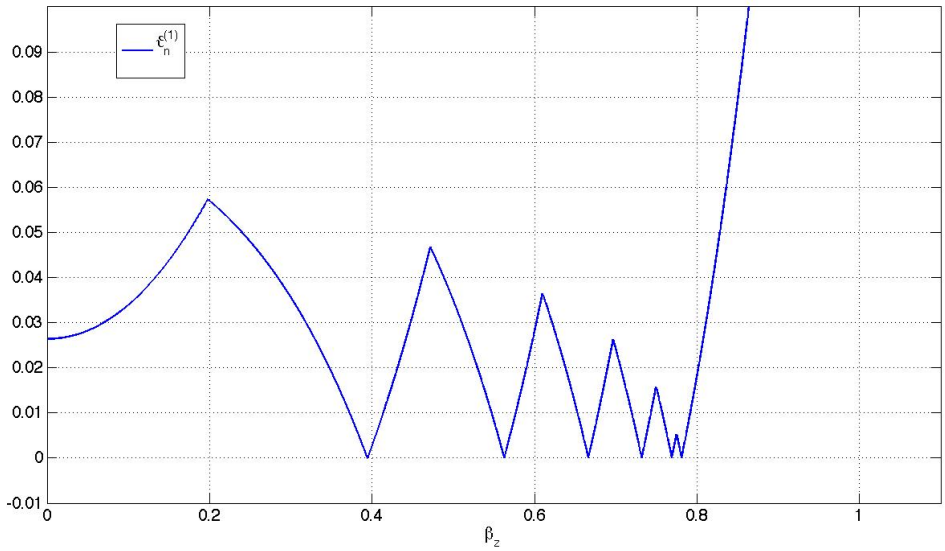

(a) $\vartheta_n^{(1)}$

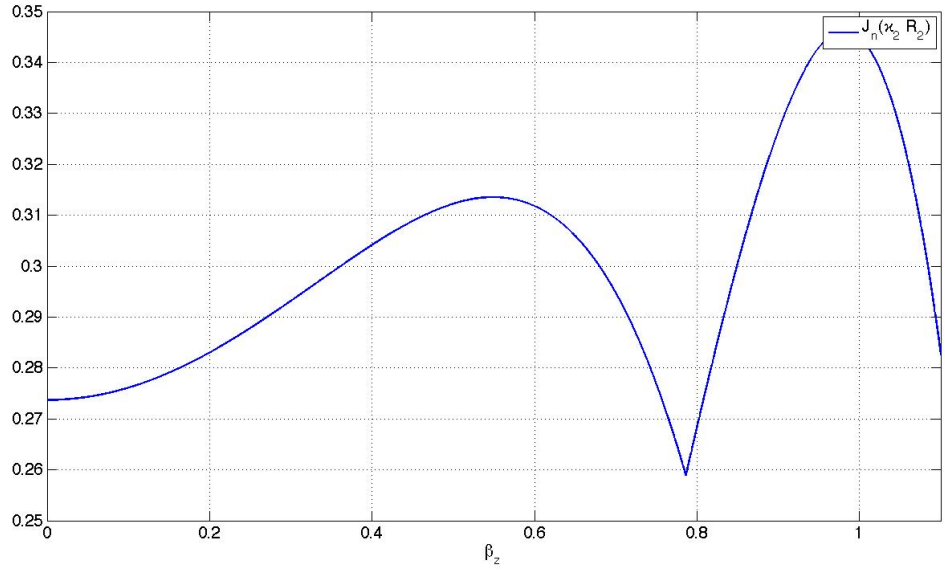

(b) $J_n(\kappa_2 R_1)$

Figure 8.5: The minimum absolute values of $\vartheta_n^{(1)}$ and $J_n(\kappa_2 R_1)$, for $n = 0, 1, \ldots, MN_{\text{tr}}$. When both functions vanish at the same time, β_z is a possible propagating mode corresponding to case (1).

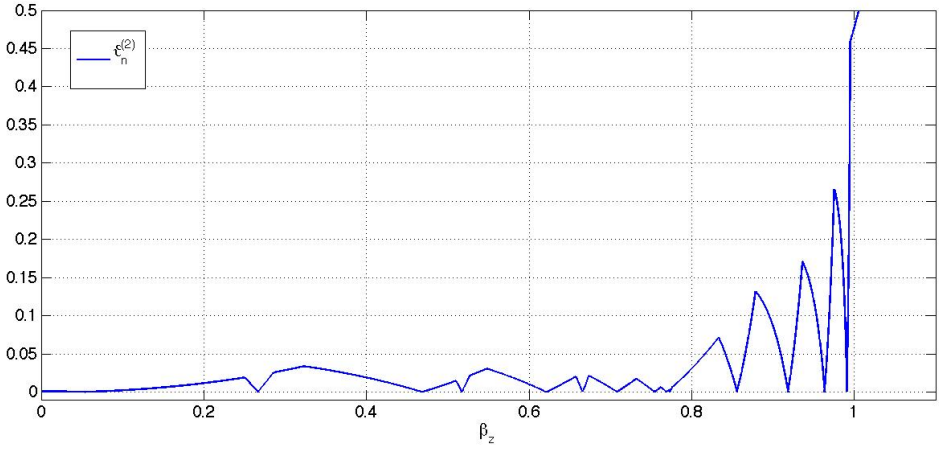

(a) $\vartheta_n^{(2)}$

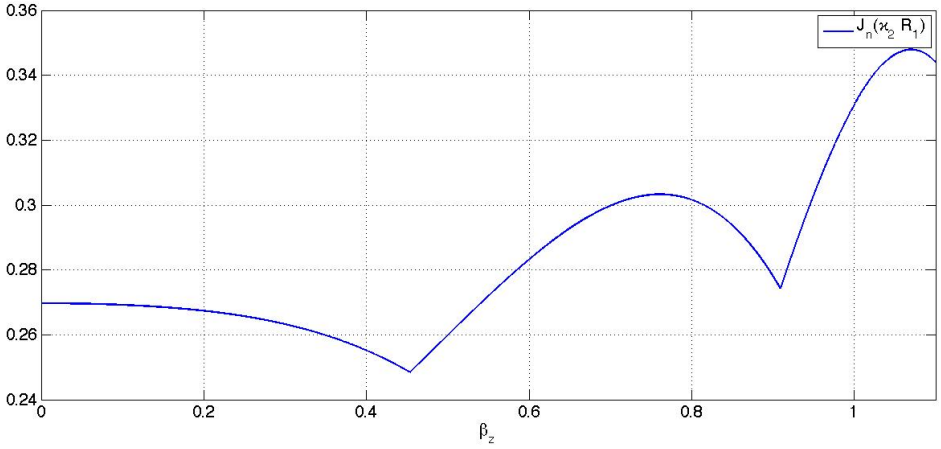

(b) $J_n'(\kappa_2 R_1)$

Figure 8.6: The minimum absolute values of $\vartheta_n^{(2)}$ and $J_n'(\kappa_2 R_1)$, for $n = 0, 1, \ldots, MN_{\text{tr}}$. When both functions vanish at the same time, β_z is a possible propagating mode corresponding to case (2).

Chapter 9

Conclusions

The research work documented in this thesis extends the MoR presented in [84] to the analysis of a wider selection of open, dielectric cylindrical structures. The modeling for the interaction of electromagnetic fields with these structures has been driven by their myriad of practical applications in fields ranging from radar, antenna design, telecommunications, and other imaging technologies. Accurate and reliable predictions of the interaction is fundamental in the assessment of behaviors and compatibility of these electrical devices and equipment.

Due to the discontinuities of the boundary condition on the contour of the cylindrical structures considered, the Maxwell's equations are essentially a MBVP. A wide selection of numerical methods have been presented over the last few decades to solve these problems. Many of them enjoy the advantages of being applicable to wide classes of general structures, and easy to implement. However, it is often hard to ascertain the accuracy and convergence of the computed solution of these numerical methods, especially in the vicinity of the sharp edges. The advantage of employing the semi-analytical MoR is to transform the Maxwell's equations to a well-conditioned system, so that when numerical matrix inversion is applied, the instability of the computed solution can be eliminated. The approach based upon the MoR is also uniformly valid for a wide frequency range, including at or near the resonant frequency. Any preassigned accuracy level can be achieved, by taking sufficiently large truncation number of the infinite system, before numerical inversion of the matrix. The solutions hence computed give reliable benchmark results for a wider class of problems with increased complexity where the analysis based on MoR becomes impossible, and purely numerical approaches must be employed.

The study of an axially-slotted PEC cylinder excited by a normal plane wave based on the MoR, together with various problems involving open spherical and spheroidal structures, was originally reported in [85]. For the first problem considered in this

thesis, this semi-analytical method is extended to its 3D counterpart when the CLR is illuminated by an oblique incident plane wave (bot TM_z and TE_z cases). Under the oblique incidence, both E- and H- polarizations are mixed, and when solved simultaneously using the MoR, two decoupled 2-by-2 block matrix equations of the second kind Fredholm are obtained. Chapter 4 contains the first rigorous treatment of this problem imposing the analytical regularization approaches that have previously appeared in the literature. Extensive numerical validation of the formulation and codes have been carried out using both internal and external tests. The computed solution is also tested for warranty of stability and convergence numerically. We also propose an approach to accelerate the series convergence of physical quantities, with details given for the case of J_z particularly. It is observed that, by choosing $N_{\mathrm{tr}} \approx [\kappa_1 R + 100]$, a 3 decimal places accuracy can be guaranteed for the computation of RCS. As the oblique incident angle, where $\theta_z^{\mathrm{pw}} \in \left(0, \frac{\pi}{2}\right)$, decreases in value, more energy is stored in the interior of the CLR (as the wave propagates down the cylinder) and less is diffracted back. In addition, the surface current possess both the z- and ϕ-components, for an oblique incident problem. As θ_z^{pw} moves away from $\frac{\pi}{2}$, the value of J_z decreases, while that of J_ϕ increases.

In Chapter 5, we can see that by properly selecting the location and size of the reflecting strip, as well as the dielectric constant of a CLR, enhancement and control of the RCS can be achieved. The desirability of the CLR (a cylindrical reflector based on a Constant K-lens) is compared with that of a CLLR (a cylindrical reflector based on a stepped-index Luneburg lens) through the studies of their spectral dependence of the RCS at a wide frequency range, and also their scanning properties at varying incident angle of the incoming plane wave. The focal spot locations of the Constant K-lens (with $\epsilon_r = 2.1$, 2.4, 3.0 and 3.5) are calculated by examining the energy density distribution, resulting from the plane wave scattering. These locations are then used for proper placement of the PEC strip of the CLR, in order to achieve optimal illumination by the focused electromagnetic flux. We observe that the CLR constructed with Constant K-lens of lower dielectric constant ϵ_r offers a more stable and reasonably high spectral dependence of the RCS, compared to those constructed with higher dielectric constant material. In addition, the scanning properties of the CLR outperforms those of the CLLR of up to 7 layers, especially at higher frequencies. We conclude that the CLR provides a cheaper and superior alternative to the CLLR (of up to 7 layers), as it offers smoother and stronger spectral dependence of the backscattering RCS, as well as better scanning performance.

In Chapter 6, a finite number M of parallel CLR (each with arbitrary size, PEC strip width and dielectric loading) are assumed located in the vicinity of one another. The scattering problem of a plane wave diffracted by these CLR is studied using the MoR. Due to the close proximity of the reflectors, the mutual interaction among them are not to be omitted in the formulation. We take the sum of the incident plane wave and all the scattered fields from other CLR to be the incident wave on each of the individual cylinder. MBC on each of the surface of the M CLR are imposed separately, and the resulted $2M$ sets of DSE are solved simultaneously using the MoR.

The MoR has also been generalized to solve the scattering problem when an arbitrary number M of conformal PEC strips are placed on a cylindrical lens. The method was originally applied to solve the potential problem involving a toroidal conductor with 2^M cuts, by first formulating the problem as a triple series equations, then exploiting the symmetry property of the Jacobi polynomials, and connecting the Jacobi polynomials with the ultraspherical polynomials in [84]. The process is repeatedly applied, halving the interval at each step, until the interval for which the series equations are defined over is reduced down to that of the periodic unit cell. The new proposed approach is less tedious in the formulation, and is applicable for a scattering problem as well as when odd number of strips are considered. Enclosing this multi-conductor cylinder gives us a grounded transmission line, which is considered in the last chapter. The hybrid electromagnetic mode (HEM) of such a multi-conductor transmission line is solved by the MoR, and the cutoff frequency is computed. We can see that there is a strong connection between the eigenvalues for the multi-conductor transmission line to those for a closed coaxial line and a metallic waveguide.

Appendix A

Vectors

A.1 Vector identities

$$\mathbf{a}\cdot(\mathbf{b}\times\mathbf{c}) = \mathbf{b}\cdot(\mathbf{c}\times\mathbf{a}) = \mathbf{c}\cdot(\mathbf{a}\times\mathbf{b})\ , \tag{A.1}$$

$$\mathbf{a}\times(\mathbf{b}\times\mathbf{c}) = (\mathbf{a}\cdot\mathbf{c})\,\mathbf{b} - (\mathbf{a}\cdot\mathbf{b})\,\mathbf{c}\,, \tag{A.2}$$

$$\nabla\cdot(\mathbf{a}\times\mathbf{b}) = \mathbf{b}\cdot(\nabla\times\mathbf{a}) - \mathbf{a}\cdot(\nabla\times\mathbf{b})\ , \tag{A.3}$$

$$\nabla\times(\nabla\times\mathbf{a}) = \nabla\,(\nabla\cdot\mathbf{a}) - (\nabla\cdot\nabla)\,\mathbf{a}\,. \tag{A.4}$$

A.2 Relationships among unit vectors

Denote the unit vectors encountered in the Cartesian coordinates by $(\mathbf{i}_x, \mathbf{i}_y, \mathbf{i}_z)$ and those in the polar cylindrical coordinates by $(\mathbf{i}_\rho, \mathbf{i}_\phi, \mathbf{i}_z)$. Suppose ϕ is the angle $\mathbf{i}_\rho$ at a fixed point makes with the positive $x-$axis. The relationships among these unit vectors are

$$\mathbf{i}_x = \cos\phi\,\mathbf{i}_\rho - \sin\phi\,\mathbf{i}_\phi\,, \tag{A.5a}$$

$$\mathbf{i}_y = \sin\phi\,\mathbf{i}_\rho + \cos\phi\,\mathbf{i}_\phi\,, \tag{A.5b}$$

and

$$\mathbf{i}_\rho = \cos\phi\mathbf{i}_x + \sin\phi\mathbf{i}_y\,, \tag{A.6a}$$

$$\mathbf{i}_\phi = -\sin\phi\mathbf{i}_x + \cos\phi\mathbf{i}_y\,. \tag{A.6b}$$

Appendix B

Special functions

The formulas and identities of the special functions used in the problem formulations are listed in this section. More extended and thorough treatments of these special functions, including those not used in this thesis, can be found in [1, 45, 52, 87].

B.1 Gamma functions

The Gamma function, $\Gamma(x)$, is defined as

$$\Gamma(x) := \int_0^\infty t^{x-1} e^{-t} \mathrm{d}t \,. \tag{B.1}$$

From this integral definition, we can see that $\Gamma(x)$ is an analytic function of x, $\forall \mathrm{Re}(x) > 0$. When x is an non-negative integer n,

$$\Gamma(n) = (n-1)! \,. \tag{B.2}$$

The following are some useful properties of $\Gamma(x)$ that have been established:

$$\Gamma(x+1) = x\Gamma(x) \,, \tag{B.3}$$

$$\Gamma(x)\Gamma(1-x) = \frac{\pi}{\sin(\pi x)} \,, \tag{B.4}$$

$$\Gamma(x) \approx \sqrt{\frac{2\pi}{x}} e^{x \ln x - x} \,, \text{ as } z \to \infty \tag{B.5}$$

$$\int_0^1 t^{p-1}(1-t)^{q-1} \mathrm{d}t = \frac{\Gamma(p)\Gamma(q)}{\Gamma(p+q)} \,. \tag{B.6}$$

B.2 Bessel functions

The Bessel function of the first kind $J_\nu(x)$ (also called the Bessel function) and the second kind $Y_\nu(x)$ (also called the Neumann function) are the commonly employed solutions to the Bessel's equation of order ν

$$x^2\frac{\mathrm{d}^2y}{\mathrm{d}x^2}+x\frac{\mathrm{d}y}{\mathrm{d}x}+\left(x^2-\nu^2\right)y=0\,. \tag{B.7}$$

For non-integer ν, $J_\nu(x)$ and $Y_\nu(x)$ are defined respectively as

$$J_\nu(x):=\sum_{m=0}^{\infty}\frac{(-1)^m}{m!\Gamma(m+\nu+1)}\left(\frac{x}{2}\right)^{2m+\nu}\,, \tag{B.8}$$

$$Y_\nu(x):=\frac{J_\nu(x)\cos(\nu\pi)-J_{-\nu}(x)}{\sin(\nu\pi)}\,. \tag{B.9}$$

For integer-valued $\nu=n$, the functions take the following forms, where $\Psi(m)=1+1/2+1/3+\ldots+1/m$ and $\gamma=0.577215\ldots$ is the Euler's constant

$$J_n(x):=\sum_{m=0}^{\infty}\frac{(-1)^m}{m!(m+n)!}\left(\frac{x}{2}\right)^{2m+n}\,, \tag{B.10}$$

$$\begin{aligned}Y_n(x):=&\frac{2}{\pi}J_n(x)\log\left(\frac{e^\gamma x}{2}\right)-\frac{1}{\pi}\sum_{m=0}^{n-1}\frac{(n-m-1)!}{m!}\left(\frac{x}{2}\right)^{2m-n}\\&-\frac{1}{\pi}\sum_{m=0}^{\infty}\left[\Psi(m)+\Psi(n+m)\right]\frac{(-1)^m}{m!(n+m)!}\left(\frac{x}{2}\right)^{2m+n}\,.\end{aligned} \tag{B.11}$$

Alternative solutions to the Bessel's equation (B.7) are the Hankel functions of the first kind $H_\nu^{(1)}(x)$ and the second kinds $H_\nu^{(2)}(x)$,

$$H_\nu^{(1)}(x):=J_\nu(x)+jY_\nu(x)\,, \tag{B.12}$$

$$H_\nu^{(2)}(x):=J_\nu(x)-jY_\nu(x)\,. \tag{B.13}$$

Any two of the four functions, $J_\nu(x)$, $Y_\nu(x)$, $H_\nu^{(1)}(x)$ and $H_\nu^{(2)}(x)$, form a pair of linearly-independent solutions to (B.7).

B.2.1 Some useful properties

Let $B_n(x)$ represent generically $J_n(x)$, $Y_n(x)$, $H_n^{(1)}(x)$, $H_n^{(2)}(x)$, or a linear combination of them.

Recurrence relations:

$$B_{-n}(x)=(-1)^nB_n(x)\,, \tag{B.14}$$

$$\frac{2\nu}{x}B_\nu(x) = B_{\nu-1}(x) + B_{\nu+1}(x)\,, \tag{B.15}$$

$$\frac{\mathrm{d}}{\mathrm{d}x}B_\nu(x) = \tfrac{1}{2}\left[B_{\nu-1}(x) - B_{\nu+1}(x)\right]\,. \tag{B.16}$$

Wronskian identity:

$$J_\nu(x)H_\nu^{'(2)}(x) - J_\nu^{'}(x)H_\nu^{(2)}(x) = -\frac{2j}{\pi x}\,. \tag{B.17}$$

Large argument approximations ($x \gg n$):

$$J_n(x) \approx \sqrt{\frac{2}{\pi x}}\cos\left(x - \frac{2n+1}{4}\pi\right)\,, \tag{B.18}$$

$$Y_n(x) \approx \sqrt{\frac{2}{\pi x}}\sin\left(x - \frac{2n+1}{4}\pi\right)\,, \tag{B.19}$$

$$H_n^{(1)}(x) \approx \sqrt{\frac{2}{\pi x}}e^{j\left(x-\frac{2n+1}{4}\pi\right)}\,, \tag{B.20}$$

$$H_n^{(2)}(x) \approx \sqrt{\frac{2}{\pi x}}e^{-j\left(x-\frac{2n+1}{4}\pi\right)}\,, \tag{B.21}$$

With time-dependence $e^{j\omega t}$, physical interpretation of the above asymptotic expressions when x is real is that both J_n and Y_n represent standing waves, $H_n^{(1)}$ represents incoming waves, while $H_n^{(2)}$ represents outgoing waves. When x is complex, both J_n and Y_n represent localized standing waves, while $H_n^{(1)}$ and $H_n^{(2)}$ represent attenuated traveling waves. For purely imaginary x, all four of the functions represents evanescent waves.

Large order approximations ($n \gg x$):

$$J_n(x) \approx \frac{x^n}{n!2^n}\left[1 - \frac{x^2}{4(n+1)} + \frac{x^4}{32(n+1)(n+2)} + O\left(\frac{x^6}{n^3}\right)\right] \tag{B.22}$$

$$J_n'(x) \approx \frac{x^{n-1}}{(n-1)!2^n}\left[1 - \frac{(n+2)x^2}{4n(n+1)} + \frac{(n+4)x^4}{32n(n+1)(n+2)} + O\left(\frac{x^6}{n^3}\right)\right] \tag{B.23}$$

$$H_n^{(2)}(x) \approx \frac{j(n-1)!2^n}{\pi x^n}\left[1 + \frac{x^2}{4(n-1)} + \frac{x^4}{32(n-1)(n-2)} + O\left(\frac{x^6}{n^3}\right)\right] \tag{B.24}$$

$$H_n^{'(2)}(x) \approx -\frac{jn!2^n}{\pi x^{n+1}}\left[1 + \frac{(n-2)x^2}{4n(n-1)} + \frac{(n-4)x^4}{32n(n-1)(n-2)} + O\left(\frac{x^6}{n^3}\right)\right] \tag{B.25}$$

Addition theorem:

$$B_\nu(w)e^{j\nu\beta} = \sum_{m=-\infty}^{\infty} B_{\nu+m}(u)\,J_m(v)e^{jm\alpha}\,, \quad \left|ve^{\pm j\alpha}\right| < |u|\,. \tag{B.26}$$

where the relationship of the parameters are depicted in Figure B.1.

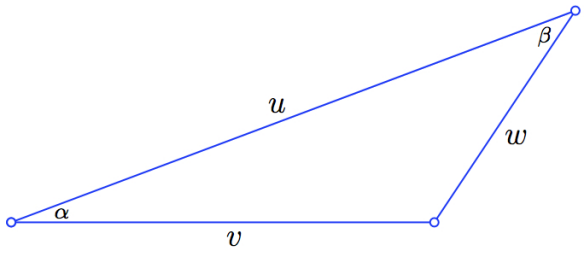

Figure B.1: The addition theorem of the Bessel function.

Generating function expansion:

$$e^{jx\cos\theta} = \sum_{n=-\infty}^{\infty} j^n J_n(x) e^{jn\theta}\,. \tag{B.27}$$

B.3 Jacobi polynomials

The Jacobi polynomials, $P_n^{(\alpha,\beta)}(x)$, are solutions to the following Jacobi differential equation

$$\left(1-x^2\right)\frac{\mathrm{d}^2y}{\mathrm{d}x^2} + \left[\beta-\alpha-(\alpha+\beta+2)\,x\right]\frac{\mathrm{d}y}{\mathrm{d}x} + n(n+\alpha+\beta+1)y = 0\,. \tag{B.28}$$

They form a complete orthogonal system in the interval $[-1,1]$ with respect to the weighting function $w_{\alpha,\beta}(x) = (1-x)^\alpha(1+x)^\beta$, for $\alpha,\beta > -1$ and $n = 0,1,2,\ldots$

$$\left(P_n^{(\alpha,\beta)}, P_m^{(\alpha,\beta)}\right) := \int_{-1}^{1} w_{\alpha,\beta}(x) P_n^{(\alpha,\beta)}(x) P_m^{(\alpha,\beta)}(x)\mathrm{d}x = h_n^{(\alpha,\beta)}\,\delta(n-m)\,, \tag{B.29}$$

where the inner square norm, $h_n^{(\alpha,\beta)}$, is

$$h_n^{(\alpha,\beta)} := \frac{2^{\alpha+\beta+1}}{2n+\alpha+\beta+1}\,\frac{\Gamma(n+\alpha+1)\Gamma(n+\beta+1)}{n!\Gamma(n+\alpha+\beta+1)}\,. \tag{B.30}$$

B.3.1 Normalized Jacobi polynomials

The Jacobi polynomial is normalized with respect to (B.29) when $n = m$. The normalized Jacobi polynomials, $\hat{P}_n^{(\alpha,\beta)}(x)$, is defined as

$$\hat{P}_n^{(\alpha,\beta)}(x) := \left[h_n^{(\alpha,\beta)}\right]^{-\frac{1}{2}} P_n^{(\alpha,\beta)}(x)\,. \tag{B.31}$$

It has the property of orthonormality, as

$$\left(\hat{P}_n^{(\alpha,\beta)}, \hat{P}_m^{(\alpha,\beta)}\right) = \int_{-1}^{1} w_{\alpha,\beta}(x)\hat{P}_n^{(\alpha,\beta)}(x)\hat{P}_m^{(\alpha,\beta)}(x)\mathrm{d}x = \delta_{nm}\,. \tag{B.32}$$

B.3.2 Some useful properties

Symmetry relation:

$$P_n^{(\alpha,\beta)}(-x) = (-1)^n P_n^{(\beta,\alpha)}(x)\,. \tag{B.33}$$

Large order approximation:

$$P_n^{(\alpha,\beta)}(\cos\phi) = \frac{\cos\left\{\left[n+\frac{1}{2}(\alpha+\beta+1)\right]\phi - \frac{\pi}{4}\left[2\alpha+1\right]\right\}}{\sqrt{\pi\, n}\,\left(\sin\,\frac{1}{2}\phi\right)^{\alpha+\frac{1}{2}}\left(\cos\frac{1}{2}\phi\right)^{\beta+\frac{1}{2}}} + O\left(n^{-\frac{3}{2}}\right). \tag{B.34}$$

Relations with trigonometric functions:

$$\sin n\phi = \frac{\sqrt{\pi}\, n!}{2\,\Gamma\left(n+\frac{1}{2}\right)}\,(\sin\phi)\,P_{n-1}^{\left(\frac{1}{2},\frac{1}{2}\right)}(\cos\phi)\,, \tag{B.35a}$$

$$\cos n\phi = \frac{\sqrt{\pi}\, n!}{\Gamma\left(n+\frac{1}{2}\right)} P_n^{\left(-\frac{1}{2},-\frac{1}{2}\right)}(\cos\phi)\,. \tag{B.35b}$$

Integral relations for $\eta \in [0,1)$:

$$P_n^{(\alpha,\beta)}(x) = \frac{(1-x)^{-\alpha}\Gamma(n+1+\alpha)}{\Gamma(1-\eta)\Gamma(n+\alpha+\eta)}\int_x^1 \frac{(1-t)^{\alpha+\eta-1}P_n^{(\alpha+\eta-1,\beta-\eta+1)}(t)}{(t-x)^\eta}\mathrm{d}t\,, \tag{B.36a}$$

$$P_n^{(\alpha,\beta)}(x) = \frac{(1+x)^{-\beta}\Gamma(n+1+\beta)}{\Gamma(1-\eta)\Gamma(n+\beta+\eta)}\int_{-1}^x \frac{(1+t)^{\beta+\eta-1}P_n^{(\alpha-\eta+1,\beta+\eta-1)}(t)}{(x-t)^\eta}\mathrm{d}t\,. \tag{B.36b}$$

Differential relations:

$$-2n(1-x)^\alpha(1+x)^\beta P_n^{(\alpha,\beta)}(x) = \frac{\mathrm{d}}{\mathrm{d}x}\left[(1-x)^{\alpha+1}(1+x)^{\beta+1}P_{n-1}^{(\alpha+1,\beta+1)}(x)\right] \tag{B.37}$$

for $n \geq 1$.

$$\frac{\mathrm{d}}{\mathrm{d}x}\left[(1-x)^{\alpha+1}\,\hat{P}_n^{(\alpha+1,\beta-1)}(x)\right] = -\sqrt{(n+\alpha+1)(n+\beta)}\,(1-x)^\alpha\,\hat{P}_n^{(\alpha,\beta)}(x) \tag{B.38}$$

for $\alpha > -1, \beta > 0$.

$$\frac{\mathrm{d}}{\mathrm{d}x}\left[(1+x)^{\beta+1}\,\hat{P}_n^{(\alpha-1,\beta+1)}(x)\right] = \sqrt{(n+\alpha)(n+\beta+1)}\,(1+x)^\beta\,\hat{P}_n^{(\alpha,\beta)}(x) \tag{B.39}$$

for $\alpha > 0, \beta > -1$.

Recurrence relation:

$$\hat{P}_{n+1}^{(\alpha,\beta)}(x) = (b_n + x a_n)\,\hat{P}_n^{(\alpha,\beta)}(x) - c_n\hat{P}_{n-1}^{(\alpha,\beta)}(x)\,, \tag{B.40}$$

with the two lowest degree polynomials as the initializations:

$$\hat{P}_0^{(\alpha,\beta)}(x) = \left[h_n^{(\alpha,\beta)}\right]^{-\frac{1}{2}}, \tag{B.41a}$$

$$\hat{P}_1^{(\alpha,\beta)}(x) = \tfrac{1}{2}\left[\alpha - \beta + x\left(\alpha + \beta + 2\right)\right]\hat{P}_0^{(\alpha,\beta)}(x). \tag{B.41b}$$

The coefficients are given by

$$a_n = \sqrt{\frac{h_n^{(\alpha,\beta)}}{h_{n+1}^{(\alpha,\beta)}}} \times \frac{(2n+\alpha+\beta+1)(2n+\alpha+\beta+2)}{(2n+2)(n+\alpha+\beta+1)}, \tag{B.42a}$$

$$b_n = \sqrt{\frac{h_n^{(\alpha,\beta)}}{h_{n+1}^{(\alpha,\beta)}}} \times \frac{(2n+\alpha+\beta+1)(\alpha^2-\beta^2)}{2\,(n+1)(n+\alpha+\beta+1)(2n+\alpha+\beta)}, \tag{B.42b}$$

$$c_n = \sqrt{\frac{h_{n-1}^{(\alpha,\beta)}}{h_{n+1}^{(\alpha,\beta)}}} \times \frac{(n+\alpha)(n+\beta)(2n+\alpha+\beta+2)}{(n+1)(n+\alpha+\beta+1)(2n+\alpha+\beta)}. \tag{B.42c}$$

B.4 Incomplete scalar products

The incomplete scalar product of two normalized Jacobi polynomials for $\alpha, \beta > -1$, $x \in [-1, 1]$ and $n, m = 0, 1, 2, \ldots$, is denoted as

$$\hat{Q}_{nm}^{(\alpha,\beta)}(x) := \int_x^1 (1-t)^\alpha (1+t)^\beta \hat{P}_n^{(\alpha,\beta)}(t)\hat{P}_m^{(\alpha,\beta)}(t)\mathrm{d}t. \tag{B.43}$$

Hence, it is clear that $\hat{Q}_{nm}^{(\alpha,\beta)}(1) = 0$.

B.4.1 Some useful properties

$$\hat{Q}_{nm}^{(\alpha,\beta)}(x) = \hat{Q}_{mn}^{(\alpha,\beta)}(x), \tag{B.44}$$

$$\hat{Q}_{nm}^{(\alpha,\beta)}(x) = \delta_{nm} - (-1)^{n-m}\hat{Q}_{nm}^{(\beta,\alpha)}(-x), \tag{B.45}$$

$$\hat{Q}_{nm}^{(\alpha,\beta)}(x) = \sum_{k=0}^{\infty} \hat{Q}_{nk}^{(\alpha,\beta)}(x)\hat{Q}_{km}^{(\alpha,\beta)}(x). \tag{B.46}$$

When $\alpha > -1$, $\beta > 0$,

$$\hat{Q}_{nm}^{(\alpha,\beta)}(x) = \frac{(1-x)^{\alpha+1}(1+x)^\beta}{\sqrt{(n+\alpha+1)(n+\beta)}}\hat{P}_n^{(\alpha+1,\beta-1)}(x)\hat{P}_m^{(\alpha,\beta)}(x)$$

$$+\sqrt{\frac{(m+\alpha+1)(m+\beta)}{(n+\alpha+1)(n+\beta)}}\hat{Q}_{nm}^{(\alpha+1,\beta-1)}(x)\,. \tag{B.47a}$$

When $\alpha > 0$, $\beta > -1$,

$$\begin{aligned}\hat{Q}_{nm}^{(\alpha,\beta)}(x) =& -\frac{(1-x)^{\alpha}(1+x)^{\beta+1}}{\sqrt{(n+\alpha)(n+\beta+1)}}\hat{P}_{n}^{(\alpha-1,\beta+1)}(x)\hat{P}_{m}^{(\alpha,\beta)}(x)\\ &+\sqrt{\frac{(m+\alpha)(m+\beta+1)}{(n+\alpha)(n+\beta+1)}}\hat{Q}_{nm}^{(\alpha-1,\beta+1)}(x)\,.\end{aligned} \tag{B.47b}$$

(B.47a) and (B.47b) are deduced from the integral relations involving Jacobi polynomials given in (B.36a) and (B.36b) (with $\eta = 0$).

B.4.2 Computation of the incomplete scalar product

When $n \neq m$, $\hat{Q}_{nm}^{(\alpha,\beta)}(x)$ may be calculated in terms of $\hat{P}_{n}^{(\alpha,\beta)}(x)$ using the following expressions

$$\begin{aligned}\hat{Q}_{nm}^{(\alpha,\beta)}(x) =& \frac{(1-x)^{\alpha+1}(1+x)^{\beta}}{(n+\alpha+1)(n+\beta)-(m+\alpha+1)(m+\beta)}\\ &\times\Big[\sqrt{(n+\alpha+1)(n+\beta)}\hat{P}_{n}^{(\alpha+1,\beta-1)}(x)\hat{P}_{m}^{(\alpha,\beta)}(x)\\ &-\sqrt{(m+\alpha+1)(m+\beta)}\hat{P}_{n}^{(\alpha,\beta)}(x)\hat{P}_{m}^{(\alpha+1,\beta-1)}(x)\Big]\,,\end{aligned} \tag{B.48a}$$

when $\alpha > -1$, $\beta > 0$ and

$$\begin{aligned}\hat{Q}_{nm}^{(\alpha,\beta)}(x) =& -\frac{(1-x)^{\alpha}(1+x)^{\beta+1}}{(n+\beta+1)(n+\alpha)-(m+\beta+1)(m+\alpha)}\\ &\times\Big[\sqrt{(n+\beta+1)(n+\alpha)}\hat{P}_{n}^{(\alpha-1,\beta+1)}(x)\hat{P}_{m}^{(\alpha,\beta)}(x)\\ &-\sqrt{(m+\beta+1)(m+\alpha)}\hat{P}_{n}^{(\alpha,\beta)}(x)\hat{P}_{m}^{(\alpha-1,\beta+1)}(x)\Big]\,,\end{aligned} \tag{B.48b}$$

when $\alpha > 0$, $\beta > -1$.

The above expressions are derived from the differential relations involving the Jacobi polynomials given in (B.38) and (B.39) by using integration by parts.

When $n = m$, $\hat{Q}_{nm}^{(\alpha,\beta)}(x)$ can be calculated using the following recurrence relation

$$\hat{Q}_{n+1,n+1}^{(\alpha,\beta)}(x) = \frac{a_n}{a_{n+1}}\hat{Q}_{n+2,n}^{(\alpha,\beta)}(x) + \left(b_n - b_{n+1}\frac{a_n}{a_{n+1}}\right)\hat{Q}_{n+1,n}^{(\alpha,\beta)}(x)$$

$$+ c_{n+1}\frac{a_n}{a_{n+1}}\hat{Q}^{(\alpha,\beta)}_{n,n}(x) - c_n\hat{Q}^{(\alpha,\beta)}_{n-1,n+1}(x)\,, \tag{B.49}$$

with the initialization

$$\hat{Q}^{(\alpha,\beta)}_{00}(x) = \left[h^{(\alpha,\beta)}_n\right]^{-1}\int_x^1 (1-t)^\alpha(1+t)^\beta \mathrm{d}t\,. \tag{B.50}$$

The above recurrence relation for the case when $n = m$ is derived from (B.40) directly, for the order n and m:

$$\hat{P}^{(\alpha,\beta)}_{n+1}(z) = (b_n + za_n)\,\hat{P}^{(\alpha,\beta)}_n(z) - c_n\hat{P}^{(\alpha,\beta)}_{n-1}(z)\,, \tag{B.51a}$$

$$\hat{P}^{(\alpha,\beta)}_{m+1}(z) = (b_m + za_m)\,\hat{P}^{(\alpha,\beta)}_m(z) - c_m\hat{P}^{(\alpha,\beta)}_{m-1}(z)\,. \tag{B.51b}$$

The term containing z is eliminated by first multiplying (B.51a) by $\hat{a}_n\hat{P}^{(\alpha,\beta)}_n(z)$ and (B.51b) by $\hat{a}_m\hat{P}^{(\alpha,\beta)}_m(z)$, then subtracting the two. The recurrence relation for $\hat{Q}_{n,n}(x)$ can be readily derived by multiplying by the $(1-z)^\alpha(1+z)^\beta$ and integrating over $(x, 1)$. The recurrence relation (B.49) has m set to be $n + 1$.

Appendix C

Abel's integral transformation

C.1 Abel's integral equations

The generalized Abel's integral equation of the following form is considered

$$f(x) = \int_a^x \frac{u(\xi)}{(x-\xi)^\lambda} \mathrm{d}\xi \,, \tag{C.1}$$

where $0 < \lambda < 1$, f is a known function, x is some fixed value in (a, b), and u is the unknown function to be determined. The companion form of (C.1) is given by

$$f(x) = \int_x^b \frac{u(\xi)}{(\xi-x)^\lambda} \mathrm{d}\xi \,. \tag{C.2}$$

C.2 Derivation of the inversion formula

The solution to (C.1) can be obtained by considering the following integral [25, 58]

$$\int_a^x \frac{f(z)}{(x-z)^{1-\lambda}} \mathrm{d}z \,. \tag{C.3}$$

The unknown function $u(\xi)$ is assumed to be continuous on (a, b) (hence, bounded). The conditions for this continuity will become clear once the inversion is described.

By substitution of (C.1) into (C.3) and interchanging the order of integration of the resulted Dirichlet formula [89], it can be derived that

$$\int_a^x \frac{f(z)}{(x-z)^{1-\lambda}} \mathrm{d}z = \int_a^x u(\xi) \int_\xi^x \frac{1}{(z-\xi)^\lambda (x-z)^{1-\lambda}} \mathrm{d}z \, \mathrm{d}\xi \,. \tag{C.4}$$

Using the change of variable $t = (x-z)/(x-\xi)$ and noting that $z-\xi = (1-t)(x-\xi)$, the inner integral reduces to a constant for fixed λ as

$$\int_\xi^x \frac{1}{(z-\xi)^\lambda (x-z)^{1-\lambda}} \mathrm{d}z = \int_0^1 t^{\lambda-1} (1-t)^{-\lambda} \mathrm{d}t = \frac{\pi}{\sin(\pi\lambda)} \,. \tag{C.5}$$

This reduction makes use of (B.6) with $p = \lambda$ and $q = 1 - \lambda$ as well as (B.4) with $x = \lambda$.

As a result, the original integral in (C.3) is reduced to

$$\int_a^x \frac{f(z)}{(x-z)^{1-\lambda}} \mathrm{d}z = \frac{\pi}{\sin(\pi\lambda)} \int_a^x u(\xi) \mathrm{d}\xi \,. \tag{C.6}$$

The final step in the derivation of the solution involves differentiating of both sides of (C.6) with respect to ξ. The solution to (C.1) is thus,

$$u(\xi) = \frac{\sin \lambda\pi}{\pi} \frac{\mathrm{d}}{\mathrm{d}\xi} \int_a^\xi \frac{f(x)}{(\xi - x)^{1-\lambda}} \mathrm{d}x \,, \tag{C.7}$$

which is often referred to as the inversion formula to (C.1).

The inversion formula to (C.2) can be derived in similar manner to be

$$u(\xi) = -\frac{\sin \lambda\pi}{\pi} \frac{\mathrm{d}}{\mathrm{d}\xi} \int_\xi^b \frac{f(x)}{(x - \xi)^{1-\lambda}} \mathrm{d}x \,. \tag{C.8}$$

C.3 Conditions for uniqueness and continuity of solution

The solution given in (C.7) is unique and continuous (including at the point a, where it equals zero) if the following conditions are satisfied [25, 69]

1. f is continuous in (a, b),
2. $f(a) = 0$,
3. derivative of f is finite almost everywhere in (a, b).

Similar conditions are required for the uniqueness and continuity of solution given in (C.8), with the second condition replaced by

(2) $f(b) = 0$.

Appendix D

Methods of summation

This chapter summarizes two of the alternative methods of summation of a series: the Abel- and Cesàro-summation methods. For more details of the summability of divergent series, please refer to [23, 40].

D.1 Abel-summation

An alternative method to calculate the sum of a series $\sum_{n=1}^{\infty} a_n$, which may be divergent, is by computing the Abel summation defined as $\lim_{r\to 1^-} \sum_{n=1}^{\infty} a_n r^n$.

D.1.1 Definitions of Abel-summability

A series $\sum_{n=1}^{\infty} a_n$ is said to be Abel-summable[1] to the limit L and is written as

$$\sum_{n=1}^{\infty} a_n = L \quad (A)\,, \tag{D.1}$$

if $\lim_{r\to 1^-} \sum_{n=1}^{\infty} a_n r^n = L$ exists, as $r \to 1^-$.

An Abel-summable series $\sum_{n=1}^{\infty} a_n(x)$ is uniformly Abel-summable on $[a, b]$ to $L(x)$ if for all $\epsilon > 0$, there exists some $\delta > 0$, such that

$$\left| \sum_{n=1}^{\infty} a_n(x) r^n - L(x) \right| < \epsilon\,, \tag{D.2}$$

for $(1 - \delta) < r < 1$ and all $x \in [a, b]$.

[1] It is worth noting that, by using Poisson's integral formula, the Fourier series of a continuous function f of period 2π can be shown to be Abel-summable.

D.1.2 Conditions for (ordinary) convergence

Although the convergence of the series implies Abel-summability, for r lying within any Stoltz angle (as stated in Abel's theorem), the converse is not always true. Tauber proved the theorem stating that: an Abel-summable series $\sum_{n=0}^{\infty} a_n$ is convergent if and only if the following is satisfied as $n \to \infty$,

$$\frac{a_1 + 2a_2 + \ldots + na_n}{n} = s_n - \frac{s_0 + s_1 + \ldots + s_{n-1}}{n} \to 0\,, \tag{D.3}$$

where $s_N := \sum_{n=0}^{N} a_n$. The conditions necessary and sufficient for the step from Abel-summability to convergence are called the Tauberian conditions.

Fejér shows that the area condition below implies (D.3),

$$\sum_{n=1}^{\infty} n|a_n|^2 < \infty\,. \tag{D.4}$$

Therefore, (D.4) is often referred as the Fejér's Tauberian condition for the Abel-summable series $\sum_{n=1}^{\infty} a_n$. In fact, for $p > 1$, the following condition

$$\sum_{n=1}^{\infty} n^{p-1}|a_n|^p < \infty\,, \tag{D.5}$$

has been shown to be a Tauberian condition from Hölder's inequality. More relaxed conditions are validated, when the Littlewood's theorem in 1911 states that:

$$\sum_{n=1}^{\infty} a_n \text{ is Abel-summable} \quad \& \quad |na_n| \le C \quad \Rightarrow \quad \sum_{n=1}^{\infty} a_n \text{ converges;} \tag{D.6}$$

while the Hardy–Littlewood's theorem in 1914 states that:

$$\sum_{n=1}^{\infty} a_n \text{ is Abel-summable} \quad \& \quad na_n \ge -C \quad \Rightarrow \quad \sum_{n=1}^{\infty} a_n \text{ converges.} \tag{D.7}$$

D.2 Cesàro-summation

For a series $\sum_{n=1}^{\infty} a_n$, convergent or not, its Cesàro-summation of order 1 — written as $(C, 1)$ — is an arithmetic mean of the partial sums of the original series. It is defined as

$$c_k^1 = \frac{s_1 + s_2 + \cdots + s_k}{k} = \frac{1}{k}\sum_{n=1}^{k} s_n \tag{D.8}$$

$$= \frac{1}{k}\sum_{n=1}^{k}(k-n+1)a_n\,. \tag{D.9}$$

where s_n is the nth partial sum of the original series; *i.e.*, $s_n := \sum_{m=1}^{n} a_m$. It is worth noting that, for a convergent series, where $\sum_{n=1}^{\infty} a_n = L$, the Cesàro-summation yields the same sum; *i.e.*, $\lim_{k\to\infty} c_1^{\alpha} = L$.

Bibliography

[1] M. Abramowitz and I. A. Stegun, editors. *Handbook of mathematical functions with formulas, graphs, and mathematical tables*. A John Wiley & Sons-Interscience Publication. John Wiley & Sons, New York, 1984. Reprint of the 1972 edition, Selected Government Publications.

[2] N. I. Akhiezer and I. M. Glazman. *Theory of linear operators in Hilbert space. Vol. I & II*, volume 9 &10 of *Monographs and Studies in Mathematics*. Pitman (Advanced Publishing Program), Boston, Mass., 1981. Translated from the third Russian edition by E. R. Dawson, Translation edited by W. N. Everitt.

[3] N.G. Alexopoulos and A. Nakatani. Cylindrical substrate microstrip line characterization. *Microwave Theory and Techniques, IEEE Transactions on*, 35(9):843 – 849, September 1987.

[4] K. E. Atkinson. *The numerical solution of integral equations of the second kind*. Number 4 in Cambridge Monographs on Applied and Computational Mathematics. Cambridge University Press, September 1997.

[5] C. A. Balanis. *Antenna theory: analysis and design*. John Wiley & Sons, New York, 1982.

[6] C. A. Balanis. *Advanced engineering electromagnetics*. John Wiley & Sons, New York, 1989.

[7] J. Beren. Diffraction of an h-polarized electromagnetic wave by a circular cylinder with an infinite axial slot. *Antennas and Propagation, IEEE Transactions on*, 31(3):419–425, May 1983.

[8] A. Boag and Y. Leviatan. Analysis of scattering from cylinders with a periodically corrugated periphery using a current-model technique. *Antennas and Propagation, IEEE Transactions on*, 41(9):1265 –1272, September 1993.

[9] J. J. Bowman, T. B. A. Senior, and P. L. E. Uslenghi, editors. *Electromagnetic and acoustic scattering by simple shapes*. A Summa Book. Hemisphere Publishing Corp., New York, 1987. Revised reprint of the 1969 edition.

[10] C. H. Chan and R. Mittra. Analysis of a class of cylindrical multiconductor transmission lines using an iterative approach. *Microwave Theory and Techniques, IEEE Transactions on*, 35(4):415 – 424, April 1987.

[11] M. V. K. Chari and P. P. Silvester. *Finite elements for electrical and magnetic field problems*. John Wiley & Sons Series in Numerical Methods in Engineering. John Wiley & Sons, Chichester, 1980.

[12] D. Colton and R. Kress. *Integral equation methods in scattering theory*. Pure and applied mathematics. John Wiley & Sons, New York, 1983.

[13] N. Dib, T. Weller, M. Scardelletti, and M. Imparato. Analysis of cylindrical transmission lines with the finite-difference time-domain method. *Microwave Theory and Techniques, IEEE Transactions on*, 47(4):509 –512, April 1999.

[14] C.F. Du Toit. A procedure for determining the largest computable order of bessel functions of the second kind and hankel functions. *Antennas and Propagation, IEEE Transactions on*, 41(12):1741 –1742, December 1993.

[15] N. Dunford and J. Schwartz. *Linear operators and spectral theory*, volume I & II. Wiley-Interscience, New York, February 1988.

[16] A. El-Hajj and K.Y. Kabalan. Scattering from and penetration into a dielectric-filled conducting cylinder with multiple apertures. *Electromagnetic Compatibility, IEEE Transactions on*, 36(3):196–200, August 1994.

[17] A. El-Hajj, K.Y. Kabalan, and R.F. Harrington. Characteristic modes of a slot in a conducting cylinder and their use for penetration and scattering, TE case. *Antennas and Propagation, IEEE Transactions on*, 40(2):156–161, Feb 1992.

[18] A. Z. Elsherbeni. A comparative study of two-dimensional multiple scattering techniques. *Radio Science*, 29(4):1023–1033, Aug 1994.

[19] A. Z. Elsherbini, Y. Ying, C. E. Smith, and V. Rodriguez-Pereyra. Finite difference analysis of cylindrical two conductor microstrip transmission line with truncated dielectrics. *Journal of Franklin Institute*, 333(6):901 – 928, 1996.

[20] L. B. Felsen and G. Vecchi. Wave scattering from slit coupled cylindrical cavities with interior loading. ii. resonant mode expansion. *Antennas and Propagation, IEEE Transactions on*, 39(8):1085 –1097, August 1991.

[21] G. GASPER. *Fractional calculus and its applications*.

[22] B. Guizal and D. Felbacq. Numerical computation of the scattering matrix of an electromagnetic resonator. *Phys. Rev. E*, 66(2):026602, Aug 2002.

[23] G. H. Hardy. *Divergent Series*. Oxford, at the Clarendon Press, 1949.

[24] R. F. Harrington. *Field computation by moment methods*. IEEE Computer Society Press, May 1993.

[25] H. Hochstadt. *Integral equations*. John Wiley & Sons, New York-London-Sydney, 1973. Pure and Applied Mathematics.

[26] D. Homentcovschi. A cylindrical multiconductor stripline-like microstrip transmission line. *Microwave Theory and Techniques, IEEE Transactions on*, 37(3):497 –503, March 1989.

[27] G.C. Hsiao and R.E. Kleinman. Mathematical foundations for error estimation in numerical solutions of integral equations in electromagnetics. *Antennas and Propagation, IEEE Transactions on*, 45(3):316–328, March 1997.

[28] M. Hussein and M. Hamid. Scattering by a perfectly conducting circular cylinder with two infinite slots. In *Antennas and Propagation Society International Symposium, 1992. AP-S. 1992 Digest. Held in Conjuction with: URSI Radio Science Meeting and Nuclear EMP Meeting., IEEE*, volume 3, pages 1579 –1582, July 1992.

[29] G. Hyde. Studies of the focal region of a spherical reflector: Stationary phase evaluation. *Antennas and Propagation, IEEE Transactions on*, 16(6):646–656, November 1968.

[30] V. I. Istrăţescu. *Introduction to linear operator theory*, volume 65 of *Monographs and Textbooks in Pure and Applied Mathematics*. Marcel Dekker Inc., New York, 1981.

[31] Y. Ji and K. Hongo. *Journal of the Optical Society of America*, 8(11):1721–1728, November 1991.

[32] W. A. Johnson and R. W. Ziolkowski. The scattering of an h-polarized plane wave from an axially slotted infinite cylinder: A dual series approach. volume 19, pages 275–291. Radio Sci., Jan–Feb 1984.

[33] D. S. Jones. *Acoustic and electromagnetic waves*. Oxford Science Publications. The Clarendon Press Oxford University Press, New York, 1986.

[34] L. V. Kantorovich and G. P. Akilov. *Functional analysis in normed spaces*, volume 46 of *International series of monographs in pure and applied mathematics*. Pergamom Press, Oxford, New York, 1964. Translated from Russian by D. E. Brown, Translation edited by A. P. Robertson.

[35] A.A. Kishk and P. S. Kildal. Asymptotic boundary conditions for strip-loaded scatterers applied to circular dielectric cylinders under oblique incidence. *Antennas and Propagation, IEEE Transactions on*, 45(1):51–56, January 1997.

[36] M. Kline. An asymptotic solution of Maxwell's equations. *Communications on Pure and Applied Mathematics*, 4:225–262, 1951.

[37] M. Kline and I. W. Kay. *Electromagnetic theory and geometrical optics*, volume 12 of *Pure and Applied Mathematics*. Wiley-Interscience [John Wiley & Sons], New York-London-Sydney, 1965.

[38] M. A. Kolbehdari. Quasi-static characteristic of a shielded cylindrical coupled microstrip transmission line by finite-element method. In *Southeastcon '94. 'Creative Technology Transfer - A Global Affair'., Proceedings of the 1994 IEEE*, pages 170 –174, April 1994.

[39] M.A. Kolbehdari and M.N.O. Sadiku. Finite and infinite element analysis of coupled cylindrical microstrip line in a nonhomogeneous dielectric media. In *Southeastcon '95. 'Visualize the Future'., Proceedings., IEEE*, pages 269 –273, March 1995.

[40] J. Korevaar. *Tauberian theory*, volume 329 of *Grundlehren der Mathematischen Wissenschaften [Fundamental Principles of Mathematical Sciences]*. Springer-Verlag, Berlin, 2004. A century of developments.

[41] V. N. Koshparenok and V. P. Shestopalov. *Diffraction of a plane electromagnetic wave by a circular cylinder with a longitudinal slot*. USSR Comput. Maths. Phys. (English Translated), 1971.

[42] S. G. Kreĭn. *Linear equations in Banach spaces*. Birkhäuser Boston, Mass., 1982. Translated from the Russian by A. Lacob, With an introduction by I. Gohberg.

[43] R. Kress. *Linear integral equations*, volume 82 of *Applied Mathematical Sciences*. Springer-Verlag, Berlin, 1989.

[44] T. Kushta and K. Yasumoto. Electromagnetic scattering from periodic arrays of two circular cylinders per unit cell. volume 29, pages 69–85. Progress In Electromagnetics Research, PIER, 2000.

[45] N. N. Lebedev. *Special functions and their applications*. Dover Publications Inc., New York, 1972. Revised edition, translated from the Russian and edited by Richard A. Silverman, Unabridged and corrected republication.

[46] Alon Ludwig and Yehuda Leviatan. Analysis of bandgap characteristics of two-dimensional periodic structures by using the source-model technique. *J. Opt. Soc. Am. A*, 20(8):1553–1562, Aug 2003.

[47] R. K. Luneburg. *Mathematical theory of optics*, volume RI. Brown University Notes, Providence, 1944.

[48] M. A. Martens, R. W. Brown, and E. M. Haacke. Conformal mapping analyses of microstrips with circular and elliptical cross-sections. *Microwave Theory and Techniques, IEEE Transactions on*, 40(9):1836–1840, September 1992.

[49] J. Meixner. The edge condition in the theory of electromagnetic waves at perfectly conducting plane screens. volume 6, pages 2–9. Ann. Physik, Sep 1949.

[50] J. Meixner. The behavior of electromagnetic fields at edges. *Antennas and Propagation, IEEE Transactions on*, 20(4):442–446, July 1972.

[51] R. Mittra and W. Lee. *Analytical techniques in the theory of guided waves*. Macmillan series in electrical science. Macmillan, New York, 1971.

[52] P. M. Morse and H. Feshbach. *Methods of theoretical physics. 2 volumes*. McGraw-Hill Book Co., Inc., New York, 1953.

[53] S. Nakamura. *Computational methods in engineering and science*. Wiley-Interscience [John Wiley & Sons], New York, 1977. With applications to fluid dynamics and nuclear systems.

[54] A. Nakatani and N.G. Alexopoulos. Coupled microstrip lines on a cylindrical substrate. *Microwave Theory and Techniques, IEEE Transactions on*, 35(12):1392 – 1398, December 1987.

[55] B. Noble. The solution of Bessel function dual integral equations by a multiplying-factor method. *Proc. Cambridge Philos. Soc.*, 59:351–362, 1963.

[56] A.I. Nosich. The method of analytical regularization in wave-scattering and eigenvalue problems: foundations and review of solutions. *Antennas and Propagation Magazine, IEEE*, 41(3):34 –49, June 1999.

[57] A. F. Peterson, S. L. Ray, and R. Mittra. *Computational methods for electromagnetics*. IEEE/OUP Series on Electromagnetic Wave Theory. IEEE Press, New York, 1998.

[58] D. Porter and D. S. G. Stirling. *Integral equations*. Cambridge Texts in Applied Mathematics. Cambridge University Press, Cambridge, 1990. A practical treatment, from spectral theory to applications.

[59] A. Ye. Poyedinchuk, Y. A. Tuchkin, and V. P. Shestopalov. New numerical-analytical methods in diffraction theory. *Mathematical and Computer Modelling*, 32(9):1029–1046, 2000. Mathematical and computer modelling in engineering sciences.

[60] J.S. Rao and B.N. Das. Analysis of asymmetric stripline by conformal mapping. *Microwave Theory and Techniques, IEEE Transactions on*, 27(4):299 – 303, April 1979.

[61] M. N. O. Sadiku. A simple introduction to finite element analysis of electromagnetic problems. *Education, IEEE Transactions on*, 32(2):85–93, May 1989.

[62] M. N. O. Sadiku. *Numerical Techniques in electromagnetics*. CRC Press, 2 edition, 2000.

[63] H. Sakurai, T. Hashidate, M. Ohki, K. Motojima, and S. Kozaki. Electromagnetic scattering by the luneberg lens with reflecting cap. *Electromagnetic Compatibility, IEEE Transactions on*, EMC-40(2):94–96, May 1998.

[64] M.V. Schneider. Computation of impedance and attenuation of tem-lines by finite difference methods. *Microwave Theory and Techniques, IEEE Transactions on*, 13(6):793 – 800, November 1965.

[65] T. B. A. Senior. Electromagnetic field penetration into a cylindrical cavity. *Electromagnetic Compatibility, IEEE Transactions on*, EMC-18(2):71–73, May 1976.

[66] V. P. Shestopalov. Method of Riemann-Hilbert problem in theory of electromagnetic wave diffraction and propagation. Kharkov, 1971. Publishing house of Kharkov state university.

[67] J. D. Shumpert and C. M. Butler. Penetration through slots in conducting cylinders – part I: Te case. *Antennas and Propagation, IEEE Transactions on*, 46(11):1612–1621, Nov 1998.

[68] J.D. Shumpert and C.M. Butler. Penetration through slots in conducting cylinders. part 2: Tm case. *Antennas and Propagation, IEEE Transactions on*, 46(11):1622 –1628, November 1998.

[69] I. N. Sneddon. *Mixed boundary value problems in potential theory*. North-Holland Publishing Co., Amsterdam, 1966.

[70] R. Spencer and G. Hyde. Studies of the focal region of a spherical reflector: Geometric optics. *Antennas and Propagation, IEEE Transactions on*, 16(3):317–324, May 1968.

[71] R. Spencer and G. Hyde. Studies of the focal region of a spherical reflector: Polarization effects. *Antennas and Propagation, IEEE Transactions on*, 16(4):399–404, July 1968.

[72] H. C. Su and K. L. Wong. Quasi-static solutions of cylindrical coplanar waveguides. volume 14, pages 347–351. Microwave and Optical Technology Letters, 1997.

[73] A. Thom and C. J. Apelt. *Field computations in engineering and physics*. D. Van Nostrand Co., Ltd., London-Toronto-New York-Princeton, N.J., 1961.

[74] A. N. Tikhonov and V. Y. Arsenin. *Solutions of ill-posed problems*. Winston, New York, 1977.

[75] A. N. Tikhonov and A. V. Goncharsky. *Ill-posed problems in the natural sciences*. Oxford University Press, Oxford, 1987.

[76] C. J. Tranter. *Dual trigonometric series*, volume 4. Proc. Glasgow Math. Assoc., 1959.

[77] C. J. Tranter. Some triple integral equations. *Proc. Glasgow Math. Assoc.*, 4:200–203, 1960.

[78] S. V. Tsynkov. Numerical solution of problems on unbounded domains. A review. *Applied Numerical Mathematics. An IMACS Journal*, 27(4):465–532, 1998. Absorbing boundary conditions.

[79] Y. A. Tuchkin. Analytical regularization method for wave diffraction by bowl-shaped screen of revolution. volume 5 of *Ultra-wideband, short-pulse electromagnetics*, pages 153–157. Kluwer Academic: Plenum Publishers, 2002.

[80] Y. A. Tuchkin. Method of analytical regularization: state of art and new approaches. volume 2 of *IV-th International workshop on electromagnetic wave scattering*, pages 43–49, Turkey, 2006. Gebze.

[81] V. Twersky. On scattering of waves by the infinite grating of circular cylinders. *Antennas and Propagation, IRE Transactions on*, 10(6):737 –765, November 1962.

[82] A. M. van de Water, B. P. de Hon, M. C. van Beurden, A. G. Tijhuis, and P. de Maagt. Linear embedding via green's operators: A modeling technique for finite electromagnetic band-gap structures. *Phys. Rev. E*, 72:056704, Nov 2005.

[83] S. S. Vinogradov, P. D. Smith, J. S. Kot, and N. Nikolic. Radar cross-section studies of spherical lens reflectors. volume 72, pages 325–337. Progress In Electromagnetics Research, PIER, 2007.

[84] S. S. Vinogradov, P. D. Smith, and E. D. Vinogradova. *Canonical problems in scattering and potential theory. Part I*, volume 122 of *Chapman & Hall/CRC Monographs and Surveys in Pure and Applied Mathematics*. Chapman & Hall/CRC, Boca Raton, FL, 2001. Canonical structures in potential theory.

[85] S. S. Vinogradov, P. D. Smith, and E. D. Vinogradova. *Canonical problems in scattering and potential theory. Part II*, volume 127 of *Chapman & Hall/CRC Monographs and Surveys in Pure and Applied Mathematics*. Chapman & Hall/CRC, Boca Raton, FL, 2002. Acoustic and electromagnetic diffraction by canonical structures.

[86] J.L. Volakis and L.C. Kempel. Electromagnetics: computational methods and considerations. *Computational Science Engineering, IEEE*, 2(1):42–57, 1995.

[87] G. N. Wastson. *A Treatise on the Theory of Bessel Functions*. Cambridge University Press, Cambridge, England, 1944.

[88] A. Wexler. Computation of electromagnetic fields. *Microwave Theory and Techniques, IEEE Transactions on*, 17(8):416–439, August 1969.

[89] D. V. Widder. *Advanced Calculus*. Prentice-Hall Inc., New York, 1947.

[90] W. E. Williams. The solution of dual series and dual integral equations. *Proc. Glasgow Math. Assoc.*, 6:123–129, 1964.

[91] K. Yasumoto and H. Jia. Three-dimensional electromagnetic scattering from multilayered periodic arrays of circular cylinders. volume 29, pages 301–304. Proc. 2002 China-Japan Joint Meet. Microwaves, Apr 2002.

[92] Wen-Yan Yin, Le-Wei Li, Tat-Soon Yeo, and Mook-Seng Leong. Multiple penetration of a te_z-polarized plane wave into multilayered cylindrical cavity-backed apertures. *Electromagnetic Compatibility, IEEE Transactions on*, 42(4):330–338, Nov 2000.

[93] Wen-Yan Yin, Le-Wei Li, Tat-Soon Yeo, Mook-Seng Leong, and Pang-Shyan Kooi. The near-zone field characteristics of an e-polarization plane wave penetrating through cylindrical multiple apertures (non) coated with lossy and lossless media. *Electromagnetic Compatibility, IEEE Transactions on*, 44(2):329–337, May 2002.

[94] J. W. Yu and N. H. Myung. Oblique scattering and coupling to a slit coaxial cable: TM case. volume 14, pages 931–942. Journal of Electromagnetic Waves and Applications, Dec 2000.

[95] L. R. Zeng and Y. X. Wang. Accurate solutions of elliptical and cylindrical striplines and microstrip lines. *Microwave Theory and Techniques, IEEE Transactions on*, 34(2):259– 265, February 1986.

[96] R. W. Ziolkowski. n-series problems and the coupling of electromagnetic waves to apertures: a Riemann-Hilbert approach. *SIAM Journal on Mathematical Analysis*, 16(2):358–378, 1985.

[97] R. W. Ziolkowski and J. Grant. Scattering from cavity-backed apertures: The generalized dual series solution of the concentrically loaded *e*-pol slit cylinder problem. *Antennas and Propagation, IEEE Transactions on*, 35(5):504–528, May 1987.

[98] R. W. Ziolkowski, W. A. Johnson, and K. F. Casey. Application of Riemann-Hilbert problem techniques to electromagnetic coupling through apertures. volume 19, pages 1425–1431. Radio Sci., Nov–Dec 1984.